

**EXPERIMENTAL AND COMPUTATIONAL EVALUATION OF
THERMAL PERFORMANCE AND OVERHEATING IN
DOUBLE SKIN FACADES**

Mauricio Hernandez Tascón

**Thesis submitted to the University of Nottingham for the degree of Doctor of
Philosophy**

August 2008

ABSTRACT

Double Skin Facades (DSFs) have been developed as an alternative technology to improve the thermal performance of conventional fully glazed buildings. Nevertheless, there is little test information on the behaviour and real performance of DSFs. This is specifically the case when the façade has to perform under extreme or moderate summer conditions. The characteristics of thermal overheating of a specific type of DSF with various configurations and its practical control have not been subjected to systematic experimental and computational investigations. This research which is based on an existent load of knowledge, carried out experiments of a full-scale one-storey laboratory chamber of a selected type of Double Skin Façade in which a comparative analysis of the thermal performance is assessed, CFD simulations of the experimental model and a Field Case Study of an existing building in the United Kingdom is also monitored. The basic thermal behaviour in the façade cavity and adjacent room is investigated by a series of parametric studies and basic flow field investigations. Section models of the DSF chamber and the case building were made and modelled using CFD in order to visualise the thermal and airflow behaviour inside the DSF complementing the experimental and field work.

The modelling work has demonstrated the feasibility and versatility of the technique for probing the flow and thermal behaviour of double skin facades. It was found that natural ventilation through the cavity by a series of controlled opening shafts on the upper and lower facade are effective means to reduce DSF overheating. It was also observed that the optical properties of cavity elements, cavity depth size, solar control and the basic operation of the facade are key issues to address in order to prevent overheating and additional heat loads from the facade.

ACKNOWLEDGEMENTS

I would like to thank Prof. Li Shao for providing me the guidance and support on the accomplishment of this project. Special thanks to Prof. Brian Ford for his assistance, advice and encouragement than any word can match. I would also like to thank the staff of the School of The Built Environment for providing help, feedback and information required for this project. I also like to thank Dr. Mikkel Kragh at ARUP for his valuable support.

I would also like to express my special gratitude to the board of Directors of The Universidad Piloto de Colombia for the generous grant that allowed me to accomplish this project. It is also a pleasure to acknowledge the help of colleagues in the School of Architecture at the Universidad Piloto de Colombia as well as other friends at other academic institutions.

And of course, this thesis would never have become a reality without the patience and support of my wife Eliana. She has kept me full of joy and smiles during all these years.

Mauricio Hernandez T

November 2007

TABLE OF CONTENTS

Abstract	ii
Acknowledgments	iii
Table of Contents	iv
List of Figures	xi
List of Tables	xxi
1. INTRODUCTION	1
1.1 Problem Statement and Objective of Study	1
1.2 Research Methodology	2
1.3 Outline of the Thesis	3
REFERENCES	5
2. BACKGROUND OF DOUBLE SKIN FACADES	6
2.1 INTRODUCTION	6
2.2 BUILDING ENVELOPE	9
2.2.1 Sustainable Architecture and Energy Context	9
2.2.2 Responsive Building Envelope	11
2.3 GLASS IN ARCHITECTURE	14
2.3.1 Definition	14
2.3.2 Glass in Buildings	15
2.3.3 Glass and the Environment	22
2.4 CONCEPT OF DOUBLE SKIN FACADE	23
2.5 DEFINITION OF DOUBLE SKIN FACADE	26
2.6 HISTORY OF DOUBLE SKIN FACADES	28
2.7 TECHNICAL DESCRIPTION OF DSF	37
2.7.1 Types of Facade construction	37
2.7.2 Building Integration of DSF	43

2.8	DSF ECONOMICS	45
2.8.1	Cost and Investments	45
2.8.2	Cost calculation and Energy assessment	48
2.9	ADVANTAGES / DISADVANTAGES OF DSFs	50
2.9.1	Advantages	50
2.9.2	Disadvantages	52
2.10	MONITORING / PREVIOUS MEASUREMENTS	53
2.11	DSF BUILDINGS IN THE UNITED KINGDOM	56
2.11.1	One Plantation Place Building	56
2.11.2	One Triton Square	58
2.11.3	BT Brentwood	59
2.11.4	Watling House	60
2.11.5	Glaxo Wellcome	61
2.11.6	Greater London Authority (GLA)	62
2.11.7	Helicon Building	64
2.11.8	Darwin Centre phase I (Natural History Museum)	65
2.11.9	Wellcome Trust Building	67
2.11.10	Ashcroft International Business School	68
2.11.11	University of Bath – Library Building	69
2.11.12	Portcullis House	70
2.11.13	Swiss Re HQ Building – ‘The Gherkin’	72
2.11.14	Fitzrovia Building, ARUP HQ	73
2.11.15 1	Deansgate Street Building	75
2.11.16	Willis Building	76
2.11.17	Beetham Tower – Manchester	78
2.11.18	Beetham Tower – London	79
2.11.19	Urbis Exhibition Centre	81
2.12	DISCUSSION AND CONCLUSION	82

REFERENCES	84
3. PHYSICAL BASIS OF THE CONCEPT OF DSFs	89
3.1 INTRODUCTION	89
3.2 PHYSICAL PARAMETERS OF DSFs	89
3.2.1 Spatial Form / Structure	90
3.2.2 Materials	95
3.2.2.1 Glazing	96
3.2.2.2 Optical Properties of Glass	97
3.3 PHYSICS OF LIGHT	103
3.3.1 Solar Radiation	103
3.3.2 Natural Lighting and DSFs	106
3.4 THERMAL ENVIRONMENT	108
3.4.1 Thermal Buoyancy	109
3.4.2 Heat Transfer Model of a DSF	110
3.4.3 Heat Fluxes in a DSF	112
3.4.4 Theoretical model of the Facade	114
3.4.5 Thermal Performance of DSFs	116
3.4.6 Overheating in DSFs	118
3.5 AIR FLOW – VENTILATION	120
3.6 CONCLUSIONS	125
REFERENCES	127
4. EXPERIMENTAL FACILITY AND SETUP	130
4.1 INTRODUCTION	130
4.2 EXPERIMENTAL FACILITY	131
4.2.1 Test Chamber	133
4.2.2 Solar Simulator Rig	135
4.3 TEST PROCEDURES	139

4.4	EXPERIMENTAL MEASURING / LOGGING	140
4.4.1	Instrumentation	140
4.4.2	Experimental Measurements	143
4.4.2.1	External measurements	144
4.4.2.2	Cavity Measurements	144
4.4.2.3	Room Measurements	147
4.4.3	Radiation measurement	148
4.4.4	Illuminance measurement in the experimental chamber	149
4.4.5	Temperature measurement in the experimental facility	150
4.4.6	Air Velocity measurement inside the cavity	152
4.5	PHYSICAL CONFIGURATIONS OF THE DSF CHAMBER	153
4.5.1	DSF Opening Position	154
4.5.2	DSF Structure	155
4.5.2.1	Reflective Shading Devices	155
4.5.2.2	Blinds	155
4.5.2.3	Louvers	157
4.5.3	Types of glass used in the DSF chamber	158
4.5.4	Cavity Depth	159
	REFERENCES	160
5.	EXPERIMENTAL ANALYSIS	162
5.1	INTRODUCTION	162
5.2	DSF OPENINGS POSITION	164
5.2.1	Standard Cases (ST)	165
5.2.2	Standard Ventilated Cases (STV)	166
5.2.3	Inlet / Outlet Size	172
5.2.4	Effect of Diffuse Radiation	177
5.3	ROOM OPENING ARRANGEMENTS	182
5.4	DEVICES IN DSF	187

5.4.1	Reflective Panels as Shading Devices	188
5.4.2	Blinds	191
5.4.2.1	Position on External Skin	192
5.4.2.2	Position on Internal Skin	194
5.4.3	Louvers	200
5.4.3.1	Position of Louvers	201
5.4.3.2	Colour of Louvers	205
5.5	GLASS TYPE	215
5.6	CAVITY DEPTH	223
5.6.1	Cavity Depth Variation	223
5.6.2	Depth Variation using Shading Devices	225
5.7	CONCLUSIONS	229
	REFERENCES	233
6.	CFD ANALYSIS OF THE EXPERIMENTAL CHAMBER	234
6.1	INTRODUCTION	234
6.2	FUNDAMENTALS OF AIRFLOW MODEL	237
6.2.1	Computational Fluid Dynamics Model	239
6.2.2	Turbulence Model	240
6.2.3	Radiation Model	243
6.3	MODEL SETUP FOR CFD SIMULATIONS	246
6.3.1	Model Grid	246
6.3.2	Model Settings	248
6.3.3	Boundary Conditions	252
6.4	AIRFLOW DESCRIPTION	255
6.4.1	DSF Openings Position	255
6.4.1.1	Sealed Cavity (ST)	255
6.4.1.2	Ventilated Cavity (STV)	258
6.4.1.3	Inlet / Outlet size	261

6.4.2	Room Openings Position	264
6.4.3	DSF Structure	266
6.4.3.1	Shading panels on Glazed Skins	266
6.4.3.2	Louvers	269
6.4.4	Glass Type	274
6.4.5	Cavity Depth	276
6.4.5.1	Depth Variation	276
6.4.5.2	Depth Variation with Louvers	278
6.5	DISCUSSION OF RESULTS	280
6.5.1	Air Velocity	280
6.5.2	Temperature	283
6.5.3	Validation of Results	286
6.6	CONCLUSIONS	288
	REFERENCES	291
7.	FIELD CASE STUDY OF MONITORING A DSF	294
7.1	INTRODUCTION	294
7.2	CLIMATE AND WEATHER DATA	296
7.3	PILOT MONITORING	298
7.3.1	Monitored Building	295
7.3.2	Monitored areas	300
7.3.3	Parameters assessed	303
7.3.4	Instrumentation	304
7.3.5	Methodology for Monitoring	305
7.3.5.1	Procedures	305
7.3.5.2	Problems encountered	307
7.3.5.3	Lessons learnt	308
7.4	FACADE PERFORMANCE MONITORING	309
7.4.1	Facade Cavity	309

7.4.2	Monitored Room	320
7.5	DOUBLE SKIN FAÇADE AIRFLOW ANALYSIS	325
7.5.1	Model Description	326
7.5.2	Model settings and Boundary Conditions	326
7.5.3	Airflow Models Results	328
7.5.3.1	Winter Day Model	328
7.5.3.2	Winter Night Model	329
7.5.3.3	Mid Season Model	330
7.5.3.4	Summer model with ventilated cavity	332
7.5.3.5	Summer model with cavity closed	333
7.5.4	Validation of CFD Results	334
7.6	OCCUPANTS PERCEPTION ASSESSMENT	336
7.6.1	Natural Lighting levels satisfaction	337
7.6.2	Facade performance perception	338
7.6.3	Natural ventilation and air quality awareness	339
7.6.4	User's interaction and operation of DSF	340
7.7	CONCLUSIONS	341
	REFERENCES	343
8.	DISCUSSION AND CONCLUSIONS	344
8.1	DISCUSSION OF FINDINGS	344
8.1.1	Thermal Performance	344
8.1.2	Airflow Performance	346
8.1.3	Natural Lighting	346
8.1.4	User's Perception	346
8.1.5	Design Implications	347
8.2	CONCLUSIONS	348
8.3	FUTURE WORK	349

LIST OF FIGURES

Figure 2.1	Glass stained windows at Notre Dame Cathedral in Paris	16
Figure 2.2	The Crystal Palace, London, By Joseph Paxton, 1851	17
Figure 2.3	Bauhaus Dessau workshops building	19
Figure 2.4	Paimio Tuberculosis Sanatorium at Paimio, Finland	21
Figure 2.5	St. George’s School, Wallasey near Liverpool	21
Figure 2.6	Basic elements comprising a Double Skin Façade	26
Figure 2.7	Steiff Factory, 1903	30
Figure 2.8	Narkomfin building in Moscow in 2007, (M. Ginzburg, 1928).	31
Figure 2.9	Salvation Army Hostel ‘Cite de Refuge’ in Paris, 1929-1933	32
Figure 2.10	Sun breakers facade in Rio de Janeiro, 1936.	32
Figure 2.11	Le Corbusier’s sketch of the of the ‘sun breakers’	33
Figure 2.12	Le Corbusier’s sketches illustrating UN building in 1947.	34
Figure 2.13	IBM Plaza, Chicago, Illinois (Van der Rohe, L. M., 1950)	35
Figure 2.14	The Hooker Building southeast Double Skin Facade, 1980	35
Figure 2.15	The Debis Tower designed by Renzo Piano, 1996-1998	36
Figure 2.16	Box Windows	38
Figure 2.17	Shaft box windows	38
Figure 2.18	Corridor Façade	39
Figure 2.19	Multi-storey façade	40
Figure 2.20	Estimated initial costs of Single and Double Skin Facades	47
Figure 2.21	Estimated maintenance costs of Standard facade vs. DSF	47
Figure 2.22	Estimated total cost in the UK for a ten storey DSF building	48
Figure 2.23	Advantages of Double Skin Facades	51
Figure 2.24	Disadvantages of Double Skin Facades	53
Figure 2.25	1 Plantation Place building views	56
Figure 2.26	1 Triton Square building views	58
Figure 2.27	BT Brentwood: General view of the building	59
Figure 2.28	Watling House: View of the facade	60
Figure 2.29	Glaxo Wellcome: General view of the building	61
Figure 2.30	GLA: General view of the building	62
Figure 2.31	Helicon Building: Views of the DSF	64
Figure 2.32	Darwin Centre phase I: General view of the building	65
Figure 2.33	Wellcome Trust: General view of the building’s north facade	67
Figure 2.34	Ashcroft I Business School: General view of the building	68
Figure 2.35	University of Bath Library: General view of the building DSF	69

Figure 2.36	Portcullis House: General view of the building on Bridge Street	70
Figure 2.37	Swiss Re HQ: General views of the building	72
Figure 2.38	Fitzrovia Building: General views	73
Figure 2.39	1 Deansgate Street: General view of the building	75
Figure 2.40	The Willis: General views of the building	76
Figure 2.41	Beetham Tower – Manchester: General views of the building	78
Figure 2.42	Beetham Tower – London: General rendered views	79
Figure 2.43	Urbis Exhibition Centre: General views of the building	81
Figure 3.1	Relative Efficiencies of Window Openings	93
Figure 3.2	Light transmittances through a Pane of Glass	98
Figure 3.3	Spectral transmittance of Clear and tinted glass	99
Figure 3.4	Spectral transmittance of clear glass depending of pane thickness	100
Figure 3.5	Optical properties of inorganic and organic glazing materials	101
Figure 3.6	Evolution of physical properties of current commercial glasses	103
Figure 3.7	Spectral distribution of solar radiation	104
Figure 3.8	Electromagnetic spectrum of visible light	105
Figure 3.9	Spectral transmittance of most common coloured floated glass	106
Figure 3.10	Thermal buoyancy leads to vertical pressure differences which drive to stack effect.	110
Figure 3.11	Heat transfer through a DSF on Summer Conditions	111
Figure 3.12	Main heat fluxes in the chamber	112
Figure 3.13	Stack effect and upward airflow inside a DSF	120
Figure 3.14	Laminar velocity profiles inside a double skin façade	125
Figure 4.1	Experimental Facility: Box-Double Skin Facade	131
Figure 4.2	DSF Experimental Chamber: Front and Side Elevations	132
Figure 4.3	DSF Experimental Chamber Plan view	132
Figure .4.4	DSF Experimental Chamber: Section	133
Figure 4.5	Experimental chamber description and materials: Section	134
Figure 4.6	Experimental chamber description and materials: Plan	135
Figure 4.7	Solar simulator structure of the experimental facility	137
Figure 4.8	Wavelengths for various black body spectra as a function of temperature	138
Figure 4.9	Spectral Output of tungsten-halogen lamps	138
Figure 4.10	Data-logging equipment connected to the measuring instruments	141
Figure 4.11	Location of sensors inside the Experimental Chamber	144
Figure 4.12	Shielded K-type thermo-couples inside the cavity	145
Figure 4.13	Location of Radiation sensors in the experimental chamber	145

Figure 4.14	Shielded K-type thermocouples for measuring surface temperatures	146
Figure 4.15	Air velocity transducer v inside the cavity, next to the inner skin	146
Figure 4.16	Shielded K-type thermo-couples placed inside the chamber room	147
Figure 4.17	Illuminance sensors placed inside the experimental room	148
Figure 4.18	Measurement point array and average measured radiation levels	148
Figure 4.19	Total radiation measured on the geometric centre of the external skin	149
Figure 4.20	Illuminance measured inside the room of the experimental chamber	150
Figure 4.21	Example of measured and average external temperatures	151
Figure 4.22	Example of measured and average air temperatures v in the cavity	152
Figure 4.23	Example of measured and average air temperatures in the room	152
Figure 4.24	Air Velocity in the cavity for ST and STV	153
Figure 4.25	Standard Configuration of the cavity (ST)	154
Figure 4.26	Standard Ventilated Configuration of the cavity (STV)	154
Figure 4.27	Location of reflective panels as shading devices	155
Figure 4.28	Blinds as shading devices next to the external skin of the DSF	156
Figure 4.29	Blinds as shading devices next to the inner skin of the DSF	156
Figure 4.30	Cavity configurations with horizontal louvers	157
Figure 4.31	Clear, Textured and Green tinted glasses in the experimental chamber	158
Figure 4.32	Depth size settings of the cavity	159
Figure 5.1	Main configurations of the cavity openings	165
Figure 5.2	Air temperatures in cavity with inlets and outlets closed (ST)	166
Figure 5.3	Air temperatures in the cavity with inlets and outlets open (STV)	167
Figure 5.4	Air temperatures in the cavity for various openings positions	168
Figure 5.5	Air temperatures in the room for various cavity openings configurations	169
Figure 5.6	Total incident radiation on the experimental chamber	169
Figure 5.7	Visible light energy measured on external and internal skins	170
Figure 5.8	Illuminance in the room of the experimental chamber	170
Figure 5.9	Temperature comparison values in experimental chamber	171
Figure 5.10	Inlets and outlet sizes adjusted with reflective panels	172
Figure 5.11	Air temperatures in the cavity for various inlet sizes	173
Figure 5.12	Average temperature values inside the cavity for various inlet sizes	174
Figure 5.13	Air temperatures inside the room for various inlet sizes	175
Figure 5.14	Air temperatures in the cavity for various outlet sizes	175
Figure 5.15	Average temperature values inside the cavity for various outlet sizes	176
Figure 5.16	Air temperatures inside the room for various outlet sizes	177
Figure 5.17	Configuration of the experimental chamber using screen diffuser	177

Figure 5.18	Light transmission and reflection of external screen diffuser fabric	178
Figure 5.19	Total incident radiation using screen diffuser	179
Figure 5.20	Illuminance in the room using screen diffuser	179
Figure 5.21	Air temperatures in the cavity for ST and STV using screen diffuser	180
Figure 5.22	Air temperatures in the room for ST and STV with screen diffuser	181
Figure 5.23	Location of openings in the experimental chamber	182
Figure 5.24	Air temperatures in the cavity for various openings positions	183
Figure 5.25	Air temperatures in the cavity for cross ventilation with the DSF	184
Figure 5.26	Air temperatures in the cavity in STV for various opening configurations on the inner skin	184
Figure 5.27	Air temperatures in the room in ST for various configurations	185
Figure 5.28	Temperatures inside the room in ST and STV using different openings configurations on the rear wall of the room	186
Figure 5.29	Air temperatures in the room for various inlets and outlets positions on the rear wall, with open inlets and outlets on the external and internal skins	186
Figure 5.30	Air temperatures in the room with ventilated cavity and open outlet on internal skin, using various inlets and outlets configurations on the rear wall	187
Figure 5.31	Air temperatures inside the cavity for ST and STV using reflective shields on external and internal skins	189
Figure 5.32	Air temperatures inside the room for ST and STV using reflective panels on external and internal skins	190
Figure 5.33	Comparison between maximum temperature values in the cavity, the room and outside the chamber in ST and STV for various areas of glass covered on the external and internal skins	191
Figure 5.34	Air temperatures in the cavity in ST and STV with blinds on the external skin.	192
Figure 5.35	Air temperatures in the room for ST and STV using blinds in front and behind the external skin	193
Figure 5.36	Temperatures inside the cavity for ST and STV using blinds in front and behind the internal skin	195
Figure 5.37	Air temperatures in the room for ST and STV using blinds in front and behind the internal skin	196
Figure 5.38	Air temperatures in the cavity for STV for various positions of blinds next to the external and internal skins	196

Figure 5.39	Air temperatures in the room for STV for various positions of blinds next to the external and internal skins	197
Figure 5.40	Illuminance in the room for various positions of blinds	198
Figure 5.41	Comparison between maximum temperature values in the cavity, the room and outside the chamber in ST for various areas of glass covered by the blinds on the external and internal skins.	198
Figure 5.42	Comparison between maximum temperature values in the cavity, the room and outside the chamber in STV for various areas of glass covered by the blinds on the external and internal skins	200
Figure 5.43	Main configuration of the DSF cavity using horizontal louvers as shading devices	200
Figure 5.44	Louvers configurations at the front and behind the external skin	201
Figure 5.45	Louvers configurations inside the cavity before the inner skin	202
Figure 5.46	Air temperatures in the cavity for ST with various louvers positions	203
Figure 5.47	Air temperatures in the cavity for STV with various louvers positions	203
Figure 5.48	Air temperatures inside the room for ST with various louvers positions	204
Figure 5.49	Air temperatures in the room for STV with various louvers positions	205
Figure 5.50	Surface colours on horizontal louvers inside the DSF chamber	206
Figure 5.51	Air temperatures in the cavity for ST cases for various louver colours	207
Figure 5.52	Temperature performances of louvers in ST for various surface colours	208
Figure 5.53	Air temperatures in the room in ST for various louver colours	208
Figure 5.54	Air temperatures in the cavity in STV for various louver colours	209
Figure 5.55	Temperature performances of louvers in STV for various louver colours	210
Figure 5.56	Air temperatures in the room in STV for various louver colours	211
Figure 5.57	Air temperatures in the cavity for STV cases for white or black colours on exposed louvers surfaces	211
Figure 5.58	Air temperatures in the room for STV cases shifting white or black colours on exposed louvers surfaces	212
Figure 5.59	Illuminance in the room for various louvers colours	213
Figure 5.60	Illuminance in the room for grey scale colours on louvers surfaces	214
Figure 5.61	Illuminance in the room for white/black colours on louvers surfaces	215
Figure 5.62	Air temperatures in the cavity for various glass types (ext skin)	216

Figure 5.63	Air temperatures in the room for various glass types (ext skin)	217
Figure 5.64	Air temperatures in the cavity for various glass types (int skin)	219
Figure 5.65	Air temperatures in the room for various glass types (int skin)	220
Figure 5.66	Thermal performances of the cavity in STV using various glass types	221
Figure 5.67	Thermal performances of the room in STV using various glass types	222
Figure 5.68	Illuminance in the room depending on the of glass type on both skins	222
Figure 5.69	External and internal views of the DSF cavity	223
Figure 5.70	Air temperatures in the cavity for ST cases varying the cavity depth	224
Figure 5.71	Air temperatures in the cavity for STV cases varying the cavity depth	224
Figure 5.72	Air temperatures in the room for STV cases varying the cavity depth	225
Figure 5.73	Air temperatures in the cavity for STV cases with louvers and various cavity depths	226
Figure 5.74	Air temperatures in the room for STV cases with louvers and various cavity depths	227
Figure 5.75	Temperatures inside the cavity for STV and three cavity depths using black/white louvers	224
Figure 5.76	Temperatures inside the room for STV and three cavity depths using black/white louvers	228
Figure 6.1	2D grid of the DSF experimental chamber model.	241
Figure 6.2	2 dimensional grid model of the cavity.	248
Figure 6.3	Main configurations of the 2D model boundaries for ST and STV.	249
Figure 6.4	Cavity configurations for various inlets and outlets sizes on external skin.	249
Figure 6.5	Openings location in the 2D model of the experimental chamber.	250
Figure 6.6	Model settings for shading control of glazing and inside the cavity with shading devices.	251
Figure 6.7	Grid models for various cavity depths.	252
Figure 6.8	Boundary definition of the DSF Experimental Chamber.	251
Figure 6.9	Air velocity and temperature contours of the cavity in ST.	256
Figure 6.10	Velocity magnitude contours in a section of the experimental chamber in ST.	257
Figure 6.11	Velocity vectors grey scaled by velocity magnitude (m/s) in ST.	257
Figure 6.12	Air velocity and temperature contours in STV.	259
Figure 6.13	Velocity magnitude contours in a vertical section of the experimental chamber in STV (m/s).	259
Figure 6.14	Calculated temperature values in the vertical centre of the cavity in ST and STV.	260

Figure 6.15	Calculated values of air velocity in the centre of the cavity in ST and STV.	261
Figure 6.16	Temperature performances for various opening sizes of the cavity.	262
Figure 6.17	Velocity magnitude (m/s) contours inside the cavity for various inlet/outlet openings sizes.	262
Figure 6.18	Velocity magnitude contours (m/s) inside the cavity for various inlet sizes and 200mm fixed outlet.	263
Figure 6.19	Velocity magnitude contours (m/s) inside the cavity with fixed 200mm inlet size and various outlet sizes.	264
Figure 6.20	Velocity magnitude vectors inside the experimental chamber for various opening positions on the internal skin.	265
Figure 6.21	Velocity magnitude vectors inside the experimental chamber for various opening positions on the back wall of the room.	266
Figure 6.22	Velocity magnitude and temperature contours of the cavity assuming shading panels on the external skin.	264
Figure 6.23	Velocity magnitude and temperature contours of the cavity assuming shading panels on the internal skin.	268
Figure 6.24	Temperature performances of the cavity for various positions of shading surfaces on external and internal skins.	268
Figure 6.25	Air velocities in the cavity for various positions of shading surfaces on external and internal skin.	269
Figure 6.26	Velocity magnitudes contours (m/s) for various positions of louvers at 45° inside the cavity.	270
Figure 6.27	Velocity magnitude contours (m/s) for various positions of horizontal louvers inside the cavity.	271
Figure 6.28	Temperature performances of the cavity calculated for various positions louvers.	272
Figure 6.29	Velocity magnitude contours (m/s) inside the cavity for various colours of louver surfaces.	273
Figure 6.30	Air velocity performances inside the cavity for various surface colours of louvers.	273
Figure 6.31	Temperature values of the cavity for various surface colours of louvers.	274
Figure 6.32	Velocity magnitudes along the centre of the cavity for various glass types.	275
Figure 6.33	Velocity magnitude contours (m/s) inside the cavity for various glass types.	275

Figure 6.34	Temperature in the centre of the cavity for various glass types.	276
Figure 6.35	Velocity magnitude contours (m/s) for various cavity depths.	277
Figure 6.36	Temperature performances in the cavity for various cavity depths in STV.	278
Figure 6.37	Velocity magnitude contours (m/s) for various cavity depths with louvers.	279
Figure 6.38	Temperature contours (°C) for various cavity depths with louvers.	280
Figure 6.39	Mean air velocity magnitude in sealed and ventilated cavity.	281
Figure 6.40	Average velocity magnitude values inside the cavity for various opening sizes.	281
Figure 6.41	Mean velocity magnitude inside the cavity for various surface colours of louvers.	282
Figure 6.42	Average velocity magnitude values inside the cavity for various depths of the DSF.	283
Figure 6.43	Mean temperature values calculated inside the cavity ST and STV.	283
Figure 6.44	Average temperature values inside the cavity for various opening sizes.	284
Figure 6.45	Average temperatures inside the cavity for various surface colours of louvers.	285
Figure 6.46	Average temperatures along the vertical centre of the DSF, calculated using CFD for various cavity depths.	285
Figure 6.47	Temperature Values at three points for the experimental (m) and simulated cases (s) for various cavity openings positions.	286
Figure 6.48	Temperature values at three points inside the cavity for the experimental (m) and simulated (s) cases using shading devices.	287
Figure 6.49	Temperature values at three points for the experimental (m) and simulated cases (s) using depths of 800, 600 and 400mm.	287
Figure 6.50	Temperature values at three points for the experimental (m) and simulated cases (s) for various glass types on the cavity's external and internal skins.	288
Figure 7.1	Monthly average temperature values for London	297
Figure 7.2	Recorded hourly inlet temperature values for ARUP HQ on south-east facing façade	297
Figure 7.3	Mean temperature values measured at inlet level for 2006-07	298
Figure 7.4	Facade selected for monitoring and detail of monitored area	300
Figure 7.5	Location of equipment and room selected for monitoring	301
Figure 7.6	Vertical section of sensors location within the facade cavity	302

Figure 7.7	Location of sensors inside the selected room	302
Figure 7.8	Total Solar Radiation on vertical surface measured inside the external skin of the south-east facing DSF (380 -1050 nm)	309
Figure 7.9	Total Solar radiation energy measured on vertical surfaces inside the facade cavity	310
Figure 7.10	Temperature measured inside the DSF cavity	311
Figure 7.11	Ambient temperatures measured on 2 nd and 5 th floor levels inside the facade cavity during 3 days of winter	312
Figure 7.12	Ambient Temperature measured on 2 nd and 5 th floor levels inside the facade cavity during 3 days of spring	313
Figure 7.13	Total solar radiation on vertical surface passing through the external glass of the façade	313
Figure 7.14	Ambient Temperature measured on 2 nd and 5 th floor levels inside the facade cavity during 3 days of summer	314
Figure 7.15	Ambient Temperature measured on 2 nd and 5 th floor levels inside the facade cavity during 3 days of autumn	315
Figure 7.16	Measured and mean dry bulb temperature of the facade cavity at 5 th floor level	316
Figure 7.17	Surface temperatures of the two skins of glass inside the facade cavity	317
Figure 7.18	Monthly dry bulb and surface temperatures of sun shading devices temperatures measured inside the DSF	318
Figure 7.19	Surface temperature measured on upper and lower louvers inside the facade cavity at 5 th level during 3 days of late summer	319
Figure 7.20	Values of temperature inside the cavity measured at 12:00h on selected dates for each season (m=measured, s=simulated)	320
Figure 7.21	Monthly mean and measured Dry Bulb Temperature in the room	321
Figure 7.22	Radiation measured inside the room on the vertical plane of the inner glass of the façade	322
Figure 7.23	Direct radiation hitting inside the room on walls and floor as the shading devices were not totally able to shield efficiently part of the inner façade	322
Figure 7.24	Surface temperature of the inner facade glass measured inside the room	323
Figure 7.25	Monthly ambient Relative Humidity room	323
Figure 7.26	Illuminance on horizontal surface measured next to the inner glass of the facade inside the room	324

Figure 7.27	Illuminance on horizontal surface measured on the back wall of the room at 3.55m from the façade	325
Figure 7.28	Total temperature inside the channel (°C)	328
Figure 7.29	Velocity magnitude contours of the winter (day) model (m/s)	329
Figure 7.30	Total temperature contours for the winter model at night (°C)	330
Figure 7.31	Contours of Velocity magnitude for the winter case at night (m/s)	330
Figure 7.32	Contours of total temperature for the mid season case (°C)	331
Figure 7.33	Velocity magnitude contours for the airflow inside the facade channel (m/s)	331
Figure 7.34	Contours of temperature of the ventilated summer model (°C)	332
Figure 7.35	Velocity magnitude contours of the summer model with outlet shafts open (m/s)	333
Figure 7.36	Total temperature contours of the closed facade channel on the summer model (°C)	333
Figure 7.37	Contours of Velocity magnitude inside the facade cavity with closed outlets on the summer model (m/s)	334
Figure 7.38	Validation of CFD results with the measured steady state temperature values according to each season case	335
Figure 7.39	Occupants satisfaction with natural light quality and solar radiation control by the DSF	338
Figure 7.40	Occupants perception of the façade efficiency	339
Figure 7.41	Occupants perception of of air quality and ventilation	340
Figure 7.42	Occupants opinion about the possibility of manual operation of lighting levels and solar protections of the façade	340

LIST OF TABLES

Table 2.1	One Plantation Place: General description of the building	56
Table 2.2	One Triton Square: General description of the building	58
Table 2.3	BT Brentwood: General description of the building	59
Table 2.4	Watling House: General description of the building	60
Table 2.5	Glaxo Wellcome: General description of the building	61
Table 2.6	Greater London Authority: General description of the building	63
Table 2.7	The Helicon: General description of the building	64
Table 2.8	Darwin Centre phase I: General description of the building	66
Table 2.9	Wellcome Trust: General description of the building	67
Table 2.10	Ashcroft Business School: General description of the building	68
Table 2.11	University of Bath Library: General description of the building	69
Table 2.12	Portcullis House: General description of the building	71
Table 2.13	Swiss Re HQ ‘The Gherkin’: General description of the building	72
Table 2.14	Fitzrovia Building: General description	74
Table 2.15	1 Deansgate Street: General description of the building	75
Table 2.16	The Willis Building: General description	77
Table 2.17	Beetham Tower Manchester: General description of the building	78
Table 2.18	Beetham Tower – London: General description of the building	80
Table 2.19	Urbis Exhibition Centre: General description of the building	81
Table 4.1	Main thermal parameters of the experimental chamber	135
Table 4.2	Technical specification of light source simulator	137
Table 4.3	Instrumentation used for experimental measurements	140
Table 4.4	Technical Information sensors – specifications	143
Table 4.5	Mean air velocities according to inlet / outlet position	183
Table 5.1	Main optical properties of the glass used in the experimental chamber	215
Table 6.1	Main parameters of the chamber’s experimental conditions	253
Table 6.2	Main boundary conditions of the experimental model	253
Table 6.3	Main boundary conditions of the facade cavity	254
Table 7.1	General information ARUP Headquarters Building	299
Table 7.2	Technical description of sensors	305
Table 7.3	Main boundary conditions of the facade cavity models	327
Table 7.4	Occupant’s perception survey results	336

CHAPTER I

INTRODUCTION

1.1 Problem Statement and Objective of Study

Large glazed areas are becoming a common element in the design of office buildings. Justification of the use of glass is mainly based on the argument that fully glazed envelopes contribute to improved natural lighting [1]. Nevertheless, these types of facades also add significant heat gains and heat losses to the total energy employed for heating and cooling. A Double Skin Facade (DSF) is an envelope system, which has an external and internal layer that contains a buffer space used for controlled ventilation and solar protection [2]. The use of multilayered skins enhances building insulation against thermal variations and external noise.

DSFs can achieve reduction of winter heating requirements [3]. However, when the building is under summer conditions or located in moderate or hot climates, heat gains are predominant and the cost of cooling becomes a major issue [4]. The improvement of the system is necessary when working under hot climatic conditions. Previous research suggested that the use of ventilated facades contributes towards the energy reduction of indoor thermal gains [5]. The use of a ventilated channel reduces temperatures in the facade, though indoor thermal conditions have to be assessed in relation to the facade configuration as part of the compliance of the system to the building requirements.

Recently, double Skin Facades have been widely used as a way to reduce the thermal instability of inner spaces caused by the growing use of large glazed areas in

buildings. This concept has provided the possibility of improved sound insulation, pre-heating air for ventilation, and protection of solar shading in urban areas. However, little has been done in the field of thermal control reduction and monitoring of full-scale buildings in the UK.

This research project is based on an existent load of knowledge in the field, a parametric study using a full-scale laboratory model of a Shaft Box Double Skin Facade type, a pilot monitoring of an existing building in the UK, and a comparative assessment of the thermal and airflow behaviours of these cases, modelled using CFD. The results are used to identify the key elements in preventing and controlling overheating of a DSF.

1.2 Research Methodology

The study of overheating in a Double Skin Facade is based on the investigation of the following topics:

- Assessment and characterization of the envelope and the concept of Double Skin Facades.
- Parametric assessment of the thermal performance inside a laboratory chamber, built at the University of Nottingham.
- CFD modelling of the laboratory results.
- Case Study of monitoring a DSF building in a UK context.
- CFD modelling of the DSF cavity in the existing monitored building.

1.3 Outline of the Thesis

Beginning with a general review of previous literature, Chapter 2 describes and explains the historical background and definition of Double Skin Facades: The effects on issues such as sustainability, while technical and economic implications are also discussed, it presents an overview of the concept of sustainable envelopes, illustrating the implications of glass in architecture. The concept and technical characteristics of DSF in buildings are described, highlighting from previous literature the economic implications and costing of DSFs, alongside its advantages and disadvantages. This provides an overall picture of the current state of the artistic application of DSFs.

Chapter 3 describes the main aspects relative to the physical basis of DSFs. A general description is presented of the physical parameters based on the spatial configuration and materials used on the facade. The main characteristics of glass and its correlation with the physics of light are also illustrated in this chapter. Previous literature in the fields of thermal environment and airflow basis are described. The main aspects relative to the physical basis of DSFs are also identified, fundamentally by its incidence on the thermal behaviour of the facade.

Chapter 4 provides a general account of the physical configurations, equipment, specifications and procedures of the Experimental Chamber of a Box-Double Skin Facade. This was built at ‘The School of the Built Environment of Nottingham University’, which was used to study the thermal performance of the facade under critical summer conditions. This chapter particularly describes the experimental facilities, test procedures, methodology and physical configurations of the

experimental chamber for investigating the performance of the double glass façade. In chapter 5, the assessment of thermal behaviour inside the DSF chamber is analysed, based within four main parameters depending on the configuration of the facade cavity. This chapter particularly analyses the implications on the thermal performance by the variation of these physical parameters. The performance of the facade is compared based on the position of openings of the cavity and the room, the structure configuration of the DSF, the type of glass used on the cavity skins and depth sizes of the DSF. This chapter also shows comparative analysis of transmitted radiation, temperature performance of the cavity and room and the illuminance inside the room of the experimental chamber. These comparative analyses are used to identify the physical conditions and critical parameters, which influence the development of overheating in the facade and room.

Chapter 6 is concerned with a comparative study carried out using Computational Fluid Dynamics software, based on the previous results of the full-scale laboratory chamber. As the experimental study was formulated based on various configurations of a DSF, and the identification of the causes of overheating in critical radiation conditions; 2D models of the experimental chamber are built and modelled by CFD to visualise and assess the airflow within the system. Commercial CFD software is used to predict the flow and movement of air and temperature response of the laboratory model. The air flow and the temperature response are simulated assuming a steady state model of the facade cavity. Thermal performance and airflow are modelled and compared identifying the main aspects that contribute to the overheating development.

Chapter 7 presents the results of a full scale field monitoring of an existing Double Skin Facade building in London. This study was used to test a pilot methodology, and to acquire a set of measured data in order to assess the performance of the DSF, with special interest in any possible overheating problems and daylight performances during mid-season and summer conditions.

Finally, Chapter 8 summarizes the findings and highlights any limitations of this study. It also suggests further research related for post-occupancy monitoring and design guidance on DSFs.

REFERENCES

1. Krewinkel, H.W., *Glass Buildings: Material, Structure and Detail*. 1st ed. 1998, Basel: Birkhäuser. 155.
2. Oesterle, L., Lutz & Heusler, *Double Skin Facades: Integrated Planning*, ed. Prestell. 1999. 208.
3. Saelens, D., *Energy Performance Assessment of Single Storey Multiple-Skin Facades*, in *Faculteit Toegepaste Wetenschappen, Arenbergkasteel*. 2002, Katholieke Universiteit Leuven, Kasteelpark Arenberg 51, B-3001 Leuven, Belgium. p. 272.
4. Faggembauu, D., et al., *Strategies to reduce thermal overheating in Mediterranean climates using large glazed areas*. in *Fier 2002: International Forum on Renewable Energies*. 2002. Tetuan: FIER 2002.
5. Gratia, E. and A. De Herde, *Natural ventilation in a double-skin facade*. *Energy and Buildings*, 2004. 36(2): p. 137-146.

CHAPTER II

BACKGROUND OF DOUBLE SKIN FACADES

2.1 INTRODUCTION

The envelope is one of the building systems that play a key role in the achievement of energy conservation and indoor thermal comfort. According to Sala, it is directly responsible for the immediate and delayed response in climatic changes [1]. It has been suggested that the correct selection of materials and an understanding of the climatic conditions resolve most of the issues regarding thermal instability. The conscious assessment of the appropriate materials according to the climatic and functional requirements has nowadays become a key element in the design process of any building.

In the past, architectural design mainly focussed on aesthetical and functional requirements. The importance of façade materials was more about aesthetics, their availability and feasibility of use, rather than the overall performance of the building, which was often a secondary consideration. The selection and application of materials for the façade was based solely on the designer's criteria, and there was usually no real understanding of the effect on the building with regard to energy usage and potential present or future environmental issues. In the case of commercial buildings, the selection was usually based on financially viable options that merely complied to basic regulations, without taking into account the possible effects of the envelope materials, in matters such as thermal comfort, energy efficiency and sustainability.

Nowadays, there is growing concern about the repercussions of poor building performance, and the rational use of materials in construction, which indirectly affect global warming. This is due to the environmental impact of energy use throughout the entire life cycle of the built environment, and the increased cost for its generation. However, the selection of new materials and technologies for building envelopes are still influenced by the economics of a project. The compliance with regulations, which demand increased air tightness, is done without a complete understanding of the balance between natural ventilation of buildings, and any potential health related issues. The growing interest in energy-efficient buildings is exploited as a marketing ploy, rather than being a conscious application which takes into account the future implications for the building and the well-being of its occupants, nor indeed the energy and environmental impact it may cause. These issues still leave a gap in the perception of the overall performance of the building and its materials, especially the real effects of the envelope on the total energy-related impact of a building. The development of building façade technology has encouraged designers, planners and engineers to do research into the possibility of achieving energy-efficient buildings through the development of environmentally responsive envelopes.

The application of double-skin facades is a growing trend in office buildings in Europe. This trend is due to the fact that the system can be applied as a way to improve transparency and natural lighting, together with the possibility of combining an acceptable indoor environment with a reduction in energy use. It is known that double-skin façade systems were originally developed mainly for temperate European climates. Developers and designers typically apply this system as a

feature to achieve novel and architecturally attractive solutions, whilst reinforcing their "Green" corporate image, without a full understanding of the real justifications of the system, in relation to building performance in critical conditions. The advantages and disadvantages are hotly debated [2], as there is still a lack of reliable data on the real performance and possible consequences of current buildings with DSF.

Improvements in glass technology, and the popularization of glass as a distinctive feature of commercial buildings, are contributing to the increasing number of fully glazed facades on buildings. Large glazed areas are becoming common in the design of office buildings. The justification of the use of glass is mainly based on the argument that a glazed envelope contributes to improving natural lighting within the workplace. Nevertheless, this type of facade also contributes to significant thermal gains, and losses to the total energy employed for heating and cooling. As a result of these difficulties, the concept of the double glazed envelope was developed to solve some of these problems. However, if the building is in summery conditions, or located in moderate to hot climates, the heat gains are predominant and the cost of cooling develops into a major issue. Improvement of the system is necessary when working under such hot climatic conditions. Previous research suggests that the use of ventilated facades facilitates the reduction of indoor thermal gains [3]. The use of a ventilated channel reduces the temperature within the façade, though the indoor thermal conditions have to be assessed in relation to the façade configuration, as part of the integration of the system with the building requirements.

The historical background and definition of the concept of Double Skin Facades are

explained in this chapter. Sustainability, plus technical and economic issues are also discussed. The following will be considered in the order set out below:

- Overview of the general approach regarding the concept of sustainable envelopes in architecture.
- Implications of glass in architecture.
- Concept and technical characteristics of DSF in buildings.
- Preliminary findings on the economic implications and costing of DSFs.
- Advantages and disadvantages of DSFs discussed in previous literature.
- Overall picture of the current state of the artistic application of DSFs.

2.2 BUILDING ENVELOPE

2.2.1 Sustainable Architecture and Energy Context

The World Commission on Environment and Development Report: "Our Common Future", defines environment as *"the place where we all live"* and development as *"what we do in attempting to improve our lot within that abode"*. The term "Sustainable Development" was first used to define the search for balanced economic growth without compromising the well-being of future generations, and the ecological balance of the planet. The growing use of natural resources, an increased hunger for energy in the modern world, and the alarming manifestation of pollution in the biosphere, has become a more relevant issue on the political and energy agendas of developed nations. The efficient use of energy and the impact of its production are critical factors which affect the concept of Sustainable Development. The combustion of fossil fuels in conventional power stations and the growing energy demand of today's buildings are directly related to global warming and acid

rain [4]. In order to limit or reduce this damage, and the level of pollutants and greenhouse gasses released into the atmosphere, the energy used in the building's life cycle must be minimised or replaced by another source. These concerns, in relation to sustainability, have begun to be included in the architectural design of buildings.

Before sustainability became an important architectural issue, Victor Olgyay initially mentioned the term "bioclimatic architecture" in the early 1950's. The architectural design process involves many stages, which allow the transformation of an abstract idea into a real building. During this process, many factors are analysed and organized. The process takes into account the aesthetical, functional and technological aspects used by architects and construction teams to create a new building. Olgyay started to include the process of combining elements such as human psychology, climatology and building physics, in order to develop a strong relationship between the building and its context. This concept, which was called "bioclimatic architecture", included the importance of the physical, regional and cultural context on the overall design and construction process [5].

The role of the built environment and the question of sustainability are important issues in any environmental policy. Building designers are now responsible for producing buildings, which have to take into account the occupant's ever-growing number needs. However, these requirements need to be satisfied while minimising the use of non-renewable resources. Sustainable Building technologies and Passive solar systems play an important role in today's project decision-making. The use of energy, for building activities, accounts for significant quantities of the total energy consumption. The amount of energy related to the built environment depends on the

energy consumption during the whole of the building's life cycle. Therefore, included in this, is the energy needed for its construction, operation and the final disposal of the building when it is demolished. From the total energy used, during the building's life span, about 15% is used for the construction process and about 5% for the demolition. A staggering 80% is actually used for its operation [6]. The indirect implications of this energy usage on global warming has been thoroughly researched and discussed. The growing demand for thermal, naturally lit and ventilated buildings, with less energy usage, is a standard requirement for future projects, which is why energy-efficient buildings are becoming more popular. However, the concept of efficiency is a complex issue, which involves many strategies having to be applied to the functional and formal design, the construction technologies, occupant health and comfort throughout the building's life, and finally, the ecological impact of the building on the environment. These are key elements involved in the achievement of a holistic approach to the sustainability requirements of the built environment. When all of these criteria are taken into account, it becomes clear that all of the elements working within a building should follow this basic relationship, resulting in the recognition that the building envelope acts as one of the *key* elements in achieving this model.

2.2.2 Responsive Building Envelope

Prof. M. Wiggington defined the concept of the responsive envelope as an intelligent skin. He described the building envelope as an active component, which has a controlled reaction to the variations that occur between the exterior and the internal spaces, providing comfort by adjusting itself automatically. Thus the building envelope acts as an enclosure which protects against the weather. [7].

The concept of intelligent skin is related to a responsive envelope that consciously reacts to environmental changes. Like the human skin, this is able to modify some of its physical characteristics in order to keep away the external, physical, chemical and bacterial threats that may affect the body. It also adjusts its water content to maintain a constant internal temperature. Hence, the sustainable envelope can be associated to a passive and active component of the building that constantly controls the amount of air and heat exchanged. It has the ability to vary the heat fluxes according to the user's requirements. It takes advantage of the materiality of the facades and its exposure to the external and internal elements reacting passively or actively, to facilitate a constant controlled environment for lighting, ventilation and thermal comfort inside the building.

The envelope also has to contribute to the reduction of the maintenance requirement of the external layers of the building. As the envelope has an important role in energy reduction, it has cost and life cycle implications, which are considered in the design process. In some cases, the term "sustainable envelope" can be related to a system that helps to achieve zero-energy operation, or a considerable reduction in energy consumption. This is one of the aspects that make the envelope a key factor in energy efficiency in buildings. Recent research has suggested that there is no general solution regarding a sustainable envelope [8]. The choice of an appropriate envelope for a building, single or double, depends on the local climate, availability of materials, type of building, user requirements and cultural aspects associated with the development of local communities.

The building skin relates to, and also separates the external and internal environments. This is one of the main parts of the building, which is responsible for most of its energy consumption. Although other elements of the building, such as the roof and ground floor, are also part of the building envelope, the facade is regarded as the main feature of the building skin. The role of the building envelope can be associated with the term, "boundary". The Oxford Dictionary defines boundary as *"a real or notional line marking the limits of an area"*. It also defines the envelope as *"the outer part of a building enclosing the interior volumes and a waterproof protective cladding, e.g. glass and metal frames, protecting the structure, as in curtain-walling"*. Although the envelope acts as a boundary or limit, the understanding of its meaning varies depending on the discipline. By definition, it is where mediation rather than delineation takes place. For this reason, the physical phenomenon that occurs through it is the result of the interaction of different factors affecting its behaviour. Schittich made a clear distinction between the roles that the facade and roof play, as the main elements that directly affect the performance of the building for ventilation, shading, natural lighting, insulation and energy use [9]. The correct combination of materials, the fenestration balance and the basic overall design of the facade are still factors of constant concern among academics, designers, constructors, planners and environmental agencies. The achievement of highly efficient envelopes is something of a key issue in building related disciplines.

In order to obey the dynamic energy stimuli that affect the building envelope, it is important to embrace the idea of multiple energy environments interacting fluidly. Recently, there has been a convergence in the research of building skins, resulting in the development of new materials, sometimes referred to as 'smart materials'. The

advances in technology and physics are opening the opportunity to various disciplines to adopt its use. Thus, the implementation of this alternative on the built environment is a new field that is starting to deliver applications for facade, lighting, energy and structural systems [10]. In the specific case of the building envelope, the concept of intelligent skin and smart materials acting together was envisioned by Mike Davis as the ‘Polyvalent Wall’ in his paper ‘A Wall for all Seasons’ [16], in which the building skin combined electronics, photovoltaics, conductive glass, thermal radiators and more. This approach to a responsive envelope served as a model of the ultimate façade, which in 1984 was hotly debated as just a promise due to the economic cost of this technology. Research into the ‘super material’, for a complex façade, has produced some other examples, such as the application of aero gel for transparent insulation, thermo chromic glass for ‘smart windows’, Semi-conducting materials for solid state lighting and Photovoltaic cells for energy generation. The implications of this idea have affected the overall concept of the application of materials on building facades; especially glass, which is nowadays one of the most researched and applied building material.

2.3 GLASS IN ARCHITECTURE

2.3.1 Definition

Glass resembles the structure of a liquid but solidified at room temperature. According to *The Schott Glaslexicon*; glass is defined as “*a material which structure resembles a liquid whose viscosity at normal ambient temperatures is so high that it can be considered to be solid. More strictly, the term ‘glass’ is applied to all inorganic compounds having this basic property. This distinguishes glass from the plastics family, all of which have an organic base and for this reason should not be*

referred as glass even if they are transparent” [11]. The main component of glass is sand (Silicon Dioxide SiO_2). It is an inorganic product of fusion that has been cooled in controlled methods and develops into a transparent rigid state solid without crystallizing. The most common elements used for glass production are: Oxides of silicon (Si), boron (B), germanium (Ge), phosphorus (P) and arsenic (As). Normal float glass contains 71-75% of silica sand (SiO_2), 12-16% soda (Na_2O), 10-15% lime (CaO) and a small percentage of other materials such as FeO_3 , which are used to give colour effect.

2.3.2 Glazing in Buildings

Glass is a very common construction material. It is used in windows, doors, facades and curtain walling. According with the Encyclopaedia of Architectural technology, the term glazing is used to denote [12]:

- Glass or transparent plastic material that covers a building or fills an opening.
- Process of placing glass into a frame or onto a building.
- Process and/or materials used in bonding glass to a frame, as in structural silicone glazing or structural sealant glazing.

The Romans started using glass in their buildings for windows and mosaics. Yet, it was made very popular during the Gothic period, when glass appeared as a very prominent feature of buildings. The physical properties of glass had a very important significance on the use of light in Gothic Cathedrals (figure 2.1). The Benedictine abbot, Abbot Suger, of the Abbey of St. Denis, rebuilt his church and kept a detailed record of this work. According to his writings, in a pamphlet called ‘Consecration of

the Church of St-Denis’, and a ‘Report on the Administration’, he stated the thesis that “the dull mind rises to truth through what is material” [13]. He believed that the presence of beautiful objects would raise men's souls closer to God. Medieval man experienced the window as a means of understanding and learning biblical passages while submerged in celestial light. Windows and stained glass made the church that special, sacred dwelling place of an all powerful God.

The emphasis of light in Suger’s writings is fundamental to gothic aesthetic. He described the importance of light “For bright is that which is brightly coupled with the bright, and bright is the noble edifice which is pervaded by the new light”. The chevet of St-Denis was an important precedent for the emphasis of stained glass, especially glass in Gothic interiors. According to Watkin [14], glass has an obvious role in Suger’s Gothic world. It was an object for contemplation and a medium to provide contact with the spiritual light as a suitable background for religious reflection and aesthetic experience.

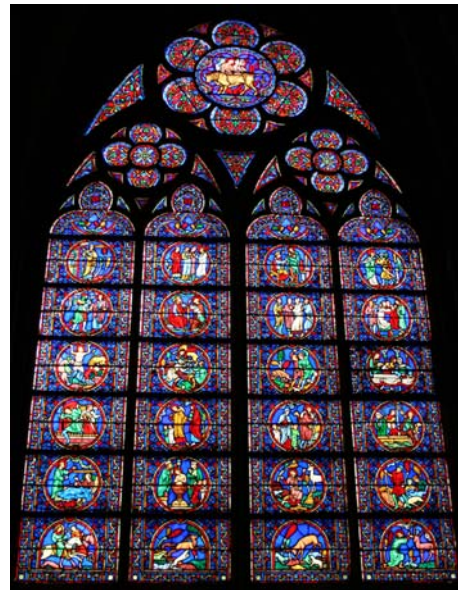


Figure 2.1 Glass stained windows at Notre Dame Cathedral in Paris.

It was not until the XIX century, that glass started to be applied in architecture as an important functional and aesthetic feature [15], when it was mainly employed for palm houses and greenhouses. According to M. Wiggington, [16], the development of the conservatory at the end of the sixteenth century to the middle of the nineteenth century, “is one of the important stories of Western architecture”. The author stated that conservatories brought together two strands of horticultural thinking by which the “creation of large glass buildings as homes for plants became a celebratory experience which was to transform architecture, particularly as their social significance became clear. There are various examples of conservatories built during this time, some of the most known being the Royal Botanical Gardens, designed and built by Richard Turner and Decimus Burton at Kew, London.

One of the great manifestations of British industrial pre-eminence was the Crystal Palace designed by Joseph Paxton for the Great Exhibition of London in 1851 (figure 2.2). The manufacturing techniques and the various systems in this building represent the sophistication that mid-century Victorian engineers and builders have attained and a culmination of a new typology of buildings.

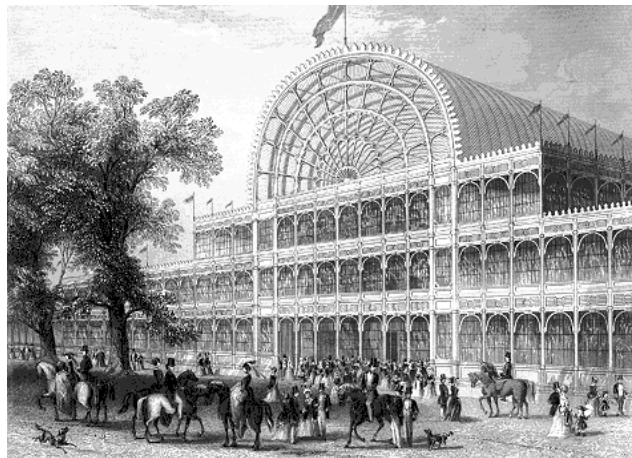


Figure 2.2 The Crystal Palace, London, By Joseph Paxton, 1851.
Source: History and Criticism of the Crystal Palace, 1852 [15].

The exhibition building was the product of mechanization, mass production, prefabrication, standardization, modular construction, systems-integration, critical path, rapid site assembly, dismantling and ingenuity [17a]. During this time, glass was functionally applied for its characteristics of light transmittance. All of these are a cornerstone of contemporary building constructions in which glass plays a very vital role.

The most important exhibition from the point of view of structural engineering and glasshouse design was the exhibition in Paris in 1889, which commemorated the centenary of the storming of the Bastille. It consisted of a complex of interconnected buildings and Eiffel's famous tower. In this complex, the Galerie des Machines was the culmination of engineering confidence in steel structure and glass enclosure. This huge structure was unfortunately dismantled in 1910 but Eiffel's three hundred metre tower still remains as a tribute to what must have been a magnificent exhibition [17b]. In the early 20th century, the German expressionist writer Paul Scheerbart (1863-1915) was described by the architect Bruno Taut (1880-1938) as the 'the only poet in architecture' due to his utopian phantasmagoria describing glass architecture. Scheerbart had an obsessive love for glass architecture and hate for brick buildings. In his writings *Glasarchitektur* [18] wrote:

"Colourful glass destroy hate

Without a glass palace life is a burden

Light permeates everything and is alive in crystal

Glass brings us the new era; brick culture is a burden

Bricks pass away; coloured glass endures".

These lines vividly allegorize the expressionism of glass architecture as light - crystal clear, colourful, mobile - and were meant to liberate the Europeans from their brick boxes. According to Hix [17c], Scheerbart visions were not impractical at all. He saw the problems of heat loss, heat gain and condensation with glass materials and suggested that several skins of glass combined with air-conditioning units could provide better indoor environments. Early modern architects were influenced by the application of glass as key material in architectural language. Glass was made popular between architects, thanks to the *Neues Bauen* movement on the 1920's. There was an influential impetus of modernism in architecture, where technological improvements on building structures were allowed to release the facade from its structural purpose and made it a vehicle for natural lighting and heat.

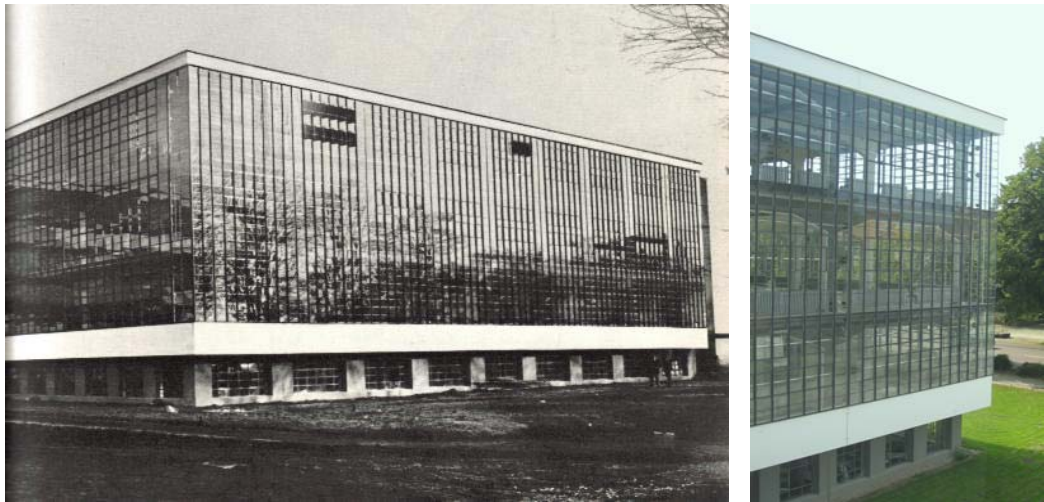


Figure 2.3 Bauhaus Dessau workshop used the first fully glazed curtain wall. (Gropius, 1926)
Source: http://en.wikipedia.org/wiki/Image:Bauhaus-Dessau_Atelier.jpg

The use of the facade as a curtain wall with more glazed surfaces, supported by steel frames, was first used by Walter Gropius. In 1926, he designed the fully glazed workshop wing of the Bauhaus in Dessau (figure 2.3). After this, the utilization of glass on the facade was widely included by modernist architects such as Le

Corbusier and Mies van der Rohe. At that time, the climatic control inside buildings was not fully developed and the glass clearly started to show some of its restrictions for glare control and thermal insulation. It was after the Second World War, with the availability of climatic control air conditioning and the development of float glass manufacture by Sir Alistair Pilkington [19], when the use of great surfaces of glass on building facades would continue and develop.

The use of glass in post-war architecture gave us examples of the developments of glass technology. However, these applications were single-glazed and environmentally insufficient. The greenhouse effect created by glass and applied before by gardeners during the nineteenth century was applied in the early twentieth century to take advantage of sun's energy to heat buildings. In 1931, Martin Wagner designed in Germany 'The Growing House', in which an external glass skin protected the house walls from external environmental changes and used incoming solar radiation to reduce heat losses.

Another example shown in figure 2.4 is Alvar Aalto's Sanatorium at Paimio, completed in 1933. This building has a good combination of passive solar design, where orientation, building form and solar penetration make an interesting example of the relationship between architecture and the sun. During this decade the Mur Neutralisant for the Cité de Refuge was developed by Le Corbusier in an attempt to overcome the environmental deficiencies such as the pan verre, which was exhibited in the Pavillon Suisse of 1931.



Figure 2.4 Paimio Tuberculosis Sanatorium at Paimio, Finland.
(Aalto, 1929-1933)
Source: <http://www.designboom.com/history/aalto/paimio.html>

According to M. Wiggington [20], the idea of using glass as part of a solar energy collection system was really started to be applied after the war. By 1948, Telkes and Raymond Peabody built the first real ‘Solar House’ in Dover, Massachusetts. The first European solar houses were built in 1956 in England by Gardner and Curtis. This sort of example of passive solar design was also applied in 1961 by A E Morgan in one of the most relevant buildings of this kind, The Saint George’s School in Wallasey. The building shown on figure 2.5 is an early example of a double glazed curtain wall with skins separated 600mm.



Figure 2.5 St. George’s School, Wallasey near Liverpool.
(A E Morgan, 1961)

The south facing double skin facade used in this building has an external fully clear glass curtain wall with an inner skin with some translucent glazed panels, which were designed to provide thermal comfort by absorbing and reflecting solar radiation. The significance of this building is due to its location at latitude 55, 5°N and the design. This idea of combination of glazed solar wall and heat accumulation was the basis of the Trombe Wall which was applied in the first solar French house in 1962. These two examples, however, are not quite successful in terms of architectural functionality. Transparency is denied through the facade at Wallasey's College and the black painted wall of Trombe's system is also deprived. Nevertheless, these two examples gave the foundation of correcting the environmental unsteadiness of buildings which became an issue when the new energy consciousness at the end of the 60's.

2.3.3 Glass and the Environment

As a result of the growing environmental awareness due to the energy crisis of the 1970's, the development on glass technology, such as double-glazing, made architects and manufacturers reconsider the use of glass in a more energy efficient manner. Manufacturers and suppliers are nowadays considering the real environmental effects of new and refurbished buildings on local communities and its occupants. The full implication of the life cycle of glass on energy efficiency and CO₂ emissions has become a matter of deep research. In the UK, the Building Research Establishment estimates that these emissions can be reduced by about 17% by taking energy efficient measures on buildings [21]. Glass has become widely used in office building design; its transparency being associated with concepts of clear corporative and modern images. Nonetheless, it is creating a huge fashion

trend in building design, in which the environmental impact and the CO₂ emissions associated with the use of fully glazed facades are not as widely assessed compared to its popularity of use.

The implication of glass for achieving energy efficiency has become an issue of imperative importance [22]. The full understanding of glass facades in terms of natural lighting and provision of adequate insulation to prevent overheating are key issues of energy efficiency in any building. However, improvements on thermal insulation of glazing with thin coatings and additional layers of glass are not the only main concern. The holistic approach to the design of the facade, balance of fenestration, thermal comfort and adequate ventilation are modern variables, determining the development of new technologies on the design of facades.

2.4 CONCEPT OF DOUBLE SKIN FACADE

Historically, the building envelope has been modified and adjusted with the purpose of offering better indoor environmental conditions. The use of different materials and colours in facades, make the envelope a part that absorbs, reflects and transmits, in different manners, the solar radiation captured by the building. The envelope also determines the thermal mass of the building, which directly affects its thermal response. Although opaque envelopes, exposed to daily thermal variation and solar radiation, allow some heat to flow inside the building, most of the heat received by the internal spaces is transmitted through the glazed areas of the envelope.

The understanding of the building envelope as an interactive layer of the building, which has to respond to climate, is mentioned in the early 1980's by M. Davies, as a

Polyvalent Wall [23], where the envelope has to be a dynamic element responding to the technical, environmental and aesthetic requirements of modern buildings. The development of Double Skin Facades (DSF) was integrated into the built environment with arguments such as sustainability, ecology, free ventilation and energy efficiency. For this reason, double skin buildings are gaining more interest amongst architects.

Other authors refer to the concept of the DSF, as the “Active Wall” or “Climate Wall”, in which there is an external screen, a ventilated cavity and an internal screen. It is here where solar protections are placed inside the ventilated channel. According to Kragh, there are three types of DSF: The Naturally ventilated Wall, the Active Wall and the Interactive wall. The differences between them are more based on the use of mechanical and controlled ventilation or air conditioning, which works as stand-alone or interacting with the façade [24]. The use of multilayered skins enhances building insulation against thermal variations and external noise.

Uuttu describes the DSF concept as “*a pair of glass skins separated by an air corridor ranging in width from 20cm to several meters*”. The author also identifies that the cavity is connected with the exterior, allowing the internal windows to be opened thus creating natural ventilation and night time cooling in summer, crucial for tall buildings where external wind pressures are high. For winter the author identifies the cavity of the DSF as a thermal buffer, which improves the thermal insulation, reduces heat losses and allows passive solar heating through the envelope [25].

Other authors added to the concept, the use of shading devices and external noise influence. Compagno defines the concept of Double Skin Facade as “*an arrangement with a glass skin in front of the actual building facade. Solar control devices are placed in the cavity between these two skins, which protects them from the influences of the weather and air pollution, a factor of particular importance in high rise buildings or ones situated in the vicinity of busy roads*” [19].

With the same concept as the ‘Polyvalent Wall’, other authors, like Faggenbauu, defines a DSF as a Multi-Functional Ventilated Facade or “*Ventilated glazed facades are made up of two layers of different materials, opaque or transparent, that are separated by an air channel used to collect or evacuate the solar radiation that is absorbed by the façade*” . The author includes, on this concept, the flexibility of integration with different types of designs using Photo-voltaic, transparent insulation (TIM) and also Phase Change Materials (PCM) inside the facade channel to enhance the thermal overall mass of the facade [26].

Poirazis [27] summarizes the concept of Double Skin Facade fundamentally on the three elements defined by Saelens [51]:

- The envelope construction, which requires two layers on the facade.
- Transparency, which has to be achieved by the use of glass.
- The intermediate ventilated cavity that can be opened or closed allowing air flow within the facade.

2.5 DEFINITION OF DOUBLE SKIN FACADE

Osterle, et al, gave the most comprehensive definition of DSF. For the authors, a double skin façade consists of “a multi layered façade envelope, which has an external and internal layer that contains a buffer space used for controlled ventilation and solar protection” [28]. Identified, was the use of multilayered skins to allow building insulation against thermal variations and external noise.

The External skin provides protection against weather and improves acoustic insulation of single glazed facades. This layer contains openings that allow air to exchange with the intermediate space and the internal rooms, if the internal skin has openings (figure 2.6). This provides the possibility to adapt the building according to the climatic variations. At that time, building facades were basically built by a single layer, which made the envelope susceptible to extreme comfort variations inside the building. The multi-layered facades provide improved insulation. However, research in this field has suggested that buildings located in predominantly hot climates, results in the large glazed areas to cause critical daily solar gains and important nocturnal heat losses.

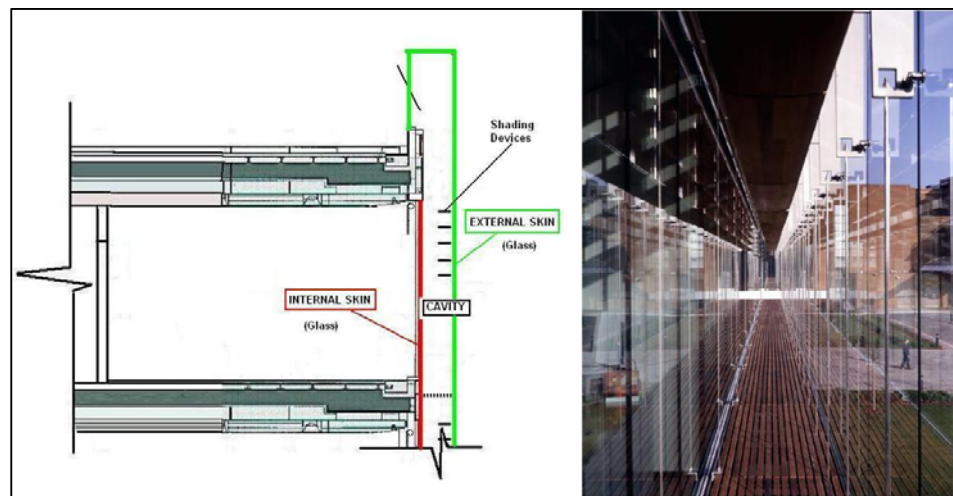


Figure 2.6 Basic elements comprising a Double Skin Façade [27].

There are various definitions of DSF. Most authors coincide on the multi-layered and ventilated concept of the facade. However, some also specified the qualities and characteristics:

Harry Poirazis [27] defined, *“The Double Skin Façade is a system consisting of two glass skins placed in such a way that air flows in the intermediate cavity. The ventilation of the cavity can be natural, fan supported or mechanical. Apart from the type of the ventilation inside the cavity, the origin and destination of the air can differ depending mostly on climatic conditions, the use, the location, the occupational hours of the building and the HVAC strategy. The glass skins can be single or double glazing units with a distance from 20cm up to 2 meters. Often, for protection and heat extraction reasons during the cooling period, solar shading devices are placed inside the cavity.”*

Harrison and Meyer-Boake [29] defined it as *“Essentially a pair of glass ‘skins’ separated by an air corridor. The main layer of glass is usually insulating. The air space between the layers of glass acts as insulation against temperature extremes, winds, and sound. Sun-shading devices are often located between the two skins. All elements can be arranged differently into numbers of permutations and combinations of both solid and diaphanous membranes”*.

The Belgian Building Research Institute (BBRI) gives a concise definition of DSF [30] as *“a traditional single facade doubled inside or outside by a second, essentially glazed facade. Each of these two facades is commonly called a skin. A ventilated cavity – having a width, which can range from several centimetres to several metres*

– is located between these two skins. Automated equipment, such as shading devices, motorized openings or fans, are most often integrated into the facade”. In this definition, they also differentiated this type of double ventilated facade with the air-tight multiple glazed facade on the basis that the purpose of a DSF is to allow controlled ventilation of the cavity.

Most of the descriptions agreed identifying DSFs by their multi-layered construction and the existence of a ventilated cavity between the two transparent ‘skins’. Their physical configuration is mostly defined by functional and environmental issues. In this sequence of ideas and based on the definition given by Osterle et al., a Double Skin Facade can be described as a multi-layered transparent envelope which contains a ventilated cavity used to increase thermal and sound insulation, pre-heat air for ventilation and provide solar protection for highly glazed buildings.

2.6 HISTORY OF DOUBLE SKIN FACADES

Buildings have evolved from structures based and surrounded by massive walls with small openings, to the transparent enlarged glazed skins used today. As a consequence of this enlargement of glazed surface on the facade; the building has become more sensitive to climatic variations and also dramatically dependant on environmental control systems. The awareness about energy efficiency involving the building envelope started to be an important issue when modern architecture included glass as a tool of the exploration of new spatial dynamics in building design.

After the energy crisis in the 1970’s, the general awareness was greater than before

as ecology and resource depletion were issues that became more important concerns among government and industry. The increased use of glass as an architectural feature for natural lighting is related to problems of thermal losses due to the low insulation given by glazed areas. Some variations of glazing were developed in order to increase the level of insulation. However, the increased insulation levels and the optical properties of glass allowing IR radiation to pass but not to be released, brought another problem - overheating.

In cold climates, it is well known that the use of double framed windows acts as an alternative in protecting internal spaces from extreme cold weather outside. Usually, the external layer is a wood framed panel and the inner layer is a single glazed window. Both work together as an insulating skin with an air cavity between them. The oldest known building with a curtain wall façade is the Steiff Factory (1903) [31] designed by Richard Steiff in Giengen Germany (Figure 2.7). Richard Steiff initially designed the building as a toy factory. The main characteristics of the building was to provide enhanced natural lighting and improved insulation against the extreme cold weather and high exposure of the building to the strong winds of the region. The building comprises of a three-storey structure with a ground floor for storage and the upper floors designated to workspaces. The building basically uses steel frames for the double skin and there are some additions of timber frames. The building is still in use.



Figure 2.7 Steiff Factory, 1903.
Source: <http://www1.flickr.com/photos/troutwerks/420220019>

Another example of the early use of Double skin frames in envelopes can be seen in the Post Office Savings Bank in Vienna; developed by Otto Wagner. This building uses a steel structure to hold a glass and aluminium skylight. Here, the concept of a double skin was used on the skylight over the main banking hall [32]. The building is currently in use; some renovations were made to accommodate air conditioning and lighting.

During the 1920's, there were some developments of buildings using the concept of Double Skin Facade. Moisei Ginzburg used the double skin concept on the facade of the communal housing project of Narkomfin building, designed in 1928 and finished in 1932 [33]. This was one of his most famous works. However, at the present time, it is in a decaying state (figure 2.8). It has been without maintenance for decades and

the building is on the UNESCO's endangered buildings list.



Figure 2.8 Narkomfin building in Moscow in 2007, (M. Ginzburg, 1928).
Source: Wikipedia.org.
Copyright licence: Creative Commons, Attribution-Share Alike 2.5.
<http://creativecommons.org/licenses/by-sa/2.5>

The concept of the double skin was also mentioned and applied by Le Corbusier. He created the idea of ‘Mur Neutralizant’. He applied this idea for the Ministries of Light Industries in Moscow. However, it was rejected by the client and not installed on the project. This concept comprised of a system of a double pane of glass with a ventilated cavity. In the design of Cite de Refuge (1928), shown on figure 2.9, and the Immeuble Clarte (1930), he mentioned the system within his designs. He described the facade as a free facade consequence of the non load-bearing function of the walls, since the structural frame releases the facade from this function. As a consequence of this, Le Corbusier was able to replace traditional windows (punched in the wall) with the ribbon window and the glass wall [34]. Nevertheless, the system was not applied yet as it was considered at that time to be very expensive to build and very inefficient [35].

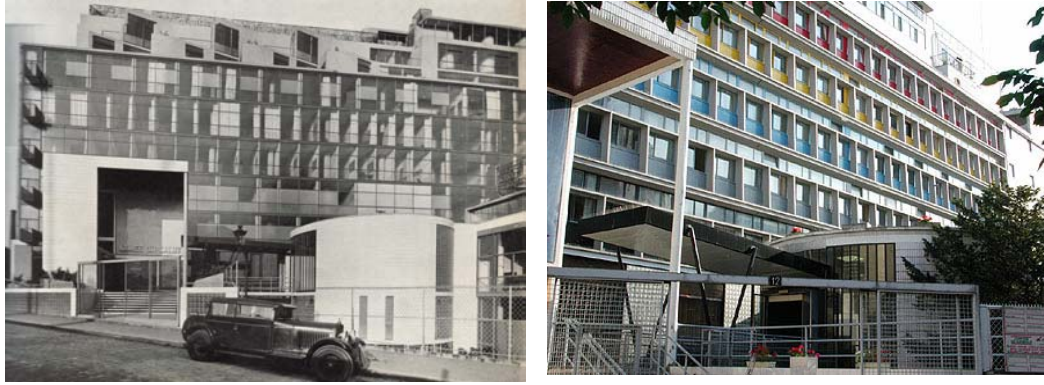


Figure 2.9 Salvation Army Hostel 'Cite de Refuge' in Paris, 1929-1933, before and after the building was altered (Besset, M., 1968).
Source: Le Corbusier Foundation, Paris.

In the year of 1936, Le Corbusier established collaboration with Brazilian architects for the design of the Ministry of National Education in Rio de Janeiro and commissioned the construction to Oscar Niemeyer (figure 2.10). This building included the use of solar protections called by him, 'brise-soleil or sun breakers', in which he developed the control of solar radiation through the facade being dependent on the solar position [36]. Figure 2.11 illustrates a sketch of the 'brise-soleil' elements relative to solar seasonal solar positions.

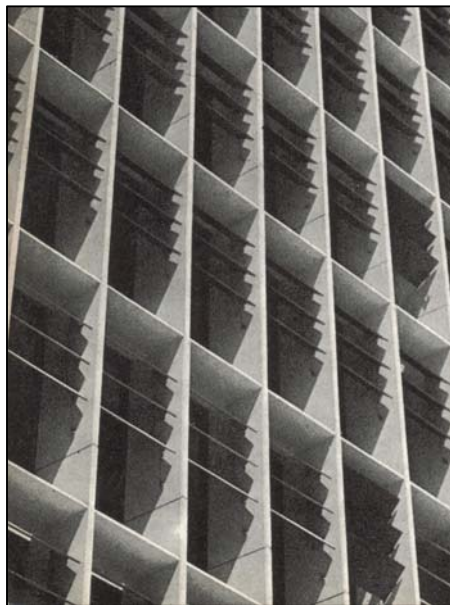


Figure 2.10 Sun breakers on the Ministry of Education facade in Rio de Janeiro, 1936. (Besset, M., 1968)

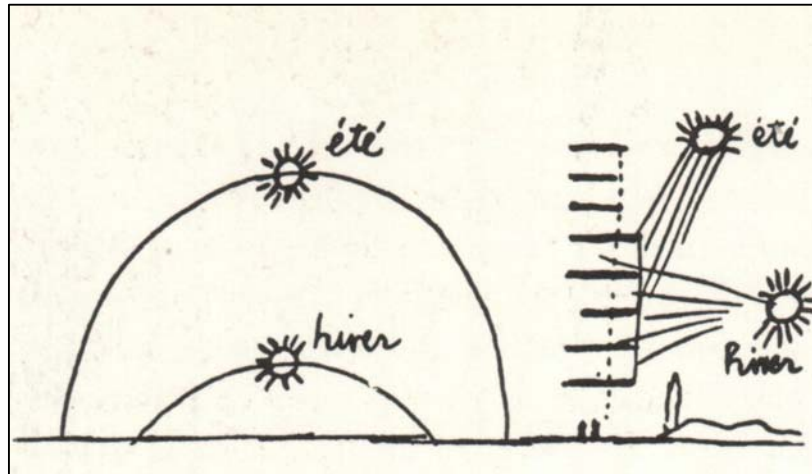


Figure 2.11 Le Corbusier's sketch of the 'sun breakers' showing the need for solar control louvers adjustable according with the sun's position. (Besset, M., 1968)

During the design process of the UN building in New York, Le Corbusier sent a letter to Senator Warren Austin in 1947 [37]. As one of the requirements for the facade of the building was to be a glass curtain wall; he referred again to his 'neutralizing wall' invention as the *"large glass panes set in aluminium frames; the panes would be double, spaced one foot apart; in this space there would be circulated hot air in winter and cold air in summer and would allow solar heat to penetrate in winter"*. He also mentions that the building façade, due to the extreme conditions of New York's summer, would critically require the 'brise-soleil' to avoid dangerous overheating. In his letter, he explained in detail the implications of light, fenestration and the orientation of the facade for which the necessity of a 'Mur Neutralizant' with ventilated cavity was vital for the east facade. Figure 2.12 illustrates the drawings included with the letter, explaining the ideas of the neutralizing wall and the solar implications on the facade and occupants of the building.

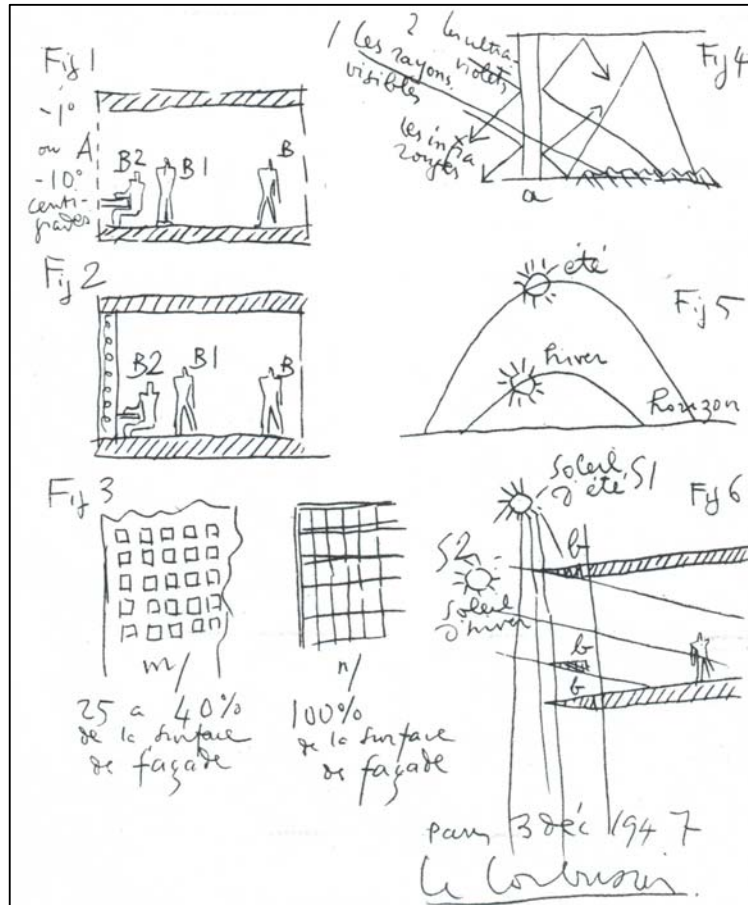


Figure 2.12 Le Corbusier's sketches, illustrating his ideas on the letter sent to Senator Warren Austin about the UN building in 1947. (Architectural Review, 1950)

As modernism became more widely accepted, the concept of the curtain wall, with the use of single glass skin as a main feature of the façade, became a characteristic of that time; regarding the feature of design trends. The resonated ideas of the almost forgotten 19th century Chicago School style, with origins in the socialist International Style became an accepted mode of building for large American corporations. The German architect, Mies Van der Rohe who emigrated to the U.S, can be highlighted as one of the precursors in America, using curtain walls in high rise buildings. In 1950, the IBM headquarters building in Chicago (figure 2.13) was one of the many buildings that apply the concept of curtain fully glazed facade.



Figure 2.13 IBM Plaza, Chicago, Illinois (Van der Rohe, L. M., 1950).
http://en.wikipedia.org/wiki/Image:2004-09-02_1580x2800_chicago_IBM_building.jpg
Photo: J. Crocker.

After preliminary attempts of Le Corbusier to apply the concept of double skin, there is no relevant progress made on this until late 1970's. The first building in North America, which incorporated Le Corbusier's Double Skin concepts, was the Occidental Chemical Centre, also known as The Hooker Office Building in Niagara Falls (N.Y). This building was designed by Cannon Design and HOK designs in 1978 and completed in 1980 it has become one of the oldest examples of contemporary Double Skin Facade (figure 2.14) [29].



Figure 2.14 The Hooker Building southeast Double Skin Facade, 1980.
(Harrison, 2003)
http://www.architecture.uwaterloo.ca/faculty_projects/terri/ds/hooker.pdf

Other building which incorporated DSF elements on the facade was the Lloyds Building designed by Richard Rogers in the late 1970's. In this building, some parts of the facade include a buffer cavity with a double skin for insulation and controlled ventilation [55]. In Britain the concept of DSF became more popular in the 1980's. Arup Associates, in the Briarcliff House Office building in Farnborough, first incorporated it. The building incorporates a double skin, which is used for sound insulation, solar protection and ventilation. There is a combination of mechanical and natural ventilation in the building, where a plant handles the air collected in the cavity and recovers heat collected within the façade for heating purposes [19].

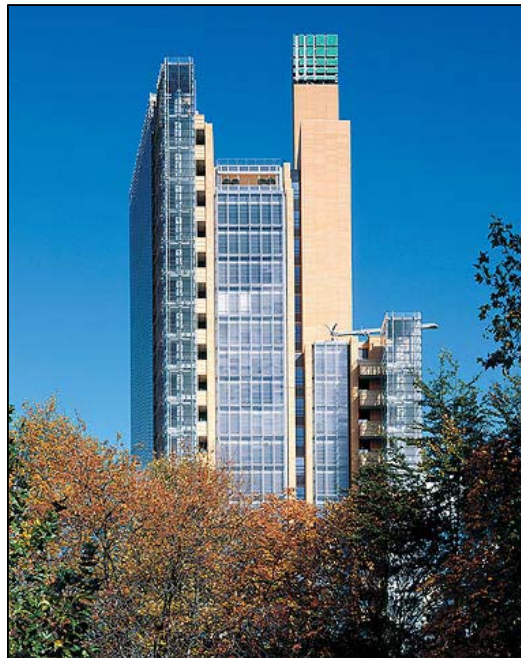


Figure 2.15 The Debis Tower designed by Renzo Piano, 1996-1998.

The growing awareness of environmentally friendly buildings motivated by corporate and political reflection influenced the proliferation of DSF concepts on high-rise office buildings. Buildings like GSW Headquarters by Sauerbruch & Hutton, the Debis building by Renzo Piano, shown in figure 2.15, and the Commerzbank Headquarters by Foster and Partners are some of the publicised

examples using Active and Interactive façades in Buildings [24]. As a result of growing fascination from both architects and clients, for the use of transparency as a feature for office buildings, there have been increased numbers of new projects in the last few years, especially in Europe, where the use of Double Skin Facades is a feature of these typologies. One later example of this trend is the Swiss Re building, known as ‘The Gherkin’, designed by Norman Foster. This building has been publicised by most architectural journals as a cornerstone example of sustainable architecture.

2.7 TECHNICAL DESCRIPTION OF DSF

2.7.1 Types of Facade construction

There are various approaches to the classification types of DSF. These depend on the Cavity Geometry, Airflow Function and Cavity configuration in relation to the operation. According to Eberhard Oesterle [2], the classification is based on the form of the cavity and then the functionality of the facade in terms of ventilation. There are four construction types of DSF:

Box Windows consist of a frame with inward opening casements. The cavity is horizontally and vertically partitioned, dividing the façade into smaller and independent boxes (figure 2.16). It is especially applicable in cases with high external noise and special requirements relating to the sound insulation between adjoining rooms. This type is suited for solid facades with punched openings and mostly used for buildings where privacy is important.

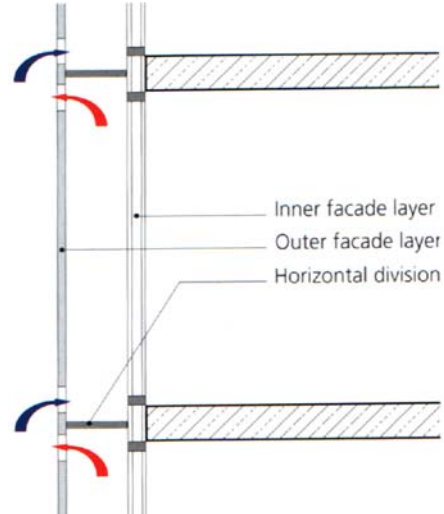


Figure 2.16 Box Windows.
(Osterle et al., 1999)

Shaft-Box Windows: Consist of a series of box windows with continuous vertical shafts (Figure 2.17). The shaft-box façade is a special form of box-window construction, based in the “twin-face” concept, which consists of a system of box windows with continuous vertical shafts extended over a number of stories to produce a stack effect.

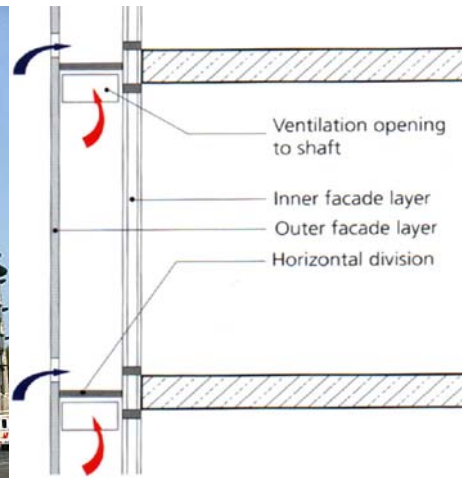


Figure 2.17 Shaft box windows.
(Osterle et al., 1999)

The façade layout consists of an alternation of box windows and vertical shaft segments, which are linked by means of bypass openings. These types of facades are

suited for buildings located in high noise areas where a high level of sound insulation is required inside the building. Due to limitations in the height of the stacks, this system is recommended for lower-rise buildings.

Corridor Facades: In this type, there is a horizontal intermediate space between the two skins (Figure 2.18). It is closed at the level of each floor. Divisions are positioned along the horizontal length of the corridor only where it is necessary for fire protection, acoustic, or ventilation reasons. The cavity inlet and outlet openings are located near ground level and the building ceiling respectively. These openings are usually placed in a staggered form on every level to prevent a mix of polluted air being removed from lower floors with the fresh air of the inlet of the next floor.

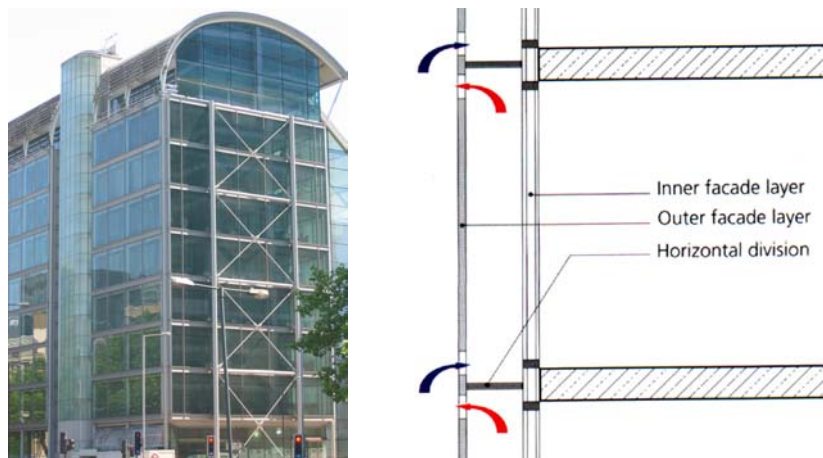


Figure 2.18 Corridor Facade.
(Osterle et al., 1999)

Multi-storey Facades: In this case, the intermediate space between the two layers is connected vertically and horizontally by a number of rooms (Figure 2.19). In some circumstances, it can be extended around the building without intermediate partitions. The ventilation of the cavity occurs via large openings near the ground floor and the roof. For winter conditions, the façade space can be closed at the top

and bottom to exploit the greenhouse effect created within the cavity and optimise solar-energy gains.

For summer conditions, the cavity is kept open in a manner to cool down the façade by means of the buoyancy created. This type of DSF is most commonly used where it is not possible to exchange air without mechanical ventilation and glazed areas without openings are required. It is essential for this system that the rooms next to the façade be mechanically ventilated, and then the façade can be used as a joint air duct.

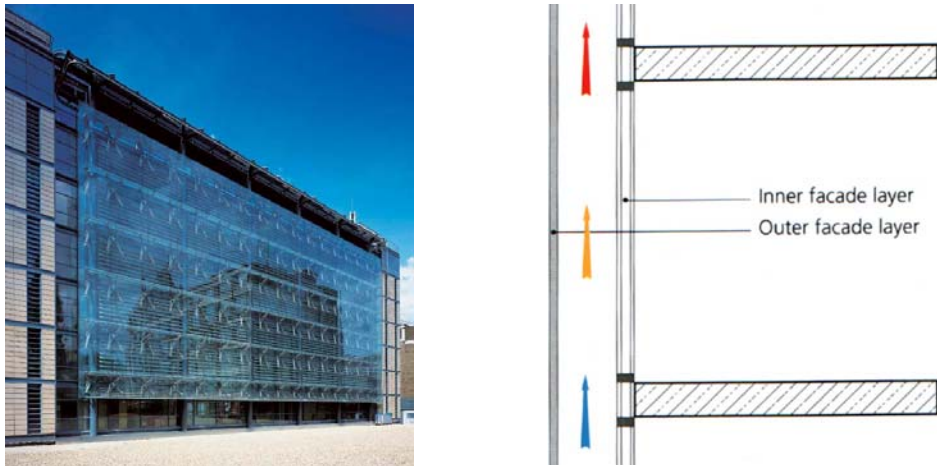


Figure 2.19 Multi-storey facade.
(Osterle et al., 1999)

The Belgian Building Research Institute (BBRI) [30] adds another category to the previous four suggested by Osterle et al. They include the Category Louver Facades, in which the exterior skin can be operable in order to function as louvers when open and an almost airtight external skin when closed.

Another author who classifies the DSF by the geometry of the cavity is Uuttu (2001). She also defines four types of facade [25]:

- Box double-skin facade: The concept here is basically a box double-façade. The horizontal dimension of the cavity is limited by the size of the modular box and the vertical dimension is usually smaller than the height of each storey. In this case, the airflows from the horizontal shafts placed on the bottom to the top of each of the cavity boxes. This type is classified the same as Box windows above.
- Shaft facades: This concept is similar to the previous one. However the location of inlet/outlet shafts is on the vertical sides of the cavity connected to a vertical air duct, extracting heated air from each box. Osterle defines this type as the Shaft-box façade.
- Storey-high double-skin facade: The cavity height is divided on each storey. However, the horizontal dimension of the facade can vary from a small section to the whole facade length. The air flows separately on each storey. It is similar to the corridor facade defined by Osterle.
- Building-high double-skin facade: The cavity continues through the whole building height without any separation and can also cover the whole horizontal length of the facade. The concept depends on the stack effect by the hot air accumulated on top of the facade. This is the same type as the multi-storey facade mentioned before.

Harrison and Meyer-Boake defined four basic typologies of the Double Skin Facade based on ventilation function [38]:

- Buffer Facade: The cavity acts as a buffer zone providing insulation, the airflows only within the buffer zone.
- Extract Air Facade: The cavity acts as a chimney, which combined with HVAC,

extracts air from the building.

- Twin-Face Facade: The DSF acts in two ways, providing pre-heated air in winter and extracting air by natural means in summer.
- Hybrid Facade: The combination of the systems above, in which the external skin can be also opened and the inlet/outlet position varied.

Kragh (2000) also classified the DSF types by the ventilation function of the cavity [24]:

- Natural Ventilated Wall: The facade acts as an insulator in winter and a chimney in summer and the airflows only within the cavity. The author recommended this for temperate climates.
- Active Wall: The facade works with the HVAC, helping to preheat air and recover heat in winter and remove air in summer. The air flow depends of the stack effect on the facade. He recommended this facade for cold climates.
- Interactive Wall: The facade acts similarly to the naturally ventilated facade. However the airflow within the cavity is forced and does not depend solely on the stack effect. The author recommends this system for hot climates.

Other authors like Aarons [39], (2000) and Magali [40], (2001) classified the facade by the height of the cavity in relation to the height of each storey or the building.

They classified the following type of facades:

- Airflow facades / Double Skinned Facades on several floors.
- Airflow windows / Double Skinned Facade per floor.

The two authors divided each category into subcategories depending on airflow patterns, cavity height, layering composition; depth and horizontal extend of the cavity, operability and materials. The difference between each author's classifications is mainly the air-tightness of the cavity, in which Magali relates the possibility of openings on the inner skin (windows) of the facade.

Finally, depending on the facade configuration and operation, the Environmental Engineering practice Battle McCarthy in the UK [27], categorized the type of DSF into five main categories:

- Sealed Inner Skin.
- Open able Inner and Outer Skin with single story cavity height.
- Open able Inner Skin with mechanically ventilated cavity.
- Sealed Cavity either on each floor on the total height of the facade.
- Acoustic barrier with massive or lightweight exterior skin.

2.7.2 Building Integration of DSF

The integration of a Double Skin Facade system in regards to the building; is defined by some authors by the support that this system is able to provide to the Heating Ventilation and Air Conditioning Systems of the Building. Basically, a DSF can be used to pre-heat air during winter, recover heat during winter and mid season and extract hot air during summer conditions. According to Osterle et al [28], it is expressed but not widely confirmed that the construction of a DSF can help to reduce the size of the HVAC plant. However, this depends of each individual case in which a DSF is applied. There are some cases where the lack of mechanical ventilation

combined with the facade can lead to discomfort inside the building and such assessment of the performance by the users varies considerably. The authors stated that the integration of DSF in buildings “*make sense technically especially when they facilitate natural ventilation for as much of the year as possible, despite adverse external conditions such high noise levels or strong winds*”. They determine that the following conditions have to be met when DSF is working without support of mechanical ventilation:

- Provides adequate sound insulation.
- Met statutory guidelines of opening areas and the limitations of depth according to the requirements of natural ventilation of workspaces.
- The maximum cooling load of the building should not exceed 35-40W/m².
- DSF construction should provide a perceptible contact with the outdoor environment.
- The facade must allow night time cooling when required.
- Lower thermal comfort can be accepted when operating without air conditioning.

Other authors relate the optimal thermal and energy performance of DSF according to how the facade should be combined with the HVAC system. Wojtek and van Paassen studied by means of a simulation model and validated with test facilities, the integration of DSF within buildings [41]. They stated that in order to achieve an adequate application of DSFs, “*it is strongly necessary detailed design of the facade and its integration with the indoor climate systems of the building*”. The authors suggested that the following tasks be included within the design procedure of the building when integrating a DSF:

- Define the functions of the DSF in the building according to the requirements of airflow, thermal performance, noise reduction and control of the facade.
- Selection of the type of facade, materials, dimensions and components according to the requirements.
- Optimization of the HVAC system to couple it with the DSF.
- Selection of control strategies to supervise the system.

Di Maio and van Paassen (2000) highlighted the importance of the cavity depth as a relevant factor to determine air temperatures inside the cavity [42]. They concluded that thin cavities lead to high temperatures with limited air flow and those wide cavities temperatures depend more from the heat transfer of elements inside the façade, which prompt the stack effect.

The choice of a particular DSF system is determined by the architectural, functional and economic factors. This choice has far reaching implications for the project planning. However, the decision depends on a very relevant priority of the climatic conditions and the predicted behaviour of the façade under critical conditions.

2.8 DSF ECONOMICS

2.8.1 Cost and Investments

It is widely agreed in most literature that DSFs have higher investment costs when compared with single glazed facades. The solely extra layer of glass and structure produces an extra investment cost. Streicher (2005) [43] has estimated the total cost of a DSF, including shading devices, from 500 to 700 EUR/m². Stribling and Stigge from Buro Happold estimated the construction costs of facades in the U.S. from

£300/m² for a conventional curtain wall facade and £800/m² for a simple flat double Facade [44].

According to Osterle et al [28], there is controversy amongst project designers' teams regarding the viability of investing the extra cost of this system because of the energy savings versus initial costs. Contradictions are often found on the position of some authors, regarding the energy saving qualities of DSF, whilst other authors refer to the increment of energy consumption and extra cost is as a result of the *use* of this technology. Moreover, the construction and maintenance cost is not often mentioned in existing literature. Poirazis [27] highlighted the importance of an appropriate design as a means to reduce energy consumption of heating, cooling and ventilation and therefore the operational costs. He stressed that a careful design has to include parameters related to the use of the building and its location. Other authors like Straube (2003) [44], concluded that DSFs are merely a solution that tries to resolve the problem of fully single glazed, increasing the cost if compared with other more simple technologies, which are often able to resolve the problem more efficiently.

Some authors give an estimate of the investment costs for different glazed facade alternatives. Figure 2.20 shows a comparative graph of the investment costs in Northern Europe by WSP-Shücco (2003) [43] and the cost of the facade in Central Europe estimated by Jager (2003) [45]. This clearly proves that the cost increase from a single skin to a double skin is nearly 90% of the investment cost per square metre. Jager (2003) also compared the running costs of standard facades compared with Double Skin Facades. The figure 2.21 shows how the running costs are also

doubled by the DSF, which is somewhat evident as the amount of surface to maintain and clean is greater.

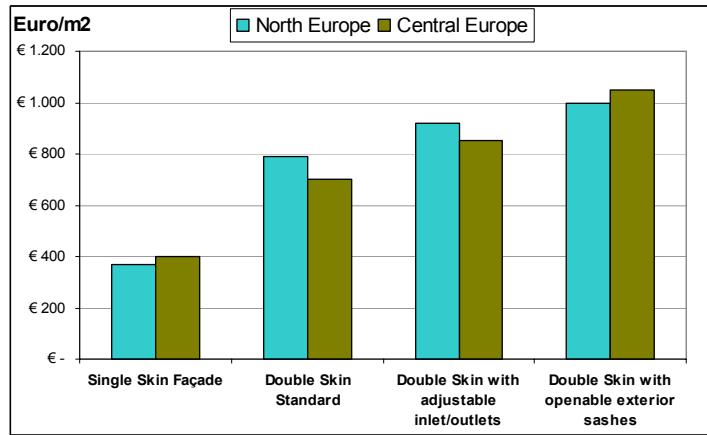


Figure 2.20 Estimated initial investment costs of Single and Double Skin Facades.

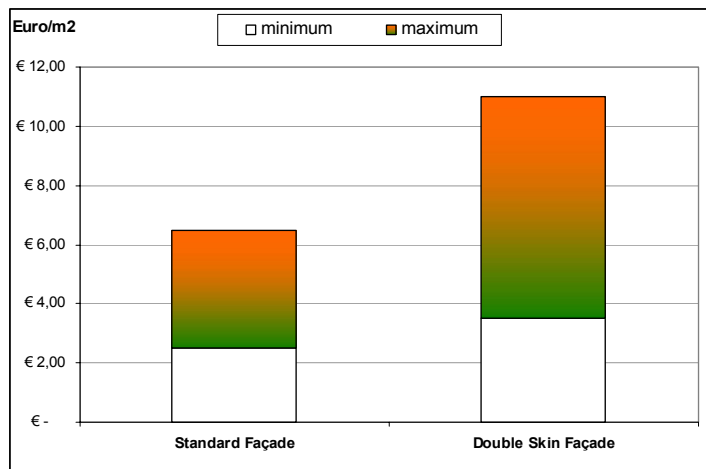


Figure 2.21 Estimated maintenance costs of Standard facade compared with Double Skin Façade.

In the U.K., Wiggington and McCarthy (2000) [46] estimated the capital costs of a conventional narrow and deep plan building with double-glazing and DSF with single and double-glazing. They found, in general, the DSF to be 20% more expensive than a comparable conventional facade. After considering the reductions in plant costs (due to improved environmental performance), the narrow plan double skin building was found to be 7.5% more expensive (figure 2.22), whilst the deep

plan building was found to be 4% more expensive. Nevertheless, the study showed that the specific cost of the facade is almost double from single to double. The total cost of the building is not affected so dramatically.

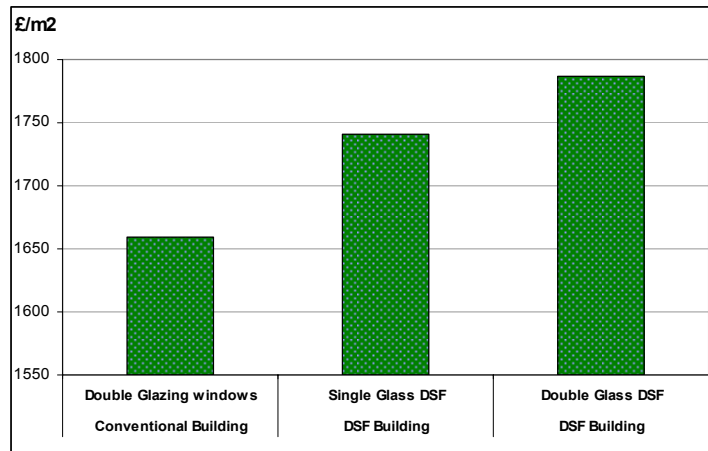


Figure 2.22 Estimated total cost in the UK for a ten storey building with a footprint of 60m by 15 (narrow plan).
Source: Environmental Second Skin Frames, Wiggington, M [46].

2.8.2 Cost calculation and Energy Assessment

Osterle et al [28] stated that there are no comprehensive, conclusive cost calculations or generally applicable methods of assessing cost effectiveness of Double Skin Facades. The authors affirm that the economic analysis of facade alternatives should take into account all investment, operating and maintenance costs. In this case, the energy assessment variable was not included. As this is a key variable supporting the efficiency and sustainability of the system, it must be included in any further analysis.

Although a detailed analysis of the benefits or detriments of Double Skin Facades are not yet fully explored; Stribling and Stigge from Buro Happold have studied the energy savings and payback issues through dynamic thermal models [47]. They modelled representative office buildings in seven cities around the world to compare

the energy consumption of conventional and double facades. They concluded the following issues:

- Double skin facades are able to achieve better energy savings when oriented SW, South and SE.
- Double façades are able to achieve energy savings from 10 to 50%. This depends on their individual climate orientation, detailing, and the construction cost and energy prices.
- They found averaged projected payback periods of around 118 years, making double facades seen to be a financially poor decision with today's energy prices.
- The economic viability of double skin facades is mostly based on the cost of construction, energy savings and especially the future prices of energy.

Osterle et al [28] and Aarons [39] coincide on the importance of the total life cycle in regards to the payback of double skin facades. They identified some issues like maintenance costs and reduced sizes of HVAC plants, as issues that directly affect energy cost reduction. However, there are also other issues not easily quantifiable, which influence productivity and can be associated in cost reduction. Such issues include glare control, increased daylight, operable windows, noise reduction, reduction of CO₂ emissions and aesthetic value and therefore are important to the added value that the building may achieve indirectly by reducing environmental impact and energy usage.

Wigginton and McCarthy [46] also found an overall reduction of energy consumption in buildings with Double Skin Facades when compared with conventional buildings. They found on average a reduction between 22 to 65%

depending on the type of DSF. In general, the additional benefits of double facades have not been fully explored and further research on this specific field is recommended.

2.9 ADVANTAGES / DISADVANTAGES OF DSFs

Poirazis (2004) [27] compiled some author's views about the assets and drawbacks of Double Skin Facades in office buildings. The main issue raised from previous literature is that the performance and efficiency of the system depends mainly on the accurate and detailed assessment carried out during the design stages.

2.9.1 Advantages

The main agreement of all authors was in regard to thermal and sound insulation. There is some discrepancy about the cost of the system and the incidence on thermal comfort. Yet, there is good agreement regarding natural ventilation, especially for night-time cooling, which was highlighted as a good quality of the facade. The percentages of these issues identified in the literature are illustrated in the figure 2.23 and is summarized as follows:

- Reduced construction costs when compared with smart technologies on facades [27].
- There is just a slight increase on the initial investment cost but in overall the cost can be balanced with a reduction on running costs [46].
- Most of the literature agrees on the improvement on thermal insulation, especially in winter due to the additional skin and the buffer zone.
- It is also suggested that the stack effect created by the facade when heated by the sun encourages air movement and air removal.

- DSFs allow night-time ventilation and heat discharge from the building, protecting from the rain without compromising security [49].
- Natural ventilation can be achieved through accurate design of the facade, which encourages airflow through the cavity and the building [49].
- Most authors agree that energy savings can be achieved through the use of DSF. This also means that indirect reduction of environmental impact and CO₂ emissions can be achieved.
- The facade cavity allows the placement of solar protections, thus improving shading coefficients and reducing direct heat loads.
- DSFs can reduce to some extent variable pressures of the facade from sudden gusts of wind.
- DSFs are able to reduce noise levels inside office buildings. Authors agree that this is one of the most important reasons for the use of this system.
- Due to glass properties and cavity configuration, reduced U-Value and g-value are also a quality highlighted by previous literature [24].
- Improved aesthetic value and transparency [49].

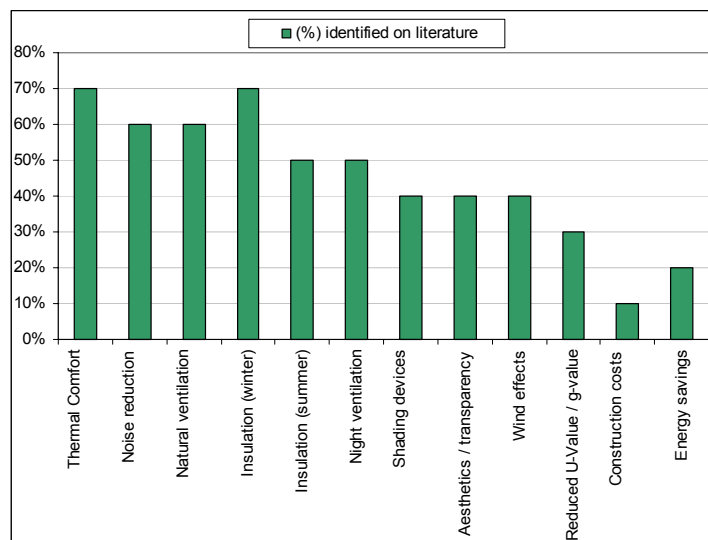


Figure 2.23 Advantages of Double Skin Facades identified by some of the authors on previous literature [27].

2.9.2 Disadvantages

The literature also suggests the problem of overheating as an important issue to be assessed in detail. The increased operational, maintenance and construction costs are also some issues that make DSFs not a very feasible option in some cases. According to Osterle et al [28], *“no one would dispute that double skin facades are more expensive than single skin forms: the construction of the outer layer and the space between the two skins make the former type more elaborate”*. The percentage of these issues identified, based on the literature, are illustrated in figure 2.24 and summarized as it follows:

- Additional maintenance and operational costs.
- Overheating problems can be a critical issue when the facade is not properly designed and assessed during design stages [26].
- Increased construction costs due to the extra facade required [28].
- Vulnerability for fire protection due to the connectivity to the facade channel, which could encourage propagation in case of fire [45].
- Reduction of usable areas due to the space required for the facade cavity.
- Increased weight to the building structure [28].
- Acoustic problems in terms of internal noise in relation to sound transmitted from room to room through the façade, or increased internal noise due to reverberation [28].

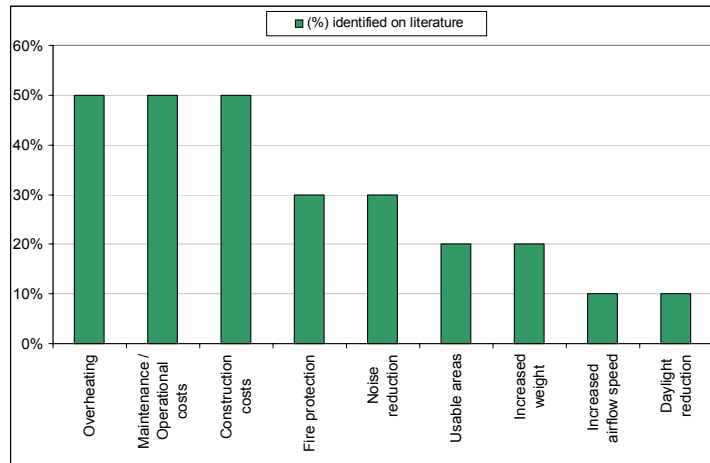


Figure 2.24 Disadvantages of Double Skin Facades identified by some of the authors on previous literature [27].

2.10 MONITORING / PREVIOUS MEASUREMENTS

There is some evidence from previous work carried out on full scale testing facilities and on site measurements. However, there is more work carried out on the performance of fully glazed buildings (single and double) based on modelling studies. Most of the models have shown that the increased cooling loads due to solar and internal heat gains dominate the energy consumption.

Kragh et al [50] carried out full-scale monitoring of eight test rooms located at Permasteelisa headquarters in Italy. It consisted of four types of facades classified by the authors as Bioclimatic Wall, Shading Wall, Interactive Wall and Active Wall. The rooms were continuously controlled and monitored in terms of room temperature, surface glass temperature, energy consumption and outdoor climate. The authors' findings demonstrated a 70% reduction of the peak cooling loads inside perimeter offices when compared with fully glazed non-ventilated curtain-wall buildings, and 25% if compared with offices behind mechanically ventilated double-skin facades cavities.

Saelens [51] in his PhD thesis monitored two existing buildings under the real climatic conditions of Brussels, Belgium. The first building was the DVV Headquarters, which is equipped with an airflow window with downward ventilation. The second building was a renovation project on the city centre, equipped with a naturally ventilated double skin facade. He analysed the performance of these buildings to assess and identify the influence of workmanship, to illustrate the complexity of real-life monitoring and evaluate the thermal behaviour of multiple skin facades. He also measured two single storey-testing facilities located on the Vliet test building, which comprised of a double skin facade and a traditional facade test room. These measurements provided data to develop and validate a numerical model, which helped to assess how the inlet temperature of the DSF should be determined.

Shang-Shou [52] proposed a protocol to determine experimentally the performance of a south facing double glass envelope. He applied this protocol based on his experimental study of a single story south facing ventilated wall system on two modular full-scale double glazed window models. Each of the models had naturally and mechanically assisted ventilation. The models were monitored with a range of weather conditions of Blacksburg, Virginia-USA. Using the test protocol, the author compared the cavity heat removal rates on the testing facilities for the mechanically ventilated system, the single naturally ventilated facade and naturally ventilated DSF.

Marquez et al (2006) [53] carried out a post-occupancy monitoring of a building with DSF, located in Lisbon. This made up part of a major project to monitor various buildings under different weather conditions, to determine under which climate and

performing conditions DSFs are most acceptable. They monitored one office located on the 11th floor of the NW facade inside an eleven-storey building that has mechanically ventilated DSFs on all the facades and a central atrium. The monitoring was carried out for 15 days during the month of September 2005. In their preliminary findings, they suggested that the air temperature in the façade cavity is mainly a function of the outdoor air, the incoming radiation and to a lesser extent, the indoor temperature.

According to Streicher et al [43], there have been other previous measurements in Continental Europe. In Belgium, BBRI has carried out some measurements in situ and an outdoor laboratory facility with DSFs in order to assess energy, ventilation, acoustics and daylight. Some universities have also performed measurements in a laboratory or in situ. All the measurements were carried out at facade level and not on all of the building. In other countries such as Greece, Germany and Sweden the studies are still concentrated in simulations rather than on site monitoring.

In the United States, the behaviour of a solar chimney added to an existing building of the College of Architecture and Urban Planning, studied by Cook and Robertson [54]. The solar chimney was based on the characteristics of a DSF. They also built a 1:10 scale model of the building to demonstrate the principles of DSFs. The full-scale solar chimney was used for gathering information during two weeks, on the behaviour of the facade in different conditions. They found direct implication of solar radiation on temperature response and stack effect and also the important effect of thermal buffering created by the DSF.

In the case of the U.K., there is no widely available data from monitored buildings. Therefore, there is a requirement for monitoring data in the U.K. to provide the opportunity to learn more about the performance of DSF in a specific location, as a relevant source of information for designers and consultant engineers.

2.11 DSF BUILDINGS IN THE UNITED KINGDOM

Over the last years there has been a dramatic growth on the use of Double Skin Facades in office buildings in the United Kingdom. Most of the buildings have been built or refurbished in the London area. The buildings referenced as examples are described briefly accordingly with the type of construction, use and type of façade.

2.11.1 One Plantation Place Building



Fig. 2.25 General view of the building from the south west and close view of the North-east facing corner Double Skin Facade.
Photos: M. Hernandez T (2006).

Table 2.1 General description of the building [56,57]

Identification

Official name: Plantation Place

Location

Address: 31-35 Fenchurch Street, London. EC3

Bordering street: Fenchurch Street

Complex: Plantation Place

Borough: City of London

City: London

Technical Data

Height: 68 m

Number of Storeys: 16

Area: 50.170m²

Construction end 2004

Façade Clear Glazed, Multi-Story Double Skin Façade
Double Skin Façade is used to increase thermal and acoustic insulation of offices providing natural ventilation for upper floors.

Building in General

Type of construction: High-rise building

Main usages: Offices for the financial, insurance and trading markets

Status: completed

Architect: Arup Associates

Consultants: Arup Associates, Hayden Young

Main Contractor: Bovis Lendlease

Quantity Surveyor: Gardiner & Theobald

Websites

<http://www.arup.com/controlsandcommissioning/project.cfm?pageid=5532>

<http://www.cityoffices.net/properties/plantation-place-1-plantation-place-fenchurch-street-building-31-35-fenchurch-street-london.cfm>

<http://www.skyscrapernews.com/buildings.php?id=250>

2.11.2 One Triton Square



Figure 2.26 View of the south-east main entrance from Triton Square and close view of the north facing Double Skin Facade.
Photos: M. Hernandez T (2006)

Table 2.2 General description of the building [56]

Identification

Official name: Triton Square

Location

Address: 1 Triton Square

Bordering street: Triton Square

Postcode: NW1 3DX

Complex: Triton Square

Borough: Camden

City: London

Country: United Kingdom

Technical Data

Number of Storeys: 5

Area: 26.000m²

Structure: Concrete frame with steelwork cores.

Façade: Clear Glazed, Multi-storey DSF integrated with HVAC through main ducts

Ventilation: Fully HVAC via under floor supply system.

Building in General

Type of construction: High-rise building

Main usages: Offices, retail

Status: completed

Consultant: Arup Associates

Websites

http://www.arupassociates.com/AAH_Projects.asp?strTag=Triton

2.11.3 BT Brentwood



Figure 2.27 General view of the building
Source: <http://www.arup.com>
Photo: Richard Bryant/Arcaid.

Table 2.3 General description of the building [58, 59]

Identification

Official name: BT Brentwood

Location

Address: One London Road

City: Brentwood, Essex

Country: United Kingdom

Technical Data

Number of Storeys: 3

Structure: Reinforced Concrete

Façade: Clear Glazed, Double Skin with cladding of preassembled factory panels on inner skin. Solar blinds manually controlled inside the façade cavity.

Ventilation: Natural Ventilation system operating in mixed mode. Sash windows manually opened for natural ventilation. The under floor air cooling provides backup cooling for inner zones.

Building in General

Type of construction: Low-rise building
Main usages: Offices.
Status: Completed
Consultant: Arup Associates

Websites

<http://www.arup.com/assets/download/download51.pdf>

<http://www.cibse.org/pdfs/7caustin.pdf>

2.11.4 Watling House



Figure 2.28 Facade view of the main entrance on Cannon Street and close view of a Shaft Box Double Skin Facade module.
Photos: M. Hernandez T (2006).

Table 2.4 General description of the building [60]

Identification

Official name: Watling House

Location

Address: 31-37 Canon Street
Bordering street: Watling Street
Postcode: EC4
City: London
Country: United Kingdom

Technical Data

Number of Storeys: 7
Built area: 7,900m²

Façade: Solid Components and full height triple glazed,
 Box Double skin Facade.
 Ventilation: Fully HVAC.
 Construction end: 1992.
 Consultant: Arup Associates
 Architect: GMW

Websites

http://www.arup.com/_assets/_download/download41.pdf

2.11.5 Glaxo Wellcome



Figure 2.29 General view of the building
 Source: <http://www.cabe.org.uk/CaseStudies.aspx?csid=100&imgid=5>
 Photo: Chris Gascoigne.

Table 2.5 General description of the building [7, 61]

Identification

Official name: Glaxo Wellcome West, Greenford.

Location

Address: 891-995 Greenford Road, Greenford,
 Middlesex
 Bordering street: Greenford Road
 Postcode: UB6 0HE

Borough: Greenford
City: West London

Technical Data

Number of Storeys: 4
Size of building: 72m long, 36m wide.
Area: 8.300m²
Structure: Concrete frame with steelwork cores.
Façade: Clear Glazed, Corridor Double Skin integrated with sun shading devices inside the cavity.
Ventilation: HVAC with load reduction through passive ventilation with double skin façade.

Building in General

Type of construction: Low-rise building
Main usages: Open plan offices.
Status: completed
Consultant: RMJM London Ltd, Arup Facade Engineering, Yeoman & Edwards, Mace.
Architect: RMJM Architect
Date: 1995-1997

Websites

http://www.rmjm.com/images/portfolio/Glaxo%20Wellcome%20HQ_portfolio.pdf
<http://www.cabe.org.uk/library/casestudy.asp?id=141>
<http://www.arup.com/facadeengineering/project.cfm?pageid=1789>

2.11.6 Greater London Authority (GLA)

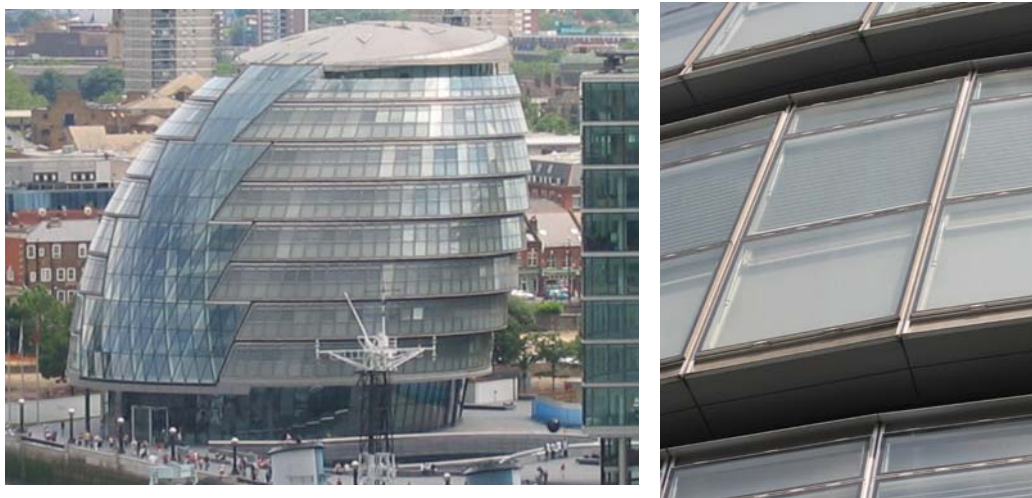


Figure 2.30 General view of the building from the monument on the north bank and close view a box module of the Double Skin Façade.
Photos: M. Hernandez T (2006).

Table 2.6 General description of the building [62]

Identification

Official name: Greater London Authority, City Hall

Location

Address: The Queen's Walk, London SE1 2AA

Bordering street: Tooley Street

City: London

Country: United Kingdom

Technical Data

Height: 45m

Structure: Steel frame with circular hollow columns.

Storeys: 11

Façade: Highly insulated panels combined with high performance box double skin modules.

Building in General

Type of construction: High rise building

Floor area: 15.000m²

Main usages: Offices for the recently created for the GLA.

Status: completed

Consultant: Arup Associates

Architect: Norman Foster

Websites

http://www.greenarch.hku.hk/research/Rock%20Museum/website/html/case_studies.html

<http://www.arup.com/advancedtechnologyandresearch/project.cfm?pageid=4345>

<http://www.arup.com/europe/project.cfm?pageid=186>

2.11.7 Helicon Building



Figure 2.31 View of the DSF over the main entrance at Finsbury Pavement and view of the Corridor DSF facing Finsbury Pavement.
Photos: M. Hernandez T (2006).

Table 2.7 General description of the building [63,64]

Identification

Official name: The Helicon

Location

Address One South Place
 Bordering street South Place
 Borough City of London
 City London

Technical Data

Floors: 8
 Area: 95.000m²
 Construction end 2000
 Facade: Clear Glazed, Multi-storey DSF above the main entrance.
 Corridor DSF on the facade along Finsbury Pavement

Building in General

Type of construction High-rise building

Main usages	Office retail development
Status	Completed
Facts:	The building features chilled ceilings and solar control via louver blinds for a low energy environment.
Architect:	Sheppard Robson
Date:	1992-1996
Consultants:	Ove Arup & Partners, Bruce Shaw Partnership, Permasteelisa (UK) Ltd., HSBC Holdings PLC. Permasteelisa Group Ove Arup & Partners Energy Consultant

Websites

www.permasteelisa.com.sg/eng/projects/theelicon/theelicon.html

www.sheppardrobson.com

http://www.architecture.uwaterloo.ca/faculty_projects/terri/366essaysW03/sharma_helicon.pdf

2.11.8 Darwin Centre phase I (Natural History Museum)



Figure 2.32 General view of the building from the South-east and general view of the south facing Multi-story Double Skin Facade.

Source: <http://www.archnewsnow.com/features/Feature62.htm>

Photos: Peter Durant/Arcblue.com.

Table 2.8 General description of the building [65]

Identification

Official name: The Darwin Centre, Natural History Museum

Location

Address: Natural History Museum, Cromwell Road,
SW7 5BD

Bordering street: Cromwell Road

City: London

Country: United Kingdom

Technical Data

Storeys: 10

Façade Clear Glazed, Multi-Story Double Skin Façade with shading protecting louvers inside the cavity.

Building in General

Type of construction: High rise building

Built area: 11,148m²

Main usages: Museum, Specimen display and storage, Laboratories.

Status: completed, September 2001

Consultant: Arup Associates: Arup Façade Engineering

General Contractor: Shepherd Construction

Architect: HOK international

Websites

www.hok.com

<http://www.archnewsnow.com/features/Feature62.htm>

2.11.9 Wellcome Trust Building



Figure 2.33 General view of the building's north facade from Houston Road and close view of the Corridor type Double Skin Facade.
Photos: M. Hernandez T (2006).

Table 2.9 General description of the building [66]

Identification

Official name: The Wellcome Building

Location

Address: 183 Euston Road, NW1 2BE
 Bordering street: Euston Road
 Complex: The Wellcome Trust
 City: London
 Country: United Kingdom

Technical Data

Storeys: 15
 Construction end: 2002
 Façade: Clear Glazed, Corridor Double Skin Facade

Building in General

Type of construction: High-rise building
 Area: 28,000m²
 Main usages: Offices, Research centre.
 Status: Completed
 Consultant: Arup Associates
 Architect: Michael Hopkins

Websites

<http://www.hopkins.co.uk>

http://www.architectureweek.com/2002/0109/tools_1-2.html

<http://www.hughpearman.com/articles5/hopkins.html>

2.11.10 Ashcroft International Business School



Figure 2.34 General view of the building
Source: www.wilkinsonseyre.com
Photo: Nick Wood.

Table 2.10 General description of the building [67]

Identification

Official name: Michael Ashcroft Business School

Location

Address: Bishop Hall Lane, CM1 1SQ

Complex: Anglia Ruskin University

City: Chelmsford

Technical Data

Storeys: 5

Construction end: 2002

Façade: Clear Glazed, South facing Multi-Storey Double Skin Facade from 1st to 3rd floors

Building in General

Type of construction: Steel framed, curtain walling and precast concrete floors and stairs.

Floor area	4.384m ²
Main usages:	Offices and teaching spaces
Status:	Completed
Architect:	Wilkinson Eyre
Consultants:	Mace Consulting, Gardiner & Theobald, Atelier 10, Buro Happold, PRP Architects, Sandy Brown Associates, William Verry, Scott Brownrigg + Turner.
Real estate management:	Anglia Polytechnic University

Websites

www.wilkinsoneyre.com

<http://www.prparchitects.co.uk/skills/skill/LandscapeArchitecture/MichaelAshcroftBS>

2.11.11 University of Bath – Library Building



Figure 2.35 General view of the building Double Skin Facade
 Source: Alec French Architects
http://www.alecfrench.co.uk/education/bu_library.html

Table 2.11 General description of the building

Identification

Official name:	Library and Learning Centre, University of Bath
----------------	---

Location

Address: Bath, BA2 7AY
Complex: The University of Bath campus
City: Bath

Technical Data

Storeys: 5
Construction end: July 1996
Façade: Clear Glazed, Corridor Double Skin Facade on 1st and 2nd floors.

Building in General

Type of construction: Extension and Refurbishment
Extension is lightweight steel/glass structure over roadway
Area: 8,000m²
Main usages: Library, 350 Public access PCs.
Status: Completed
Architect: Alec French Partnership
Management: University of Bath

Websites

<http://www.bath.ac.uk/about/campustour/index.php>
http://www.alecfrench.co.uk/education/bu_library.html

2.11.12 Portcullis House



Figure 2.36 General view of the building on Bridge Street and close view of the Shaft-Box Double Skin Facade module.
Photos: M. Hernandez T (2006)

Table 2.12 General description of the building

Identification

Official name: The Parliamentary Offices - Portcullis House

Location

Address: Bridge Street
London, SW1A 2LW
Bordering street: Bridge Street and Victoria Embankment
Complex: Houses of Parliament
City: Westminster, London

Technical Data

Storeys: 6
Construction end: 2000
Façade: Shaft-box Double Skin Facade modules

Building in General

Type of construction: Concrete arches braced by steel tension members that bridge the six supports from the tube station at the level of the first-floor cloister. Reinforced concrete columns combined with precast floors and cladding
Area: 23.000m²
Main usages: Committee, conference and meeting facilities for MPs. Retail and Coffee shops on ground floor
Status: Completed
Consultant: ARUP
Architect: Michael Hopkins & Partners
Real estate management:

Websites

<http://www.hopkins.co.uk/>
<http://www.galinsky.com/buildings/portcullishouse/index.htm>

2.11.13 Swiss Re HQ Building – ‘The Gherkin’



Figure 2.37 General view of the building from St Mary Axe and close view of the Double Skin Facade.
Photos: M. Hernandez T (2006).

Table 2.13 General description of the building [68]

Identification

Official name: 30 St Mary Axe, Swiss Re HQ

Location

Address: 14-34 St Mary Axe, London, EC3.
 Bordering street: St Mary Axe, Bury Court
 Borough: City of London
 City: London

Technical Data

Storeys: 40 – 179,8m
 Construction end: 2004
 Façade: High insulated bronze and clear Double Skin glazed facade, with internal break-out spaces that spiral up the building for air distribution drawn through opening panels on the inner facade.

Building in General

Type of construction: High-rise building
 Floor area: 47.950m²
 Main usages: Offices and retail
 Status: Completed
 Consultant: Arup , Gardiner & Theobold, Hilson Moran Partnership , Derek Lovejoy Partnership, Speirs and Major , Arup Fire, Arup Transportation,

BDSP Partnership, Emmer Pfenninger, Kontor
GTCM, Linklaters & Alliance, Montagu Evans,
Osprey Mott MacDonald, PTS, Reef UK, RWG
Associates, Sandy Brown Associates, Space
Syntax Laboratory, The Richard Coleman
Consultancy, Tricon, Van Deusen &
Associates, VIDEF

Architect:

Foster and Partners

Real estate management:

30 St Mary Axe Management Services Ltd
20 Bury Street London EC3A 5AA

Websites

<http://www.30stmaryaxe.com/home.asp>

<http://www.swissre.com/pws/about%20us/buildings%20and%20directions/london/swiss%20re%20in%20london.html>

<http://www.fosterandpartners.com/Projects/1004/Default.aspx>

2.11.14 Fitzrovia Building, ARUP HQ



Figure 2.38 General view of the building south-east facade from Howland Street and close view of the Double Skin Facade on Fitzroy Street
Photos: M. Hernandez T (2007).

Table 2.14 General description of the building [69]

Identification

Official name: ARUP HQ, Fitzrovia Building

Location

Address: 13 Fitzroy Street, W1T 4BQ
 Bordering street: Fitzroy, Howland Street
 Complex: Fitzrovia Estate
 City: London

Technical Data

Storeys: 7
 Construction end: 2002
 Façade: Clear Glazed, Multi-Storey Double Skin with sun-shading devices inside the cavity integrated with HVAC external ducts.

Building in General

Type of construction: High-rise building
 Area: 125,000-square-foot
 Main usages: Offices
 Status: completed
 Consultant: Arup Associates
 Architect: Sheppard Robson
 Real estate management: London Merchant Securities plc (LMS)

Websites

<http://archrecord.construction.com/features/digital/archives/0507dignews-1.asp>
http://www.sheppardrobson.com/sr_master.html

2.11.15 1 Deansgate Street Building



Figure 2.39 General view of the building and close views of the DSF.
Sources: <http://www.skyscrapernews.com>, Photo: Chris Wilkinson, 2005.
<http://www.merouk.co.uk/structures/2002deansgate.htm>

Table 2.15 General description of the building [70]

Identification

Official name: No 1. Deansgate

Location

Address: 1 Deansgate, Manchester, M3

Bordering street: Deansgate

City: Manchester

Technical Data

Storeys: 17

Construction end: 2002

Façade: Clear Glazed, Corridor Double Skin with external using single glazed frameless louvers that automatically adjust opening positions according to climatic variations.

Building in General

Type of construction: High-rise building

Total height: 62m

Main usages: Residential and retail on lower levels.

Flats: 84
Status: completed
Developer: Crosby Homes
Structural Engineer: Martin Stockley Associates
Construction manager: MACE Ltd.
Architect: Ian Simpson Architects.

Websites

<http://www.skyscrapernews.com/buildings.php?id=656>

http://en.wikipedia.org/wiki/No._1_Deansgate

<http://www.iansimpsonarchitects.com/site/main.htm>

2.11.16 The Willis Building



Figure 2.40 General views of the building from North-west and South-east corners.
Source: MERO-SCHMIDLIN (UK) PLC.
http://www.merouk.co.uk/curtainwalling/50001limest_construction.htm

Table 2.16 General description of the building [71]

Identification

Official name: The Willis Building

Location

Address: 51 Lime Street, City of London, London. EC3
 Bordering street: Lime Street
 City: London

Technical Data

Stores: The project consists of three interlocking blocks of 16, 23 and 29 stories adjacent to the Lloyds Building.
 Area: 44.120 m².
 Construction ends: 2007.
 Façade: Externally ventilated shaft-box double skin cladding to East elevation of the tower levels 2 to 23, and West elevation of the tower levels 2 to 15 and 17 to 22

Building in General

Type of construction: High-rise building
 Total height: 138,80m.
 Main usages: Offices.
 Status: completed.
 Client: British Land Company Plc and Stanhope Properties Plc
 Construction manager: MACE Ltd.
 Architect: Foster and Partners.

Websites

<http://www.skyscrapernews.com/buildings.php?id=78>
<http://www.britishland.com/devwillisbuilding.htm>
http://www.merouk.co.uk/curtainwalling/50001limest_construction.htm
<http://www.merouk.co.uk/news/20070329limest.htm>
<http://www.building.co.uk/story.asp?sectioncode=583&storycode=3085557&c=1>
<http://www.fosterandpartners.com/>

2.11.17 Beetham Tower - Manchester.



Figure 2.41 General views of the building.
 Sources: http://en.wikipedia.org/wiki/Image:Beetham_tower.jpg
<http://www.skyscrapernews.com/buildings.php?id=132>
 Photos: Iain Dickinson (2006), Nick Graysen (2007).

Table 2.17 General description of the building [72]

<u>Identification</u>	
Official name:	Beetham Tower Manchester, also known as Hilton Manchester.
<u>Location</u>	
Address:	301 Deansgate, Manchester. M3 4LQ
Bordering street:	Deansgate St
City:	Manchester
<u>Technical Data</u>	
Storeys:	47
Construction ends:	2006.
Façade:	Clear glass, externally ventilated Box double skin facade cladding.
<u>Building in General</u>	
Type of construction:	High-rise building
Pinnacle Height:	169m

Pinnacle Type:	Facade Overrun
Top Floor Height:	157m
Primary Use:	Hotel
Secondary Use:	Residential
Description:	279-bed hotel, 219 residential flats.
Status:	Completed.
Developer:	Beetham Organization
Structural Engineer;	Cantor Seinuk Group
Main Contractor;	Carillion Construction
Architect:	Ian Simpson Architects.

Websites

<http://www.skyscrapernews.com/buildings.php?id=132>

http://en.wikipedia.org/wiki/Beetham_Tower%2C_Manchester

<http://news.bbc.co.uk/1/hi/england/manchester/4944590.stm>

<http://technology.newscientist.com/channel/tech/mg19125631.300.html>

<http://www.thebeethamorganization.com/home.php>

2.11.18 Beetham Tower - London



Figure 2.42 General view and close rendered view of the of the tower facade.
 Sources: <http://www.skyscrapernews.com/buildings.php?id=1524>
<http://www.thebeethamorganization.com/home.php>
 Photos and renders: Ian Simpson Architects.

Table 2.18 General description of the building [73]

Identification

Official name: Beetham Tower London, also known as Jumeirah London and The Boomerang.

Location

Address: 1 Blackfriars Road, London. SE1 9UF
 Bordering street: Blackfriars Road
 City: London

Technical Data

Total floors: 51
 Status: Planning Approved
 Proposal date: 2006
 Construction start date: 2008
 Proposed completion date: 2011
 Façade: Clear glass, Multi-storey double skin facade.

Building in General

Type of construction: High-rise building
 Total height: 180m
 Primary Use: Hotel
 Secondary Use: Residential
 Description: 261-bed hotel, 96 residential flats.
 Developer: Beetham Organization
 Project Architect: Ian Simpson Architects.

Websites

<http://www.skyscrapernews.com/buildings.php?id=1524>
http://www.thebeethamorganization.com/plugins/content/content.php?content_26
http://en.wikipedia.org/wiki/Beetham_Tower%2C_London
<http://www.iansimpsonarchitects.com/site/main.htm>

2.11.19 Urbis Exhibition Centre



Figure 2.43 General views of the building.
 Sources: <http://www.skyscrapernews.com/buildings.php?id=181>
<http://en.wikipedia.org/wiki/Urbis>
 Photos: Chris Wilkinson (2004), Kaihsu Tai (2005).

Table 2.19 General description of the building [74]

<u>Identification</u>	
Official name:	Urbis
<u>Location</u>	
Address:	Cathedral Gardens, Manchester. M4
Bordering street:	Cathedral Gardens, Fennel St,
City:	Manchester
<u>Building in General</u>	
Total floors:	6
Status:	Completed
Completion date:	2002
Façade:	Clear glass, Corridor Double Skin Facade..
Type of construction:	Low-rise building
Total height:	35m
Primary Use:	Museum, temporary exhibitions.
Project Architect:	Ian Simpson Architects.
<u>Websites</u>	
http://www.skyscrapernews.com/buildings.php?id=181	
http://en.wikipedia.org/wiki/Urbis	

2.12 DISCUSSION AND CONCLUSION

The envelope has an important role on the thermal balance of a building; its implications nowadays on energy consumption are primary issues for any preliminary design. The use of glass as a main material for building envelopes has created a great concern about its direct implications on natural lighting, thermal performance and energy usage on contemporary architecture.

Glass is now widely applied as a fashionable material associated with ‘high tech’ and to symbolise a ‘transparent’ corporate image for office buildings. Its influence on the internal environment has been a matter of great research during the last century. Nevertheless, the development of new improvements on its manufacture, characteristics and applications on technologies such as Double Skin Facades are still issues, which are not completely clear in regard to how they should be applied by designers and engineering consultants.

Double Skin Facades have been developed to resolve the problem of thermal unsteadiness in single glass facades. The, argued, increased thermal and acoustic insulation with improvement of natural lighting is highlighted as some of its benefits in previous literature. However, there is argument about the flexibility and limitations on its use in places with high solar gains and temperature levels, which are factors that can lead to overheating. Some authors mention the configuration and operation of the façade, as important factors that may lead to overheating. There is some argument about the efficiency of DSFs; some authors affirm DSFs are efficient under very specific conditions, others suggest that it is not a very energy efficient system and requires deeper assessment in relation to the entire building.

Most of the literature suggests that the key elements to be considered in the design stage, which determines the efficiency of Double Skin Facades, are: Solar radiation, climatic conditions, building location, facade design, building structure, user's requirements and building regulations.

Most literature suggests the importance of good understanding of the performance by studying the physics of the cavity and the implications of different geometric configurations. The final response of the airflow and thermal performance requires to be assessed by comparing all of these possible configurations, to avoid overheating and exploit the facade adequately for insulation and natural ventilation.

There is wide assessment of the performance of DSFs through thermal and CFD models; however the development of simple CFD techniques applied for designers is still under-developed.

The data and information from site monitoring and built cases are still scarce and do not provide an overall picture of the performance of the systems during different seasons. There is a necessity for comparisons within different climatic conditions as a means to define which specific environments are suitable for DSF buildings.

The choice of a particular DSF system is determined by architectural, functional and economic factors. The choice has far reaching implications for the project planning. However, the decision depends on a very relevant priority of the climatic conditions and the predicted behaviour of the façade under critical conditions. This requires a detailed design and study of the facade for each specific case.

REFERENCES

1. Sala, M., The intelligent envelope: The current state of the art, *Renewable Energy*, 1994. 5(5-8): p. 1039-1046.
2. Fachinstitut Gebäude-Klima E.V., editor, Proceedings of "Doppelfassaden und Technische Gebäudeausrüstung". Bietigheim-Bissingen, Germany, 1997.
3. Costa, M., et al. Analysis of multifunctional ventilated facades: An European Joule Project. in *Eurosun Conference*. 2000. Copenhagen, Denmark.
4. WCDE, *Our Common Future: The Brundtland Report*. XV ed. 1987, Oxford: Oxford University Press. 400p.
5. Olgyay, V., *Design with Climate: Bioclimatic approach to architectural regionalism*. 1936, Princeton, NJ: Princeton University Press.
6. Streicher, W., et al., *BESTFACADE: Best Practice for Double Skin Facades*, 2005, Institute of Thermal Engineering, Graz University of Technology, Sweden.
7. Wigginton, M. and J. Harris, *Intelligent Skins*. 2002, Oxford: Architectural Press.
8. Neubert, S., *Double Skin Facades - a contribution to sustainability?*, in *European Postgraduate Studies in Architecture and sustainability*. 1999, Louvain-la-Neuve: Lausanne.
9. Schittich, C., in *DETAIL Building Skins: Concepts, Layers, Materials*, ed. C. Schittich. 2001: Birkhäuser. Ed. Detail. 196.
10. Addington, D.M. and D. Schodek, *Smart Materials and Technologies for the architecture and design professions*. 2005, Oxford: Architectural Press. 241.
11. Krewinkel, H.W., *Glass Buildings: Material, Structure and Detail*. 1st ed. 1998, Basel: Birkhäuser. 155.
12. Glass, J., *Encyclopaedia of Architectural Technology*. 2002, London: John Wiley & Sons Ltd. pp. 127-136.
13. Nuttgens, P., *The story of architecture*. 2nd ed. 1997, London: Phaidon. pp. 158.
14. Watkin, D., *A History of Western Architecture*. 2000, London: Laurence King Publishing, pp. 151.
15. Tallis, *History and Criticism of the Crystal Palace*, 1852.
16. Wigginton, M., *Glass in Architecture*. 2003, New York: Phaidon Press Inc.
- 17a. Hix, J., *The Glass House*. 1974, London: Phaidon Press Limited, pp.136.
- 17b. *Ibid.* pp.158-159.
- 17c. *Ibid.* pp.161.
18. Scheerbart, P., *Glasarchitektur*. 1914, Leipzig: Verlag der Sturm.

19. Compagno, A., *Intelligent Glass Facades*. 5th revised and updated ed. 2002, Basel, Boston, Berlin: Birkhäuser.
20. Wiggington, M., *Glass in Architecture*. 2003, New York: Phaidon Press Inc. pp.97-98.
21. Shorrocks, L. and G. Henderson, *Energy Use in Buildings and Carbon Dioxide Emissions*. 1989, Report BR 170, Building Research Establishment, UK.
22. Button, D., et al., *Glass in Building: Guide to Modern Architectural Glass Performance*, ed. D. Button and B. Pye. 1993: Pilkington Glass Ltd, Butterworth-Heinemann Ltd. 372.
23. Davies, M. and R. Rogers, A Wall for All Seasons. *RIBA Journal*, 1981, 2(88): p. 55-57.
24. Kragh, M. *Building Envelopes and Environmental Systems*. in: *Modern Façades of Office Buildings*. 2000. The Netherlands: Delft Technical University.
25. Uuttu, S., *Study of Current Structures in Double Skin Facades*, in Department of Civil and Environmental Engineering. 2001, Helsinki University of Technology: Helsinki, Finland.
26. Faggembauu, D., et al. Strategies to reduce thermal overheating in Mediterranean climates using large glazed areas. in *Fier 2002: International Forum on Renewable Energies*. 2002. Tetuan: FIER 2002.
27. Poirazis, H., *Double Skin Facades - A Literature Review*. 2004, Division of Energy and Building Design, Department of Construction and Architecture, Lund Institute of Technology: Lund. p. 196.
28. Oesterle, L., Lutz & Heusler, *Double Skin Facades: Integrated Planning*, ed. Prestel. 1999.
29. Harrison, K. and T. Meyer-Boake, *Tectonics of Environmental Skins: The Occidental Chemical Centre*, 2003, School of Architecture, University of Waterloo, p.6.
30. Belgian Building Research Institute, BBRI: *Ventilated Facades - Classification and illustration of facade concepts*, 2004, Department of Building Physics, Indoor Climate and Building Services.
31. Albrecht, P., 1903 Steiff Factory, in *a+t*, 1998. p. 49.
<http://www.aplust.net/paginasingles/ionce/ionceartic/ionceart01.html>
32. Leon Crespo, A.M., *History of Double Skin Facades*. 1999, Graduate School of Design, Harvard University: Cambridge, USA. p. 3.
33. Buchli, V., Moisei Ginzburg's Narkomfin Communal House in Moscow, *Journal of the Society of Architectural Historians*, 1998. 57 (2).
34. Taylor, B., *Le Corbusier, the city of Refuge, Paris 1929-33*. 1987, Chicago: The University of Chicago Press.

35. Besset, M., 1968, Who Was: Le Corbusier. Who Was?, ed. J. Leymarie. 1968, Cleveland, Ohio, USA: the World Publishing Company. 230.
36. Corbusier, L., The Sun-break, in Besset, M., Who was Le Corbusier,. 1933.
37. Letter from Le Corbusier to Senator Warren Austin, published in the Architectural Review, 1950: p. 69-71.
38. Harrison, K. and T. Meyer-Boake. The Tectonics of Environmental Skins. 2003. School of Architecture. University of Waterloo. p. 8.
39. Aarons, D., Properties and applications of double-skin building facades, in Dept. of Architecture. 2000, Massachusetts Institute of Technology (MIT): USA. p. 277.
40. Magali, B., Proposition of climatic facades classification, in IEA Task 27 Subtask A, Case 2: Double Envelope Systems. 2001, Catholic University of Leuven, Belgium: Leuven.
41. Stec, W.J. and A.H.C. van Paassen, Integration of the Double Skin Facade with the Buildings, in Energy in Built Environment. 2628 CD, Energy Technology, TU Delft: Mekelweg 2, Delft, The Netherlands.
42. Di Maio, F. and A.H.C. van Paassen, Simulation of Temperature and Air flow in a Second Skin Facade, 2000, Laboratory for Refrigeration Engineering and Indoor Climate Technology, Delft University of Technology: Mekelweg 2, Delft, The Netherlands.
43. Streicher, W., et al., WP1 Report "State of the Art", BESTFACADE: Best Practice for Double Skin Facades. 2005, Graz University of Technology: Graz, Austria. p. 151.
44. Straube, J.F. and R.V. Straaten, The Technical Merit of Double Skin Facade Buildings. 2003, School of Architecture, University of Waterloo: Waterloo, USA.
45. Jager, W., Double Skin Facades -Sustainable Concepts. Presentation of Hydro for Syd Bygg-2003, 2003: Malmo, Sweden.
46. Wigginton, M. and B. McCarthy, Environmental Second Skin Systems homepage. 2000, Michael Wigginton & Battle McCarthy. <http://www.battlemccarthy.demon.co.uk/research/doubleskin/mainpage.htm>.
47. Stribling, D. and B. Stigge. A critical review of the energy savings and cost payback issues of double facades. in 2003 CIBSE/ASHRAE Conference. 2003. UK: CIBSE: Chartered Institution of Building Services Engineers.
48. Claessens, J. and A. DeHerte, Technology module-5: Active Solar Heating and Photovoltaics, Energy Research Group, School of Architecture, University College Dublin: Dublin, Ireland. p. 32.
49. Lee, E., et al., High-Performance Commercial Building Facades. 2002, Building Technologies Program, Environmental Energy Technologies Division, Ernest Orlando Lawrence Berkeley National Laboratory, University of California: Berkeley, CA. p. 133.

50. Kragh, M., M. Colombari, and M. Zibec. Advanced Façades and HVAC Systems: preliminary results of full-scale monitoring. in Energy Efficient and Healthy Buildings in Sustainable Cities. 2002. Lyon-France: EPIC AIVC.
51. Saelens, D., Energy Performance Assessment of Single Storey Multiple-Skin Facades, PhD thesis, in Faculteit Toegepaste Wetenschappen, Arenbergkasteel. 2002, Katholieke Universiteit Leuven,: Kasteelpark Arenberg 51, B-3001 Leuven, Belgium. p. 272.
http://63.236.105.169/envelopes/content/resources/pdf/case_studies/PhD_Dirk_Saelens.pdf
52. Shang-Shou, L., A Protocol to Determine the Performance of South Facing Double Glass Façade System: A Preliminary Study of Active/Passive Double Glass Façade Systems, PhD thesis, in Faculty of the Virginia Polytechnic Institute and State University. 2001, Virginia Polytechnic Institute: Blacksburg, Virginia, USA.
<http://scholar.lib.vt.edu/theses/available/etd-04212001-152253/unrestricted/>
53. Marques da Silva, F., et al. Double-Skin Façade Thermal Monitoring. in Proceedings: Healthy Buildings. 2006. Lisbon, Portugal: Laboratório Nacional de Engenharia Civil (LNEC), Structures Dept, Building Dept.
54. Cook, S.R. and R.J. Patton, A Study of the CAP Double Skin Building Façade. 2003, Ball State University: Muncie, Indiana. p. 42.
55. Wigginton, M., Glass in Architecture. 2003, New York: Phaidon Press Inc.p. 320.
56. ARUP, Arup Projects: Controls and Commissioning. 2004, Arup Associates: London, UK.
<http://www.arup.com/controlsandcommissioning/project.cfm?pageid=5532>
57. Bradley, S., A. Rowan, and N. Pevsner, London 1: The City of London (The Buildings of England). Revised ed. Vol. 1. 1997, London: Yale University Press. 704.
58. Hughes, A. and P. Warburton, A state-of-the-art office in Brentwood, Essex. Proceedings of the Institution of Civil Engineers: Structures & Buildings, 2005. 158(SB3): p. 157–165.
59. Hughes, A. and D. O’Carroll, BT ‘Workstyle’, Brentwood, Essex, in THE ARUP JOURNAL. 2002. p. 13-18.
http://www.arup.com/_assets/_download/download51.pdf
60. Barnes, S. and M. Brundle, Watling House, in THE ARUP JOURNAL. 2001. p. 37-37. http://www.arup.com/_assets/_download/download41.pdf
61. Baird, G., The Architectural expression of environmental control systems. 2001: E & FN Spon Press. 256.
62. Turpin, M., Great Hall, in Civil Engineering Magazine—American Society of Civil Engineers. 2003. p. 36-45.
63. Evans, B., Lower Energy in a City Street. The Architects Journal, 1994. 200(2): p. 31-32.

64. Sharma, P., The Helicon in Finsbury Pavement, London A Case Study, in Principals of Environmental Design, School of Architecture, University of Waterloo. p. 14.
65. Richards, K., Architecture Parlante: The Darwin Centre by HOK International. 2002, ArchNewsNow.com. p. <http://www.archnewsnow.com/>
66. Pearman, H., His Light Materials: Michael Hopkins and the Wellcome Trust headquarters, in Gabion: Retained Writing on Architecture. 2005, Hugh Pearman. p. 1-4, <http://www.hughpearman.com/articles5/hopkins.html>
67. Evans, B. and E. Summer, Academic prowess. The Architects Journal, 2003. 217(15).
68. Foster&Partners, 30 St Mary Axe, Swiss Re HQ. 2004, Foster + Partners: London. <http://www.fosterandpartners.com/Projects/1004/Default.aspx>.
69. Gissen, D., Breathing room: Arup's new London headquarters celebrates its mechanical systems, in Architectural Record. 2005, McGraw-Hill Construction,UK. <http://archrecord.construction.com/features/digital/archives/0507dignews-1.asp>.
70. Newman, J., Skycrapersnews.com, in Skyscraper News UK. 2007: UK. <http://www.skyscrapernews.com/buildings.php?id=656>
71. Ibid. <http://www.skyscrapernews.com/buildings.php?id=78>
72. Ibid. <http://www.skyscrapernews.com/buildings.php?id=132>
73. Ibid. <http://www.skyscrapernews.com/buildings.php?id=1524>
74. Ibid. <http://www.skyscrapernews.com/buildings.php?id=181>

CHAPTER III

PHYSICAL BASIS OF THE CONCEPT OF DSFs

3.1 INTRODUCTION

The physical interaction of each of the components inside the cavity determines the overall functionality of a Double Skin Facade. The understanding of these events is a complicated task, which has to include complex mathematical models and simulations. Most of the theory assessing the physics of DSFs is based on thermal performance models, airflow and daylight simulations [1]. The main physical aspects relative to the physical basis of DSFs are identified in this chapter by the following aspects:

- *Physical parameters.*
- *Physics of Light and Natural Lighting.*
- *Thermal Environment.*
- *Airflow.*

3.2 PHYSICAL PARAMETERS OF DSFs

Double Skin Facades were classified in the previous chapter according to the cavity geometry configuration and the resulting air function. Each type has particular physical parameters and properties, which makes each facade unique in its context, its behaviour and its operation. The physical position and characteristics of the elements that configure the facade determines how the facade behaves. The physical elements that constitute the facade are expressed with the following parameters:

3.2.1 Spatial Form / Structure

Double Skin facades are arranged with a similar combination of elements. The exact nature, dimensions and interaction of these elements however, are rather open to variation and offer a comprehensive degree of tailoring to suit a given scenario and requirement. According to Uutu [2], the structure of a Double Skin Facade can be divided into various substructures:

- “*Primary Structures*” are the load bearing elements, which connect and hold the facade to the building such as beams, walls, floors and bracings.
- “*Secondary Structures*” described as the elements; although carrying secondary loads, define horizontal elements, vertical partitions and the external shape of the facade.
- “*Tertiary Structures*” are defined as the elements that are part of the facade but are not critical for the structural stability of the facade. These elements are additional and are usually placed as part of the environmental strategy of the facade.

The spatial assembly of the DSF façade is described by the author as a main characteristic that differentiates the facade operation, which is defined by “*secondary structures*”. These are basically configured by the following main components:

- Facade skins
- Cavity form
- Cavity Openings

The facade skins usually consist of either single or double glazing units. Some special coatings or films can be utilized in order to modify the properties of glass. In general, the external skin tends to be fully glazed with sealed single glass units. The Debis building for instance (figure 2.15), has the possibility of opening the external skin by operable glass louvers providing the opportunity to reduce pressure on the facade, protect the inner skin from rain and ventilate the building as a single skin building, when required. The inner skin is sometimes combined with opaque materials, which can be used for thermal storage and increasing U-values of the inner facade.

The cavity form, which is a result of the construction height, is an important factor that determines the efficiency of DSFs. Gan [3] investigated the effect of the cavity width and height of solar chimneys and double façades in relation with buoyancy-induced ventilation rate. He found that buoyancy inside a facade cavity increases with the variation of cavity size until a point where there is no significant change. However, there is also an important relationship between the cavity width and height. In the case of a 4-storey-high DSF, there is a maximum width of 700mm in which the induced buoyancy is effective. Thus, cavity form is a critical issue for discussion, in order to understand the behaviour and implications of a DSF. Osterle et al [6] also mentions the direct implications of the construction parameters in the function of the airflow of the cavity. They stated that the reduction of the cavity size creates significant pressure losses within the cavity. For this reason the airflow or ‘aero physics’ inside the cavity are directly linked to the form and size of the facade.

The cavity openings are also critical issues that determine the overall efficiency of

the air exchange rate of the facade with the exterior. Faist [4] compared the implications of an airtight facade with a ventilated facade. The author described that the most important implication of the inlet/outlet opening position is on the resultant temperature inside the cavity. He explained that the lower temperatures are always obtained when the facade is ventilated. He also stated that the cavity width is not critical when the facade is sealed, for him it is more relevant to determine the cavity width in relation to the allowed effective height and openings, if the facade is ventilated.

Some authors also illustrate the different conditions within the cavity, depending on the inlet/outlet positions. Compagno [5] described them as “*depending on the wind pressure conditions of the building skin, the stack effect and the discharge coefficient of the openings*”. In this case, the author gives priority to the pressure difference between inlet and outlet as a relevant factor that determines airflow through the cavity.

There is no extensive literature describing the implications of openings on the internal and external skin. Osterle et al [6] gives a comparison of the ventilation effectiveness between various opening types of windows on the internal skin, in relation to the area available on elevation of the opening light. Figure 3.1 shows the relative efficiency of various window casements on the inner skin of the facade. The author describes that the effectiveness of the window depends on its opening movement. In this comparison, the author does not mention the direction of the airflow inside the cavity; the airflow rate was based on the area of opening. Further assessment is required to assess the effectiveness of each opening with upward and

downward airflows.

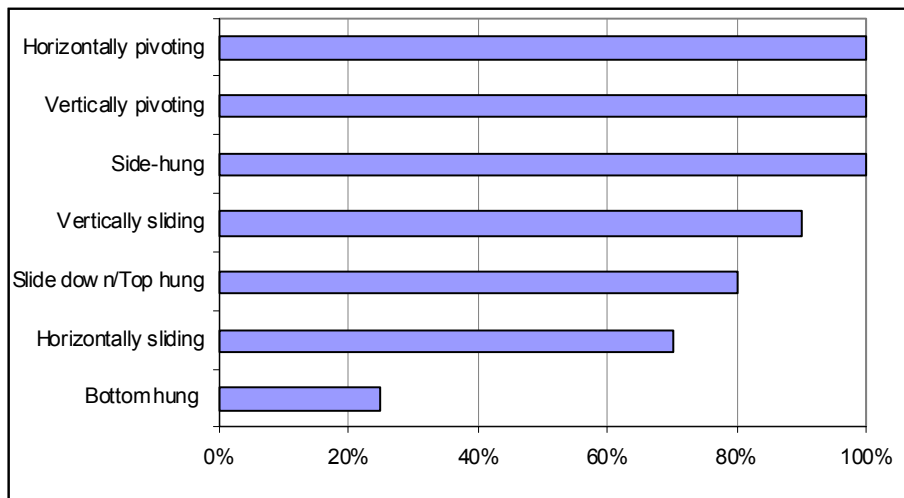


Figure 3.1 Relative efficiencies of window openings on the inner skin of the facade [6].

In relation to the influence of openings on the external skin, Osterle et al [6] focusses on the implications of the form of air inlets/outlets in relation to the quality of the air stream in the facade. The authors highlighted that “*the magnitude of the airflow is dependent upon the route that it follows within the cavity, which depends on the influence of vortices on edges of the cavity and the position of inlets and outlets. The development of eddies within inlet/outlets can reduce considerably the effective area of the opening*”. For this reason, the form and location of inlets and outlets have to be critically assessed. The impact of the openings of the double skin is stressed as very important by Gratia and De Herde [10]. They calculated an important reduction in energy consumption between airtight and ventilated cavities in relation to the elements inside the cavity.

As part of the components that have influenced the facade performance, Uutu made reference to the “*tertiary structures*”, which are defined by a series of elements such as horizontal louvers and blinds. These are placed inside the facade and do not have

structural function; their role is specifically related with the performance of the facade in terms of solar and air flow control. Some authors highlight the implications of the position the solar protection and materials have on the thermal comfort and energy performance of the facade. Osterle et al [6] puts emphasis on the direct influence that the position of the shading devices have on the thermal performance, where the elements have to be positioned towards the external skin to encourage better ventilation, and avoid excessive heat through the cavity. They suggested that the best position for the shading devices should be the first third of the cavity, providing there is good airflow above and below them. They suggested placing any shading device at least 150mm from the outer skin in order to avoid high temperatures on the external surface of the facade.

Aarons [7] mentions the influence of blind materials on the heat transfer coefficient inside the facade, in which the solar factor and the position of blinds could provide considerable reduction of the temperature difference between the cavity and the exterior. The author highlighted the importance of air movement along the blinds to allow convective heat removal.

Jager [8] suggested optimal values for optical properties and type of shading devices inside the cavity. Gratia and De Herde [10] determined that cooling consumption may be reduced by up to 23.2% by paying attention to the location of the blinds, their colour and the openings of the double-skin. Stec et al [11] studied the impact on the thermal performance of using plants as shading devices inside a DSF. The authors found favourable and effective impact on the performance results based on the reduction of temperature, cooling capacity and operation time of ventilation systems;

they suggested “*plants created a more effective shading system than blinds*”. However, further assessment is required to complement this analysis regarding the implications of plants on facades in relation with natural lighting.

3.2.2 Materials

One of the main issues during the design process of any building is the selection of its constituent materials. The method by which materials are selected often depends on their classification. Addington and Schodek (2005) described this classification based on the question “*why a material is differentiated from another*” in terms of engineering or architecture classifications. From the engineering approach, materials are selected by “*how the material performs*”. This means materials are applied based on what they can do, how they behave and if they physically resist the influence of their surroundings. From an architectural perspective, materials are selected based on “*what the material is and where it is used*”. This means that materials are selected, more, according to their standardization within the categories in construction, and where the material belongs in their use within each category [12].

In architectural design fields, materials are often selected long before the performance criteria of the material are defined. In the case of the building envelope, and especially in the case of Double Skin Facades, this selection is often described by literature as ‘obeying’, not only for its functional requirements, but also for its aesthetical and intrinsic image. The selection of materials in architecture often leans more towards aesthetic requirements, and the criteria being applied that it is pleasing to their eye. In the case of complex systems such as DSFs, the selection is dependent

upon a deep understanding of how all the materials involved in the facade behave and respond to their environment. Poirazis shows the importance of specific elements of the facade such as shading devices or panes [1]. Uutu highlights the implications of the combination of the materials with glass, in order to avoid incompatibilities with the material itself and its coatings [2]. The intrinsic relationship of the materials and the function of the envelope are issues that require coupled analysis, as the materials and the facade work together as a system. The sole application of the materials in DSFs as static elements is inadequate; it has to be assessed as a relationship between materials, technologies and the environment.

Glass is the main material, which characterizes the concept of a DSF; it plays a predominant role in facade aesthetics, integration and functionality. The main properties that affect DSFs are analyzed within this chapter as part of the energy behaviour within the luminous and thermodynamic environments.

3.2.2.1 Glazing

As mentioned before, glass is a non-crystalline solid. The main purpose of glass in buildings is to allow windows to be used as a source of natural light and heat. The evolution of glass utilisation in buildings from small portions to curtain walls was discussed in the previous chapter. This has symbolized the liberation of glass from the building structure. However the environmental implications of glass are critical issues.

In 1978, Richard Rogers carried out research for Pilkington [13] in which he defined the implications and targets required for glazed building skins: *“It is not good having*

sophisticated services systems for a building and a poor skin performance. It is only even partially effective to have a sophisticated mechanical services installation and high quality fixed performance skin. A time responsive, variable quality skin system is the only logical answer to this problem. A building becomes a chameleon which adapts. A properly equipped and responsively clothed building would monitor all internal and external variables, temperature, hygrometry and light levels, solar radiation etc., to determine the best energy equation given these conditions and modify the building and its internal systems accordingly. It is not too much to ask for a building to incorporate, in its fabric and its nervous system, the very basic vestiges of an adaptive capability”. The clear understanding of glass properties is nowadays an imperative aspect when designing the building envelope.

3.2.2.2 Optical Properties of Glass

The most relevant characteristic of glass is its transparency, basically due to the lack of a crystalline structure within its molecules. This gives its quality for light transmission. When solar radiation strikes a pane of glass, light is partly reflected, partly absorbed in the thickness and partly transmitted. According to the Glass Guide; *“the ratio of each of these three parts to the incident solar radiation defines the reflectance factor, the absorptance factor and the transmittance factor of the glazing”* [14], the tint of the glass, its thickness and the coating affects these factors as well. The definitions of these three parts are described as follows [13]:

- *‘Reflectance’* (ρ) is defined as the incident beam of light that is reflected by the material. Depending on the glass surface, the reflections of the glass can be ‘specular, diffuse or spread’.

- ‘Absorptance’ (α) is the fraction of incident radiation, which is absorbed by the body of the glass.
- ‘Light transmittance’ (τ) occurs depending on the optical properties of the glass, which determines the ratio between reflectance and absorptance. It is basically the fraction of incident radiation directly transmitted through the glass. Light transmittance is subject to variation due to refraction, diffusion and colouring.

The total light (I_L) transmitted by a panel of glass is the result of the sum of the total solar radiation, which is absorbed and reflected outside and transmitted and absorbed inside the building. This resultant is illustrated in figure 3.2, which is described by Compagno as the Total Solar Energy transmission factor (*g-value*) [5].

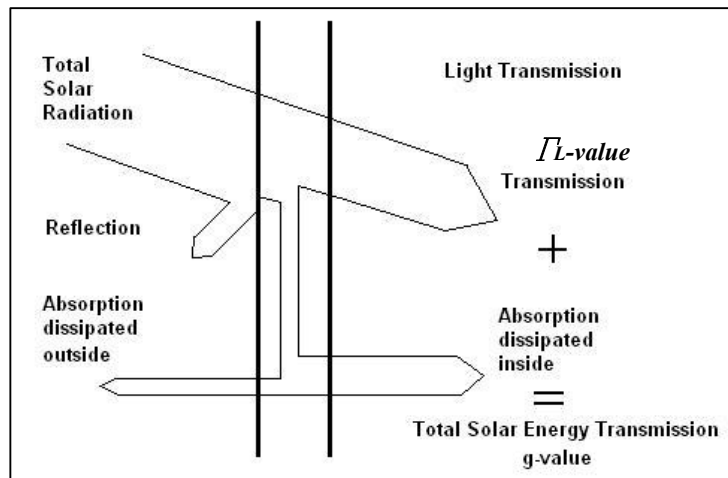


Figure 3.2 Light transmittances through a single pane of glass [5].

Glass has the characteristics to reflect, absorb and transmit solar radiation. Due to its transparency, the amount of light that glass is able to transmit (solar transmittance) is high. Depending on its chemical components, the amount of light that is absorbed and reflected varies. Soda-lime-silica glass has high transmittance levels for

radiation wavelengths between 315 to 3000nm, which means that there is almost no UV, however, visible and near IR are transmitted through it. This means that the wavelengths below 310 and higher than 3000nm are reflected and absorbed. Essentially, this is why glass has the characteristics to create a greenhouse effect as the radiation that passes through it is afterwards reflected in Long-wave by other elements, and is no longer able to pass through the glass back to the exterior.

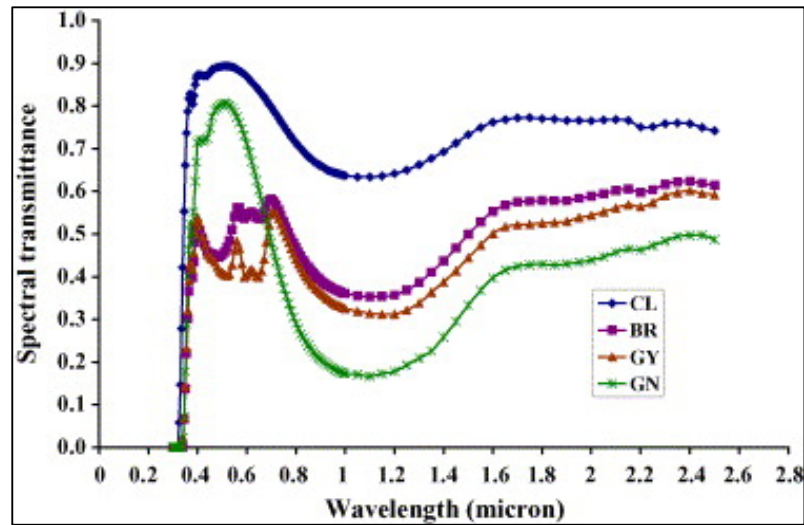


Figure 3.3 Spectral transmittance of Clear and tinted glass [15].
(Chaiyapinunt, S., et al, 2005)

Figure 3.3 show the comparison made by Chaiyapinunt, S., et al of the normal incidence spectral transmittance of clear glass and tinted glasses of 6 mm thickness [15]. In general, most glass has very low transmittance for UV radiation. Clear glass (CL) has an overall high transmittance on visible and near infrared. The capacity of the glass to transmit infrared radiation is clearly affected by its colour and its chemical composition. Green glass, for instance, has good visible light transmittance but very poor performance on the infrared. There are other types of glass available on the market today, such as bronze (BR) or grey (GY); they have a low transmittance for visible and moderate for infrared.

The thickness of glass also has a very important influence on the way that light is transmitted; Visible light transmittance is slightly reduced when thickness is increased. Nevertheless, Short-wave and Long-wave infrared is considerably reduced when thickness is increased. Figure 3.4 illustrates how the spectral transmittance is reduced by the increase of glass thickness.

Although glass and crystal can be differentiated by the reflective and sparkling pattern effects of crystal; the physical difference is basically its molecular composition; in glass the molecules are arranged in irregular patterns. This makes glass transparent but crystal is translucent at best. The most important property of glass is that it allows visible light and short-wave infrared to pass through it. However, it blocks long-wave infrared reflected from the inner building surfaces. It also works as a physical barrier for fluids. The average transmittance of clear float glass is nearly 82% [15a].

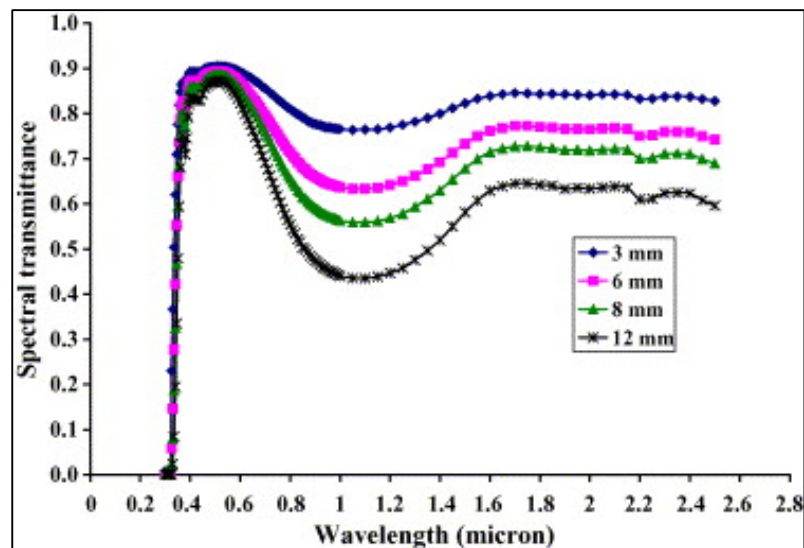


Figure. 3.4 Spectral transmittance of clear glass for various pane thicknesses [15]. (Chaiyapinunt, S., et al, 2005).

In the last century, transparency was not an exclusive property to glass; there were also other materials such as plastics, which were developed to be translucent as well. Plastics have the advantage of increased strength and reduced weight. However, these materials do not have the same durability, heat resistance and thermal transmittance as mineral glass. Although their physical and thermal properties differ from glass, transparency and light transmittance are relatively similar. The difference between glass and plastic is basically its inorganic base. Glass manufacturers attempt to develop glass with better transmittance levels. Although some glass achieves up to 95% of total solar transmittance, some polymers have similar optical properties. Figure 3.5 illustrates the similarity in light transmittance of inorganic and organic glazing materials. The main difference is for long wave IR transmittance; organic materials promote higher levels to be transmitted through them. It is also well known that due to its organic composition, acrylic glazing is rather sensitive to UV radiation, which alters its optical properties with time and suffers damaging effects [18].

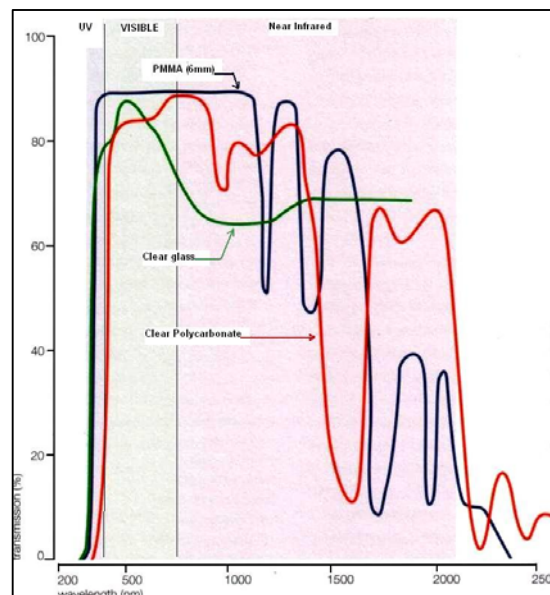


Figure 3.5 Optical properties of inorganic and organic glazing materials [18]. (Wigginton, 2003).

Advances in glass technology have allowed the application of glazing systems to achieve low thermal transmittance levels (*U-value*). This gives designers more freedom to explore the possibilities of extra glazed surfaces on buildings. However, this improvement in insulation and the natural property of glass to trap Long-wave IR, produces a contrary effect in summer conditions. Nowadays, there are more buildings with almost fully glazed envelopes with high insulating glazing. This trend is causing an evident growth in energy use in summer due to increased cooling loads. Although the development of low emissivity (ϵ) glass has allowed designers to improve the use of glass for natural lighting, there is still a necessity to understand in detail the impact on advanced façade systems that involve the increased use of glazing.

Figure 3.6 illustrates the improvement of *U-values* of glazing from approximately $6\text{W}/\text{m}^2\text{K}$ on single glazing, to about $0.5\text{W}/\text{m}^2\text{K}$ in triple glazing units. There is still a lack of reliable data for the performance of vacuum windows. However, there is still a considerable reduction of the capacity of glass to transmit visible light when the *U-value* is reduced. This effect has an important implication for the accurate selection of glass within the design stages, depending of the functionality and performance of the building [6]. Although there is also a slight reduction in the capacity of the glass to let visible light (*T_L-value*) flow when the glass insulation capacity is increased, the reduction is not considerable, when comparing the improvement in insulation and reduction of the total energy transmission factor (*g-value*).

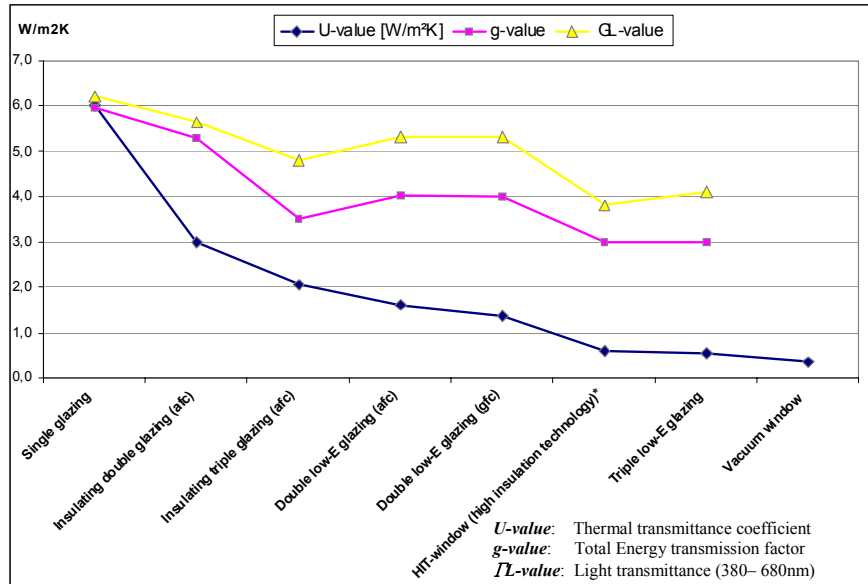


Figure 3.6 Evolution of physical properties of current commercial glass [6]. (Osterle, E., et al, 1999).

3.3 PHYSICS OF LIGHT

3.3.1 Solar Radiation

The sun is a giant fusion reactor; it uses hydrogen, which is turned into helium at a rate of 4 million tonnes per second. On these reactions, a tremendous amount of energy is released and this matter is then transformed into energy. While the sun's inner temperature is about 40million degrees Celsius, the gases at its surface are about 6.000 degrees Celsius; the energy radiated towards the earth is in virtue of this temperature [16].

One third of the solar radiation that reaches the earth is reflected back to space; the rest is absorbed and eventually transmitted as long-wave infrared radiation. The solar constant at the top of the atmosphere is 1354W/m²; about 50% of this insolation reaches the earth's surface at sea level. The earth re-radiates and absorbs energy in a balanced green house effect that permits temperatures on the surface suitable for life [17]. Figure 3.7 Shows the amount of energy reaching the earth at the top of the

atmosphere and at sea level. The minimum values at ground level are due to the absorption of this energy by some of the atmospheric gases such as water vapour, oxygen, nitrogen, carbon dioxide and ozone.

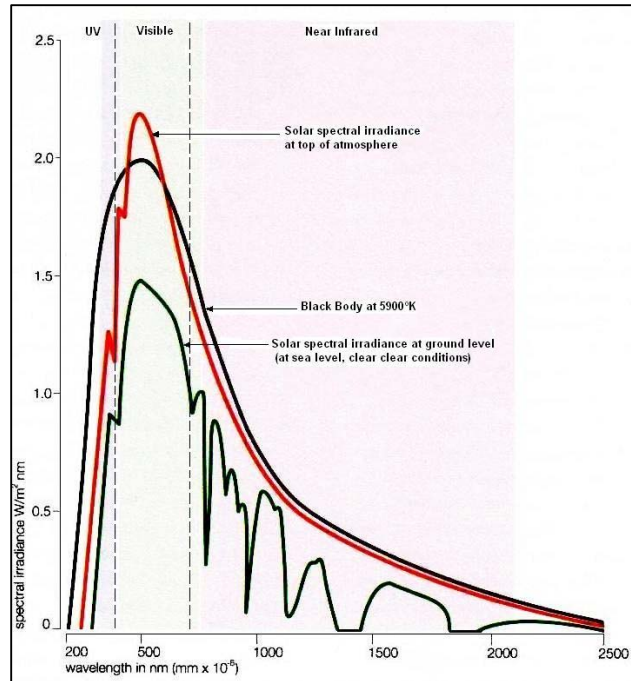


Figure 3.7 Spectral distribution of solar radiation [18].

Solar radiation is emitted in various wavelengths, which all together constitute the solar radiation spectrum. We perceive solar radiation as white light; however it spreads as a wider spectrum that ranges from ultraviolet or very short wavelength, to infrared or very long wavelengths. About 7% of the radiation is ultraviolet, 40% of the total solar radiation that reaches the surface is within the visible region and about 50% is infrared. Just a fraction of the total electromagnetic spectrum reaches the earth's surface.

The human eye is capable of perceiving radiation wavelengths from 380 to 780 nanometres, which are known as visible light. This light is part of the solar

electromagnetic radiation that reaches the surface of the earth. However, there are also other parts of the electromagnetic spectrum that the eye is not able to perceive but has an important influence on the physical environment such as Ultra-Violet radiation with wavelengths less than 380nm and Infra-red radiation with wavelengths longer than 780nm. The maximum sensitivity of the eye to solar radiation corresponds to 550nm [5]. Figure 3.8 illustrates the total electromagnetic spectrum from very short to very long wavelengths.

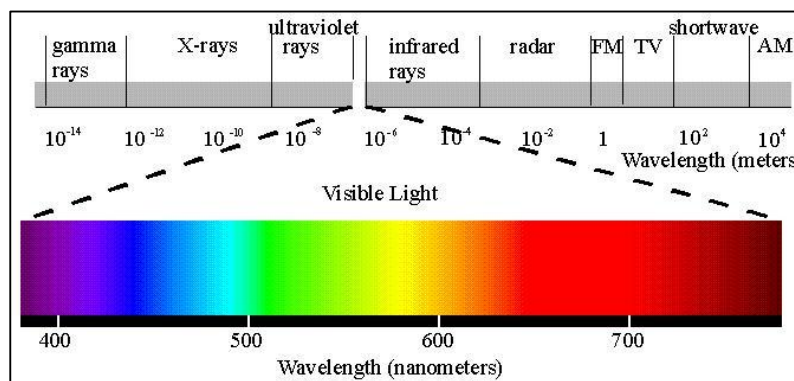


Figure 3.8 Electromagnetic spectrum highlighting visible light [13].

Almost all objects emit, reflect or transmit some light. Numerous types of spectra can be distinguished depending upon the nature of the radiation coming from an object. Building materials also have different responses to light depending on the way they absorb, reflect and transmit radiation. The temperature and chemical composition of a material determines how it emits, reflects or transmits radiation. If the spectrum is composed primarily of thermal radiation much of its emission spectrum is within infrared.

In the case of DSFs, glass is the most relevant material, as it is responsible for the transmission of most of the visible and short wave infrared segments of the spectrum. It was previously described that colour and chemical composition determines its total

transmittance. The amount of visible light and near-IR required into the building is critically dependant on the type of glass used for the facade. Figure 3.9 shows typical spectral transmittance values for common coloured glass. The graph shows how some glass is suitable for transmission of some parts of the visible spectrum and for some parts of the near infrared. This is a factor, which is not always considered by designers when applying glass to facades.

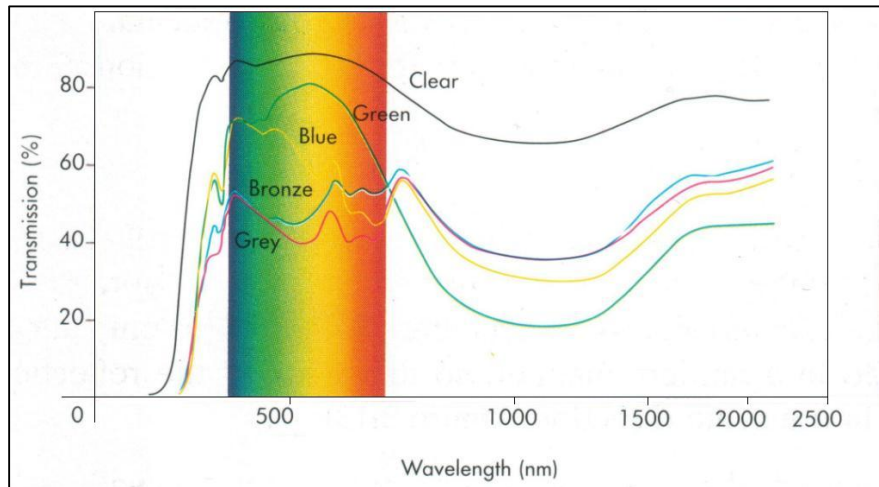


Figure 3.9 Spectral transmittance of most common coloured floated glass [13]. (Button, 1993)

3.3.2 Natural Lighting and DSFs

The growing awareness of energy efficiency in buildings and the rational use of light has been another factor that influences the proliferation of more glazed envelopes on buildings. Heerwagen (1986) [19] and Veich & Gifford (1996) [20] agreed people believe that sunlight has beneficial effects over artificial lighting. The effect of light on people's mood and performance at work is directly linked with the levels of natural lighting. Research in the field of visual comfort confirms that people enjoy having windows in their built surroundings. Studies done on the visual comfort of office workers concluded that awareness of external weather, the ability to see

people and having the option to regulate ventilation and temperature in their spaces, are some of the main reasons why people prefer having more windows in buildings [21].

According to Osterle et al, “*Good natural lighting and unimpeded views out of a building are part of the minimum standards required by guidelines for workplaces in many countries*”. The real requirement of natural lighting is not only the maximization of the amount of light but the improvement in the quality of lighting. The authors suggested that the effects of DSFs on natural lighting are specifically related to the reduction of the amount of light, additional perceived room depth, compensatory effect of large glazing areas and the implications of sun shading devices in the facade [6].

The use of daylight in buildings has become a major factor in the enhancement of the indoor environmental quality of energy efficiency (Fanchiotti et al, 2001) [22]. Nowadays, the use of computer tools, such as RADIANCE software [23], is helping designers and researchers to understand the implications of facades on daylight.

The use of DSFs as a way to improve daylight is an issue that has been analysed previously. Viljoen, A et al [24] studied scale models and computer models to establish the influence of daylight on refurbished buildings. It was found that daylight factor in DSF is slightly reduced at 5m penetration from the facade using the ‘passive zone’ rule of thumb. On both scaled and RADIANCE models they found that the influence of a DSF does not improve floor daylighting factors if compared to single glazed facades. Instead, the authors found that the influence of the plan

configuration, the reflectivity of the internal materials, and window orientation to be key factors in affecting the building's daylight performance. Osterle et al also concluded that the reduction in daylight at 5m penetrations on single glazed facades is about 1% higher than that obtained with DSFs.

Straube et al concluded that *“the amount of window area for daylighting depends on various factors, but Double Facades are certainly not the only or best way to achieve excellent daylighting in commercial buildings”*. They mentioned the pros of DSFs as allowing good daylighting in overcast conditions, but also highlighted the cons with the possibility of glare due to an excess of glazed area. Thus, DSFs and daylighting have to be assessed in the same way as any other building envelope, particularly considering the risks implied by using large glazed surfaces on the facade [25].

3.4 THERMAL ENVIRONMENT

The part of thermodynamics known as heat transfer defines and characterizes the thermal behaviours which are constantly in action everywhere. In a DSF, there are multiple complex and dynamic types of heat transfer, laminar and turbulent flows, temperature, density stratifications, wide-ranging air velocities, which all occur simultaneously. The heterogeneity of physical factors makes the analysis of DSF a complex task. However, some research has been done to develop tools, which offer the possibility of analysing the way DSF behaves and giving the potential to explore the design and thermal response under different conditions. A quick overview of heat transfer and fluid mechanics will help us to establish the complex categories of thermal behaviours relevant to a DSF.

3.4.1 Thermal Buoyancy

The concept of a Double Skin Façade was developed to create a greenhouse effect between the two parallel surfaces of glass, in order to improve thermal insulation. The heat trapped between these layers increases the density of air inside the cavity and develops a difference of pressures and temperatures along the height of the façade. This process is known as thermal buoyancy, which is dependent upon the average temperature difference between the column of warm air. This pressure difference is given by: $\Delta p = 0.043 h \Delta t$, Where p is the air pressure in Pascals, h is height of the column at mean temperature difference Δt from the surrounding air. The resulting air flow is approximately given by: $V = 0.121 A (h \Delta t)^{0.5}$, where V is the volume flow rate (m³/s) and A is the area of each opening (top and bottom equal area) [26].

The warm air inside the cavity tends to flow out of openings at the top of the DSF and cool air will flow at the bottom of the façade (Figure 3.10). The thermal buoyancy for driving natural ventilation is more efficient when the greatest average temperature difference (Δt) and a greater height of the cavity exist. The magnitude of the stack effect is dependent upon the average temperature increment over the full height of the cavity. For improved stack effect, the heat accumulated from solar gains should take place as low down the cavity/stack as possible.

Although in cold conditions the temperature difference is higher and the possibility of air removal by natural means is better, this is when minimal ventilation is required. In warm conditions, the temperatures in the cavity can be high above the comfort zone and only suitable for an unoccupied space. However the temperature

difference upon which the pressure difference, and hence the air flow, depends, is the average temperature of the column of air and not the temperature as it leaves the stack. Thus, the more efficient airflow through the cavity develops the higher and lower the cavity is heated up.

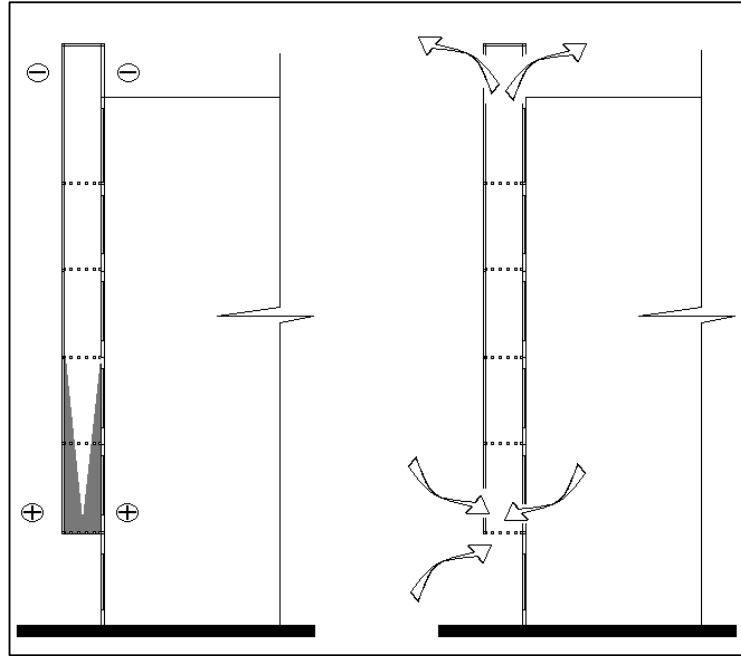


Figure 3.10 Thermal buoyancy leads to vertical pressure differences which drive to stack effect.

3.4.2 Heat Transfer Model of a DSF

The rate of heat transfer under steady state conditions is known in Europe as the *U-value*. Gan presented an analytical solution of heat transfer through a multiple glazing system derived from a double-glazing unit. The thermal transmittance in multiple glazing [27], was translated by the author with the following equation:

$$U = \frac{1}{\frac{1}{h_e} + \frac{1}{h_i} + \frac{1}{h_i}} \quad (3.1)$$

Where:

$$U = W / m^2K$$

$$h_e = \text{External heat transfer coefficient (W/m}^2\text{K)}.$$

$$h_i = \text{Internal heat transfer coefficient (W/m}^2\text{K)}.$$

$$h_t = \text{Conductance of multiple glazing units (W/m}^2\text{K)}.$$

The main heat fluxes through a multiple glazing unit are shown in figure 3.11. The heat source from the exterior is the solar radiation, which is initially reflected on about 15% of the external skin. This process, which depends on the external conditions, determines the external heat transfer coefficient (h_e) and the remaining radiation passes through the glass.

The reflection on the inner glass and inner walls of the cavity creates processes of convection and conduction, which determine the heat transfer coefficient inside the cavity (h), the accumulated and remaining heat by radiation and conduction received by the room determines the heat transfer coefficient (h_i).

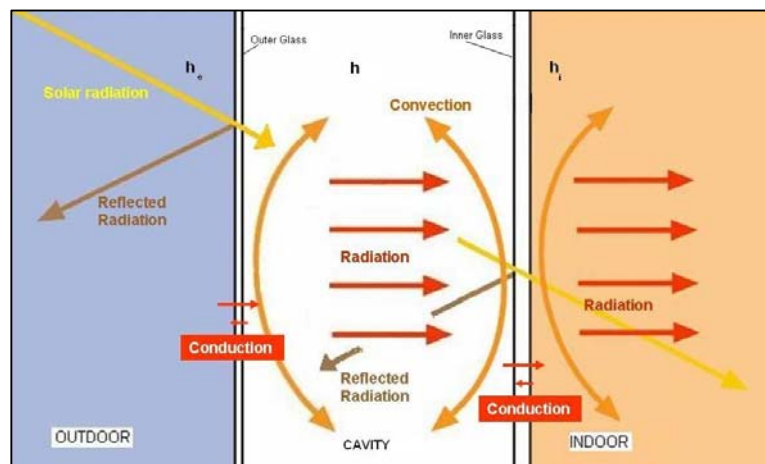


Figure 3.11 Diagram of heat transfer through a double Skin Façade in Summer Conditions

Although the steady-state natural convection flow is present in a Double Skin Façade and represented on the linear equation (3.1) and illustrated by figure 3.11, the heat transfer process in a DSF is very dynamic and complex, which includes the solution of the differential equations in x , y and z directions cited before as the transport equations for mass, momentum and energy.

3.4.3 Heat Fluxes in a DSF Model

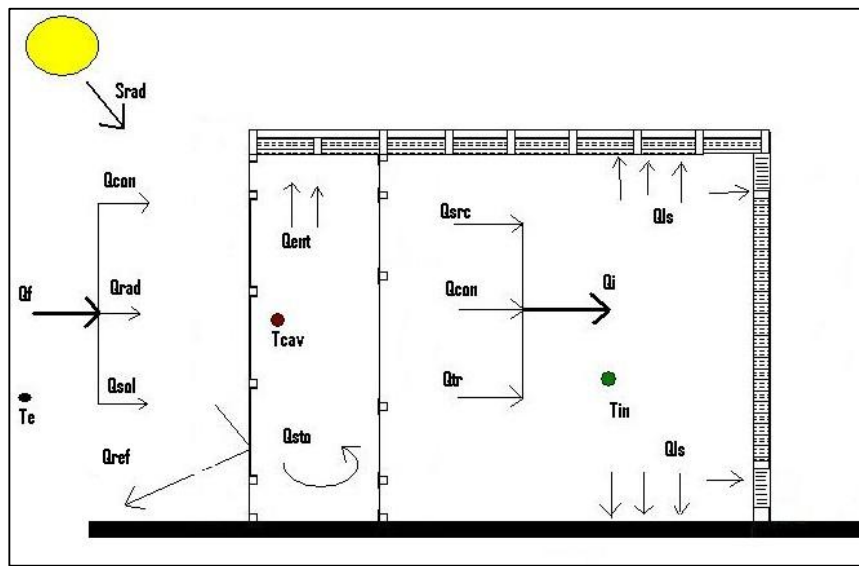


Figure 3.12 Main heat fluxes in the chamber.

According to Faggenbau et al [28], the main heat fluxes developed in a double skin façade are illustrated in figure 3.12. The external façade gain (Q_f) (W/m^2) is formed by the sum of the gains from: Convective heat gains (Q_{con}), Radiative heat gains (Q_{rad}) and Solar gains (Q_{sol}), which are the result of the Radiation received (S_{rad}) minus the radiation reflected by the façade (R_{ref}).

$$Q_{sol} = S_{rad} - R_{ref} \quad (3.2)$$

In this order, the external façade gains are:

$$Q_f = Q_{con} + Q_{rad} + Q_{sol} \quad (3.3)$$

The net heat gains inside the room (Q_i) are produced by the incident solar radiation inside the room (Q_{src}), the Convection heat transfer of the room (Q_{con}) and the thermal radiation of the surfaces (Q_{tr}). Thus;

$$Q_i = Q_{sr} + Q_{con} + Q_{tr} \quad (3.4)$$

The heat gains in the cavity (Q_c) of the Double Skin façade are; the enthalpic (convective and conductive) gains from the channel (Q_{ent}) and the gains from the energy absorbed by the façade elements (Q_{sto}). Thus the heat balance is expressed:

$$Q_f = Q_i + (Q_{ent} + Q_{sto}) \quad (3.5)$$

The total incident energy entering the room (Q_r), is the result of the net indoor gains (Q_{ni}) minus the heat losses (Q_{ls}) in the room. Thus;

$$Q_r = Q_{ni} - Q_{ls} \quad (3.6)$$

The total indoor gain is the value to keep into account when calculating the heat loads for the HVAC system. It is also the key factor in determining the performance of a DSF system.

3.4.4 Theoretical model of the Facade

Sedlak et al [29] developed the basis of a theoretical model of energy balance within the facade cavity. The model was used to estimate the temperature profile of a double skin facade with different glazing, material composition and size variations. The model is based on the following issues:

- Spectral solar transmittance (τ) and infrared reflectance (ρ) of clear float and low-e glazing on the facade.
- Temperature distribution only on z direction $\theta(x, y, z) = \theta z$
- Air velocity is constant $v(x, y, z) = v$ (m/s)

The model considered the following description for heat gains of the DSF:

Heat gain from solar radiation:

$$dQ_s = \tau I \Delta y dz \quad (3.7)$$

Heat transfer through the external or internal l skin of the facade:

$$dQ_j = U_j \Delta (\Theta(z) - \Theta_j), j = i, e \quad (3.8)$$

Heat gain within the facade cavity:

$$dQ = C_p \rho \Delta x \Delta y \Theta(z) dz \quad (3.9)$$

Where:

τ = Transmittance of solar radiation on the external skin of the facade.

I = Intensity of solar radiation (W/m²°K)

C_p = Specific heat capacity of air (J/kg°K)

ρ = Density of air (kg/m³)

Δx = distance of x direction (cavity depth)

Δy = distance on y direction (cavity width)

$\theta(z)$ = temperature within the cavity (z direction).

θ_j = temperatures; θ_e =outdoor air, θ_i =indoor air (°C)

The authors expressed the temperature distribution within the cavity on z direction, the heat gain within the cavity depending on the height (z) of the cavity and the airflow velocity (v), through the following equation:

$$\Theta(z) = \frac{\partial \Theta}{\partial \tau} = \frac{d\Theta}{dz} \frac{dz}{d\tau} v = \Theta(z)v \quad (3.10)$$

The determination of the temperature within the cavity is solved by the following equation:

$$\Theta(z, v) = \frac{1}{a} \left[a - (a - a_o \Theta_o) e^{-\frac{a_o(v)(z-z_o)}{a_1}} \right] \quad (3.11)$$

Where:

$\theta_o = \theta(z_o) =$ temperature of the air at the inlet height (z_o) of the DSF (°C).

Finally, the authors determined the total energy balance of the facade through the following equation:

$$Q = V \cdot \rho \cdot C_p \sum_{j=1}^n [\theta_{vi}(t_j) - \theta_e(t_j)] \Delta t \quad (3.12)$$

Where:

V = Volumetric air flow rate (m³/s)

C_p = Specific heat of air (J/kg°K)

θ_{vi} = Air temperature at the ventilation inlet (°C).

θ_e = External air temperature (°C).

t = time (s)

3.4.5 Thermal Performance of DSFs

Research on thermal performance of DSFs is mainly based on theoretical models developed to calculate the inter-space temperature behaviour and flow characteristics of mechanically and naturally ventilated facades. Stec & van Paassen developed a simulation model in which the temperature field was validated by measuring in test facilities and a real office building. Although the authors found reasonably accurate results for the simplified models and the experimental data, they suggested more detailed research for the assessment on the induction of the airflow due to buoyancy, analysis of the airflow in the cavity and the interior of the building, and finally, the influence of the construction details inside the double skin facade [30].

Grabe (2002) developed and validated a simulation algorithm for temperature behaviour and flow characteristics of double facades in order to provide a simple tool for calculation without the need to use fairly complicated CFD tools. As the model

was compared with controlled and monitored results, the author found that inaccuracies in some cases were based on the modelling of flow resistance according to the geometry of the facade [31].

For some authors, the accuracy of the models depended on the complexity of the numerical models and the accurate understanding of the system inter-relationships. According to Bartak et al (2001), *“a strong thermodynamic coupling exists between the air flow through the naturally ventilated double-skin façade, and the air temperature difference between the cavity of the double-skin façade and outside. This interaction can only be predicted by sophisticated and state-of-the art building energy modelling and simulation techniques”*.

Poirazis et al (2003) studied the behaviour of 4 different types of DSFs and calculated the temperature on different heights of the cavity using WIS, MathCAD software and their own numerical model. The authors determined that there is a very strong influence on the thermal insulation quality of the DSF when internal elements (blinds) are used inside the facade. The differences in temperature inside and outside, and the cavity openings, are also factors highlighted as important in order to increase or decrease *U-values* on the facade. They basically stated that the relation of inlet/outlet gaps are important to reduce the energy transmitted through ventilation air, and the presence of blinds inside the facade is also a critical factor affecting the overall *U-values* inside the facade cavity [33].

Although most literature offers various approaches of numerical models assessing the thermal behaviour of Double Skin Facades; each model is developed for very

specific conditions. As a result of the intricate processes within a DSF, there are no general tools yet available to assess simplified DSF models. The most realistic and accurate models were developed using Computer Fluid Dynamics software. However, the geometrical complexity required for accurate models, and the limitation of computational resources are still major constraints highlighted by most authors, applying CFD as a tool to simulate thermal performance.

3.4.6 Overheating in DSFs

One of the reasons for the development of Double Skin Facades was the improvement of thermal insulation of fully glazed buildings. However, the addition of a second skin is not as straightforward a solution as it seems. Thomas [34] highlights the implications of placing a second ‘skin’ on the building envelope: *“This can help to reduce heat loss while maintaining most of the benefits of solar gain directly into the building. It can also trap potentially useful solar heat between the skins”*. The possibility of uncontrolled heat accumulated within the ‘buffer’ space is mentioned by some authors, yet, detailed information about the development and specific causes of overheating have not yet been fully assessed.

Faggenbauu et al [28a,b] addressed the issue of large glazed areas, arguing that increased heat gains are a critical matter in Mediterranean countries. The authors assessed the implication of transparent insulation and phase change materials incorporated in ventilated facades. Using a numerical model, they compared the differences of total load from the facade using the different materials on the facade. They stated that the alternatives to maintain reasonable levels of heat gains of the facade in summer conditions must be based on a careful selection of glass, assessing

its behaviour with the incorporation of partially opaque shading devices or transparent insulation materials (TIM).

Gratia and De Herde (2007) analysed how favourable the greenhouse effect is in DSFs. Despite direct, indirect and casual gains; the authors stressed that the addition of an extra skin and faulty operation of the double skin facade openings, are the most critical causes contributing to overheating on fully glazed buildings. They basically found that the greenhouse effect can be moderately advantageous, depending specifically on the building orientation. The authors concluded the south facing facade is the most favourable and the east-west orientations are the most critical to prevent and assess overheating [35].

Geissler [36] investigated and compared the thermal performance of some recently built double facade constructions. The author shows various cases displaying *U-values*, *g-values* and vision area of the facade. He illustrated the two most common types of DSFs, which are based on low-e coating on inner skin and low-e coating on external skin. In general, all facade types have low *g-values*, which, according to the author, are achievable even on unventilated double facades with regard to solar control, due to the use of high quality coatings for glass products. Nevertheless, the author does not show a clear comparative assessment of how the facade actually performs in critical conditions.

Osterle et al [6] mentions within the planning steps, the necessity of avoiding overheating in the intermediate space as a requirement, depending on careful dimensioning of the openings in order to limit heat gains in summer. The author

made a qualitative reference to the stratification within the cavity, highlighting the risk of increased heat loads on the top storey and upper part of the facade.

3.5 AIR FLOW - VENTILATION

The main factor that encourages air movement inside ventilated cavities is pressure difference. This is caused by thermal buoyancy, the action of wind around the building or mechanical operation. Osterle et al [6] provided an examination of the main airflow processes that result from thermal buoyancy on Double Skin Facades.

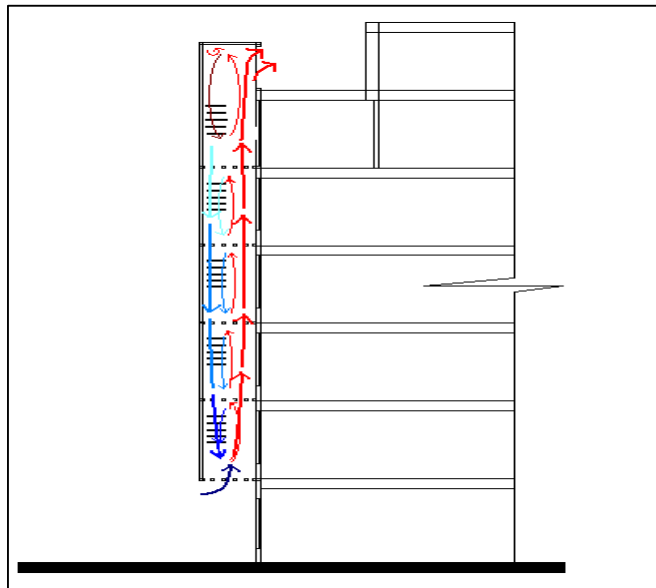


Figure 3.13 Hot air develops stack effect and upward airflow inside the cavity of a Double Skin Facade.

According to the authors, DSFs encourage air movement inside the cavity as a result of the greenhouse effect created between the two skins of glass, the heated air density is lessened and buoyancy starts to develop creating a stack effect, lifting hot air to the upper section of the facade and forcing cold air to enter from the bottom (Figure 3.13). However, the temperature difference (ΔT) between outside and inside the cavity also causes air movement within the cavity. In this case, the pressure is high

on the bottom and low on the top of the façade, creating an opposite flow down to the inlet. The thermal uplift (Δp_{th}) inside the facade cavity is expressed by the following equation:

$$\Delta p_{th} = \Delta \rho' \cdot g \cdot \Delta h \cdot \Delta T_m \quad [\text{Pa}] \quad (3.13)$$

Where:

$\Delta \rho'$ = Specific change of air density in relation with temperature change (kg/m³°K).

g = Gravitational acceleration (9,81m/s²).

Δh = Effective difference of height of the facade cavity (m).

ΔT_m = Mean excess temperature (°K)

The specific change of density ($\Delta \rho'$) is derived from the law of gases to the following formula:

$$\Delta \rho' = \frac{\rho}{T_{ab}} = [0.004 \text{ kg/m}^3\text{°K}] \quad (3.14)$$

And the absolute temperature (T_{ab}) is can be expressed by:

$$T_{ab} = T_{zu} + \Delta T_m + 273,15 \quad [^\circ\text{K}] \quad (3.15)$$

The wind outside the facade also has an influence on the airflow inside the cavity, the pressure created by pressure difference inside the facade and outside is known as ‘stagnation pressure’ (q), which is expressed as:

$$q = \frac{\rho}{2} v^2 \quad [\text{Pa}] \quad (3.16)$$

Where:

ρ = Density of air (kg/m³)

v = Outside air velocity (m/s)

The pressure of the exterior wind (p_{wind}) is given by the specific wind pressure coefficients (cp) which depend on the facade orientation. The values of these coefficients are positive on the pressure zones facing the wind and negative on the suction zones towards the wind direction. The pressure is expressed by the following formula:

$$p_{wind} = cp \cdot q \quad [\text{Pa}] \quad (3.17)$$

According to Osterle et al, *“the pressure differences between upper and lower openings are regarded as forces acting on the areas of the openings, whereby the motive force is the product of the pressure difference taken in conjunction with the opening area”*. This is known as pressure loss (Δp_{loss}), which is formulated as:

$$\Delta p_{loss} = \zeta \cdot q \quad [\text{Pa}] \quad (3.18)$$

The balance of the volume of air admitted at the inlet (V_{in}) is equivalent to the amount of air leaving the cavity through the outlet (V_{out}), known as the continuity equation, which is expressed basically by:

$$\dot{V}_{in} = \dot{V}_{out} \quad \text{or} \quad A_{in} \cdot v_{in} = A_{out} \cdot v_{out} \quad [\text{m}^3] \quad (3.19)$$

Where:

V = Airflow volume (m³)

A = Opening area (m²)

v = Air velocity (m/s)

This relation establishes that when there is an alteration of the opening area, the air velocity must be increased in order to keep the continuity balance. The concept of pressure equilibrium (Δp_{loss}) is expressed as:

$$\Delta p_{loss} = \Delta p_{th} + \Delta p_{wind} \quad [\text{Pa}] \quad (3.20)$$

Where:

Δp_{th} = Thermal buoyancy pressure (Pa)

Δp_{wind} = Wind pressure (Pa)

The previous basic equations provide an overall idea of the airflow from the inside to the outside of the facade. However, the variation of the airstreams inside a DSF are very complex and depend on the interaction of all the elements, which contributes to the local and total heat transfer coefficients of the facade that determine the manner in which the flow behaves. For this reason, CFD analysis is a very useful tool to calculate detailed flow patterns, because the momentum, mass, energy and radiation equations are discretized and calculated to obtain the flow behaviour inside the facade.

The two basic types of airflows present inside a DSF are defined as *turbulent* when high inertia forces are present and *laminar* when friction forces prevail over the forces of inertia. Turbulent flows depend on air velocity and the viscosity of the fluid, known as the Reynolds number, which is the relationship between centrifugal force and adhesion. This is expressed as:

$$\text{Re} = v \cdot \frac{L}{\nu} \quad (3.21)$$

Where:

v = Air velocity (m/s).

L = Dimension of the change of direction of the air stream (m)

ν = Kinematic viscosity of air [$\sim 15.5 \times 10^{-6}$ m²/s]

There is a critical Reynolds number value when turbulence occurs. According to Osterle, the critical Re in DSFs is from 10.000 to 20.000. Grabe (2002) [31] stated that “*with natural ventilation inside the cavity, the driving force is the reduction of the density due to the increase of air temperature. This increase is greater near the heat sources, thus near the panes and the shading device. Further on it might be non-symmetrical because of different magnitudes of the heat sources*”. This means that the laminar flow created within the facade is higher on the inlet and sharply decreased half way down the total height, and finally increased in reduced magnitude on the outlet. This means that the inlet/outlet relationship plays a key role in determining the quality of the laminar flow in the cavity. Figure 3.14 illustrates the profile of the velocity inside a double skin facade with inlets on the bottom and outlets at the top of the cavity.

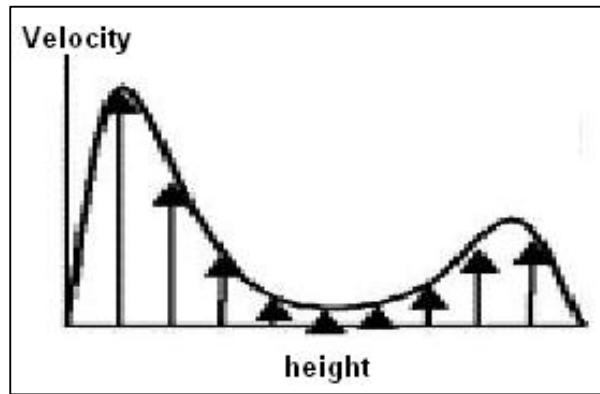


Figure 3.14 Laminar velocity profile inside a double skin facade [31].
(von Grabe, 2002)

As previously discussed, one of the main features of DSFs is the capacity to accumulate heat and promote stack effect. Nevertheless, the necessity of air exchange is important. Thus, in order to prevent overheating, appropriate removal of warm air at the top during summer is important. The amount of heat removed by convection (Q_{conv}) can be expressed by the following equation:

$$Q_{conv} = \rho \cdot C_p \cdot \dot{V} \cdot \Delta T \quad [\text{Kw}] \quad (3.22)$$

Where:

ρ = Density of air (kg/m^3)

C_p = Specific heat of air (1.20kg/m^3 at 20°C)

\dot{V} = Resultant air stream volume (m^3)

ΔT = Difference of temperature between air supply and exhaust air.

3.6 CONCLUSIONS

The main physical aspects relative to the physical basis of DSFs were identified in this chapter fundamentally by its effect on the thermal behaviour of the facade.

According to previous literature, the following aspects can be summarized as the

main physical aspects, which affect the thermal behaviour of a Double Skin Facade:

- It was identified that the thermal response of the facade is dependant on the type of elements used inside the cavity as ‘secondary’ and ‘tertiary’ structures.
- The selection of materials for the internal and external skin is highly dependant on the type of glass and colour, which has dramatic consequences on how solar radiation is managed through the facade.
- The importance of glass as a main material for the facade ‘skins’ is a critical issue, which has to be assessed carefully.
- The form of the facade is important but not as relevant as the openings configurations.
- Natural lighting is also an important issue, which has to be taken into account in conjunction with the thermal assessment.
- The airflow inside the cavity of a DSF determines the rate in which heat can be removed from the facade; the inlet/outlet relationship also plays a key role in determining the quality of the laminar flow in the cavity. However, the control of solar radiation and greenhouse effect inside the facade are the most critical factors that have to be considered, when assessing the thermal behaviour and overheating control in a DSF.

Heat transfer coefficients inside the facade are very dynamic and complex processes, which include the solution of the differential equations in x , y and z directions. The physics of heat transfer inside a double skin facade are complex issues, which require simultaneous analysis of the transport of heat due to conduction, convection and radiation. Some authors refer to CFD as a useful tool to analyse the airflow and thermal performance of Double Skin Facades.

REFERENCES

1. Poirazis, H., Double Skin Facades - A Literature Review. 2004, Division of Energy and Building Design, Department of Construction and Architecture, Lund Institute of Technology: Lund. p. 196.
2. Uuttu, S., Study of Current Structures in Double Skin Facades, in Department of Civil and Environmental Engineering. 2001, Helsinki University of Technology: Helsinki, Finland.
3. Gan, G., Simulation of buoyancy-induced flow in open cavities for natural ventilation. *Energy and Buildings*, 2006. 38(5): p. 410-420.
4. Faist, A.P., Double Skin Walls. 1998, Institute de Technique du Batiment: Department d'Architecture, Ecole Polytechnique Federal de Lausanne (EPFL), Switzerland.
5. Compagno, A., Intelligent Glass Facades. 5th revised and updated ed. 2002, Basel, Boston, Berlin: Birkhäuser.
6. Oesterle, L., Lutz & Heusler, Double Skin Facades: Integrated Planning, ed. Prestell. 1999. 208.
7. Aarons, D., Properties and applications of double-skin building facades, in Dept. of Architecture. 2000, Massachusetts Institute of Technology (MIT): USA. p. 277.
8. Jager, W., Double Skin FACades -Sustainable Concepts. Presentation of Hydro for Syd Bygg 2003. 2003: Malmo, Sweeden.
9. Lee, E., et al., High-Performance Commercial Building Facades. 2002, Building Technologies Program, Environmental Energy Technologies Division, Ernest Orlando Lawrence Berkeley National Laboratory, University of California: Berkeley, CA. p. 133.
10. Gratia, E. and A. De Herde, The most efficient position of shading devices in a double-skin facade. *Energy and Buildings*, 2007. 39(3): p. 364-373.
11. Stec, W.J., A.H.C. van Paassen, and A. Maziarz, Modelling the double skin facade with plants. *Energy and Buildings*, 2005. 37(5): p. 419-427.
12. Addington, D.M. and D. Schodek, Smart Materials and Technologies for the architecture and design professions. 2005, Oxford: Architectural Press. 241.
13. Button, D., et al., Glass in Building: Guide to Modern Architectural Glass Performance, ed. D. Button and B. Pye. 1993: Pilkington Glass Ltd, Butterworth-Heinemann Ltd. 372.
14. Saint-Gobain, Glass Guide. 2000, Goole East Ridding Yorkshire, UK: Saint-Gobain Glass UK. 617.
15. Chaiyapinunt, S., et al., Performance rating of glass windows and glass windows with films in aspect of thermal comfort and heat transmission. *Energy and Buildings*, 2005. 37(7): p. 725-738.

- 15a Pilkington, The Glass Range for Architects and Specifiers. 2006, Pilkington Group Limited: UK. p.18.
<http://www.pilkington.com/resources/glassrangebroanddatasheetjune2006.pdf>
16. Boyle, G., Renewable Energy: Power for a Sustainable Future. 4th ed. 2002, Oxford: Oxford University Press.
17. Hinrichs, R.A. and M. Kleinbach, Energy: Its use and the environment. 2002, New York: Brooks/Cole Thomson Learning. 585.
18. Wigginton, M., Glass in Architecture. 2003, New York: Phaidon Press Inc. 320.
19. Heerwagen, J.H. and D.R. Heerwagen, Lighting and Psychological Comfort. Lighting Design and Applications, 1986. 16: p. 47-51.
20. Veich, J.A. and R. Gifford, Assessing beliefs about lighting effects on health, performance, mood and social behavior. Environment and Behaviour, 1996. 28: p. 446-470.
21. Bell, P.A., et al., Environmental Psychology. 5th ed. 2001, Ft Worth: Harcourt Brace: Thomson Wadsworth. 634.
22. Fanciotti, A. and C. Amorim. Daylighting in Commercial Buildings: The Use of New Components and Design Solutions to Optimize Visual Comfort and Energy Efficiency. in 7th IBPSA Conference. 2001. Rio de Janeiro, Brazil.
- 23 Larson, G.W., Radiance software. 1985, Lawrence Berkeley National Laboratory (LBNL): Berkeley, California.
24. Viljoen, A., et al., Investigations for improving the daylighting potential of double-skinned office buildings. Solar Energy, 1997. 59(4-6): p. 179-194.
25. Straube, J.F. and R.V. Straaten, The Technical Merit of Double Skin Facade Buildings. 2003, School of Architecture, University of Waterloo: Waterloo, USA.
26. Baker, N. and K. Steemers, Energy and Environment in Architecture. 2nd ed. 2005, Oxon, UK: Taylor and Francis.p.p 224
- 27 Gan, G., Thermal transmittance of multiple glazing: computational fluid dynamics prediction. Applied Thermal Engineering, 2001. 21(15): p. 1583-1592.
28. Faggembauu, D., et al. Strategies to reduce thermal overheating in Mediterranean climates using large glazed areas. in Fier 2002: International Forum on Renewable Energies. 2002. Tetuan: FIER 2002.
- 28a. Faggembauu, D., et al., Numerical analysis of the thermal behaviour of ventilated glazed facades in Mediterranean climates. Part I: development and validation of a numerical model. Solar Energy, 2003. 75(3): p. 217-228.
- 28b. Faggembauu, D., et al., Numerical analysis of the thermal behaviour of glazed ventilated facades in Mediterranean climates. Part II: applications and analysis of results. Solar Energy, 2003. 75(3): p. 229-239.

29. Sedlak, J., M. Jaros, and J. Mohelnikova. Energy Assessment of Double-Skin Glazed Facade. in *Glass in Buildings*. 2005. Bath, UK: Centre of Window & Cladding Technology, University of Bath.
30. Stec, W. and D. van Paassen, Defining the performance of the Double Skin Facade with the use of Simulation model, in *Energy in Built Environment*, Energy Technology, TU Delft: Mekelweg 2,Delft, The Netherlands.
31. von Grabe, J., A prediction tool for the temperature field of double facades. *Energy and Buildings*, 2002. 34(9): p. 891-899.
32. Bartak, M., T. Dunovska, and J.L.M. Hensen. Design Support Simulations for a Double Skin Facade. in *1st International Conference on Renewable Energy in Buildings "Sustainable Buildings and Solar Energy 2001"*. 2001. Prague, Czech Republic.
33. Poirazis, H. and J.L.J. Rosenfeld, Modelling of Double Skin Facades - Results obtained using WIS. 2003, Technical University of Denmark (DTU): Sagsrapport, Denmark.
34. Thomas, R., *Environmental Design: An introduction for architects and designers*. 2005: Taylor & Francis Ltd. 272.
35. Gratia, E. and A. De Herde, Greenhouse effect in double-skin facade. *Energy and Buildings*, 2007. 39(2): p. 199-211.
36. Geissler, A. The Case for Ventilated Facades - Latest Developments to Prevent Solar Overheating of Highly Glazed Buildings. in *Glass in Buildings*. 2005. Bath, UK: Centre of Window & Cladding Technology, University of Bath.

CHAPTER IV

EXPERIMENTAL FACILITY AND SETUP

4.1 INTRODUCTION

Previous studies of the thermal performance of Double Skin Facades have been done using specific buildings. These case studies were mainly based on computer models of airflow simulations, thermal performance and daylighting. There has been no previous experimental parametric assessment of the impact of different configurations of the facade correlated with thermal performance, and specially the effects of these on overheating. For this reason, the experimental model built at the University of Nottingham represents a type of Double Skin Facade in which various physical arrangements of the cavity are analysed in order to understand their impact on thermal performance and overheating development.

For this experimental assessment, the type of DSF selected was a one storey Box-Double Skin model with an adjacent room. This facade was chosen as it can be built inside a laboratory without the direct incidence of external variations of weather,. This allows for the comparing of thermal performance for various configurations of the facade cavity. This chapter provides a general account of the physical construction, equipment, specifications and procedures of the Experimental model of the Box-Double Skin Facade chamber built at The School of the Built Environment in Nottingham University.

This chapter particularly describes the following issues:

- Experimental Facilities.
- Test procedures.
- Physical configurations of the Experimental Chamber.

4.2 EXPERIMENTAL FACILITY



Figure 4.1 Experimental Facility: Box-Double Skin Facade Chamber at the School of the Built Environment of Nottingham University.

The experimental study was carried out using the rig shown in figure 4.1. This full-scale chamber has total dimensions of 2400 x 2550 x 3400 millimetres (W x H x D). The Chamber is one storey high and located in a module of a Box-Double Skin Facade. It has the option to open and close air inlet shafts placed on the external skin. There are three inlet shafts along the top of the facade and three along the bottom. Each of the inlets and outlets shafts is 700mm wide and 200mm high, with a total dimension of 2200 x 200 millimetres (W x H) on top and bottom. Figure 4.2

illustrates the general external dimensions of the experimental chamber and the locations of the inlet and outlet shafts on the external skin. Figure 4.3 shows the total dimensions of the chamber along with the main configuration of the cavity and room.

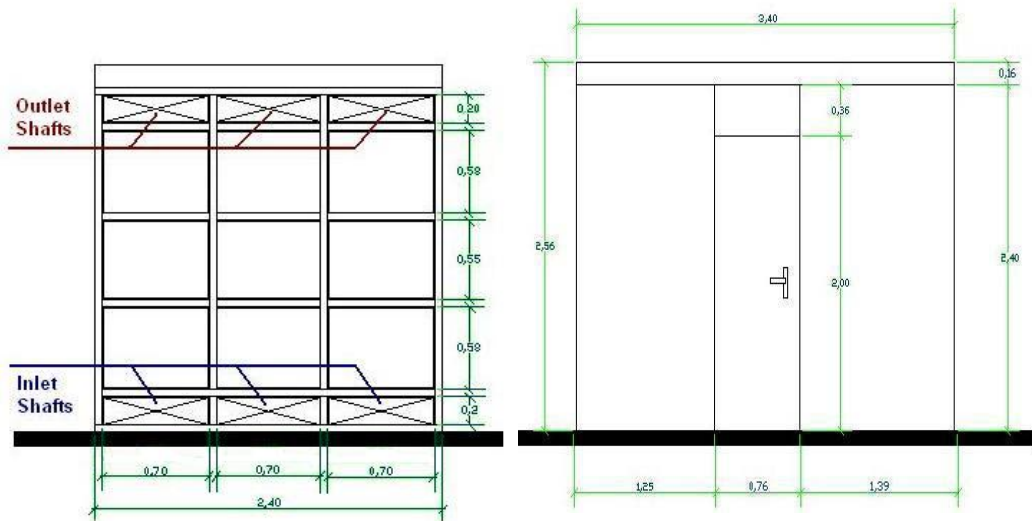


Figure 4.2 DSF Experimental Chamber: Side Elevation.

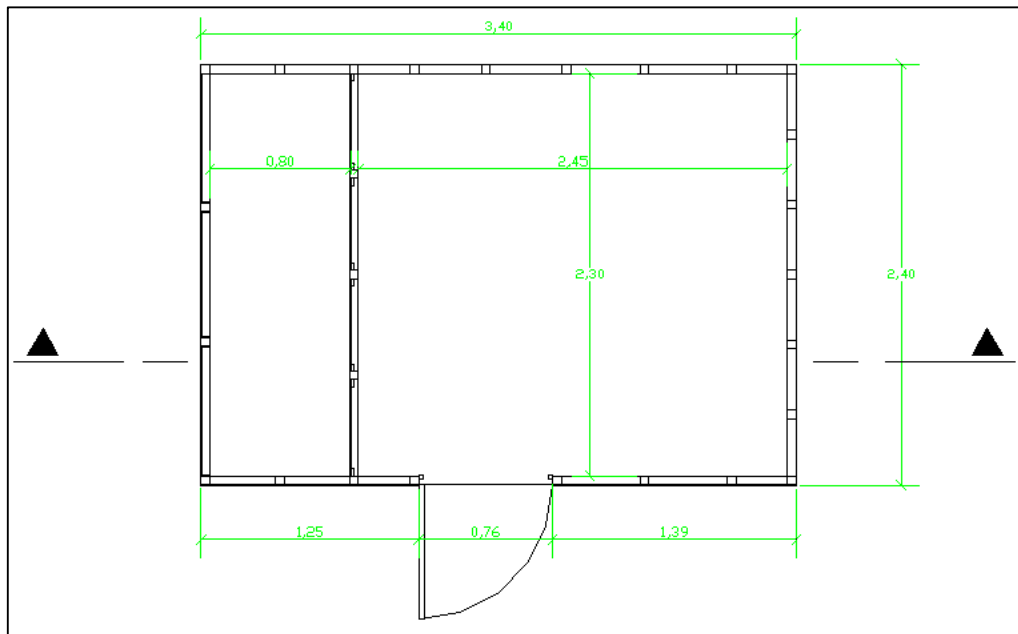


Figure 4.3 DSF Experimental Chamber Plan view.

The cavity's internal dimensions are 2300 x 2300 x 800 mm (W x H x D). The cavity depth can be modified, as the inner skin is adjustable. The room next to the DSF has internal dimensions of 2450 x 2300 x 2300 (W x H x D). The walls and ceiling of both the cavity and room are insulated.. For the experimental analysis, the room was kept sealed in order to minimise heat loss.

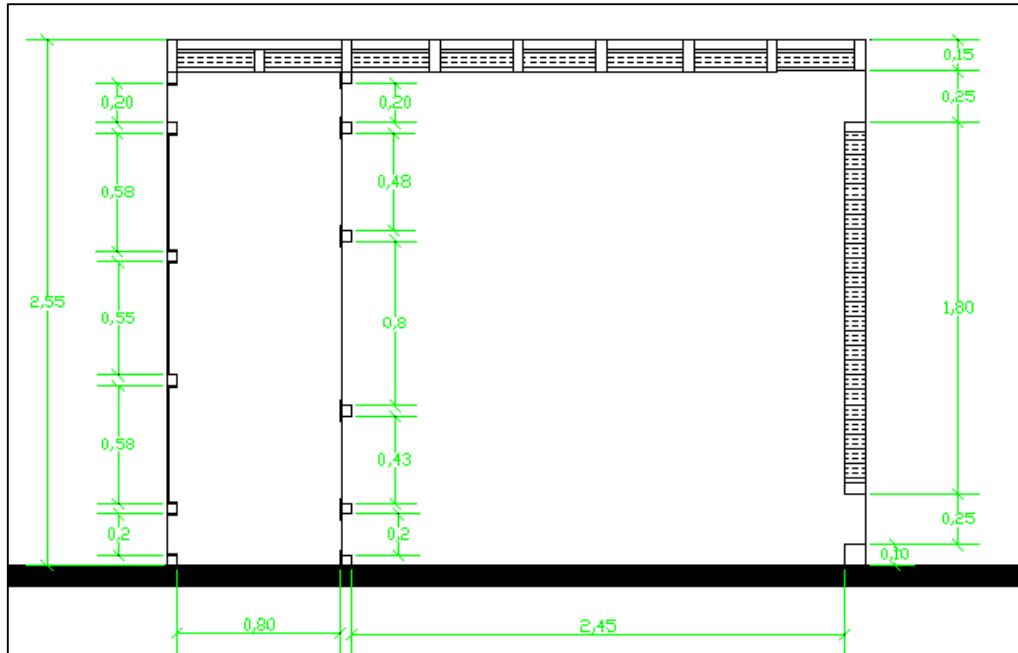


Figure 4.4 DSF Experimental Chamber: Section.

4.2.1 Test Chamber

The chamber was timber built and the walls and cavity floor insulated using rigid thermal insulation panels. The double glazed facade means that the glass panels can be replaced with reflective coated timber panels on the external skin. The room has inlet and outlet shafts located at the top and bottom of the back wall. These shafts were kept closed for most of the tests. However, in the cross ventilation test the shafts were left open so that the thermal behaviour with cross ventilation could be assessed.

The rig was insulated by panels to control heat loss from the room and side walls. According to the manufacturer, the thermal transmittance (U -value) of the panels is $0,22\text{W/m}^2\text{K}$ [1]. The chamber used the current floor of the laboratory, which is concrete, and has a U -value of $0,25\text{W/m}^2\text{K}$ [2]. The cavity floor, side walls and ceiling were fitted with the same insulation panels as used for the room and covered with reflective aluminium sheet to increase reflectance. Figure 4.5 shows a section of the chamber including a description of the materials and main configuration.

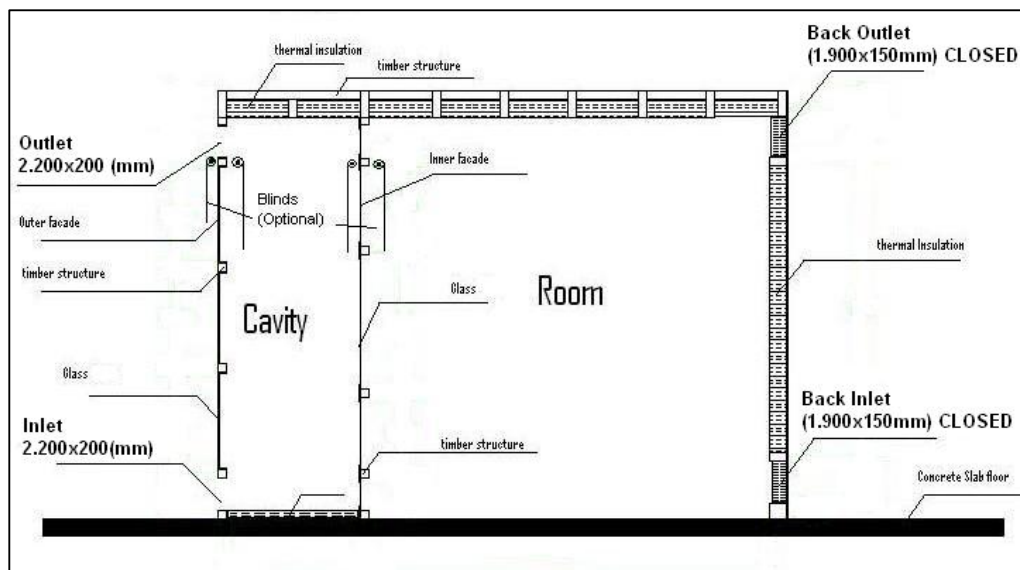


Figure 4.5 Experimental chamber description and materials: Section.

The inner skin is adjustable and can be covered by reflective coated timber panels or can be adapted to allow for the use of blinds or louvers as shading devices. Figure 4.6 illustrates the arrangement of the chamber in the plan, with openings for glazing on the external and internal skins of the cavity. The main thermal parameters (as detailed in table 4.1) were pre set in order to define the experimental conditions of the materials used in the experimental facility.

Table 4.1 Main thermal parameters of the experimental chamber

Walls thermal transmittance (U-Value):	0,22W/mt ² K [1]
Chamber floor (U-Value):	0,25W/mt ² K [2]
Blinds (g-value):	0,15W/mt ² K [3]
Blinds - fabric light transmittance:	0,42 [3]
Blinds - fabric reflectance :	0,64 [3]
Glass transmittance -clear 4mm:	0,82 [4]
Glass transmittance -textured 4mm:	0,79 [4]
Glass transmittance -green 4mm:	0,75 [4]
Clear glass U-value – single 4mm:	5,4 W/mt ² K[4]

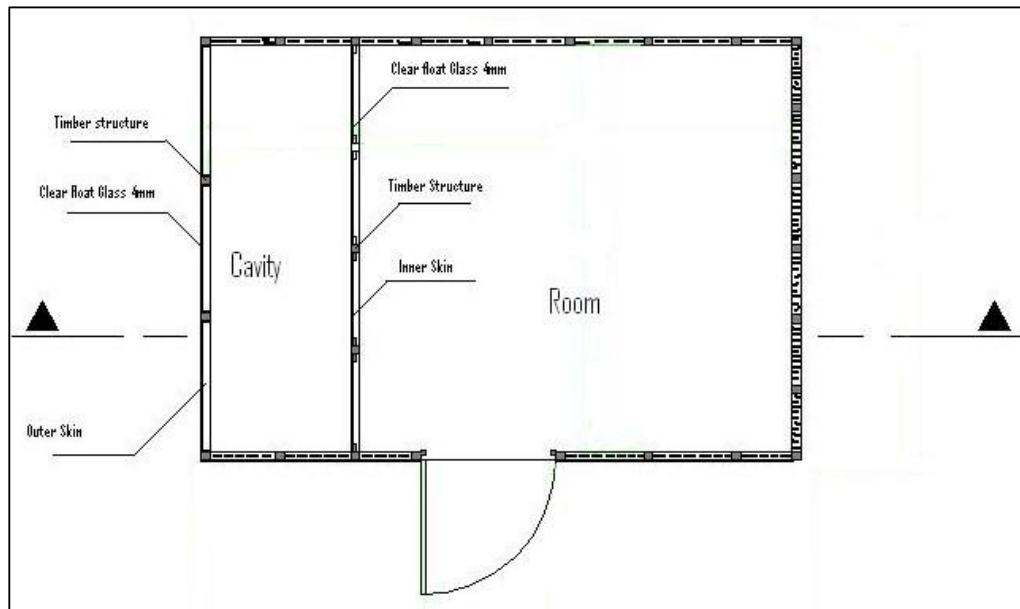


Figure 4.6 Experimental chamber description and materials: Plan.

4.2.2 Solar Simulator Rig.

The intensity of the radiation generated by the solar simulator was selected with the aim of simulating specific conditions of a non favourable orientation of the facade. As the intensity of direct solar radiation on vertical surfaces varies with solar position; a timeframe of around 1.5 hours was selected to simulate a constant short period of time, assuming an average level of radiation. The level of direct radiation produced by this solar simulator was about 600W/m². This magnitude was set so that the effect of direct solar intensity on a vertical surface of the DSF, with high levels of radiation, could be extrapolated .

As per the I.H.V.E Guide [5] and the CIBSE Guide for Environmental Design [6]; the solar radiation intensity during short periods of time, on sub-tropical and also temperate locations, on non favourable orientations, there are averages between 600 to 615W/m² on vertical surface. As detailed in Table A6.34 [5a], peak levels of direct radiation, as high as 640W/m², can be found in non favourable orientations. Such orientations include East and South-East at mid morning; during spring equinox and summer solstice; and also in locations at 50°N. High levels of direct radiation, as high as 620W/m² in East and South-East orientations at mid morning during winter solstice, in locations at 30°N can also be found (Table A.6.30 [5.b]). For this reason, the selected setting of light magnitude was adjusted to recreate the specific conditions of an average of 600W/m² of radiation assuming a moderate level of external temperature of between 22 and 25°C. Thus in order to simulate a similar level of radiation, a light rack was assembled using 20 flood halogen lights.

The rack was placed 1.500mm in front of the external glazed facade of the chamber. The lights were organised in 4 rows (A, B, C, D) with 5 lamps on each row. The horizontal distance between each lamp was 600mm. The first row of lamps started 500mm from the ground, with subsequent rows modulated by a margin of 500mm each. The rack was located in the centre in front of the external skin. The location of the rack and the vertical distances are illustrated in figure 4.7. The lamps specifications are detailed in Table 4.2.

Table 4.2 Technical specifications of light source simulator

Description:	Floodlight luminaire [7].
Type:	Encased
Lamp:	Tungsten Halogen.
Bulb Manufacturer:	Osram [8].
Wattage:	500W
Voltage:	230V
Life (Hrs):	2000
Luminous flow:	9500 lm
Colour Temperature:	3000°K
Lamp Bulb length:	114.2mm (horizontal)
Warm up time:	20 minutes



Figure 4.7 Solar simulator of the experimental facility.

The amount of light absorbed and reflected by any object is related to temperature. This phenomenon is known as Planck's law, which describes the spectral radiance of electromagnetic radiation, at all wavelengths, from a black body at temperature (T) [9].

With regard to the light source used for this solar simulation, the amount of radiation emitted by these lamps was directly related to their colour temperature. Figure 4.8 illustrates the Wien's displacement law [10], which states that the hotter an object is, the shorter the wavelength at which it will emit most of its radiation. In this specific

case, the light source colour temperature was 3000°K, which meant that a significant amount of the radiation was emitted within the near infrared wavelengths.

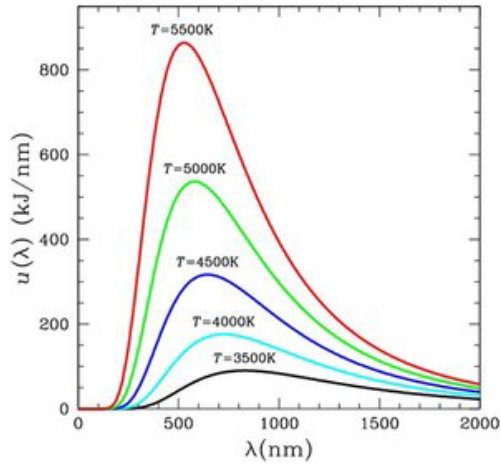


Figure 4.8 Wavelength corresponding to peak emission in various black body spectra as a function of temperature [9].

Figure 4.9 illustrates the emission spectrum of the tungsten halogen lamps. The type of lamps used produced significant amounts of radiation within the near IR spectrum; however this condition was necessary in order to recreate and assess the circumstances in which overheating develops. As can be seen in the emission spectrum (Figure 4.9), of the total radiation emitted by the lamps; about 25% was within the near-infrared spectrum, 24% within the visible and 51% within the IR.

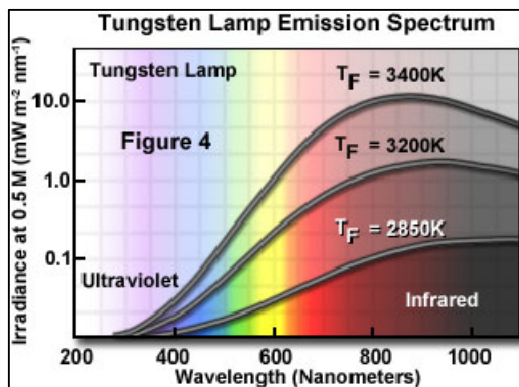


Figure 4.9 Spectral Output of tungsten-halogen lamps.
Source: <http://www.oceanoptics.com/products/spectraloutp>

4.3 TEST PROCEDURES

The following procedures were carried out for the tests using the DSF experimental facilities:

- The artificial light source was turned on.
- The thermal behaviour of the experimental chamber was measured and monitored for 1 hour 30 minutes after the light source had reached a steady level. The floodlights system required approximately 15 to 30 minutes to produce a steady luminous flow.
- Air temperature values outside the chamber, inside the cavity, and inside the room were measured.
- Surface temperature values inside the cavity and inside the room were measured
- Radiation levels inside the cavity and the room were measured.
- The horizontal and vertically reflected luminance levels inside the room were measured.
- The rig was modified according to the parameters of Opening Position, DSF Structure, Glass Type and Cavity Depth.
- Data collection through data-logging/storage equipment was carried out.
- The results were assessed to understand the thermal performance of the DSF.

The main aim of the testing was to investigate how the temperature of the cavity and the room behaved when the parameters and structure of the DSF and protections were modified. To measure temperature, radiation and illuminance, a group K-type thermocouples was installed inside the cavity, the room, and outside the chamber. The radiation was verified using radiation energy sensors installed on the outer and inner skins. To determine luminance levels; intensity lux sensors were used to

monitor the amount of light reflected by the walls of the room and the amount of light received over a horizontal level. The data was collected over a period of 2 hours for each test using a data logger connected to a PC.

4.4 EXPERIMENTAL MEASURING / LOGGING

4.4.1 Instrumentation

The equipment used for measuring environmental conditions of the experimental chamber is described in Table 4.3:

Table 4.3 Instrumentation used for experimental measurements

1	Data Logger [11].
4	Pyranometers (Bandwidth 680-1050nm) [12].
2	Visible light energy sensors (Bandwidth 380-680nm) [12].
2	Illuminance sensors (Bandwidth 480-630nm) [12].
1	Humidity/Temperature probes rht+ type [12].
18	K-type thermocouples for temperature measurement.
1	Delogger-Plus Software for recording and Monitoring [13].
1	Air Velocity transducer [14].
1	PC for data storage.

The data logger used was a dataTaker (DT500 series). The “*dataTaker DT500*” is a general purpose 12V DC / 6V Battery powered data acquisition and logging system, for measuring inputs from most sensor types. The data was stored in a battery backed RAM capable of holding up to 166.530 data point records. The measured data was also transferred and stored on a PC using “*DeLogger™ 4 Pro*” [13] software, an enhanced graphical package that allows reporting to a database, and also offers remote dataTaker management features. The data-logging equipment used for the data-collection and storage is illustrated in figure 4.10.



Figure 4.10 Data-logging equipment connected to the measuring instruments.

The sensors employed for measuring the light operated independently and had a semiconductor diode and filter system that responded to light using a silicon photocell detector with cosine corrected heads. This ensured that only light rays normal to the sensor were measured. The following types of sensors were installed in the experimental chamber:

The energy sensors were single channel Skye SKL-510 cosine corrected sensors that measure light energy in units of Watts/m² within the waveband of 380 to 680nm. The defined response curve allowed this sensor to be used with mixed lighting (artificial and/or natural light). The strong ‘out of band’ sources were ignored and only energy within 380-680nm was measured. For the solar simulator used about 28% of the visible radiation was produced within the range measured by this sensor.

The pyranometers were single channel Skye SKS-1110 cosine corrected sensors that measure near infrared light energy in units of Watts/m² which fall within the

waveband 680-1050nm. For the solar simulator used in this research, about 72% of the IR radiation was produced within the range measured by these sensors.

The photometric sensors were single channel Skye SKL-310 cosine corrected sensors that measure illuminance within the visible wavelength spectrum perceived by human vision. It has peak sensitivity at 555nm for light adapted to the eye. It measures light falling within this part of the spectrum in lux (lx) units.

Surface temperature was measured by K-type thermocouples fixed to the surface using silicone adhesive and shielded using 20mmx20mm aluminium screens placed against the light flow. The standard error of the thermocouples was +/- 0,5°C or 4%. According to Saelens [15], *“thermocouples change the local characteristics of the surface such as emissivity, conductivity and thermal capacitance”*. These variations were defined by Bentley, [16], as installation errors. In order to measure accurately the author recommends, using the smallest possible measuring set-up, positioning the thermocouple wires parallel to the isotherms; and positioning the thermocouple as close as possible to the surface. However, as this recommendation considers the overall behaviour of the cavity-chamber and the small areas where the thermocouples were installed and shielded, the manufacturer's error was instead assumed as the implication of installation error. For air temperatures, the thermocouples used were also shielded using aluminium screens to avoid being directly heated by the light source.

The Relative Humidity and Dry bulb temperatures were also measured inside the room using a two channel sensor Skye rht+ probe with PT100 temperature sensor.

This provided a linear output of temperature and humidity from 0 to 1.000mV. A radiation shield was used in order to avoid error readings from direct light sources. The accuracy levels of the equipment and parameters are shown in table 4.4.

Air velocities were measured using an air velocity transducer which measures velocities using thermal anemometry. The probe location is indicated in figures 4.11 and 4.15. The transducer was orientated to measure velocity magnitude on the vertical direction. The technical specifications and detailed descriptions of the instruments used for the experimental analysis are provided in table 4.4.

Instrument	Manufacturer	Parameter measured description	Parameter Units	Sensitivity	Working range	calibration date	Accuracy
K-type Thermo-couples	Pico Technology	Air temperature	°Centigrade	10Ω-2kΩ	-75+250°C		±0.2°C to ±2°C
Energy Sensor	Skye Instruments Ltd	Solar flux within the visible withband range	Irradiance W/m2	380-680nm 1mV/100w/m ²	0-5000 w/m ²	10/05/2005	Absolute typ. < 3% to 5% max
Pyranometer	Skye Instruments Ltd	Solar flux within the the near infrared range	irradiance W/m2	680-1050nm 1mV/100w/m ²	0-5000 w/m ²	17/05/2005	Absolute typ. < 3% to 5% max
Lux sensor	Skye Instruments Ltd	Levels of light perceived by human eye	illuminance Lux	450-650nm 1mV/10klux	0-500.000 lux	15/07/2005	Typical ± 3 to 5%
pt100 Temperature RH+ sensor	Skye Instruments Ltd	Dry bulb temperature Air Relative Humidity	°Centigrade %	0-1V	-40°C+60°C 0-100%	27/07/2005	±0.2°C (-10+60°C) ±2% RH
Air Velocity Transducer Model-8455	TSI Incorporated	Air Velocity	m/s	0-10V	0.05-1m/s	14/01/2003	±0.2%

Table 4.4 Technical Information sensors – specifications

4.4.2 Experimental Measurements

The experimental chamber was monitored in three parts; the exterior of the chamber, the cavity and the room. In each of these spaces, a series of sensors was installed to measure the environmental conditions resulting from the light incidence through the glazed facade. The main locations of the sensors are shown in figure 4.11. In each

test, the thermal environment outside the chamber, inside the cavity and inside the room, was measured.

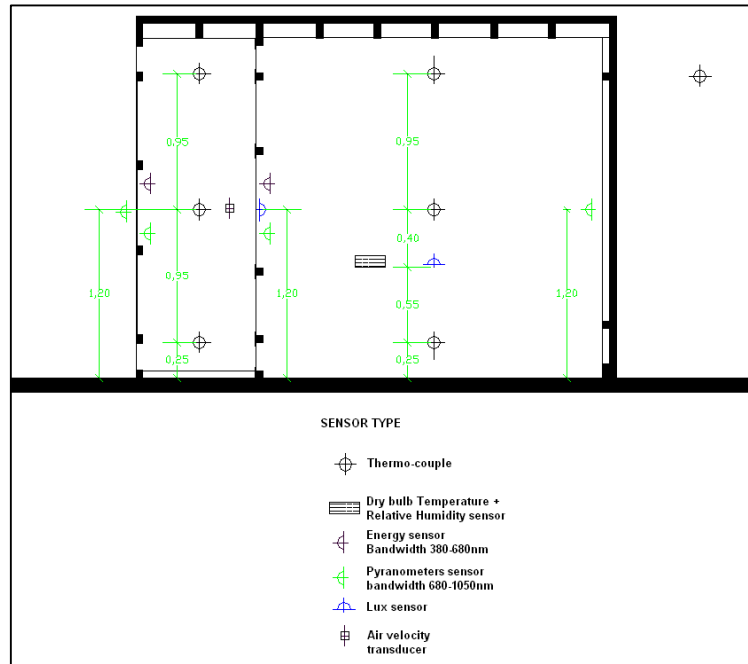


Figure 4.11 Location of sensors inside the Experimental Chamber.

4.4.2.1 External measurements

- Total radiation in front of external glass (Visible and Short-wave IR). The procedures for the validation of the average radiation received outside the cavity are explained in 4.3.3.
- External Ambient temperature (1 height, at 2.05m from ground level, on the shade at one side of the Experimental Chamber. The average reading of the laboratory temperature is explained in 4.4.5.

4.4.2.2 Cavity Measurements

- Facade channel temperatures (5 points measured with shielded K-type thermocouples at 3 heights: Three vertical points at the centre of the cavity, at 0.25m, 1.20m and 2.15m, the other two points were measured on each side of the

cavity at 1.20m from the ground and 0.5m from the side walls). Figure 4.12 illustrates two of the K-type thermo-couples used for measuring the air temperature inside the cavity.



Figure 4.12 Shielded K-type thermo-couples inside the cavity.

- Radiation on the vertical surface transmitted through the outer facade to the cavity. The radiation was measured at the vertical centre of the external glass, behind the external skin. The radiation energy was measured on visible bandwidth (380-680nm) and near shortwave infrared bandwidth (680-1050nm). Figure 4.13 illustrates the position of sensors in the cavity.



Figure 4.13 Radiation sensors located on the external, internal skins and back wall of the experimental chamber.

- Glass surface temperatures inside the facade channel: 4 points measured with K-type thermocouples. 2 were located on the outer glass and 2 were placed on the external and internal glass (Figure 4.14).

- Surface temperature of each of the cavity walls: 4 thermo-couples were placed one on each of the right and left walls, floor and ceiling (Figure 4.14).
- Surface temperature of shading devices: 2 positions were measured with K-type thermocouples on the louvers located at 0.60m and 1.50m (Figure 4.14).

The TC placed over the glass and wall surfaces were covered using reflective aluminium shields to avoid the sensor measuring the heat by direct radiation.



Figure 4.14 Shielded K-type thermocouples for measuring surface temperatures.

- Air Velocity magnitude was measured as a reference for the main tests on the inside of the centre of the cavity at 1.20m from ground level. Figure 4.15 shows the location of the hot-wire probe. The average readings obtained are explained in 4.4.6.



Figure 4.15 Air velocity transducer position inside the cavity, next to the inner skin.

4.4.2.3 Room Measurements

- Room air temperatures (3 points measured with K-type thermocouples at 3 heights: 0.25m, 1.20m and 2.15m). Figure 4.16 illustrates two examples of the shielded thermo couple positions inside the room.
- Ambient Dry bulb temperature and Relative Humidity (1 point, measured at 0,80m from floor level, at a distance of 1.25m from the inner glass pane).



Figure 4.16 Shielded K-type thermo-couples placed inside the chamber room.

- Radiation on the vertical surface transmitted through the facade to the room. This was measured at the centre behind the inner skin and back wall. The radiation energy was measured on visible bandwidth (380-680nm) and near shortwave infrared bandwidth (680-1050nm). Figure 4.11 shows the general location of the radiation sensors.
- Indoor illuminance (2 positions): One on horizontal plane at 0.80m from ground level at the centre of the room. The other measured the vertical reflected illuminance from the room. The latter was positioned at 1.20m from ground level facing toward the back of the room, at the level of the inner skin pane. Figure 4.17 shows the locations of the luminance sensors. These were placed horizontally and facing backwards inside the room.



Figure 4.17 Illuminance sensors placed inside the experimental room.

- Surface temperature of each of the room walls (4 thermo-couples placed one each on the right and left walls, floor, and ceiling).

4.4.3 Radiation measurement

To measure the radiation levels on the external glass, the external skin was divided into an equal grid of 7 columns and 7 rows. The radiation levels were measured at each intersection point and compared with each of the other points in the array. Figure 4.18 shows the grid array and distribution of radiation over the external surface, which is scattered almost evenly on the mid part of the exposed surface.

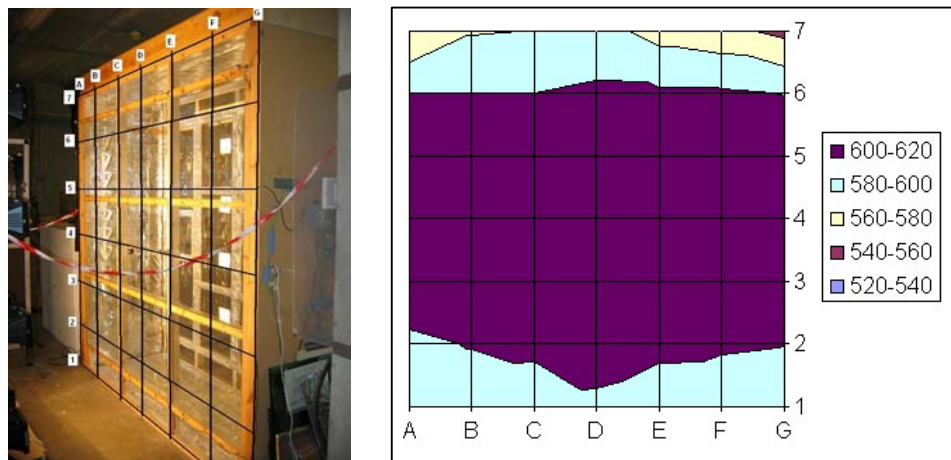


Figure 4.18 Measurement point array on external skin of the experimental chamber and average measured radiation levels.

The average radiation received on the centre of the external layer was 602.21 W/m²; with the values decreasing slightly at the top and bottom of the external glass. This average value was obtained around 30 minutes after the light source was switched on, which indicated the ‘warming up period’ of the light source. Figure 4.19 illustrates the average readings taken in the geometrical centre of the outer skin for a period of 2 hours (including this “warming up” stabilizing period.)

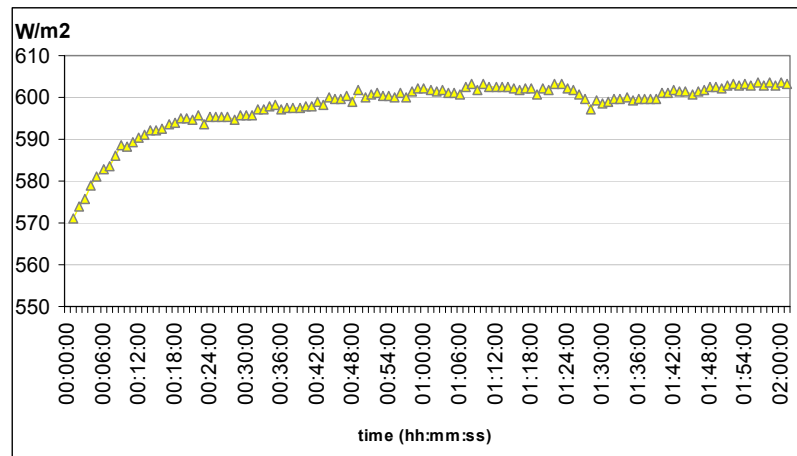


Figure 4.19 Total radiation measured on the geometric centre of the external skin.

4.4.4 Illuminance measurement in the experimental chamber

The illuminance inside the room was measured as a reference for the comparative analysis of shading devices and glass types according to the main configurations of the cavity. Illuminance levels were measured at two points inside the facade room; one measuring a horizontal plane in the centre of the room and the other measuring a vertical reflection from the room. The average interior illuminance was 1157.16lx and the average reflected was 948.20lx. The measured illuminance levels on the basic configuration of the chamber are illustrated in figure 4.20.

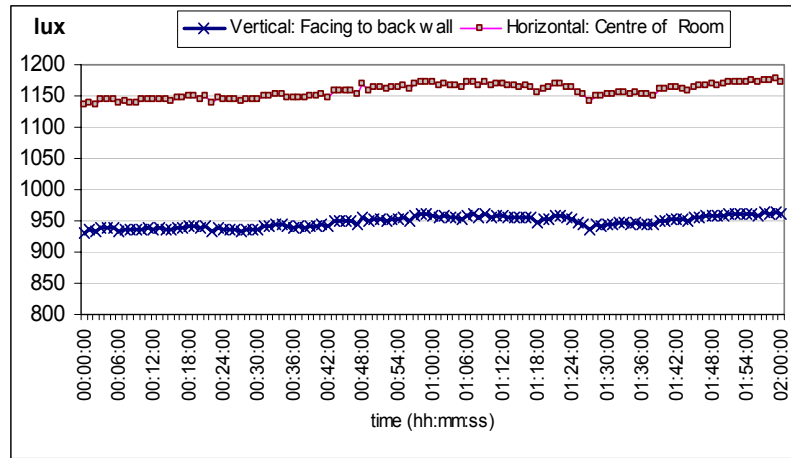


Figure 4.20 Illuminance measured inside the room of the experimental chamber.

4.4.5 Temperature measurements in the experimental facility

The experimental chamber was built in the interior of a laboratory to avoid the influence of wind and other elements of weather. The external temperature was measured over a two-hour period. In order to measure the temperature behaviour in this controlled environment; the readings of exterior temperature were taken in the shade next to the chamber, without the direct incidence of direct radiation from the lamps.

The temperatures surrounding the chamber required approximately 30 minutes to reach a steady level. These readings are identified in all the tests as external temperature. Figure 4.21 contains details of measured and average external temperatures. The results in Figure 4.21 also include the influence of the light source at the start of the tests. The average external temperature was 23.84°C.

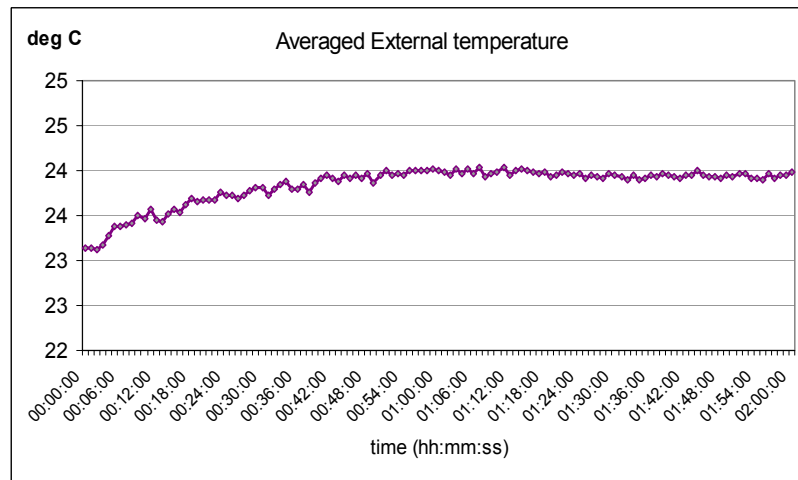
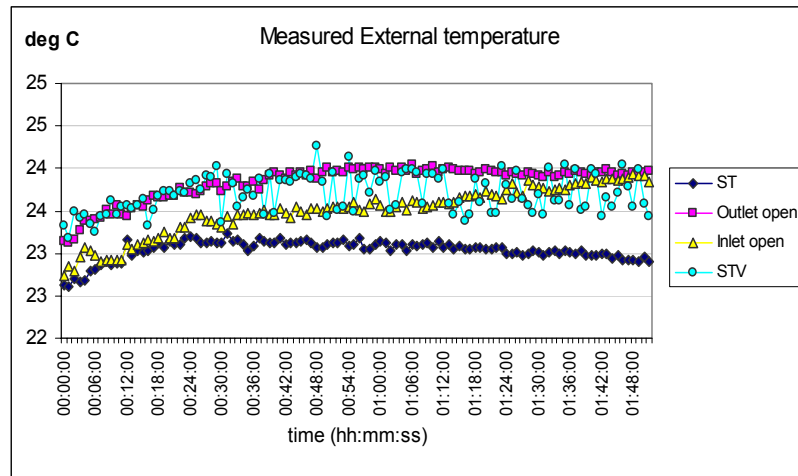


Figure 4.21 Examples of measured and average external temperatures.

The air temperature in the cavity was measured using 3 shielded thermo-couples along the vertical centre of the cavity (figure 4.11) and was averaged for the comparative analysis of each parameter. Figure 4.22 illustrates an example of the air temperatures measured inside the cavity and the averaged values for the duration of the test.

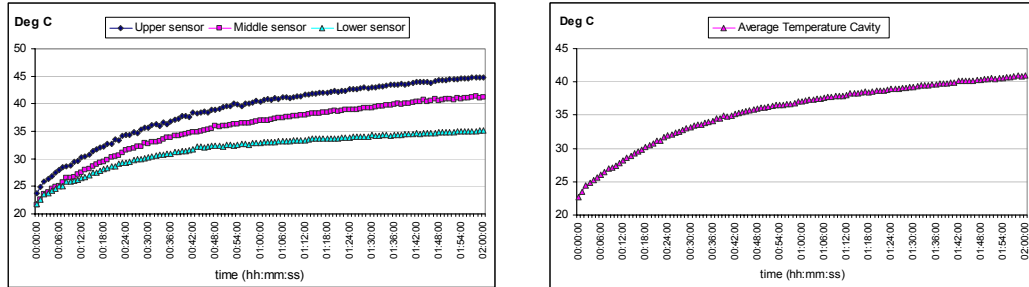


Figure 4.22 Examples of measured and average air temperatures inside the cavity.

The air temperatures inside the room were measured using 3 shielded thermo-couples along the vertical centre of the cavity (figure 4.11) and were averaged for the correlation analysis of each parameter. Figure 4.23 illustrates an example of air temperatures measured inside the room with the averaged values for the duration of the test. The next chapter contains the comparative analysis of the temperatures inside the cavity and the room using the averaged values of temperatures measured in each series of tests.

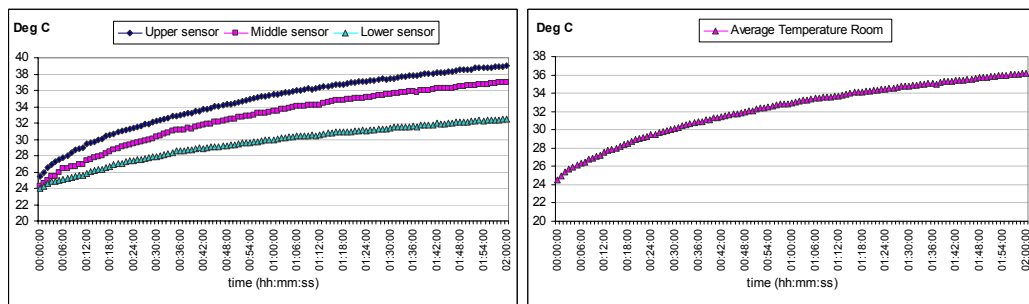


Figure 4.23 Example of measured and average air temperatures inside the room.

4.4.6 Air velocity measurements inside the cavity

The air velocity inside the cavity was measured as a reference for the CFD in the main configurations of the cavity. The airflow rate was measured at one point inside the facade cavity at 1,20m from the floor level and 0,25m to the inner skin. The location of the air velocity sensor is illustrated in figures 4.11 and 4.15. The averaged

mean velocities measured for the airflow with respect to the main configurations of the cavity openings are shown in table 4.5.

Inlet Closed	Outlet closed	STV-Inlet + Outlet Open	ST-Inlet + Outlet Closed
0,0622m/s	0,0554m/s	0,1630m/s	0,0575m/s

Table 4.5 Average air velocities according to the inlet and outlet position.

Figure 4.24 illustrates the different behaviours of the air flow as measured on each of the main configurations of the cavity. This information was used as the main reference of airflow inside the cavity.

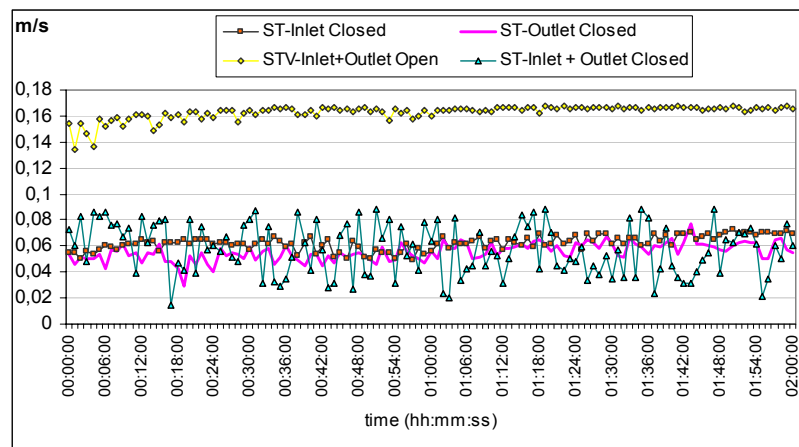


Figure 4.24 Air Velocity inside the cavity for the Standard (ST) and Standard Ventilated (STV) Cases.

4.5 PHYSICAL CONFIGURATIONS OF THE DSF CHAMBER

The experimental chamber was configured with the inlet and outlet shafts at two main positions in order to assess the incidence of overheating. Essentially the cavity was sealed or ventilated. These main configurations were included in the assessment of the other parameters, which were based on the cavity structure, glass type and cavity depth.

4.5.1 DSF Opening Position

There were two main configurations of the cavity based on the opening shafts position: The ST type (as illustrated in Figure 4.25) had the cavity inlets and outlets closed during the test; whereas the STV type (as shown in figure 4.26) had the inlets and outlets open. The main variables compared for all the cases were; external temperature, cavity temperature, room temperature and the temperature difference between the room and the cavity given the external temperature.

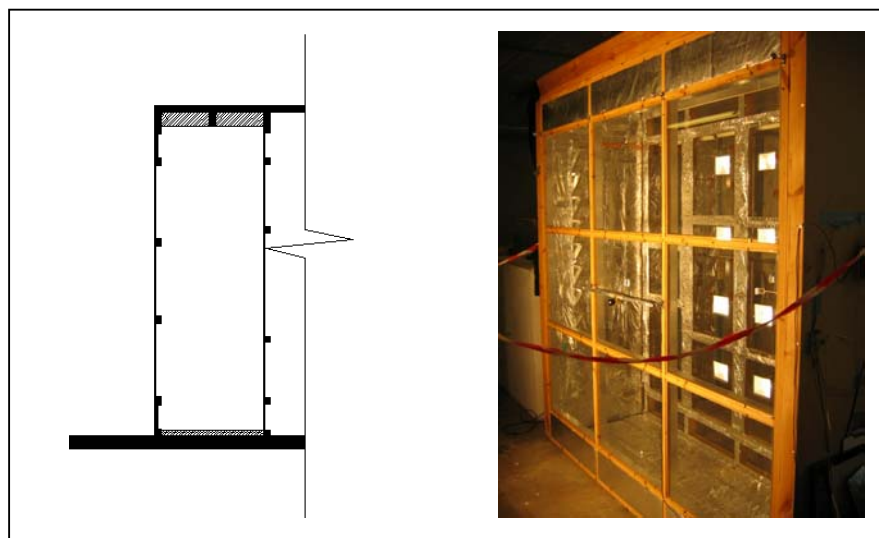


Figure 4.25 Standard Configuration (ST): Sealed cavity with inlets and outlets closed.

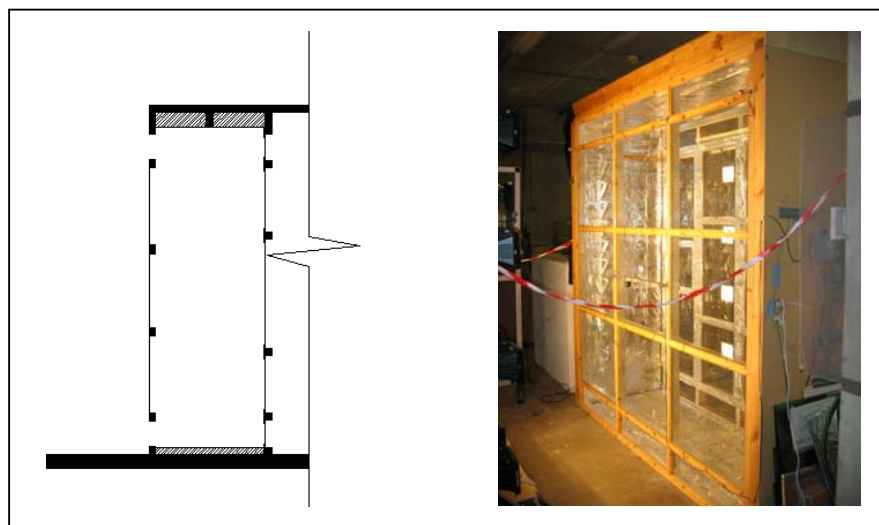


Figure 4.26 Standard Ventilated Configuration (STV): Ventilated cavity with inlets and outlets open.

4.5.2 DSF Structure

The amount of radiation received by the cavity and the chamber was controlled by the use of various shading devices:

4.5.2.1 Reflective Shading Devices

The reflective surfaces were placed on the external and internal glazed skins. The surface of each skin was covered from 33% to 66% of its total area. The protection with reflective surfaces was also exchanged from the external to the internal skin. The area covered on each glazed surface is illustrated in figure 4.27.

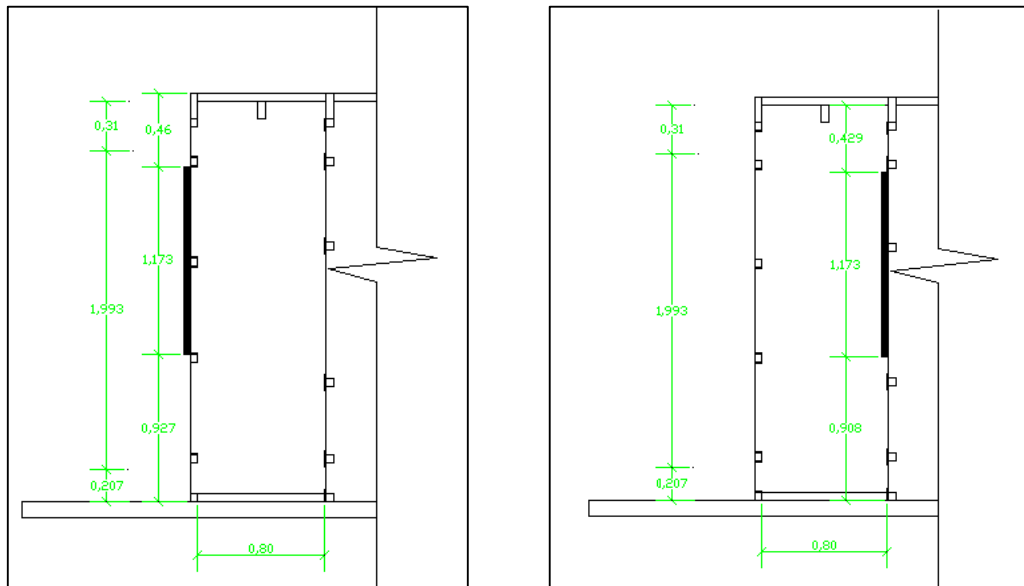


Figure 4.27 Location of opaque shading devices on the external and internal skin.

4.5.2.2 Blinds

In this configuration, the cavity was shaded with a series of three vertical PVC Polyester fabric blinds. The surface of each skin was covered from 25% to 75% of its total area. The fabric was chosen for its high reflectance of white colour. According to the manufacturer, Skyspan Limited, the light transmission of the fabric

is up to 15% [8]. The location of the blinds is shown in figures 4.28 and 4.29. They were positioned in 4 different locations:

- Outside the cavity: in front of the external skin
- Inside the cavity: behind the external skin
- Inside the cavity: before the inner skin
- Inside the room: behind the inner skin

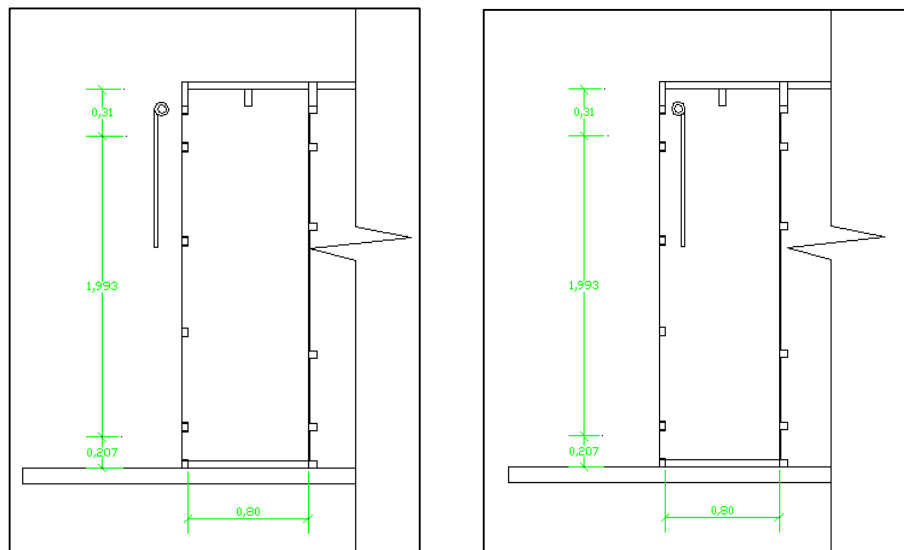


Figure 4.28 Blinds as shading devices next to the external skin of the DSF.

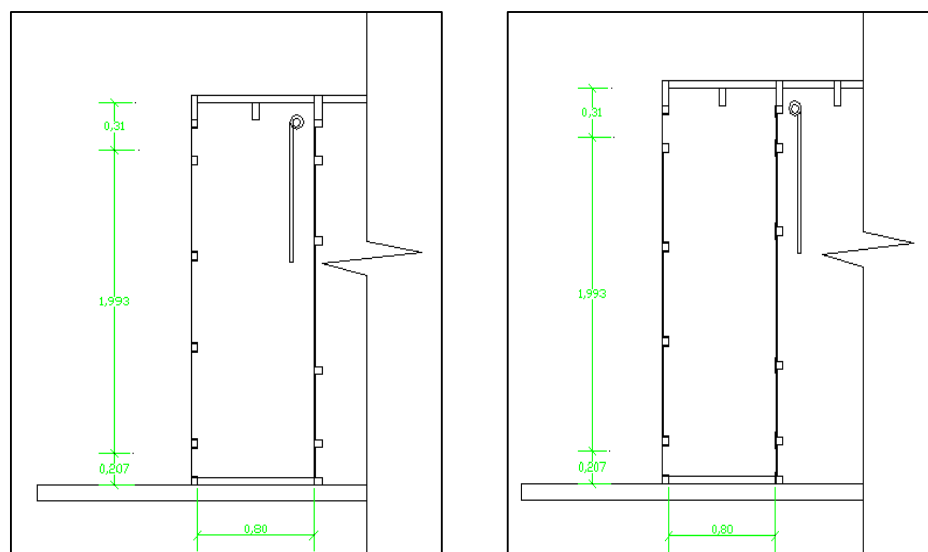


Figure 4.29 Blinds as shading devices next to the inner skin of the DSF.

4.5.2.3 Louvers

For this configuration, the cavity was shaded by a series of 11 horizontal aluminium louvers placed inside the cavity. The positions of the louvers were varied in order to test the impact of the location on the thermal response. The locations of the louvers included some outside the external skin, inside the cavity behind the external skin, in the centre of the cavity and in front of the inner skin. The colour of louvers was also modified. The main location of the louvers in the centre of the cavity (as shown in figure 4.30) was used for the rest of the tests.

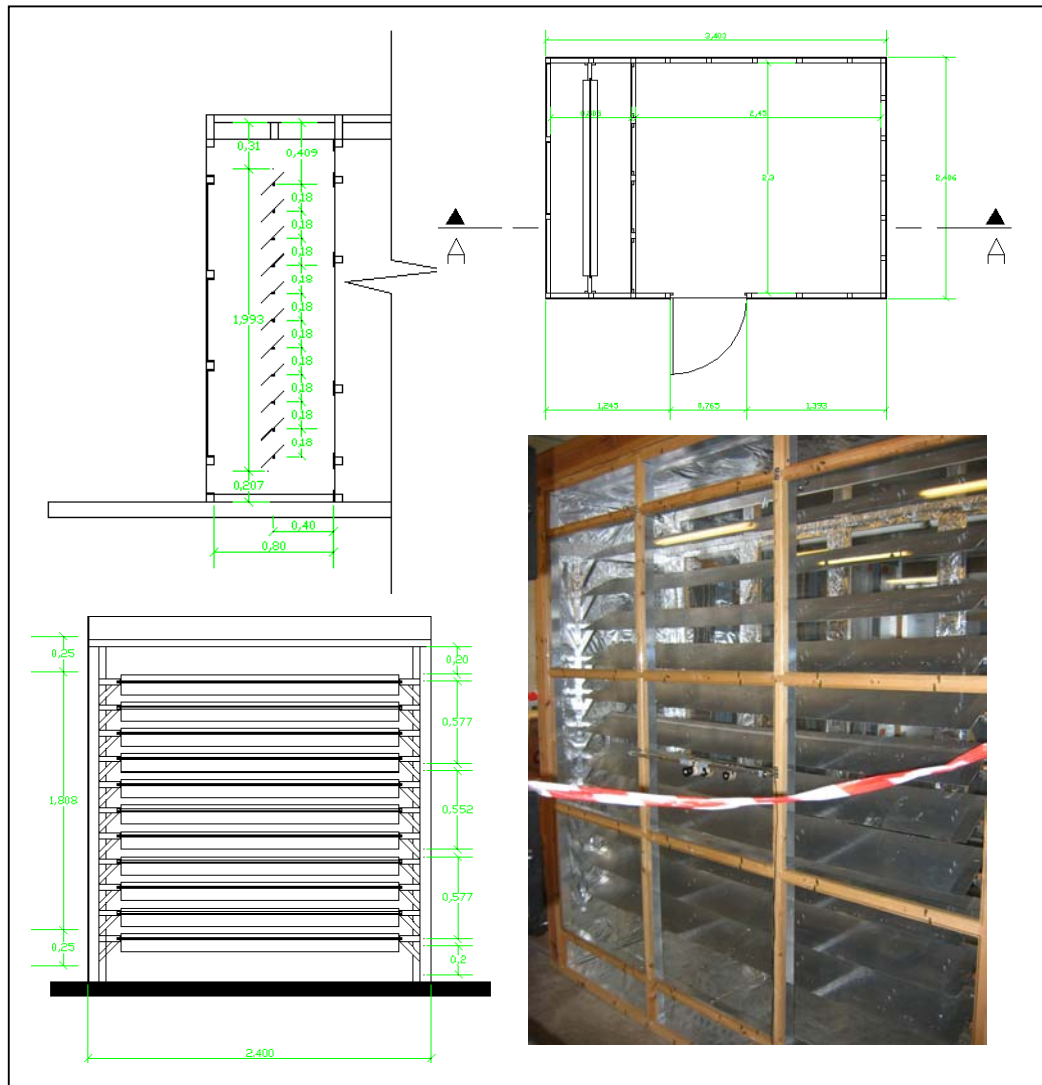


Figure 4.30 Cavity settings with horizontal louvers as shading devices.

4.5.3 Types of glass used in the DSF chamber

In this configuration, the type of glass used on the external and internal skin was changed. There were three types of glass used for this experimental analysis: Clear float glass; standard frosted glass (stippolyte pattern glass); and green tinted glass. All the glass used has 4mm thick. In order to measure the influence of the glass type on the thermal behaviour, each was tested at various positions on the external and internal skin. For the rest of the cases, the comparison is made using clear glass. Figure 4.31 illustrates examples of the external skin of the chamber using clear, textured and green tinted glass. The light and energy transmission coefficients of the glass types is shown in table 4.6.

Properties	Optifloat Clear 4mm	Texture stippolyte 4mm	Optifloat green tinted
Light transmission	0,82	0,79	0,75
Total heat transmission	0,82	0,58	0,59
Reflection (outside-in)	8%	6%	7%
Reflection (inside-out)	8%	6%	7%
Colour (outside-in)	Clear	Grey	Green
Colour (inside-out)	Clear	Grey	Green
thickness	4mm	4mm	4mm

Table 4.6 Main optical properties of glass used in the experimental facilities.
<http://www.pilkington.com/pilkington2004/both/images/productdirectory/flash/optifloat.html>



Figure 4.31 Clear, Textured and Green tinted glasses used in the experimental chamber.

4.5.4 Cavity Depth

As the inner skin of the chamber could be moved backward and forward, the depth size of the cavity was adjusted to 200, 400, 600 and 800mm. These sizes were tested and compared for this specific analysis. It should be noted however that to allow for comparison with the other parameters, the main size of the cavity depth was kept to 800mm in all the cases.

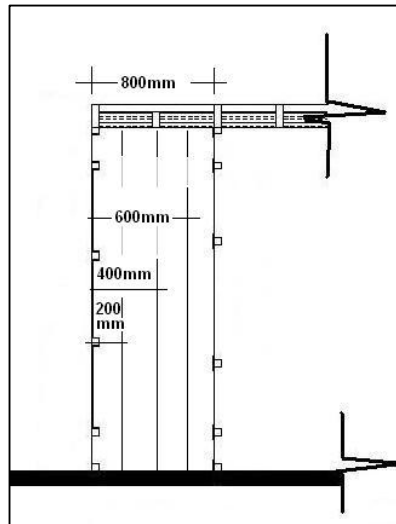


Figure 4.32 Depth size settings of the cavity

REFERENCES

1. Kingspan, Rigid Insulation System Thermal Performance. 2004, Kingspan Insulation Limited: Pembroige, Leominster, Herefordshire HR6 9LA, UK. Website: http://www.tek.kingspan.com/uk/thermal_performance.htm
2. DTLR, Building Regulations: Approved Document Part L2: Conservation of fuel and power in buildings other than dwellings. 2003, Office of the Deputy Prime Minister: UK. p. 75.
3. Skyspan, Skyspan (Europe) GmbH. 2003: Nordstrasse 10, D-83253 Rimsting, Germany. Website: http://www.skyspan.com/07_Material.html
4. Pilkington, The Glass Range for Architects and Specifiers. 2006, Pilkington Group Limited: UK. p.18.
<http://www.pilkington.com/resources/glassrangebroanddatasheetjune2006.pdf>
<http://www.pilkington.com/pilkington2004/both/images/productdirectory/flash/optifloat.html>
5. I.H.V.E, Institution of Heating and Ventilating Engineers: IHVE guide: Book B. 4th ed. 1972, London, Great Britain: IHVE, p.540.
- 5a. *ibid*, Table A6-34, Appendix A6-32.
- 5b. *ibid*, Table A6-30, Appendix A6-28.
6. CIBSE, CIBSE Guide A2, Weather and solar data. 1986, London Chartered Institution of Building Services Engineers: London, UK.
7. RS, Product Catalogue. 2007, RS Components Ltd: Birchington Road, Corby, Northants, NN17 9RS, UK. Website: <http://rswww.com>
8. OSRAM, Product Catalogue. 2007, OSRAM Gesellschaft mit beschränkter Haftung: Munich, Germany. Website: <http://catalog.myosram.com/>
9. Rybicki, G.B. and A.P. Lightman, Radiative Processes in Astrophysics. 1979, New York: John Wiley & Sons. p.p 22.
10. Mehra, J. and Rechenberg, H, "The Historical Development of Quantum Theory", Volume 1 Chapter 1, Springer, 1982
11. Datataker , DT500/600: specifications, 2007, Datataker Pty Ltd: 7 Seismic Court, Rowville, Australia, VIC 3178.
Website: <http://www.datataker.com/products/dt500.html>
12. Skye-instruments, Technical information. 2007, Skye Instruments Ltd,: 21 Ddole Enterprise Park, Llandrindod Wells, United Kingdom, LD1 6DF.
Website: <http://www.skyeinstruments.com/>
13. Datataker, DeLogger Plus Software, Ed. Software: Discbell Ltd, Manual: Data-Electronics, 1997, Australia.
14. TSI, Air Velocity transducer technical specifications: Models 8455/8465/8475, 2007, TSI Incorporated: 500 Cardigan Road, Shoreview, MN 55126 U.S.A.
Website: http://www.tsi.com/documents/2980575_8455-65-75-AVT.pdf

15. Saelens, D., Energy Performance Assessment of Single Storey Multiple-Skin Facades, in Faculteit Toegepaste Wetenschappen, Arenbergkasteel. 2002, Katholieke Universiteit Leuven,: Kasteelpark Arenberg 51, B-3001 Leuven, Belgium. p. 272.
16. Bentley, J.P., Principles of measurement systems. 4Rev Ed edition ed. 2004, Harlow: Pearson Prentice Hall. 544.

CHAPTER V

EXPERIMENTAL ANALYSIS

5.1 INTRODUCTION

Previous parametric studies on the thermal performance of facades under controlled environments mainly focused on the airflow behaviour through windows. Brandle and Boehm [1], Müller and Balowski [2], Inoue et al [3] and Bonveni et al [4] studied energy performance indicators such as the U-value and g-value of various windows configurations. Some work has been done in measuring the energy performance in specific buildings with active envelopes. Poirazis [5] highlighted two types of studies in which measurements were carried out on test rooms and real buildings. The author summarized some studies, which focused on measuring airflow, pressure differences and indoor environments based on real conditions and specific cases.

Other studies developed and calibrated numerical models for specific full-scale facilities. Park et al [6] calibrated a simulation model of a DSF based on experimental models in which the variation of ventilation regimes and weather conditions were used to predict the most relevant state variables. According to the authors, *“It was found that there is a significant difference between the estimated parameters and the theoretical/literature values”*. The authors suggested future work for validation of the models based on the variation of physical parameters and configurations of the facade. Saelens [7] measured two single storey high DSFs and a traditional envelope under real climatic conditions. The author used the measurements of the facade to relate them with energy objectives. The purpose of

this was to evaluate modelling assumptions and derive modelling parameters and relationships of the temperature and airflow measurements, under summer and winter conditions. Although these previous studies measured the implications of airflow on energy performance; the direct repercussions on the thermal performance of different configurations within the facade was not clearly assessed or illustrated.

In the previous chapter, the general experimental procedure for investigating the performance of the double glass facade system was explained. The reference values of external temperature, radiation, illuminance and air velocity inside the cavity were illustrated. The assessment of thermal behaviour and overheating development of the DSF chamber was organised into four main parameters based on the physical configuration of the facade cavity. This chapter analyses primarily the impact on the thermal performance as a result of modifying the physical parameters of the facade cavity. The performance was compared based on the following parameters:

- DSF openings position
- Room openings position
- DSF structure
- Glass type
- Cavity depth

In order to meet the research objectives, the following analysis was carried out:

1. Comparison of the fraction of transmitted radiation (visible and near infrared) through the DSF cavity to the room.
2. Evaluation of the temperature performance of the cavity and the room according to the physical variations in the DSF.

3. Comparison of the luminance levels on horizontal and vertical positions reflected from the room walls, depending of the variation of shading devices.

The data was analysed comparing the temperature performances in each of the cases during the measured periods of 2 hours. A comparative analysis was then used to identify the physical conditions and critical parameters which influence the development of overheating both in the DSF and in the room of the experimental chamber. The data obtained in this experimental analysis was later used (see chapter 6) as a basis for developing the CFD model in which the vertical airflow and thermal responses in relation to these parametric variations was visualised.

5.2 DSF OPENINGS POSITION

For the first parameter, the cavity was arranged with a basic configuration of 800mm depth using 4mm standard clear glass on both skins. The comparative analysis was based on the influence of the inlet/outlet positions in the temperature response of the cavity and room. The two main configurations of the cavity are shown in figure 5.1, these are the Standard type (ST) with inlets and outlets closed and the Standard Ventilated type (STV) with inlets and outlets open. The main variables compared in all cases were; external temperature, cavity temperature, room temperature and temperature difference between the room and the cavity in relation to the external temperature. In this parameter, the configurations of the DSF in non ventilated (ST) and ventilated cases (STV) were analysed assessing the thermal performance of the cavity and room based on the different inlets and outlets positions and opening size.

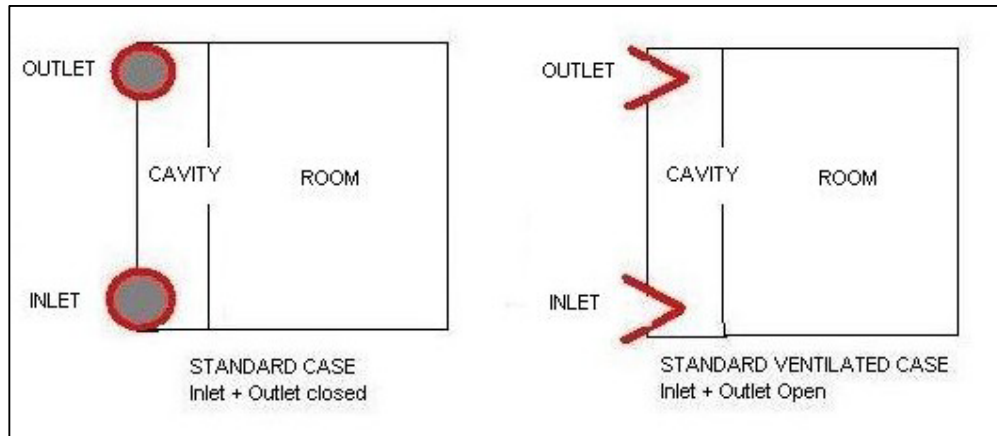


Figure 5.1 Main configurations of the cavity openings.

5.2.1 Standard Cases (ST)

The DSF cavity was arranged with the inlets and outlets closed. The temperature was measured for 2 hours using thermocouples located in three points along the mid section of the cavity, at heights of 200mm (Lower-TC), 1200mm (Mid-TC) and 2150mm (Upper-TC). Figure 5.2 illustrates the resultant temperatures of these three points in relation to the temperature of the laboratory, measured outside the experimental chamber.

Figure 5.2 illustrates how temperature levels inside the cavity increased rapidly when there was no air exchange with the exterior. Stratification of temperatures in relation to the height occurred; this reflected the influence of convective heat transfer within the internal surfaces of the cavity and the greenhouse effect created by the two layers of glass within the cavity. The difference in temperature between the cavity and the exterior increased dramatically, and the thermal buffer created by this condition enhanced the overall U-value of the facade. The averaged maximum temperature inside the cavity in the final 10 minutes was 36.35°C with a difference of 4.34°C (ΔT_c) between the upper and lower sensors and a difference of 12.51°C (ΔT_{ce})

between the cavity and the exterior . Hence an increase in temperature of 58% above the external temperature.

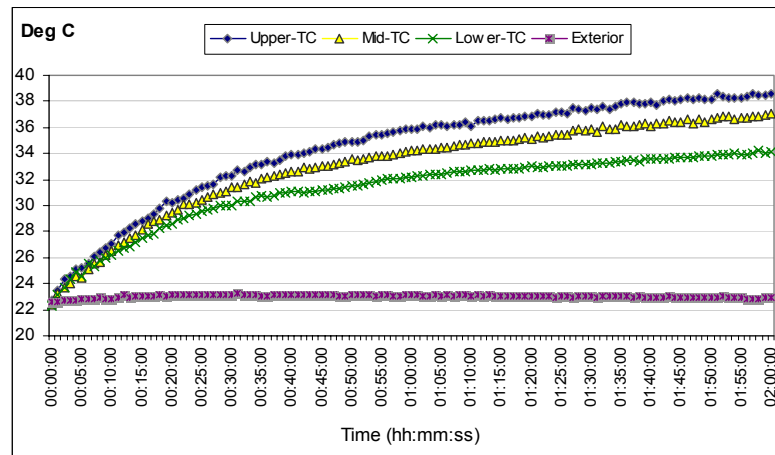


Figure 5.2 Air temperatures inside the cavity with inlets and outlets closed (ST).

5.2.2 Standard Ventilated Cases (STV)

For the ventilated configuration, the cavity was arranged initially with the inlets and outlets open. Then the opening position was adjusted so that the inlets or outlets was closed. Temperatures were also measured for 2 hours with thermocouples in the same locations as mentioned previously. Figure 5.3 illustrates the temperature response at these three points in relation to the temperature outside the chamber. The figure shows how temperature levels inside the cavity increased with the influence of the radiation. However, these increases in temperature occurred at a decreasing rate and their values were variable, illustrating the influence of buoyancy driven airflow through the cavity.

There was also stratification in relation to the height; so far the average difference of 3.42°C of the temperature within the cavity (ΔT_c) fell slightly, by about 1 degree, when air was flowing. This was as a result of the stack effect. Although there was a positive difference of 5.36°C in the temperatures between the cavity and the outside

of the chamber (ΔT_{ce}), there was a reduction of 63.87% in ΔT_{ce} when compared with the ST. The mean maximum temperatures measured with the ventilated cavity were 28.36°C, which translated to an overall reduction of 22.30% in mean temperature levels when the cavity was ventilated.

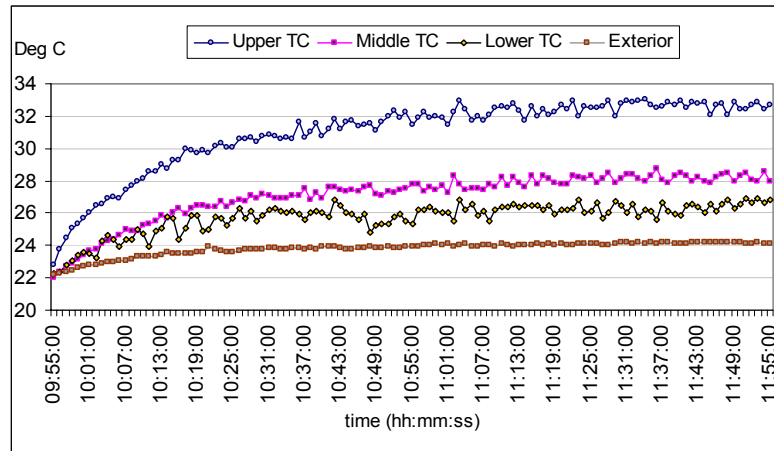


Figure 5.3 Air temperatures inside the cavity with inlets and outlets open (STV).

The temperature levels were also measured inside the cavity given various inlet and outlet positions. When the inlets or outlets positions are exchanged, the thermal response of the sealed cavity is almost similar when one each group of the openings were closed; Figure 5.4 shows the similarity in the thermal responses of the cavity when the airflow is not encouraged in the cavity. There is a mean difference of 0.11°C in the temperatures between the ST cases with maximum average temperatures of 36.71°C. In contrast, the difference with the STV case is clearly higher. This indicates that the stack effect combined with an open cavity encourages air movement and reduces cavity temperatures. Therefore, there is no relevant implication in having one of the openings sealed when the DSF is exposed to direct radiation. However, the repercussion of the openings size on the airflow and thermal behaviour will be analysed later in this chapter.

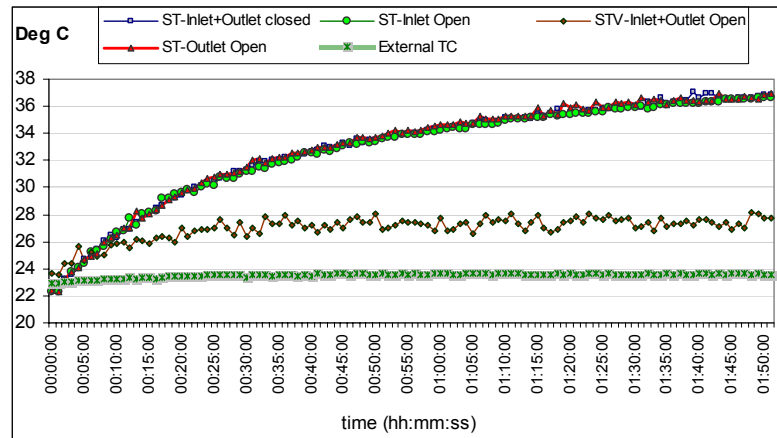


Figure 5.4 Air temperatures in the cavity for various openings positions.

With respect to the room temperatures, the thermal behaviour was relatively constant. There was no significant difference in the overall temperature response between the ST cases, despite the differing inlet and outlets positions. However, there was a slight reduction of 1.27°C in the temperature when both the inlet and outlet were closed. This was due to the fact that the panels used to close the cavity inlets and outlets were opaque, and thus there was a slight reduction in the incident radiation reflected by these surfaces. This reduction influenced the overall temperature, as clearly displayed in figure 5.5, which shows the higher temperatures in the ST cases when the inlets or outlets were closed. Although there was a reduction of 8.76% in the mean temperature in the STV, there was still a need for ventilation and further reduction of the total radiation entering the room in order to reduce heat loads. This indicates that direct gains were the main issue that affected the total heat load entering the room.

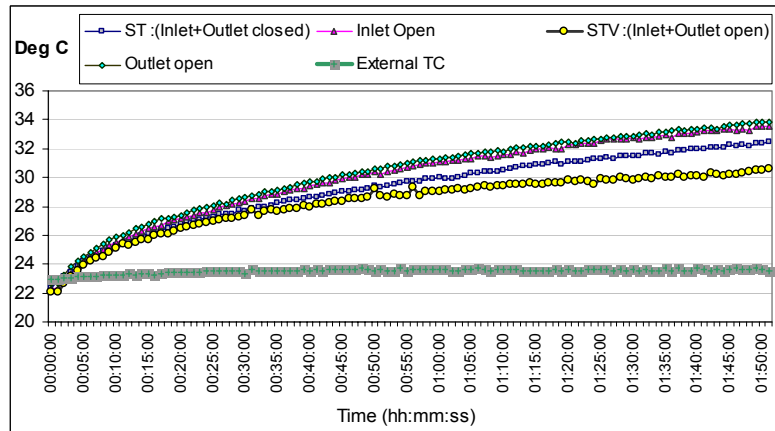


Figure 5.5 Air temperatures in the room for various cavity openings configurations.

The amount of total radiation that reached the facade and the room are illustrated in figure 5.6. The total radiation energy received on the external skin was significantly reduced by 69.85% through the two skins. This was due to the part of the short wave and visible wavelengths that were reflected and absorbed by the two panes of glass of the cavity. However, the remaining net total energy entering the room in short wave and visible was about 180W/m², which was clearly enough to develop high temperatures inside the room when no ventilation or shading was provided.

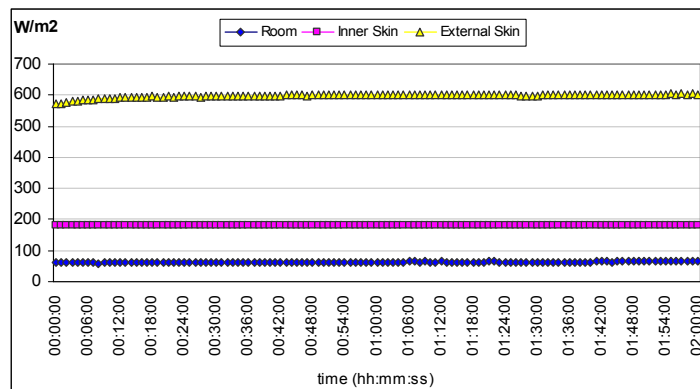


Figure 5.6 Total incident radiation on external, internal and back wall of the experimental chamber.

The visible part of the energy passing through the external and internal skins was also measured. Figure 5.7 illustrates the levels of energy measured on visible

wavelengths. This figure illustrates that the amount of energy entering the room is also reduced by reflection and absorption through the glass panes.

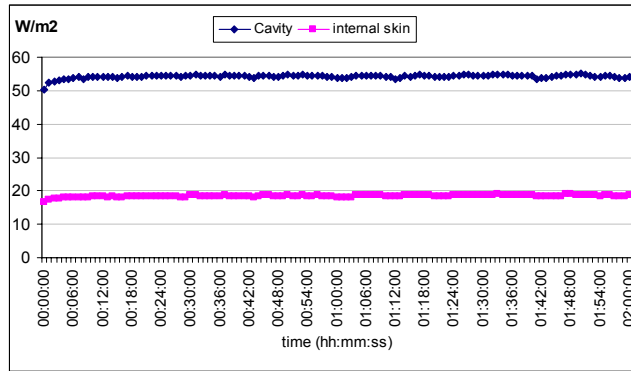


Figure 5.7 Visible light energy measured on external and internal skins of the experimental chamber.

The total illuminance levels entering the room were also measured. Figure 5.8 illustrates the illuminance received on the horizontal plane measured in the centre of the room and the vertical reflected back to the inner skin inside the room. The mean illuminance levels measured in these cases without shading devices were 1169 and 956 lux (Figure 5.8), which are quite high and require some control to reduce them to satisfactory levels.

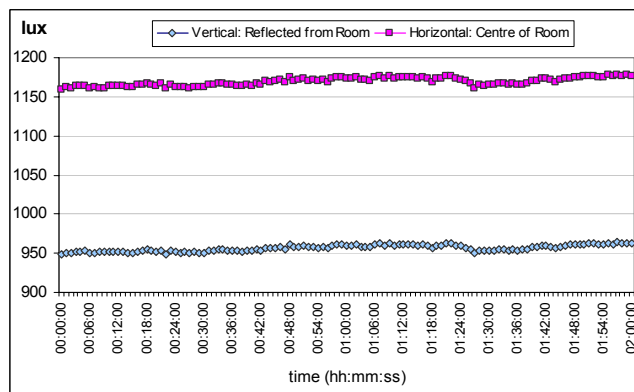


Figure 5.8 Illuminance measured inside the room of the experimental chamber.

When mean temperatures between the ST and the STV are compared; it is clear that lower temperatures in the cavity were obtained when it was ventilated. Figure 5.9

illustrates the comparative levels of thermal performance in the experimental chamber. It was found that the difference in temperature between the cavity and the room (ΔT_{cr}) in the STV was negative. This means that the heat transfer coefficient inside the cavity is clearly reduced when air is continuously flowing through it; the buoyancy effect created by the heat received and irradiated by the interior surfaces favours this behaviour inside the cavity. Although temperatures inside the DSF are lower in the ventilated case, the temperatures inside the room were almost similar to the values obtained in the standard cases. This suggests that the influence of the air movement inside the room is also needed in order to remove the heat accumulated by its surfaces and trapped by the internal glazed skin. The temperature in the room was slightly lower in the STV than in the ST cases, which suggests that there is heat transfer by conduction from the room to the cavity as a result of the lower temperature inside the cavity.

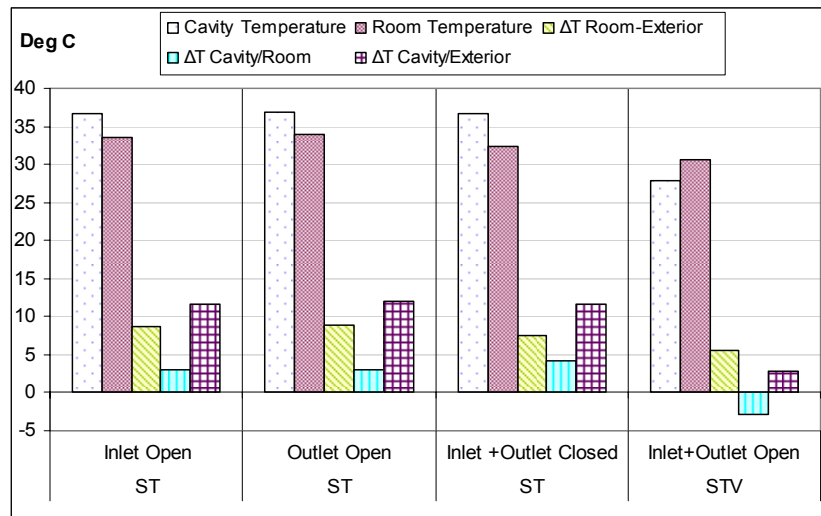


Figure 5.9 Comparison between maximum temperature values in the cavity, the room and outside the chamber for various cavity openings positions.

The temperature difference between the cavity and the exterior (ΔT_{ce}) was dramatically higher when the inlets were closed. This behaviour clearly confirms that a DSF acts as an effective insulator against the external environment, proving its use as a passive heating device when heat is required. In contrast, this behaviour illustrated the tendency for overheating when air movement in the room is restricted. As the room was not ventilated in all these cases, the difference in temperature between the room and the exterior was almost similar in the ST cases and slightly less in the STV.

5.2.3 Inlet / Outlet Size

In this parameter, the size of the openings was adjusted using sizes of 200, 150, 100, 50, 25 and 12.5mm. Each opening was adjusted to these sizes and the thermal performance relative to the sizes of the opening on the bottom to the top compared, and vice versa. The resultant temperature inside the cavity and the room was measured and compared. Figure 5.10 shows the placing of the panels to allow for the adjustment in the size of the inlet and outlet openings on the external skin of the DSF chamber.



Figure 5.10 Inlets and outlets sizes adjusted with reflective panels on the external skin.

A relationship between the reduction in inlet size and the increase in temperature levels inside the cavity was discovered. It was found that overheating starts to develop when the size of the inlets are greatly reduced, however the lowest temperatures were not obtained when the inlets were fully open; in fact, the lowest temperatures inside the cavity were achieved when Inlet-Outlet size relationships of 0.75 to 1, 0.5 to 1 and 0.25 to 1 were used.

Figure 5.11 shows the thermal performance of each case in which the lowest temperatures were reached using a size relation of 50mm inlet to 200mm outlet. The reason for this behaviour was due to the increased pressure on the inlet, which motivated and increased the airflow rate through the cavity. However, when the inlet-outlet size relation was higher than 0.25 to 1 the temperature rose and the cavity started to behave more like a sealed than a ventilated DSF. This airflow behaviour is illustrated later in chapter 6 of the CFD analysis.

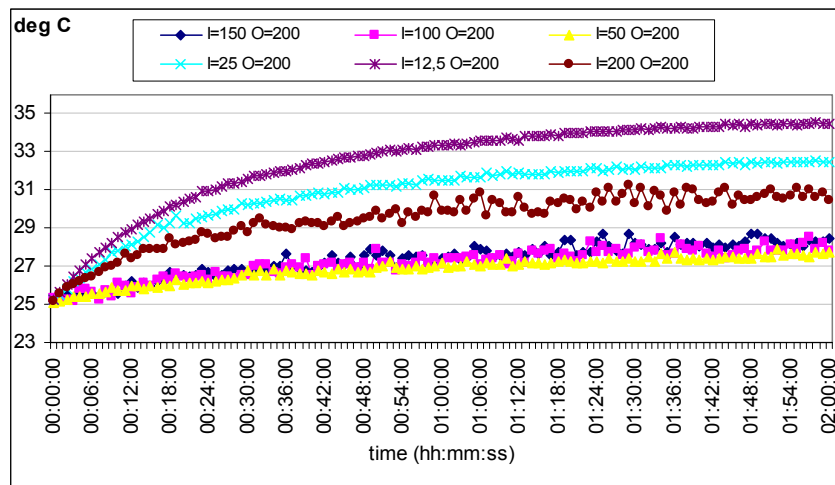


Figure 5.11 Air temperatures in the cavity for various inlet sizes (mm).

Figure 5.12 illustrates a comparative plot of average values of temperatures inside the cavity between variable inlet sizes and fixed outlet sizes. A trend was observed

whereby temperature levels in the cavity decreased when the inlet size relationship decreased to a maximum of 0.25 to 1. After this size ratio overheating started to develop in the cavity. This clearly indicates the important factor that the temperature is dependent on the inlet-outlet size ratio, establishing the efficiency of airflow rates and representing a key point to take into account for overheating control.

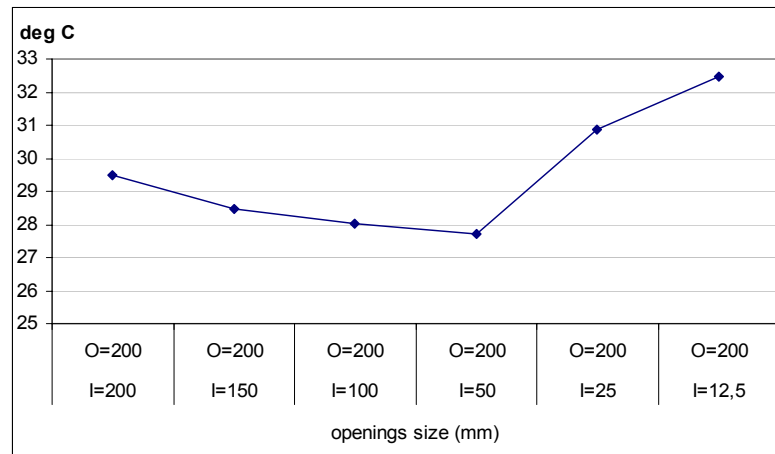


Figure 5.12 Average temperature values inside the cavity for various inlet sizes.

The variations in inlet size-ratios also had direct implications on the thermal performance of the room. A clear behaviour emerged in that the temperature levels increased rapidly when the cavity inlets size was reduced and thus better performance occurred when the inlet-outlet ratio was 0.5 to 1. This is consistent with the behaviour observed in the cavity. This indicated that the improvement in the rate of heat removal in the cavity had a comparative influence in reducing in part, the heat transferred to the room by conduction through the inner skin. Figure 5.13 shows the temperature plots for each of the variations of inlets size, in which the lowest temperatures were obtained with inlet to outlets ratios of up to 75%.

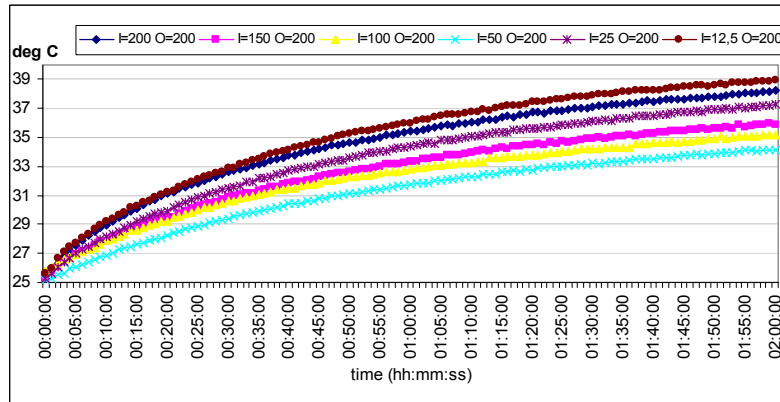


Figure 5.13 Air temperatures inside the room for various inlet sizes (mm).

In the case of the variable outlets sizes in relation to fixed inlets size (figure 5.14), the reduction in temperature levels were found to be in some manner similar to the previous case. The relationship of 1 to 1 of inlet to outlet size also proved not to be as efficient as relationships of less than 0.75 to 0.25 to 1. In this case, the highest temperatures were also obtained when a minimum outlet size of 12.5mm was used. In this case, the influence of the pressure difference on inlet/outlet size determined the increase in the airflow rate and the decrease in temperature levels. Nevertheless, the most favourable relationship here was found to be 0.75 and 0.50 to one, which indicates that the reduction in the size of the outlet is a more critical issue than the reduction in the size of the inlet.

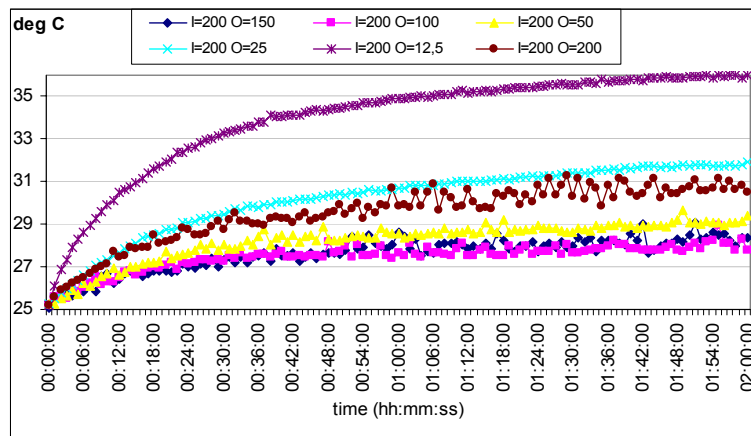


Figure 5.14 Air temperatures in the cavity for various outlet sizes (mm).

In figure 5.15, the average values of temperatures between varied outlet sizes and fixed inlet sizes have been compared. In these tests, a similar trend emerged whereby the temperature levels inside the cavity decreased when the outlet size ratio was decreased but only to a maximum of 0.50 to 1; the cavity started to develop overheating after this. Temperatures here were also dependent on the size ratio, however the implications of the stack effect inside the cavity, which increases air pressure at the top of the buffer zone, determined a limitation on the reduction of openings size at the top of the DSF. This indicated that the reduction in the outlet size is very critical and also that the outlet size cannot be reduced to more than 50% in relation to the inlet size as overheating will start to develop.

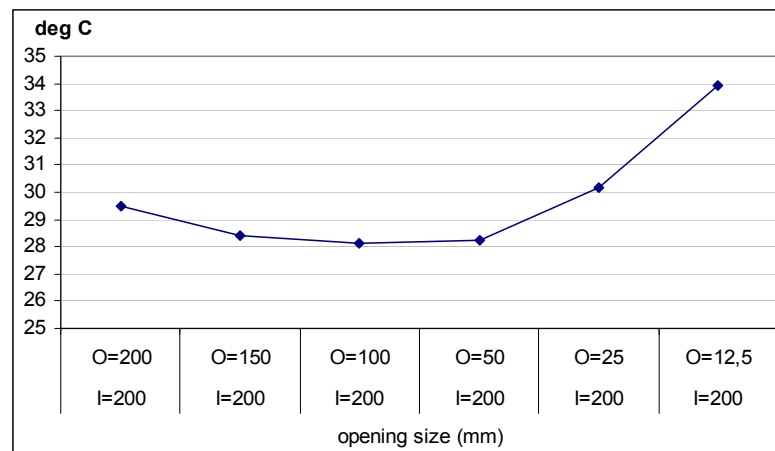


Figure 5.15 Average temperature values inside the cavity for various outlet sizes.

The variations in the performances observed with the different outlet size-ratios were relatively similar to those noted when the inlet sizes were adjusted. In this case, the most rapid increase in temperature levels was observed with the smallest outlet openings, and the lowest levels were observed when adjusting outlet ratios up to 50%. Although figure 5.16 shows a slightly lower plot on the performance when the ratio was up to 75%, the difference with the previous ratio is only 0.60°C. This may be caused by the reduction in incident light due to the enlargement of opaque areas

when the outlet size was increased rather than from the influence of heat transfer through the inner skin. In this case, it is also important to highlight that the improvement in the rate of heat removal from the cavity also had a comparative influence on the reduction of the heat transferred to the room.

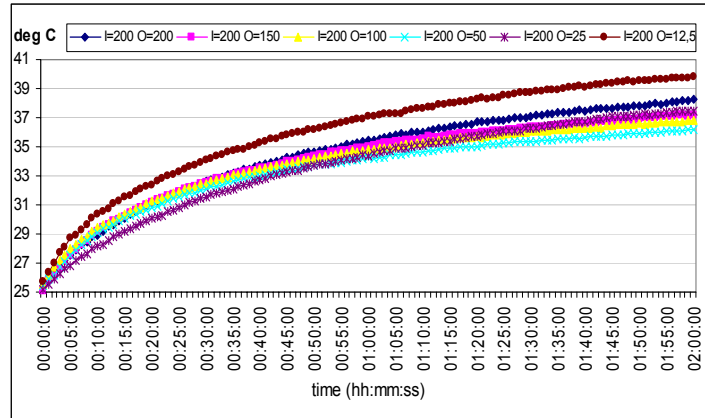


Figure 5.16 Air temperatures inside the room for various outlet sizes (mm).

5.2.4 Effect of Diffuse Radiation.

In order to observe the effect of diffuse radiation through a thin cloud on the overall performance of the chamber; a series of tests using a diffuser screen were performed. The screen was placed between the light source and the external skin at a distance of 500mm from the external skin (figure 5.17).

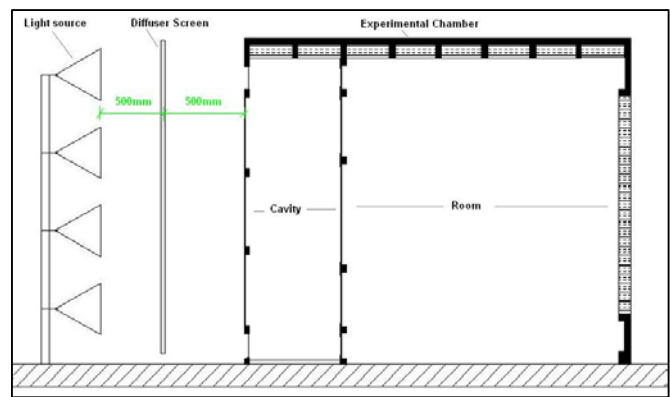


Figure 5.17 Configuration of the experimental chamber using screen diffuser in front of the external skin.

The screen has a light transmittance of 0.38 on visible and approximately 0.45 on near infrared, with a reflectivity factor of 0.60 [8]. Figure 5.18 shows the light transmission characteristics provided by the manufacturer.

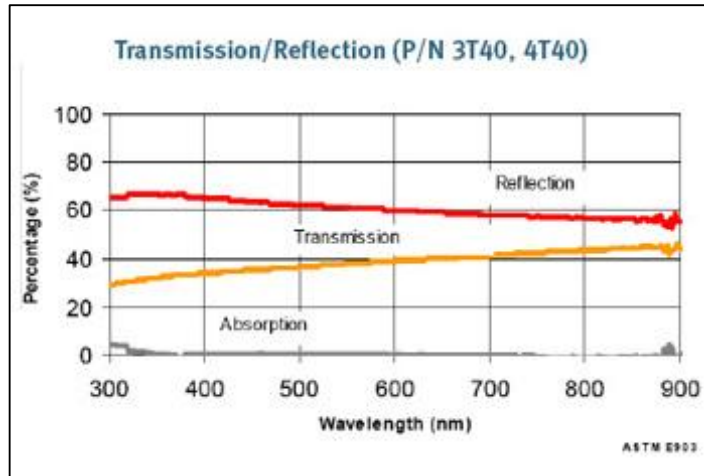


Figure 5.18 Light transmission and reflection of external screen diffuser fabric [8].
Source: GORE™ TENARA® Architectural Fabric
http://www.gore.com/en_xx/products/fabrics/index.html

The levels of radiation on the external and back wall of the room were measured. Figure 5.19 shows that the average radiation level on the external skin was 329.57W/m², which is equivalent to a reduction of 48% in the heat load from the light source. This influence can also be observed in the direct radiation received by the back wall of the room, which also showed a reduction of 54% on the direct heat load from the light source. As a high percentage of the light is reflected and absorbed by the fabric, it can be inferred that the radiative heat generated by the lamps was mostly absorbed and reflected by the diffuser screen, which allows the observation of the thermal behaviour of the chamber without the influence of this additional load.

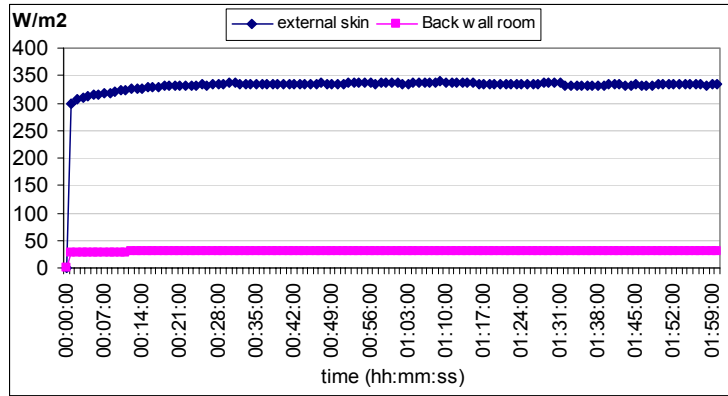


Figure 5.19 Total incident radiation using a screen diffuser in front of the external skin.

The illuminance inside the room was also measured and the mean values revealed attenuation of 45%. Figure 5.20 shows a plot of the levels measured, in which the mean average value in the centre of the room was 645.85 lux and 418.10 lux for the light reflected inside the room. This reduction also shows the influence of the fabric on reducing light transmittance in visible wavelengths.

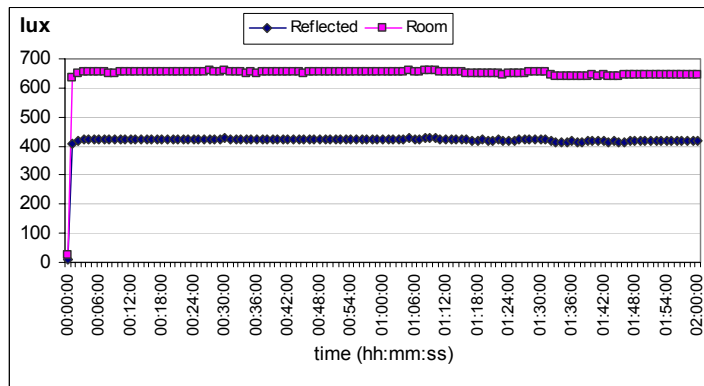


Figure 5.20 Illuminance in the room using a screen diffuser in front of the external skin.

The thermal behaviour of the cavity and the room was measured for the main configurations of the ST and STV cases. As the total heat load entering the external skin was reduced, an expected drop in the overall temperature values was observed. The temperature responses inside the cavity both with and without the screen diffuser exhibited similar physical behaviours, also reducing the additional radiative heat

created by the lights. A clear fall in the temperature levels inside the cavity was observed when the inlets and outlets were open (STV). Figure 5.21 shows that the patterns of temperatures observed were similar to those without the diffuser screen. Although in this case, the difference in temperature from ST to STV was about 8%, whilst in the case where the screen was not used a difference of 24% was observed. This indicated that there is a direct relationship between buoyancy and incident radiation. Decreasing direct radiation by using the screen slowed the buoyancy and stack effects. The heat removal rate was also affected, indicating that incident radiation played a key role on the stack effect in the DSF.

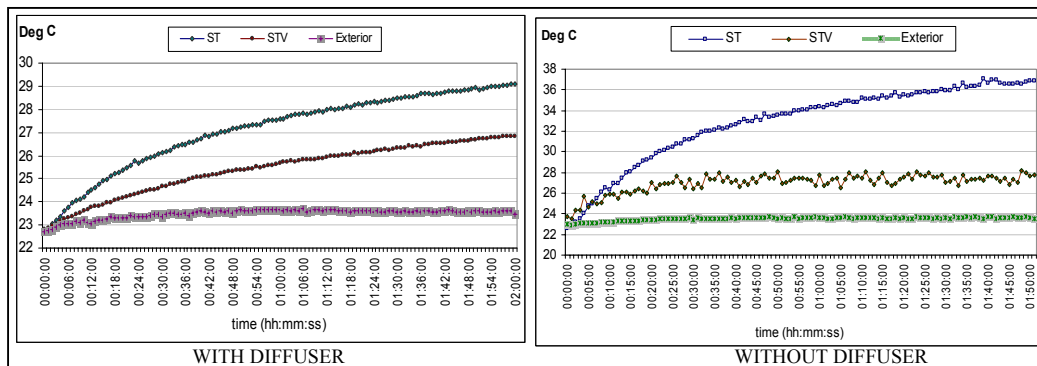


Figure 5.21 Air temperatures in the cavity for ST and STV comparing the influence of diffuser in front of external skin.

For the thermal response inside the room, there was also a clear difference between non-ventilated and ventilated cases. Figure 5.22 shows a plot of temperature readings inside the room for ST and STV cases. There is a similar difference in the temperatures between ST and STV either with or without the screen. In both set-ups, the difference inside the room is about 6% lower when the cavity was ventilated (STV), which means that the influence of the additional radiative heat load accelerates the rate of convective heat transfer inside the cavity, but it is slightly delayed by conduction through the inner skin.

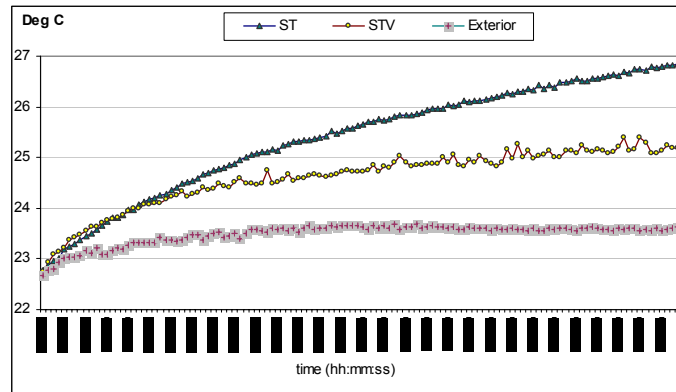


Figure 5.22 Air temperatures in the room for ST and STV using screen diffuser.

Taking into consideration that the main objective of this research was to assess the physical behaviour of the DSF, the following issues were considered in order to carry out the tests using the screen diffuser in front of the external skin:

- The amount of heat reflected and removed by the screen was noticeably high, which caused an evident reduction on the stack effect and the heat removed from the cavity.
- The experimental values of radiation measured without a diffuser screen were closer to the critical scenario assumed for a DSF facing East or West during summer at 30°N.
- The overall physical thermal behaviour of the DSF was similar when the chamber was exposed to the light source, either with or without a diffuser screen.
- The cavity temperature reduction was slightly higher than the reduction in the total radiation for the enclosed cavity. It was due to the proportionally greater reduction in IR radiation rather than the directional quality of the radiation. (The heating of the inner skin was reduced.)

The differences in thermal performance of the ST and the STV inside the room were very similar in both experimental set-ups.

5.3 ROOM OPENING ARRANGEMENTS

For this parameter, the thermal behaviour of the cavity and the room were assessed and compared using various configurations of inlets/outlets arrangements on the inner skin and the back wall of the room. The cavity depth was set at 800mm with standard clear glass on both skins. The inlets and outlets on the external skin were left open during all tests (STV). In all cases the main variables were compared in relation to the different combinations of openings (as shown in figure 5.23).

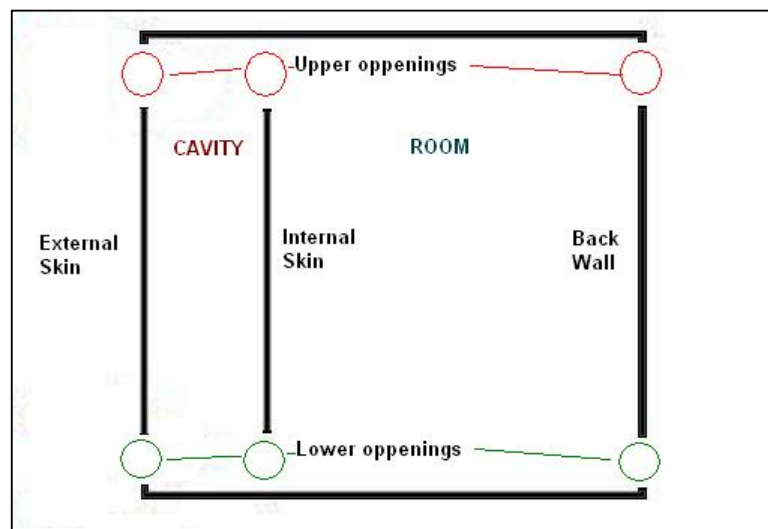


Figure 5.23 Location of openings in the experimental chamber for testing cross ventilation effect through inner skin and back wall of the room.

The first correlation of thermal behaviour was assessed according to the position of inlets on the external and internal skins, when the room and cavity were allowed to have air exchange through the openings of the inner skin. Figure 5.24 illustrates the plots of the temperature performance inside the cavity. It was observed that a slight reduction in the temperature inside the cavity occurred when air was exchanged from the cavity to the room through the upper openings of the inner skin. However, this apparent reduction meant that the heat accumulated in the cavity was induced into the room by the stack effect of the DSF. This indicates that the room will overheat in

the long term if no means of releasing the heat is provided. In the other cases, the temperatures reached were higher and generally constant, showing the importance of continuous airflow in the cavity in deterring the development of overheating.

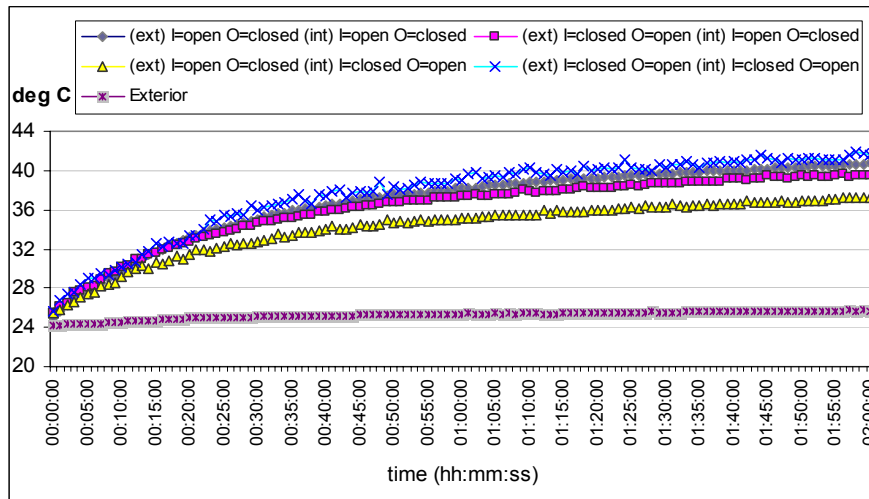


Figure 5.24 Air temperatures in the cavity for various positions of inlets and outlets on external and internal skins.

This first correlation indicated the importance of the position of the inlets and outlets on the inner skin according to ventilation and heating requirements. It can be established from these results that the aperture of upper openings on the internal skin encouraged the heated air accumulated in the cavity to flow inside the room when the outlets were closed. On the contrary, heat air removal from the room was slightly encouraged when the outlets on both skins were open.

The improvement in the cavity temperature on STV when ventilation was allowed through the inner skin is illustrated in figure 5.25. The graph illustrates a considerable reduction in overheating when airflow continuously flows through the cavity. This is another factor to bear in mind when considering overheating control. In chapter 6, the airflow of these cases is illustrated and discussed.

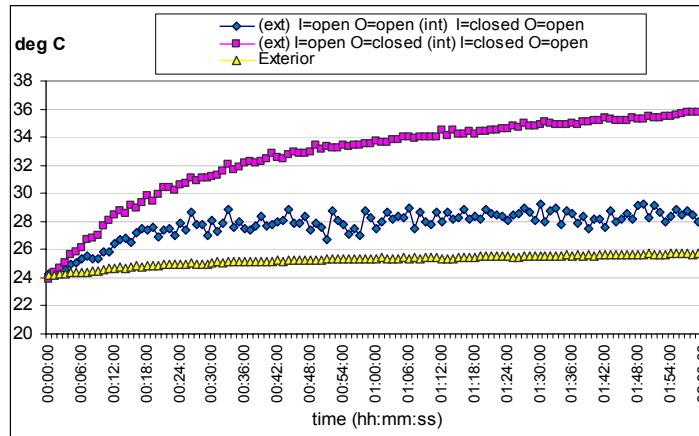


Figure 5.25 Air temperatures in the cavity using cross ventilation with the DSF.

It was previously considered that the best way to prevent overheating in the cavity was to use ventilation. In the case of the room, the position of the inlet/outlets on the inner skin contributed dramatically to the removal of heat and the prevention of overheating. Figure 5.26 illustrates how closing one of the openings on the inner skin increased the possibility of overheating developing. In both cases, closing the inlets or outlets led to a rapid increase in the temperature inside the room. When air continuously flowed through both inlets and outlets on the inner skin, the levels of temperatures were reduced by 5.5°C. However, temperature levels inside the room were still high and alternative means of heat removal were still needed.

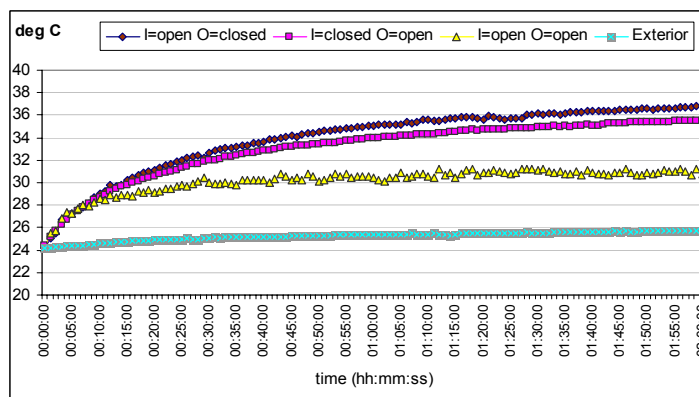


Figure 5.26 Air temperatures in the cavity in STV for various openings configurations on the inner skin

As previously discussed, the lack of air removal from the cavity was the primary cause of overheating development. Figure 5.27 shows how temperature levels inside the room rose rapidly when air from the cavity entered without exchange with the exterior. Although a slight reduction was perceptible when both the inlet and outlet on the inner skin were open, the temperature levels were still too high. This was due to the elevated convective heat from the cavity which flows faster through these openings.

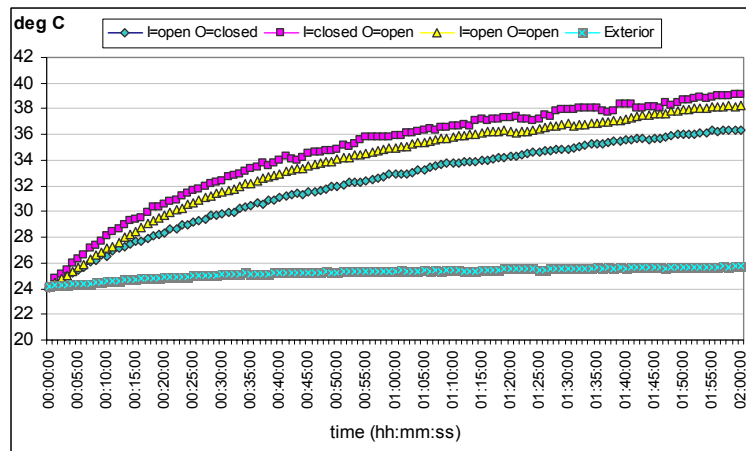


Figure 5.27 Air temperatures in the room with non ventilated cavity (ST) using various openings configurations of the internal skin.

The dramatic difference in temperatures between ventilated (STV) and non ventilated cases (ST) was evident when comparing the two cases where the room was allowed to release the excess of heat from the cavity to the exterior and where the room received the heat accumulated inside the cavity. Figure 5.28 shows a dramatic difference of 9°C in maximum room temperatures between a sealed cavity when air is allowed to enter the room, and a ventilated cavity that allows air exchange with the room. This highlights the need to consider the inlet/outlet positions in DSFs according to the passive requirements for heating, natural ventilation and air removal.

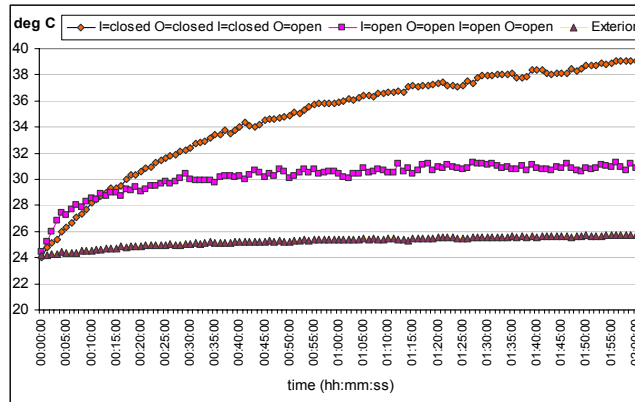


Figure 5.28 Temperatures inside the room for ST and STV using different openings configurations on the rear wall of the room.

It was observed that temperature levels dropped in ventilated cases, however the levels were still high when the inner skin was open, meaning that added heat load enters the room by means of free convective gains through the inner skin openings. The impact of heated air from the cavity to the room determines a critical design issue for setting the configurations of the DSF for ventilation and passive heating. Figure 5.29 shows how there is little influence on the temperature performance when varying the back wall openings position, because of no significant differences in pressures between the inside and outside of the room. Increased pressure differences are required to promote efficient air removal.

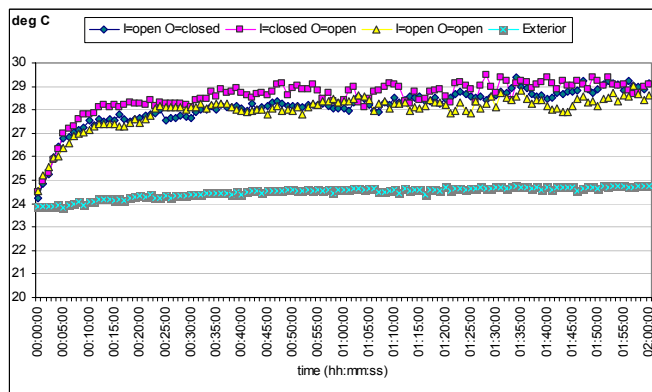


Figure 5.29 Air temperatures in the room for various inlets and outlets positions on the rear wall, with open inlets and outlets on the external and internal skins.

The internal skin was closed at the bottom openings to assess how the thermal performance of the room behaved when only dependent on buoyant heated air, which was forced to circulate to the top of the DSF. The positions of the openings of the back wall were adjusted and temperatures were measured inside the room. Figure 5.30 shows a clear difference in the temperature performances of the room when cross ventilation from the inner skin to the back wall of the room was allowed. This demonstrated that inducing a back flow combined with buoyant airflow from the cavity makes air removal from the room more efficient, somewhat reducing overheating as expected.

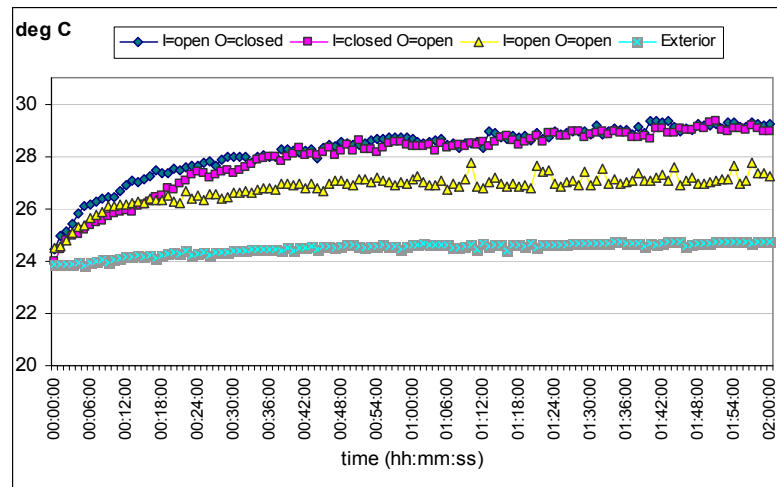


Figure 5.30 Air temperatures in the room with ventilated cavity and open outlet on internal skin, using various inlets and outlets configurations on the rear wall.

5.4 DEVICES IN DSF

For the analysis of the thermal performance of the experimental chamber with devices inside the DSF, the cavity was modified using reflective panels over the glazed skins as solid shading devices. Fabric blinds were used as translucent shading devices, and louvers were used as adjustable shading devices. Each set-up was tested

in the ST and STV; and the temperatures inside the cavity and the room were measured and compared.

5.4.1 Reflective Panels as Shading Devices

For this parameter, the areas on the external and internal skins were sheltered using reflective panels which covered from 33 to 66% of the glazed area. The thermal performance was compared for various positions of the shading panels on the external and internal skin.

In order to assess the influence of the panels on the heat transfer of the facade (both inside and outside the facade cavity); the initial set of tests were carried out by covering 33% of the glazed area of the external skin and then similarly on the internal skin. Figure 5.31 shows the plots of the thermal performance inside the cavity comparing the position and the configuration of the cavity. The graph shows a noticeable increase in the temperature inside the cavity when the inner skin was covered by the panels. This indicated a direct rise in the convective heat transfer coefficient in the buffer space as a result of the increase in the radiation reflected by the panels inside the cavity. Although the temperature levels were reduced when the cavity was ventilated, it was clear that in the cases of both the ST and STV, the main factor that contributed to the increased heat transfer in the facade was more reflected radiation within the cavity. This was as a result of adding extra surfaces in the buffer space of the facade.

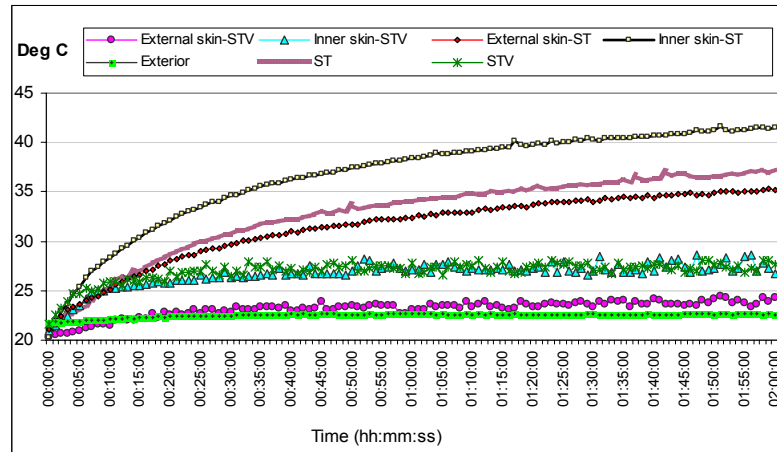


Figure 5.31 Air temperatures inside the cavity for ST and STV using reflective shields on external and internal skins.

Enlarging the shaded areas of both skins led to an overall reduction in the heat load by radiation through the double skin glazed facade. The room temperatures mostly depended on; the amount of resultant direct incident light; the conductive heat transfer passing through the inner skin; and the long-wave IR reflected on the walls of the room. Figure 5.32 shows various temperature performances in the room when the shaded on each skin of the facade were increased by 66%. In these cases a tendency to overheat was observed when the cavity was sealed. However simply reducing the level of direct incident light by adding additional shaded areas did lead to the effective reduction of the heat load in the room. The heat transfer in the cavity, the rate of heat removal when the cavity was ventilated and the reduction in the resultant incident radiation to the room were the key factors in controlling the temperature levels inside the room.

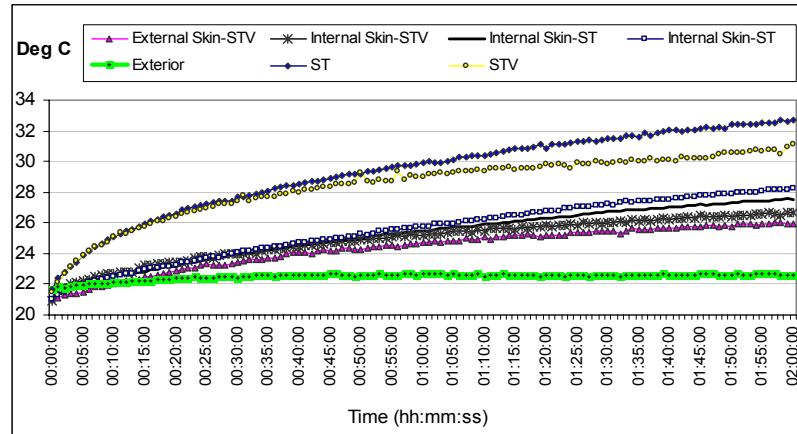


Figure 5.32 Air temperatures inside the room for the ST and STV using reflective panels on external and internal skins.

Figure 5.33 shows the values of maximum temperatures obtained for the ST and STV depending of the amount of glazed areas shielded on each skin. The cases shown in this figure validated the trend of decreasing temperatures inside the chamber and the room when external protections were used. However, when protections were placed inside the cavity, the temperature response was different due to the radiation reflected and the increased convective gains within the cavity. The difference in temperature between the cavity and the exterior (ΔT_{ce}) showed a tendency to rise when more radiation was reflected inside the DSF. The difference in temperature between the room and the exterior also seemed to rise when temperatures in the cavity were higher, thus the incidence of conductive heat transfer increased the total heat load of the room. There was an overall reduction in the temperatures in both cavity and the room when more glazed areas were sheltered; however the temperature in the cavity increased when more radiation was reflected from the panels covering the inner skin.

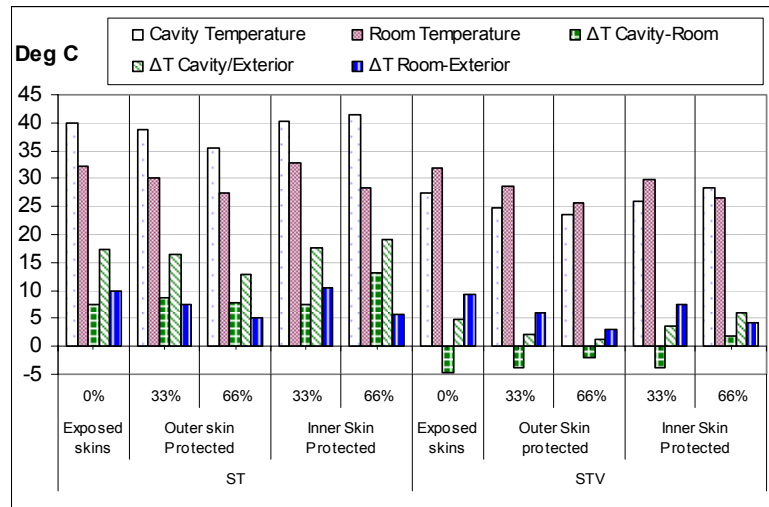


Figure 5.33 Comparison between maximum temperature values in the cavity, the room and outside the chamber in ST and STV for various areas of glass covered on the external and internal skins.

When comparing within the same case, it was confirmed that even if the cavity was ventilated or not, the room temperatures tended to be lower when more of the surface on the outer or inner skin was protected. The figure above shows that the temperatures of the room decreased as more of the surface area was covered. Nevertheless, it is clear that the amount of heat reflected by the surfaces inside the cavity increased the heat in the DSF and decreased the heat losses from the room through the glazed skin. The net result of this was an increase in the overall indoor heat level.

5.4.2 Blinds

The experimental chamber was fitted with blinds as shading devices in order to control the direct incident light on the external and internal skins. The glazed skins were covered with three white vertical PVC-Polyester fabric blinds. The total surface of each skin was covered from 25% to 75%. According to the manufacturer, Skyspan limited, the fabric has a reflectance of 0.64 and light transmission in visible

wavelength of 0.42 [9]. The blinds were positioned in configurations outside the cavity, inside the cavity and behind the internal skin. These positions can be seen in figure 4.5 of the previous chapter. The comparative analysis of the thermal performance was then based on the influence of the blinds in relation to their position in the DSF.

5.4.2.1 Position on External Skin

The influence of the blinds on the temperature was compared based on the blinds covering 50% of the glazed surfaces. For this parameter, the blinds were placed in front and behind the external skin, in both the ST and STV cases. Figure 5.34 again confirms the development of overheating in ST when the cavity was sealed. Although the resultant temperature can be reduced by nearly 5°C when placing the blinds outside the external skin, the important reduction was achieved when the cavity was ventilated in the STV. The graph also illustrates how the temperature was increased when the blinds were positioned inside the cavity.

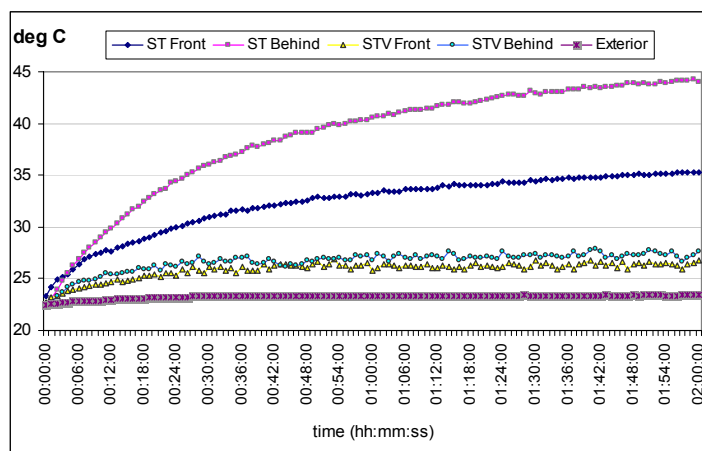


Figure 5.34 Air temperatures in the cavity for ST and STV using blinds in front and behind the external skin.

In both ST and STV cases, the highest temperature levels were reached when the blinds were placed behind the external skin. This indicated that the increase in heat transfer was due to the greater reflection of light on the blinds surfaces, which also contributed to the increase in the greenhouse effects inside the cavity. However, in the ventilated cavity, the difference in temperatures between both cases was very small (0.86°C), indicating that most of the heat reflected and accumulated by the blinds was rapidly dissipated from the cavity by means of natural convection and the favourable position of the blinds close to the external skin.

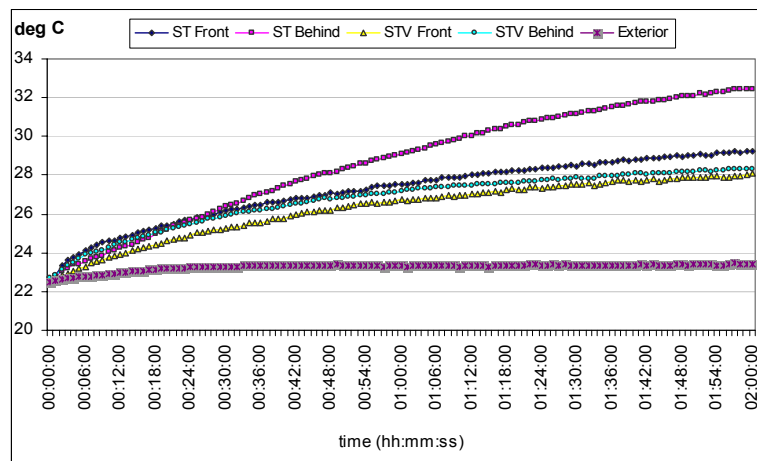


Figure 5.35 Air temperatures in the room for ST and STV using blinds in front and behind the external skin.

In the case of the thermal performance of the room (figure 5.35), a correlation could be seen between the position of blinds and the resultant temperatures. Higher temperature levels were obtained when the cavity was sealed. These temperature levels increased dramatically when the blinds were placed inside the cavity. This suggests that the amount of light reflected by the blinds, the increased convective heat transfer in the cavity (due to the position of the blinds), the conductive heat transfer through the inner skin, and the remaining direct radiation passing through the blinds add important loads to the heat balance of the room. Therefore, overheating

clearly developed in this case, indicating a critical factor which must be taken into account.

On the other hand, the position of the blinds had a positive affect in reducing overheating. The next figure illustrates how the resultant temperatures inside the room were slightly reduced by 0.78°C when the blinds were placed behind the external skin and the cavity was ventilated (STV). This highlights an important benefit to consider when blinds are used in a DSF.

5.4.2.2 Position on Internal Skin

Blinds were placed in front and behind the internal skin, in both the ST and STV cases. Figure 5.36 illustrates the sharp overheating effect, created when the blinds were placed inside the cavity when it was sealed. A dramatic difference of 17.93°C on the maximum temperature can be observed as compared with the other cases. However, when blinds were placed inside the room, the temperatures in the cavity did not reach such high levels as the blinds increased the rate of convective heat transfer in the surrounding air. This in turn led to an increase in the convective heat rate inside the room. The graph also shows how the temperature was dramatically reduced when the cavity was ventilated, even when the blinds were inside the cavity. The temperature levels were quite similar, indicating the importance of boosting convective heat transfer in combination with constant airflow in the cavity as a means of preventing overheating from occurring. The position of the blinds inside the room had no relevant influence on the thermal performance of the cavity. This was because the radiation reflected by the blinds was reflected by the internal glass.

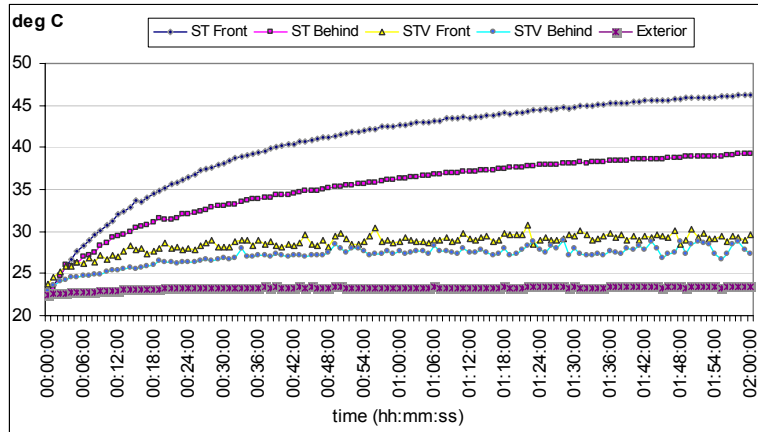


Figure 5.36 Temperatures inside the cavity for ST and STV using blinds in front and behind the internal skin.

The temperature performance of the room was critically affected by the position of blinds behind the inner skin. As mentioned before, the increase in reflected radiation on the blind's surfaces boosted the greenhouse effect in the room, by means of improving the total U-value of the inner skin.

Figure 5.37 shows how no significant differences were observed between ST and STV cases when the blinds were placed inside the room. Only when the blinds were placed inside the cavity was there a reduction in the temperature levels. The figure confirms that it is possible to achieve a reduction of 3.5°C when placing the blinds inside the cavity and allowing continuous airflow through the cavity of the DSF. This indicated that locating the blinds as shading devices inside the spaces next to the glazed facade is not helping in the prevention of overheating.

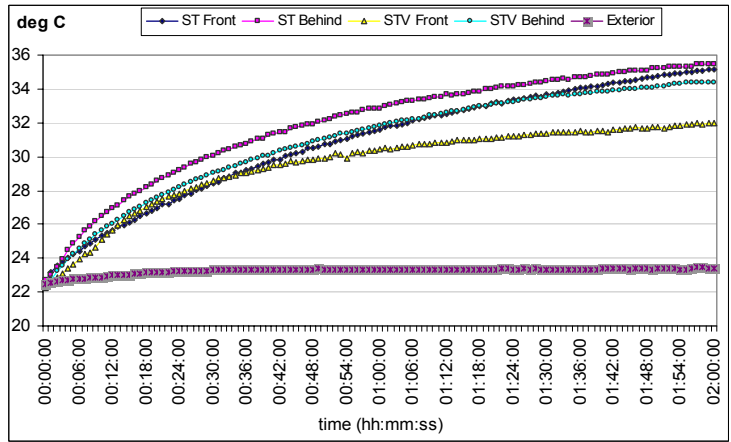


Figure 5.37 Air temperatures in the room for ST and STV using blinds in front and behind the internal skin.

Taking into account that a ventilated cavity allows for better prevention of overheating, STV cases were also compared in order to determine the best possible configuration when using blinds in combination with a DSF.

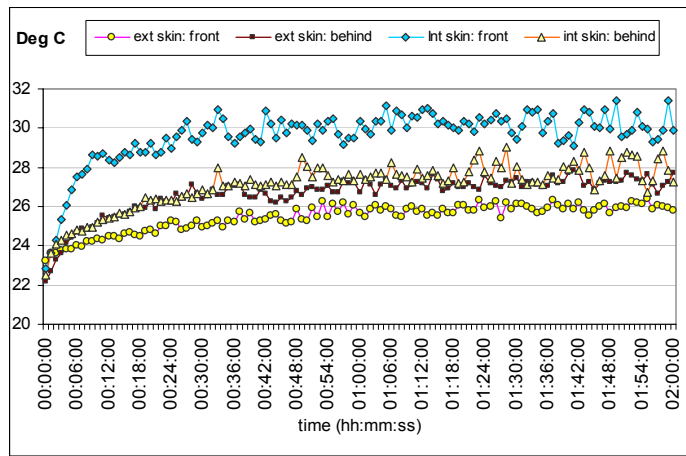


Figure 5.38 Air temperatures in the cavity for STV for various positions of blinds next to the external and internal skins.

Figure 5.38 shows that the best position for the blinds, if you want to achieve lower temperature levels in the DSF, is to place them in the cavity behind the external skin. There was a very clear difference in temperature when the blinds were placed in front of the internal skin, which means that even when the heat transfer rate was

increased, the air flow removal was more efficient when the blinds were closer to the external skin.

When comparing only between STV cases, a very clear difference in temperature levels was observed when the blinds were positioned inside the room. Figure 5.39 shows how quickly the temperature levels rose when the blinds were located behind the internal skin. Although the lowest temperatures were obtained when the blinds were located outside the external skin, the differences of temperature levels were relatively small when compared within the cases using blinds in the cavity. This indicates how the heat removal by a ventilated cavity is a key element in controlling overheating.

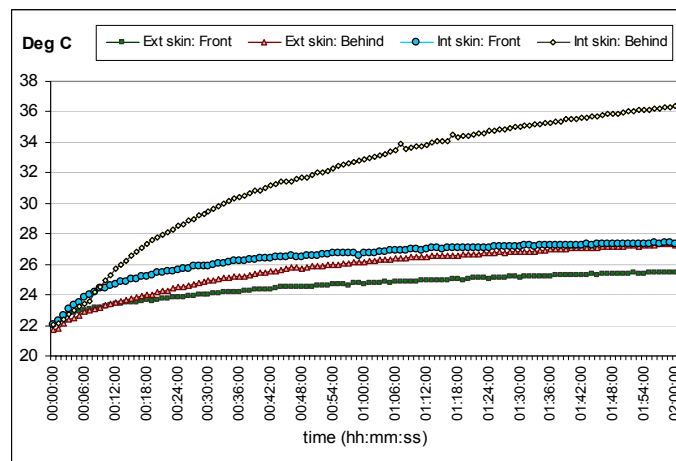


Figure 5.39 Air temperatures in the room for STV for various positions of blinds next to the external and internal skins.

The illuminance inside the room was greatly affected by the position of the blinds. Figure 5.40 shows how better levels of lighting were achieved when the blinds were positioned close to the inner skin. The lowest visible light levels were obtained when the blinds were behind the external skin. This also demonstrated that the amount of light transmitted by the blinds to the inner spaces was higher when they were placed close to the inner skin.

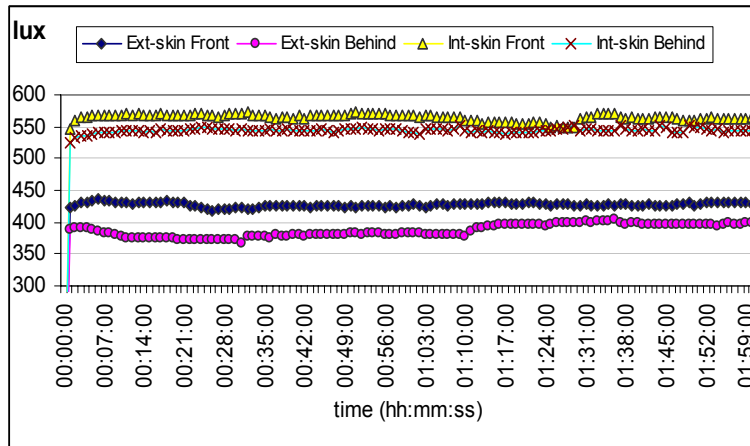


Figure 5.40 Illuminance in the room for various positions of blinds.

Figure 5.41 shows the maximum temperatures obtained in the ST depending on the variation of size and location of the blinds. It generally confirms that increasing blind surfaces outside the chamber reduces temperatures inside the cavity. In contrast, temperatures rise when blinds surfaces are increased inside the cavity. This confirms that convective heat transfer increases as a result of more reflected radiation from the blinds surface.

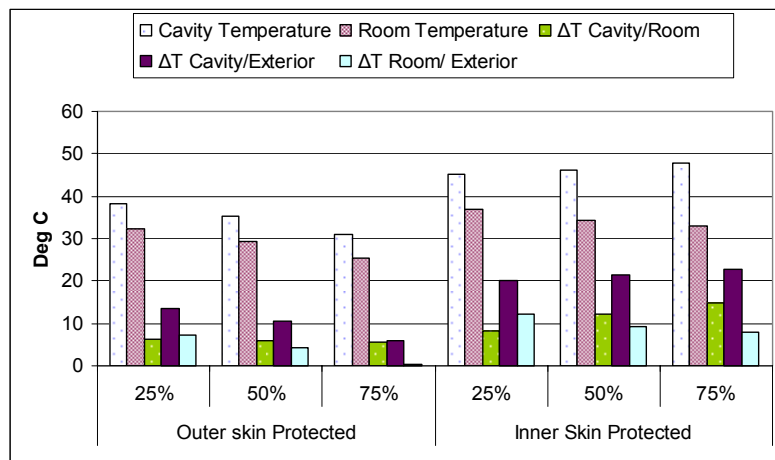


Figure 5.41 Comparison between maximum temperature values in the cavity, the room and outside the chamber in ST for various areas of glass covered by the blinds on the external and internal skins.

The difference in temperatures between the cavity and the room (ΔT_{cr}) were virtually identical when the blinds were placed outside the external skin because the load from radiation (Q_{sol}) was reduced and the radiation reflected by the facade (Q_{ref}) increased. However the external facade gains (Q_f) were considerably reduced but only when the ST was in this position. Therefore, this position is not really the most suitable as it creates practical issues for maintenance and aesthetics. On the other hand, ΔT_{cr} tended to increase as a result of the increased convective heat transfer when the blinds were inside the cavity

The difference in temperature between the room and the exterior (ΔT_{re}) tended to decrease as the blinds outside the external skin blocked the radiation received. However, it tended to increase when the inner skin was covered; therefore it proves that the increased heat transfer from the cavity contributed to the development of overheating in the room when the cavity is not ventilated.

In the ventilated cases, there was an overall reduction in the values of temperatures inside the cavity when more of the glazed area was covered. However, the temperatures inside the room were relatively similar to those obtained in the non-ventilated cases (Figure 5.42). Although the heat gains inside the cavity were lower in STV when compared with ST, a similar trend existed whereby the temperatures in the cavity increased when more radiation was reflected and absorbed by the blinds fabric.

Room temperatures tended to decrease slightly when more glazed skin was covered. Nevertheless, temperatures were always higher when the blinds were inside the

cavity, proving that the total indoor gains were increased due to an overall increase in the net indoor gains (Q_i) and a reduction in the losses (Q_l) from the room. This was due to the increased cavity temperature that effectively made the buffer space an insulator. However this effect, while a key feature of DSFs, is also the biggest problem in causing overheating.

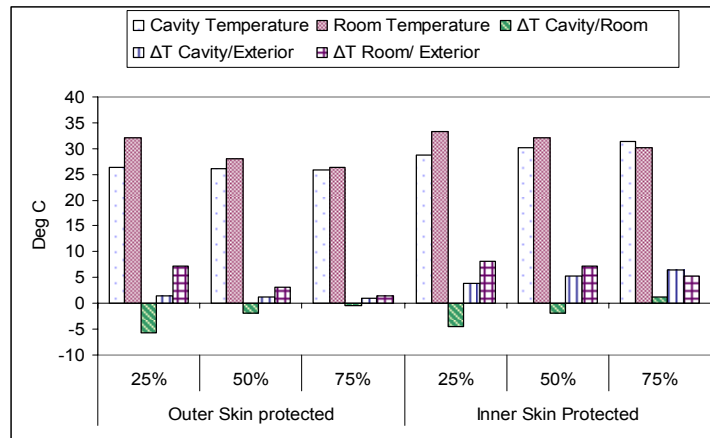


Figure 5.42 Comparison between maximum temperature values in the cavity, the room and outside the chamber in STV for various areas of glass covered by the blinds on the external and internal skins.

5.4.3 Louvers

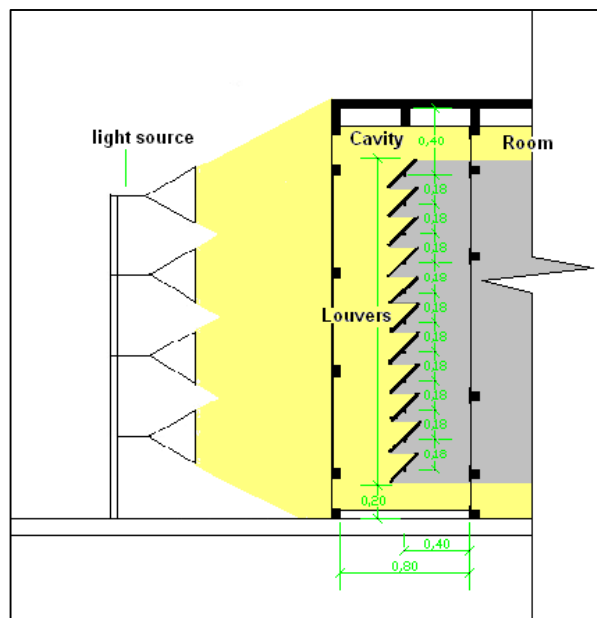


Figure 5.43 Main configuration of the DSF cavity using horizontal louvers as shading devices.

In order to identify their implications on the thermal performance of the DSF, 11 horizontal louvers were placed inside the cavity. As the incident radiation from the light source was normal to the glass surface, the louvers tilt angle was adjusted to 45° with an overlap of 10 mm on each side, increasing the shading ratio behind the louvers to 0.92. Figure 5.43 illustrates a typical section, with the main configuration of louvers inside the DSF cavity. The tests were carried out using 2mm aluminium laminates as louvers. Then, their colour was modified using three scales of grey, white and finally mat black colours.

The positions of the louvers in relation to the glazed skins were also adjusted and analysed. The colour of the louvers is also modified and analysed in this section. Each set-up was tested in the ST and the STV and the temperatures inside the cavity and the room measured and compared.

5.4.3.1 Position of Louvers

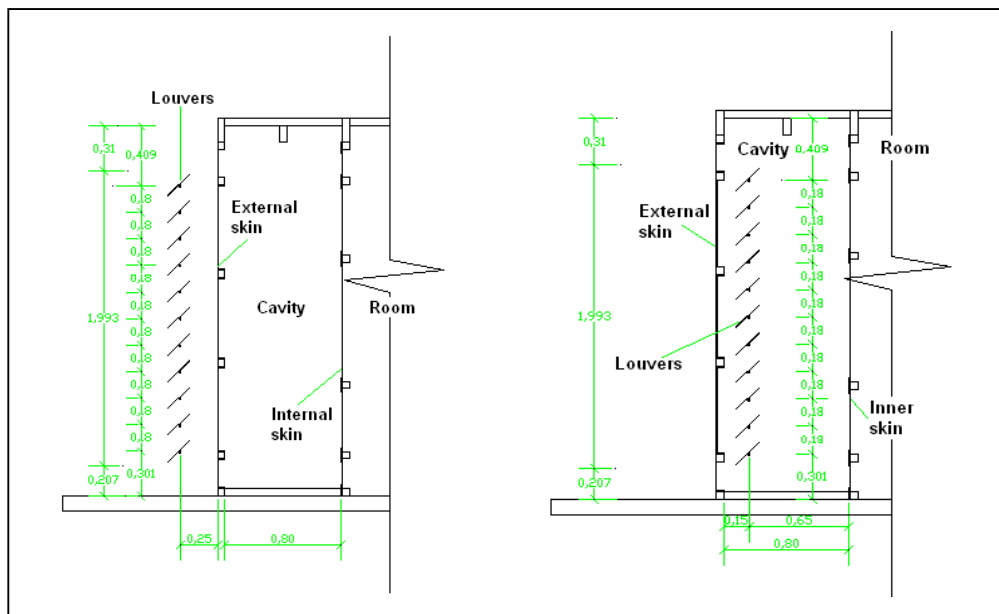


Figure 5.44 Louvers configurations at the front and behind the external skin

In this analysis, the louvers were positioned in 4 different places: outside the external skin; behind the external skin; in the centre of the cavity; and in front of the inner skin. Figure 5.44 and 5.45 show the configurations for each arrangement of the louvers position.

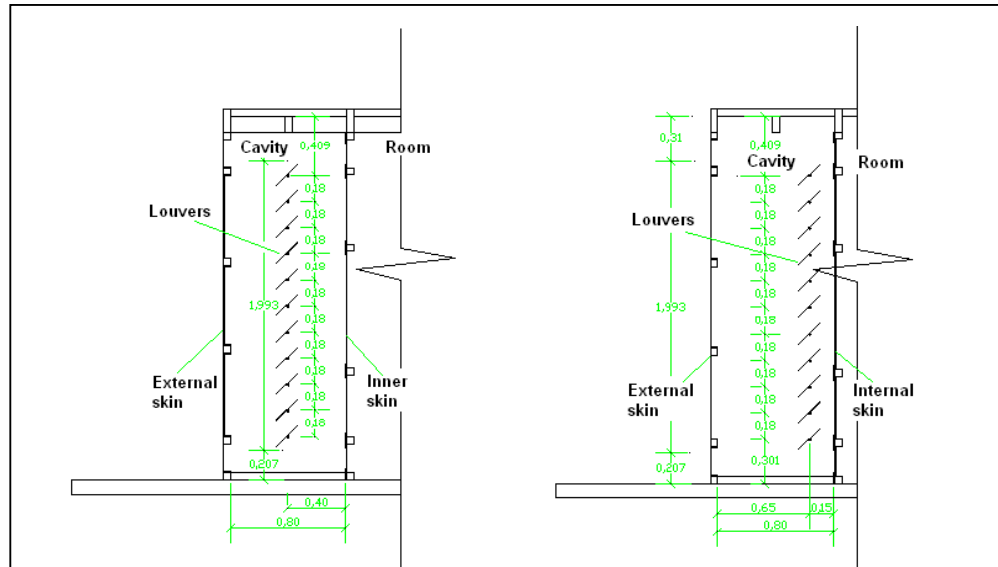


Figure 5.45 Louvers configurations in the centre of the cavity and before the inner skin.

The impact of the louvers on the temperature performance was compared based on their position in relation to the glazed surfaces. For this parameter, the set of louvers were placed in front and behind the external skin in both ST and STV cases.

Figure 5.46 illustrates the rapid development of overheating when the cavity was sealed. Although the resultant temperature was lower by 17.30°C when the louvers were outside the external skin, the position was inconvenient in terms of construction and maintenance. The graph also shows there was very little difference in the resultant temperatures when the louvers were placed inside and the cavity was sealed. The graph shows there were slightly higher temperatures when the louvers were in the centre of the cavity. This was due to the proximity of the louvers to the

thermocouples on this specific case. The significant difference in temperatures when the louvers were inside the cavity was due to the rise in the heat transfer rate caused by the additional light reflecting on the louvers surfaces.

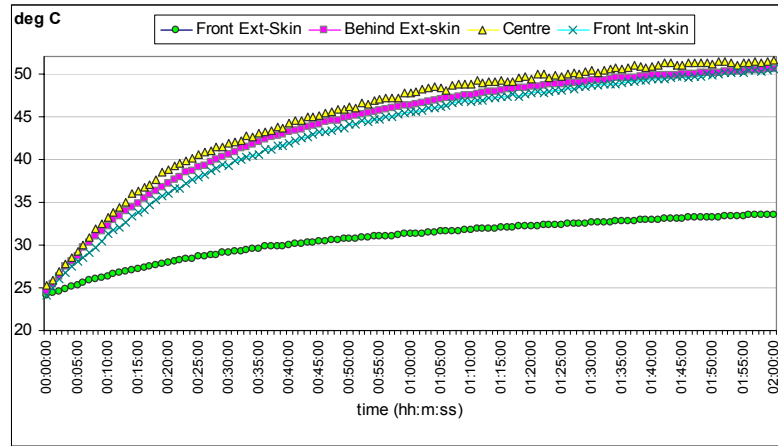


Figure 5.46 Air temperatures in the cavity for STV cases with various louvers positions.

Comparing various positions of louvers in STV, it was clear that there was a reduction in the rate of heat transfer. Temperatures were considerably lower and relatively steady. Figure 5.47 also shows the lowest temperature levels were reached when the louvers were placed outside the facade. However, the differences in temperatures in the cases of the louvers inside the facade were not as high as the ones measured with the sealed cavity.

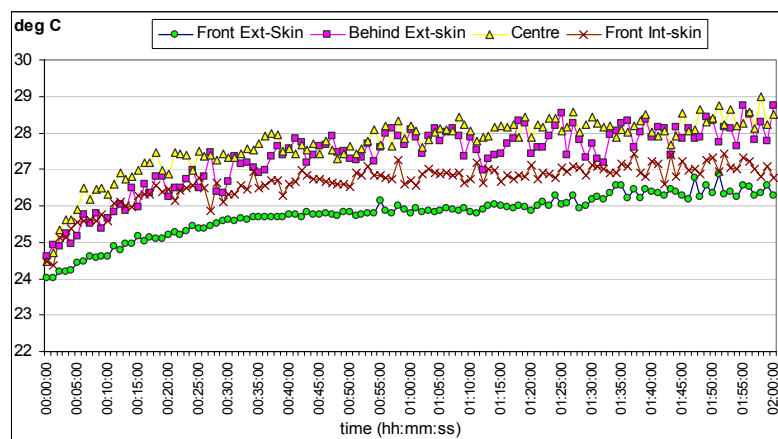


Figure 5.47 Air temperatures inside the cavity for STV with various louvers positions.

The differences between temperature performances inside the cavity were to some extent dissimilar, depending on the position of the louvers in STV. A slight reduction of 1.9°C in the maximum temperatures was observed when the louvers were behind the external skin. These results were consistent with those observed in the cases where the blinds were used as shading devices. This reiterated the importance of continuous airflow inside the cavity and the location of shading devices close to the external skin as a first step in controlling overheating in the DSF.

The thermal performances of the room were relatively similar in the ST when the louvers were inside the cavity (figure 5.48). An evident trend to develop overheating can be seen; however the lowest temperature levels were reached with louvers close to the glazed skins. This was essentially caused by the existence of two sub-buffer spaces between the louvers and the glass. This proximity induced a laminar air stream, which flowed parallel to the boundaries of the cavity, creating a continuous and cyclical flow, causing a slight reduction in the overall temperatures. The manifestation of these zones and the airflow behaviours are visualized and explained in chapter 6.

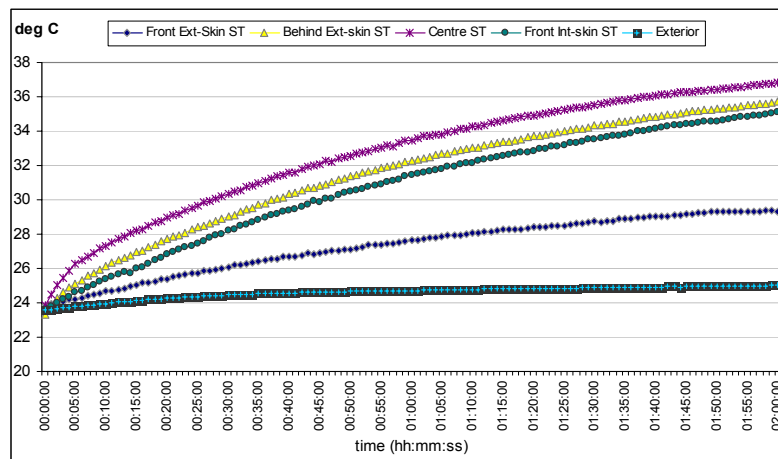


Figure 5.48 Air temperatures inside the room for ST with various louvers positions.

In the ventilated cases, a more gradual increase in the temperature levels could be seen. Figure 5.49 shows how much these temperature levels differed depending on the location of the louvers. These differences in temperature were produced by the direct influence of the louvers position on the airflow inside the cavity. With regard to temperature performance, it was clear that placing the louvers close to the external skin contributed to a reduction in the heat load rates in the room. In contrast with the temperatures inside the cavity, the room was greatly affected by the behaviour of the airflow inside the cavity. In chapter 6, these cases are visualized using CFD and explained in relation to performance of the airflow.

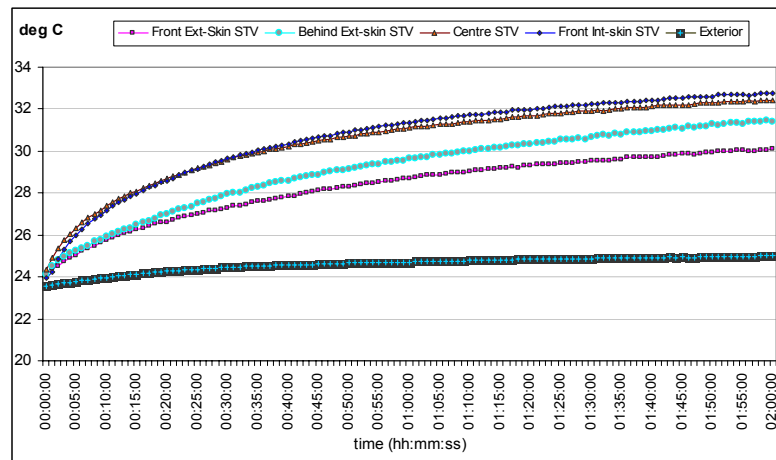


Figure 5.49 Air temperatures inside the room for STV with various louvers positions.

5.4.3.2 Colour of Louvers

In order to identify the influence of the light reflected by the louvers on the thermal performance of the DSF; the surface colour of the louvers was changed in order to modify their optical properties (figure 5.50). The thermal performance was measured with the louvers painted white, and then gradually changing the absorptivity by increasing 25% of black to the colour mix to produce three different types of greys, labelled 1 to the lightest to 3 to the darkest. Finally the louvers were painted 100% mate black.

The thermal performance of the chamber was also tested with a combination of white and black colours on each surface of the louvers. The tilt angle of the louvers, like the previous tests, was kept the same, 45°. The incident radiation from the light source was also kept normal to the external glass surface. Each set-up was tested in the ST and the STV, and the temperature inside the cavity and the room, measured and compared.



Figure 5.50 Surface colours on horizontal louvers inside the DSF chamber.

In comparing the different colour of louvers in the ST, it was noted that temperatures inside the cavity rose by levels of up to 53.2°C. In addition, a direct relationship between the reflectivity and the increased temperature levels was observed. Figure 5.51 shows how temperature levels increased when reflectivity decreased. A clear difference was observed in the temperatures inside the cavity when the louvers were white and white/black. However, it was interesting that when the louvers were black/white; temperatures were slightly lower than in the grey and black cases, indicating that the rate of heat transfer in the cavity decreased slightly with this combination as a result of the high reflectivity on the back of the louvers. Higher temperature levels were reached by decreasing reflectivity, indicating the inverse relationship of reflectivity on shading devices inside the cavity and overheating development as soon as the cavity is sealed. The results were not very different because of the dominance of IR and limited shortwave radiation.

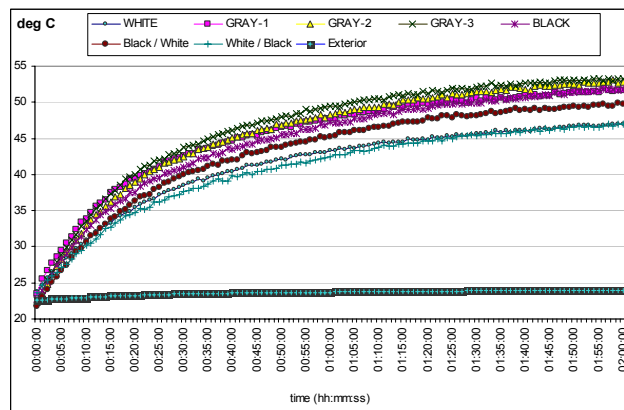


Figure 5.51 Air temperatures in the cavity for ST cases using different surface colours on louvers.

The absorptivity of each colour had a direct influence on the temperature of the louvers. Figure 5.52 shows how temperatures were higher with darker colours. The lack of constant airflow also contributed to the sharp increase in their surface temperatures, which showed a tendency to increase when the cavity was sealed.

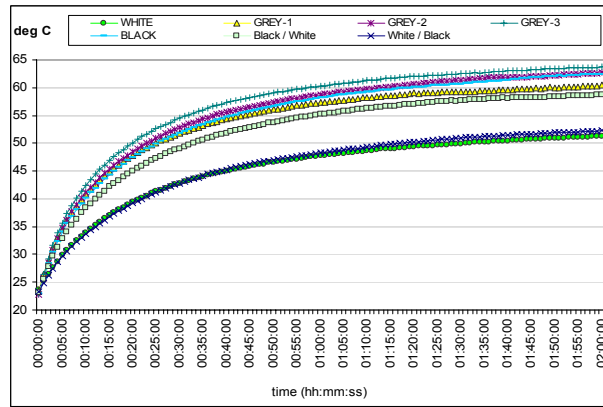


Figure 5.52 Temperature performances of louvers for ST cases for various surface colours.

The thermal behaviour of the room performed interestingly depending on the colours used for the shading devices. Figure 5.53 illustrates a particular reduction in temperature when the colours of the louvers were combined. It was observed that the highest levels were obtained using black and grey, with the lowest levels obtained with combined white/black. This indicates that dark colours reduce reflectance; the accumulated heat inside the cavity is increased as a result of the of temperature increase on the surface of the louvers. The impact of the reflectivity was greater for shortwave radiation, so the temperature difference could be larger in real climatic conditions.

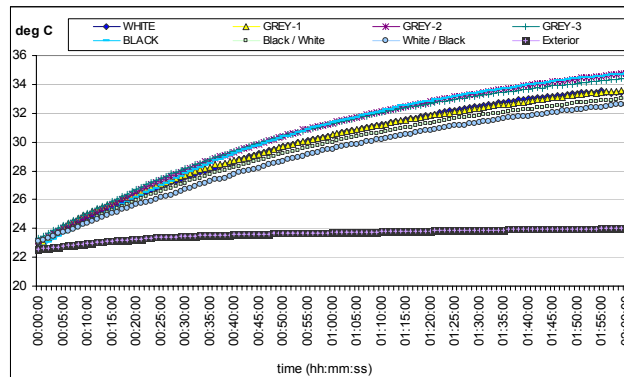


Figure 5.53 Air temperatures in the room for ST cases using different surface colours on louvers.

Once the cavity was ventilated, there was a mean reduction of about 23°C in temperature levels inside the cavity. Figure 5.54 illustrates how temperature levels were generally lower in STV. The mean lowest temperature inside the cavity was 24.39°C when louvers were painted white, demonstrating the relationship of the reflectivity of shading devices on the thermal performance of the cavity. The figure also shows how similarly the cavity performed once reflectivity was reduced. This indicates that the heat transfer rate increased at a reduced rate when the cavity had continuous airflow. The average differences in temperatures between all the cases were moderately small, demonstrating the impact on the stack effect which directly affected the airflow inside the cavity. This behaviour will be described and discussed in chapter 6.

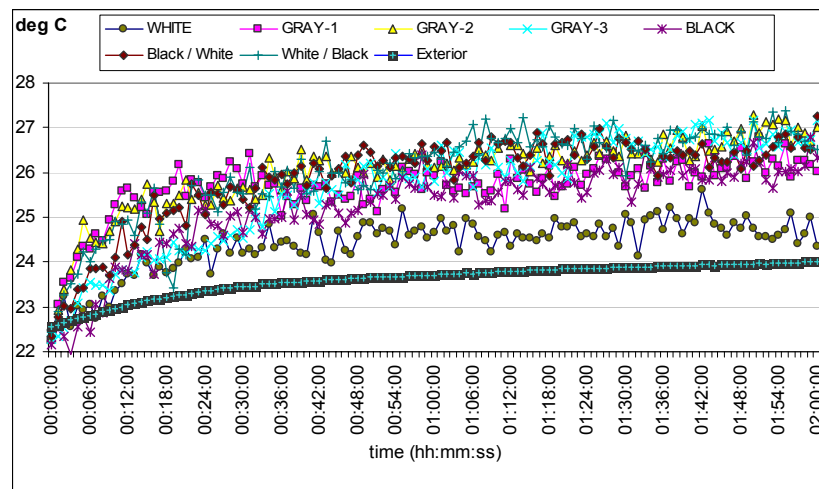


Figure 5.54 Air temperatures in the cavity for STV cases using different surface colours of louvers placed inside the cavity.

The continuous airflow induced by buoyancy and the different absorptivity of each tested colour determined the various ranges of surface temperatures reached by the louvers. Figure 5.55 shows how temperatures rose sharply, reaching steady levels which were balanced by the continuous airflow through the cavity. The graph shows

how the lowest temperatures were obtained by white louvers, and then (the temperatures) progressively increased when using less reflective louvers. It was observed that the darker the colour, the hotter the surfaces became, which indicated a clear increase in the amount of energy absorbed by the shading devices as their colour was darkened.

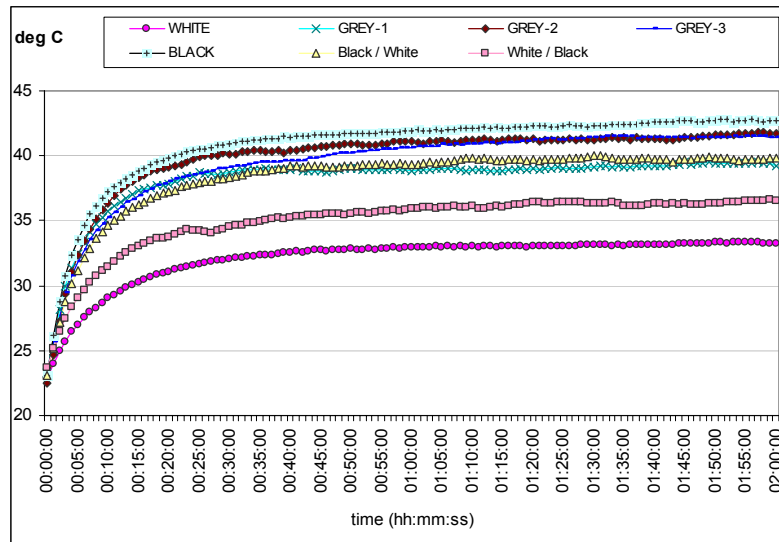


Figure 5.55 Temperature performances of louvers for STV cases using different surface colours.

The temperature performances of the room with ventilated cavity shown in figure 5.56, indicate how the absorptivity of louvers helped to reduce more efficiently the amount of heat transferred to the room. Higher cavity temperatures, but lower room temperatures for black louvers because of the lower radiation reflected to the room. When using dark coloured surfaces on the louvers; it was observed that higher temperature levels were obtained inside the cavity, increasing the resultant heat load to the room. This clearly indicates that the darker the shading devices, the more efficient the stack effect inside the cavity and airflow through the cavity. Thus for cooling: the first factor to control is shading, the second is ventilation.

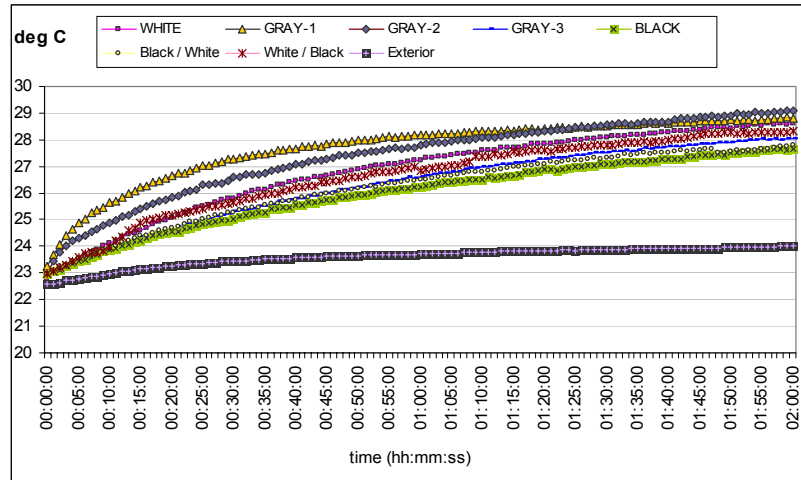


Figure 5.56 Air temperatures in the room for STV cases using different surface colours on louvers.

The similarity between the thermal performance in the cases of black and combined colours can also be observed (as described in the previous figure.) Figure 5.57 shows enlarged plots of the temperatures of louvers using black and combined surface colours. The exposed surfaces were set with the white facing upwards and the other facing downwards, and vice versa. It was observed that in comparing the three cases the lowest temperatures were obtained when the louvers were painted black.

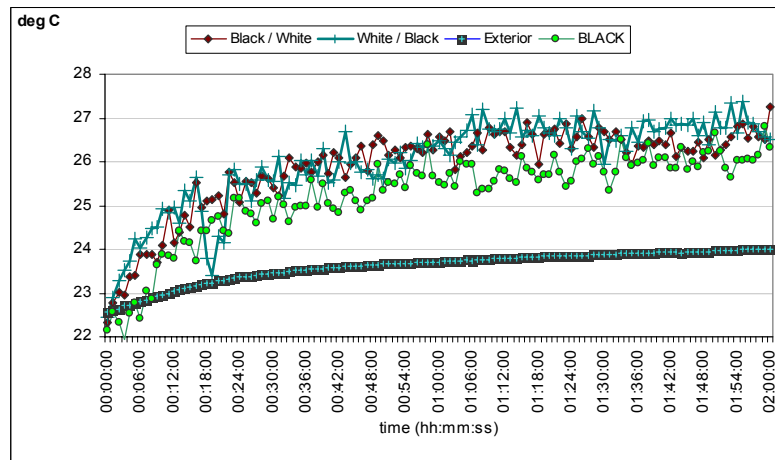


Figure 5.57 Air temperatures in the cavity for STV cases alternating white or black colours on exposed louvers surfaces.

When combined colours were used, the temperatures were slightly higher as a result of more reflective louvers surfaces on one side, which directly influenced the convective heat transfer. The more absorptive the surface, the more heat was absorbed and released in long wave IR, increasing heat exchange with the immediate air and encouraging upwards air movement. The less absorptive the surface of the louvers, the more short wave infrared reflected and less heat accumulated, which led to lower temperatures on the louvers surfaces. However, the stack effect was not as effective and the heat was removed more slowly, resulting in the slight increase in the cavity temperatures.

In the case of the room temperatures, relatively similar performances were achieved using black and combined colours on the louvers. However, even with these similar performances; the lowest temperatures were obtained using black painted louvers; proving the importance of using dark colours on louvers to improve the stack effect. Figure 5.58 shows enlarged plots of the temperatures measured inside the room using black, combined white/black and black/white louvers, inside the cavity.

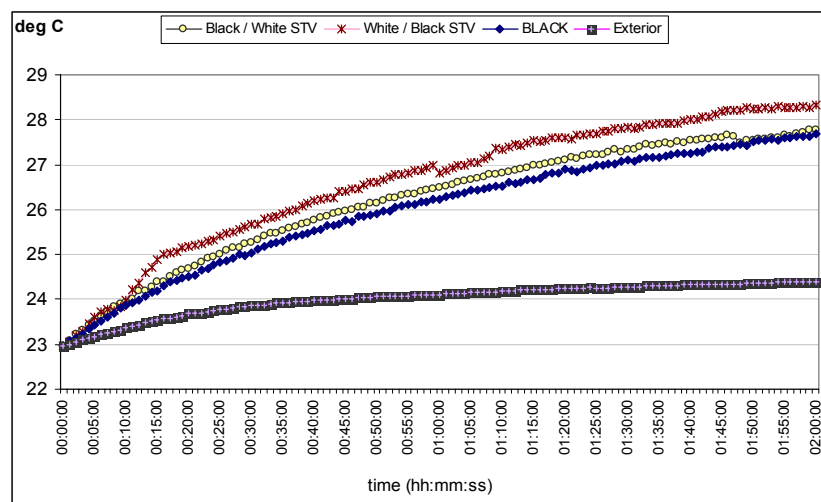


Figure 5.58 Air temperatures in the room for STV cases shifting white or black colours over the exposed louvers surfaces.

Although using darker louvers inside the cavity demonstrated a slight reduction in overheating development inside the room, the reduction of the reflectivity on the louvers had detrimental effects on the illuminance levels inside the room. Figure 5.59 illustrates a series of illuminance levels measured in each case using different colours on the cavity louvers. As predicted, the levels of light decreased dramatically when changing the scales of grey to black. The lowest illuminance levels were obtained when using black and black/white surfaces. This behaviour is a very critical factor proving that a balance between overheating control and adequate lighting levels is required.

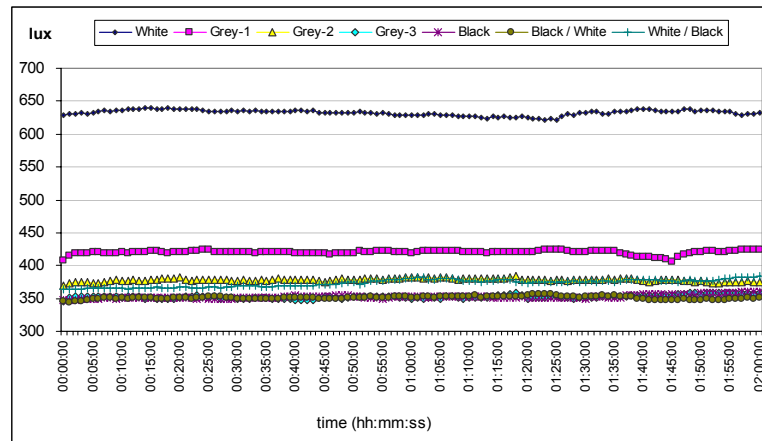


Figure 5.59 Illuminance in the room for various louvers colours.

The levels of luminance dropped from an average of 632.41 lux for the white louvers, to 419.96lx (grey-1), 378.19lx (grey-2), and 352.53lx (grey-3). This demonstrated that decreasing reflectivity also contributes to a decrease in visible light reflectance, which is the key element in natural lighting. Figure 5.60 illustrates the measured illuminance for the three shades of grey used in the tests.

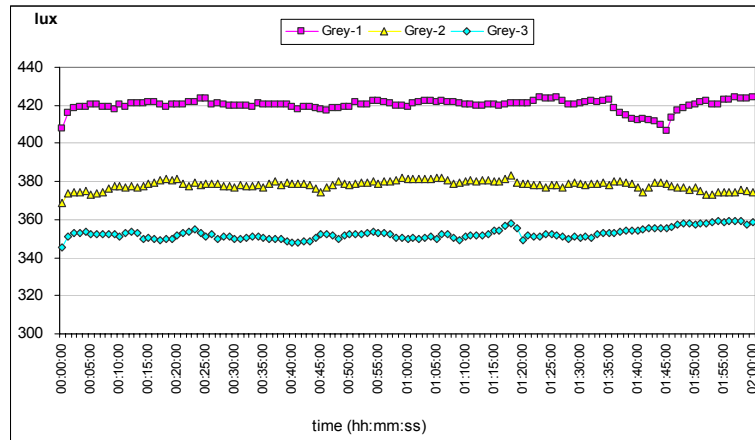


Figure 5.60 Illuminance in the room for three grey scale colours used on louvers surfaces.

In order to find a suitable balance between the improved heat transfer rate in the cavity and adequate lighting levels, the combination of colours white/black and black/white were also compared to assess the overall illuminance, within the cases where best thermal performances were obtained inside the room. Figure 5.61 illustrates how similar the luminance levels were with either black or combined white/black louvers. The mean measured levels were 352.66 and 350.94 lux respectively. However, there was a slight improvement in these levels when using black/white louvers. The black surface was facing the light source thus convective heat transfer was increased, and the white surface was facing the room and consequently the illuminance levels were not as low as when using fully black louvers. Although slightly higher, the mean measured levels were 373.33 lux, which are reasonably moderate. Moreover, this colour combination could be regarded as another factor to consider when designing the facade knowing that as a result of the climate, overheating is likely to occur.

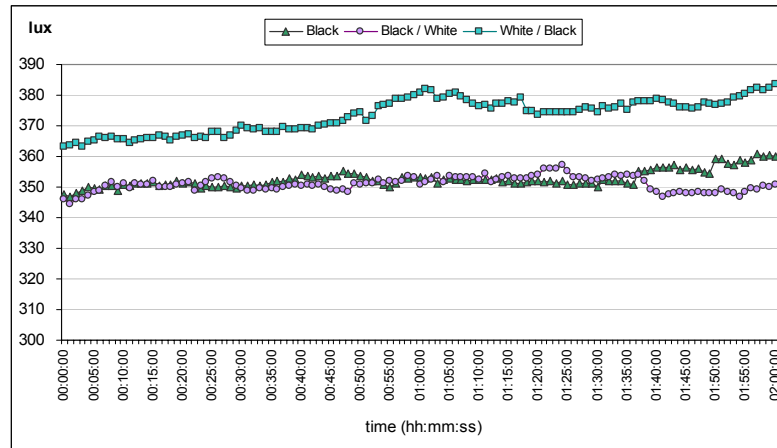


Figure 5.61 Illuminance in the room for alternating white/black colours on louvers surfaces.

5.5 GLASS TYPE

For this parameter, the glass on the external and internal skins was changed to compare the thermal performance of the experimental chamber. The glass selected for this test was clear, textured stippolyte and green tinted glass manufactured by Pilkington [10]. The main optical properties of the selected glasses are described in table 5.1.

Properties	Optifloat Clear	Textured Stippolyte	Optifloat Green tinted
Light transmission	0,82	0,79	0,75
Total heat transmission	0,82	0,68	0,59
Reflection (outside-in)	8%	6%	7%
Reflection (inside-out)	8%	6%	7%
Colour (outside-in)	Clear	Grey	Green
Colour (inside-out)	Clear	Grey	Green
thickness	4mm	4mm	4mm

Table 5.1 Main optical properties of the glass used on the experimental chamber. Source: Pilkington Group Limited / Optifloat glass [10].

In order to assess the influence of the glass on the thermal behaviour of the cavity and the room, the three types of glass were alternatively changed on the external and internal skins. Air temperatures inside the cavity and the room were measured and compared in ST and STV cases. The influence of glass type on illuminance levels was also compared.

The initial tests were carried out changing the glass type on the external skin. Figure 5.62 shows the plots of the thermal performance inside the cavity in both the ST and STV cases. It was observed again that there was an evident difference between the ventilated and the non-ventilated cases. However, the graph shows an increase in temperature levels when using green tinted glass. Even with a ventilated cavity, there was a reasonable rise in the temperatures. This is consistent with the reduced total transmittance of this type of glass, indicating its capability to enhance the greenhouse effect.

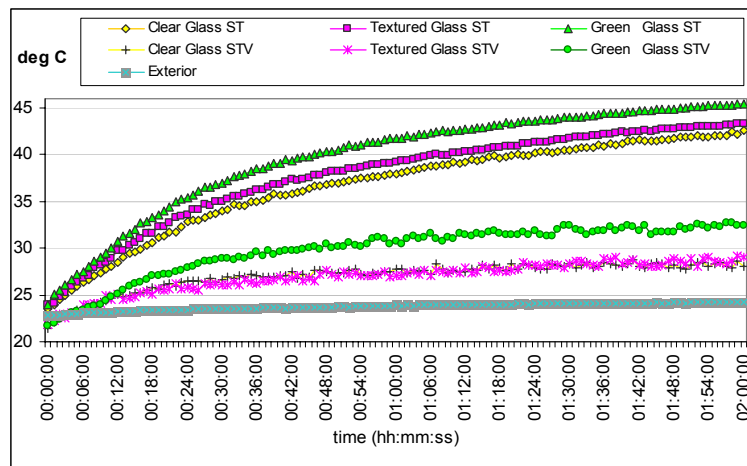


Figure 5.62 Air temperatures in the cavity for various glass types on the external skin.

Inside the room, however, a similar behaviour was observed in most of the cases (figure 5.63). There was a gradual increase in temperatures that reached values of between 34.4°C and 36.5°C. Although textured glass on the external skin reduced

somehow the maximum temperatures of the cavity on STV; the most important issue identified was the opposite thermal response using this glass in ST. The moderate total light transmitted by textured glass is partly reflected in long-wave IR, which then becomes trapped inside the cavity due to the reduced heat transmittance on the external skin. Once the cavity is ventilated, it favours the stack effect contributing to the reduction of heat in the cavity and conductive heat loads through the inner skin.

The thermal performances using green glass on the external skin showed a similar behaviour to using clear glass in the STV. This reveals the advantage of the greenhouse effect by reducing the total transmittance on the external skin, which encourages stack effect and heat removal. This principle is useful for controlling overheating as long as the cavity is ventilated.

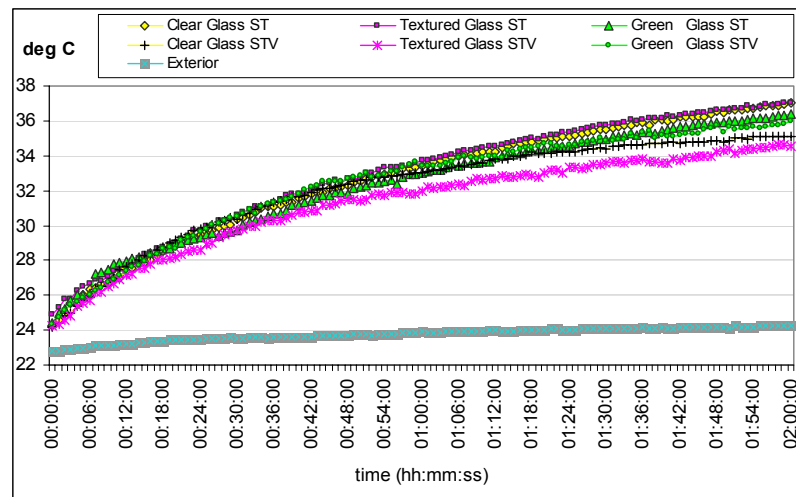


Figure 5.63 Air temperatures in the room for various glass types on the external skin.

The energy balance of incident radiation was moderately reduced by each type of glass depending of its total transmittance. However, on the external skin, this factor could be a disadvantage as the reduction in total transmittance contributes to the

greenhouse effect, which in the case of the cavity could easily lead to overheating developing if it (the cavity) is not properly ventilated.

The second series of tests were carried out when the glass type on the internal skin was changed. Figure 5.64 illustrates the thermal performance of the cavity in the ST and the STV. The graph shows the marked increase in temperature levels on ST, proving again the importance of continuous airflow throughout the cavity to prevent overheating development.

Comparing the plots in the ST on one hand, a small average increase of 1.28°C was observed on the temperature plots of the cavity when using green glass. This was caused by the slight rise of reflected heat from the inner glass by means of the reduced light transmittance of green glass. The thermal performances of the cavity using clear and textured glass were very similar. Although averaged temperatures using textured glass showed increments of only 0.26°C , it also demonstrated the effect that increased reflected radiation has on inner glass when temperatures increase inside a sealed cavity. On the other hand, the thermal performance on STV showed a slight reduction of 1.32°C in average temperatures when textured glass was placed on the inner skin. The performances of the cavity using clear and green glass exhibited similar behaviours. Although the average difference between these two cases was 0.72°C , higher temperatures were reached using clear glass on both skins. The reduced reflectance of clear glass also reduced to some extent the stack effect. As a consequence the airflow was slower through the cavity. In chapter 6, the airflow variations according to glass type are described and discussed.

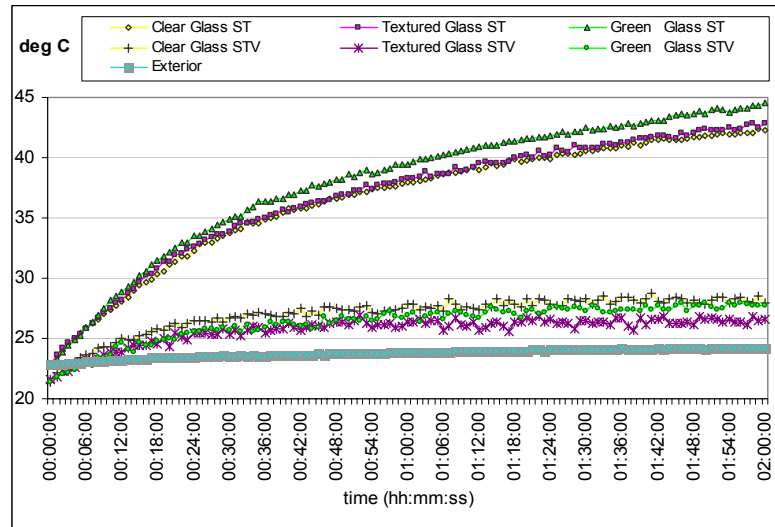


Figure 5.64 Air temperatures in the cavity for various glass types on the internal skin.

Thermal performances inside the room observed when changing the glass type on the internal skin were to some extent different from those observed when modifying the external skin. In these cases the increases in temperatures were higher those reached when changing the external glass. The maximum values reached in the ST were between 36.3°C and 36.9°C, which are about 5° higher;. This indicates that controlling radiation with glass type on the external skin is only useful for the ST.

Although it was seen that there were differences in the maximum temperatures between ST and STV cases when the inner glass was modified, it was also noticed that there was a further reduction in temperature when textured or green glass was used in the STV. While textured and green glass also reduced the maximum temperatures of the room, it was found that the thermal performances of the room were very similar in the ST. These behaviours were due to the influence of airflow through the cavity and the resultant heat load eventually transmitted into the room. The air temperature plots between all glass types were very similar because there were no real shading devices and the heat absorbed by the glass was fed to the

interior in any event. The increased airflow in the cavity and the reduced light transmittance on the inner skin helped to reduce the total heat load entering the room. This indicated that lower transmittances on the internal skins favoured a reduction in temperatures on the spaces next to the facade and more effective heat removal from the cavity when it was ventilated. However it was determined that glass low transmittance shading was not as good as the use of opaque shading devices.

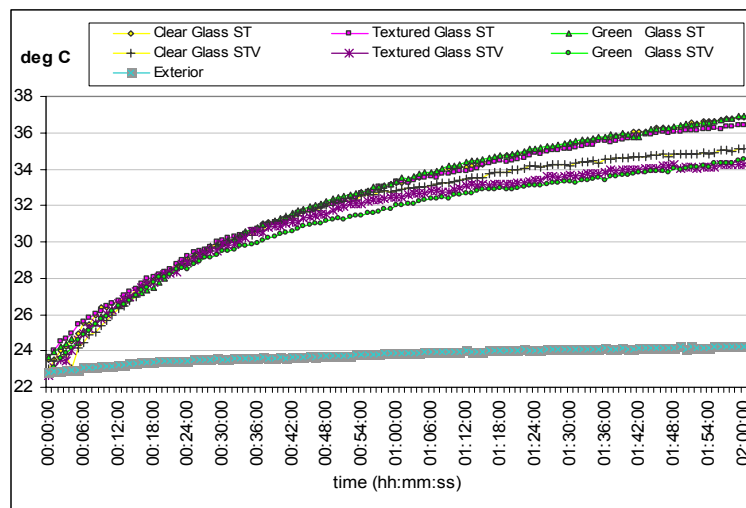


Figure 5.65 Air temperatures in the room for various glass types on the internal skin.

Finally, the glass type was changed on both skins. The resultant temperatures inside the ventilated cavity using clear, textured and green glass are illustrated in figure 5.66. The plots show clear differences in the performances of each type of glass. Temperature levels rose faster and higher when using green glass. Although the light transmitted through the external skin was lower using this type of glass, the reflected radiation inside the cavity was higher, which shows an increase in greenhouse and stack effects. Thus convective heat transfer and temperatures inside the cavity were increased. Temperature levels were lower using clear glass, as transmittance is higher with this type of glass, resulting in less radiation being reflected inside the cavity thus reducing convective heat transfer and temperatures. The average

difference in temperature using green and clear glass was 3.36°C . The graph also shows how temperatures in the cavity when textured glass was used, were slightly lower than when green glass was used but higher than when using clear glass. This indicates that slightly more radiation was reflected inside the cavity but also more radiation was transmitted, so the stack is moderately lower than using green glass and higher than when using clear glass.

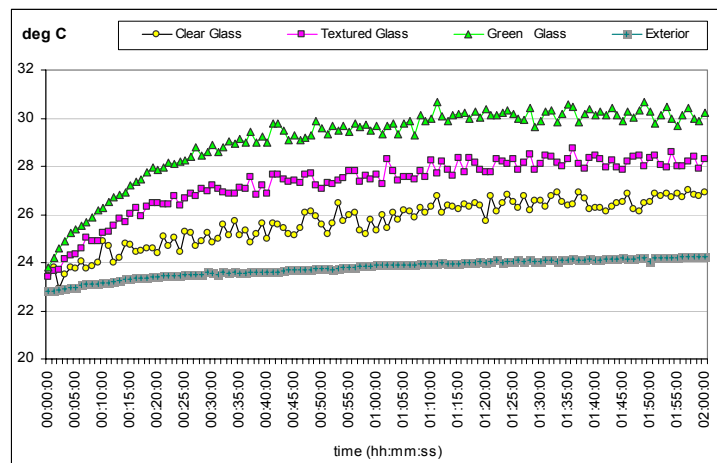


Figure 5.66 Thermal performances of the cavity for STV varying glass types on external and internal skins.

Figure 5.67 shows the temperatures inside the room using clear, textured and green glass on both skins. It was observed that the lowest temperature levels were obtained using green glass. An increase in temperature levels was observed when the glass type on both skins was replaced with another type which had higher light transmittance. This was contrary to the thermal performance of the cavity in which convective heat transfer mainly determined the thermal response. The direct incident light transmitted through the glass skins influenced the total heat load received by the room and determined its thermal performance. The heat load of the room was primarily affected by the resultant incident radiation, which occurs through the inner skin.

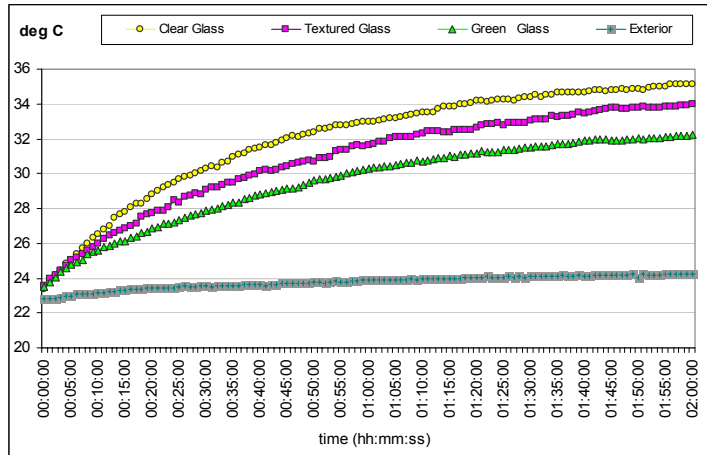


Figure 5.67 Thermal performances of the room for STV and various glass types on external and internal skins.

The light transmittance of the glass also affected the luminance levels of the room. Figure 5.68 shows the reduction in the luminance levels depending on the type of glass used. The average level when using clear glass was 945.28 lux. The illuminance was reduced to 741.49 lux when using textured glass, (a reduction of 21.56% of the lighting level inside the room.) When using green glass, the illuminance levels were further reduced to 669.19 lux, (a reduction of 29.21% in the lighting level.) This indicates that the reduction of light transmittance has a direct impact on the levels of available natural lighting through the glass.

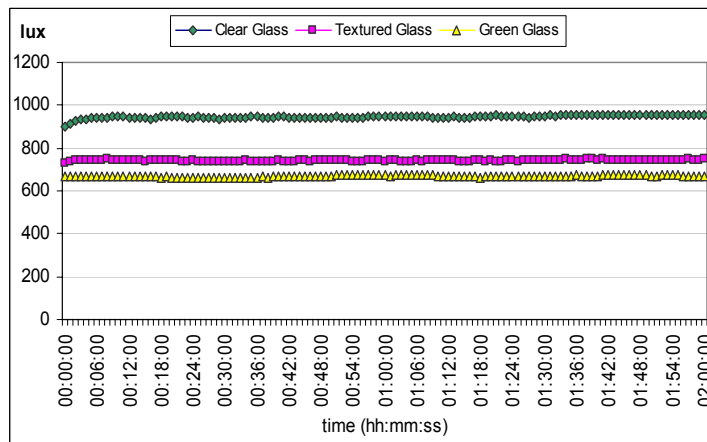


Figure 5.68 Illuminance in the room depending on the of glass type on both skins.

5.6 CAVITY DEPTH

For the analysis of the thermal performance of the experimental chamber in relation to the size of the DSF, the cavity depth sizes, measured from the external to the internal skin, were adjusted to 800mm, 600mm, 400mm, 200mm and 100mm (figure 5.69). Standard 4mm clear glass was used on both skins. Each set-up was tested in the ST and the STV and the temperatures inside the cavity and the room were measured and compared.



Figure 5.69 External and internal views of the DSF cavity adjusted to 800mm depth.

5.6.1 Cavity Depth Variation

The impact of the depth size on the thermal performance of a sealed cavity is shown in figure 5.70. Although there was a rapid increase of temperature, a slight reduction in the gradients and maximum levels reached, was observed. This was due to the fact that less volume of air is heated by the greenhouse effect when depth is reduced. These performances indicated that U-values increase with larger cavity depths inside a sealed DSF. Nevertheless, all performances showed a rapid tendency cause the development of overheating. Thus, this factor should be taken into consideration when improved thermal insulation is required.

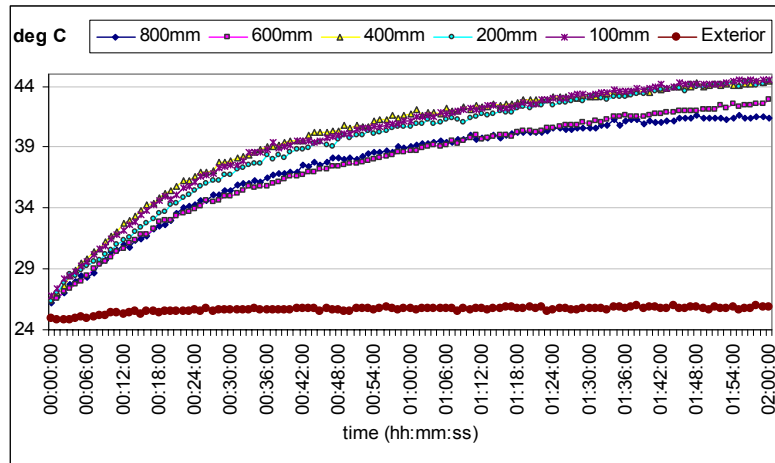


Figure 5.70 Air temperatures in the cavity for ST cases and various cavity depths.

When the cavity was ventilated, very different thermal behaviours in the DSF were exhibited. The reduction in the cavity depth increased the overall temperatures measured. Figure 5.71 shows how the thermal performances rose and remained at relatively steady levels in all cases except when using the 100mm depth. When the size was reduced to 100mm, the cavity started to behave similarly to a sealed cavity, indicating that the airflow was not adequate, so the heat removal rate fell. The relationship of size depth with airflow performance is discussed in chapter 6.

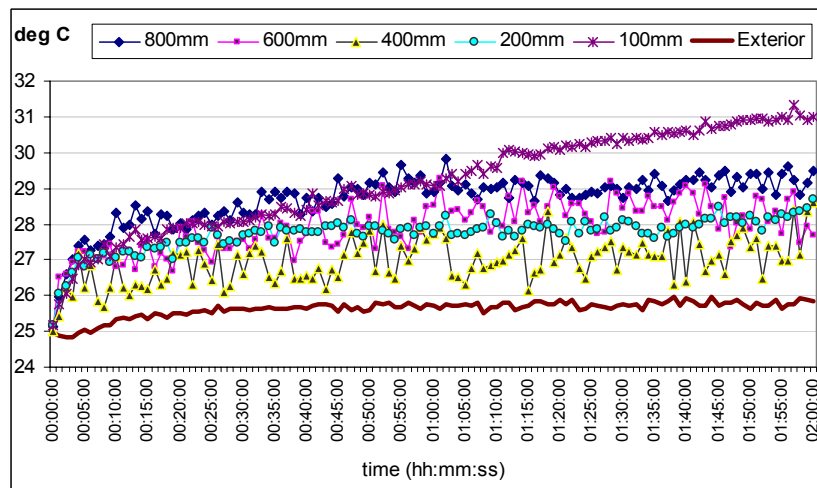


Figure 5.71 Air temperatures in the cavity for STV cases and various cavity depths.

Although the reduction in depth indicate a direct influence on the increased temperatures inside the cavity, the room temperature was more influenced by the resultant heat load from radiation and conductive loads through the inner skin. The highest room temperatures were measured when the cavity depths were reduced to 200 and 100mm, (as shown in figure 5.72.) However, the lowest temperatures were reached when the depth used was 400mm and then they (the temperatures) increased when depths of 600 and 800mm were used. This indicates the importance of the heat transfer coefficient in the cavity, which affects conductive loads through the inner skin.

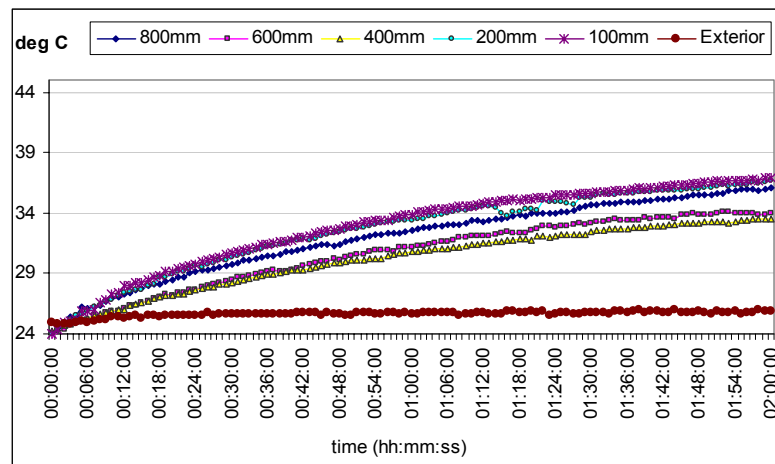


Figure 5.72 Air temperatures in the room for STV cases and various cavity depths.

5.6.2 Depth Variation using Shading Devices

The influence of louvers inside the cavity in relation to the cavity depth was also assessed. Based on previous observations relating to the restriction of space within the cavity using louvers; during this setup the depth sizes were adjusted to 800mm, 600mm and 400mm. The tilt angle of the louvers was kept at 45°, and the influence of colour on the louvers surface was also compared using white/black and black/white louvers. All settings were tested on ST and STV and temperatures in the cavity and room were measured and compared.

This series of tests were carried out using louvers painted white on top and black underneath. Figure 5.73 shows temperature plots measured inside the cavity. Maximum average levels of 35.38°C, were observed, when the cavity depth was 800mm. Relatively similar averages of 33.68°C and 33.32°C were also measured when using depths of 600mm and 400mm. It was noted that as the volume of air was reduced and the radiation reflected by louvers was increased; the stack effect provided more efficient air movement, which facilitated overheating control in the cavity.

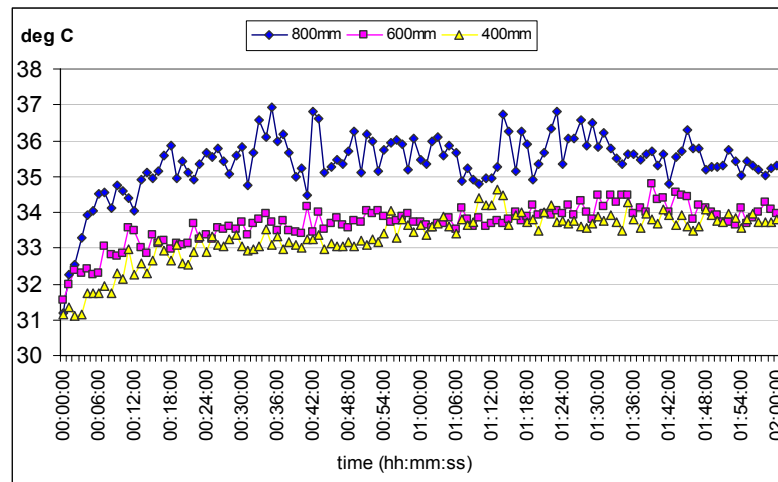


Figure 5.73 Air temperatures in the cavity for STV cases with louvers and various cavity depths.

With regard to the room temperature, figure 5.74 illustrates the clear affect of narrowing the cavity depth on improvements in the stack effect. A gradual reduction in room temperature, 4.65%, was measured, after narrowing the cavity to 600mm. A further 2.55% was achieved when the cavity was only 400mm deep. However, the average difference between the maximum and minimum temperatures was 2.64°C. Thus, it was clear, that the relationship between the cavity depth and colour of the louvers had an important role in improving the performance of the DSF.

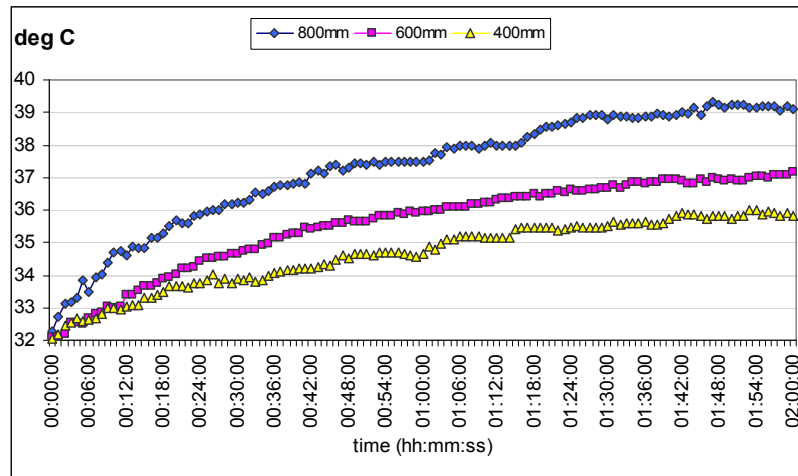


Figure 5.74 Air temperatures in the room for STV cases with louvers and various cavity depths.

The final series of tests were carried out using louvers painted black on top and white underneath. In these cases, which are shown in figure 5.75, there was a reduction in the average temperature when the cavity was 600mm deep. A trend of increasing temperature levels was observed when configured with 800mm and 400mm.

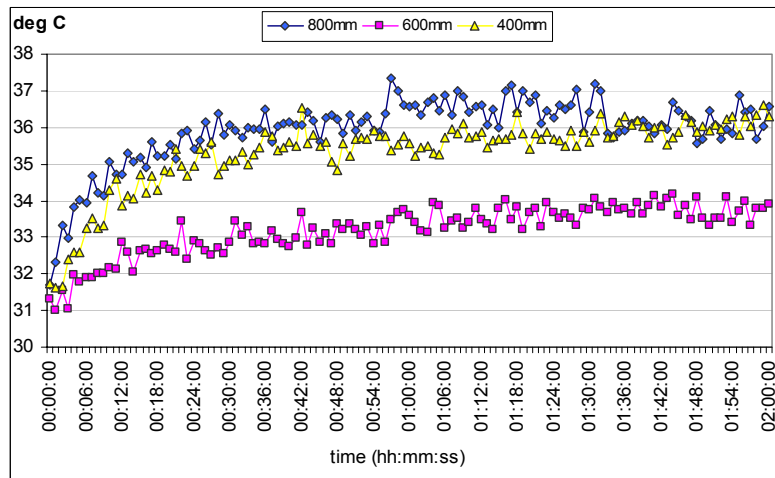


Figure 5.75 Temperatures inside the cavity for STV and three cavity depths using black/white louvers.

The previous performances illustrated a fine relationship between the heat absorbed by the louvers and the cavity depth, which in these cases confirmed that wider and

thinner cavity depths are not effective for heat removal. This indicated that in a ventilated cavity, the size relationship between the distance of the louvers from the cavity skins and their absorptiveness was a key factor to be considered when determining the height and depth of the cavity. In addition the need for heat removal or thermal insulation improvement must also be considered.

With respect to the room temperatures, figure 5.76 again illustrates how the influence of absorptivity on the exposed side of the louvers increased further the stack effect in the cavity. It was also observed that the highest temperatures were measured with a depth of 800mm. There was a slight reduction of 2.39% in average temperatures when using 400mm depth, and a further reduction of 2.47% when using a depth of 600mm.

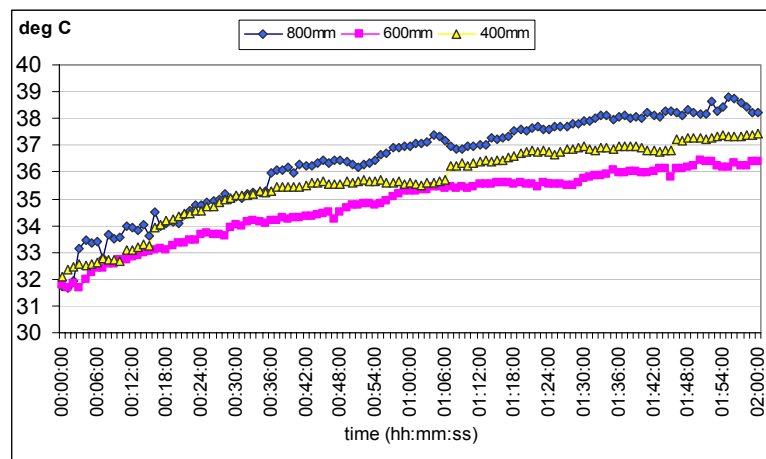


Figure 5.76 Temperatures inside the room for STV and three cavity depths using black/white louvers.

This behaviour indicates that the stack effect in the cavity speeds up the heat removal rates and decreases the total heat loads in the room. Yet, the effectiveness of the DSF in removing heat relies strongly on the airflow inside the cavity, which is greatly affected by the size of the gap between the louvers and the glazed skins. The

graph shows that a wider breadth of the cavity with louvers increased temperature fields. Nevertheless, there is a peak distance, which requires detailed calculation and analysis depending of the total height of the DSF. Thus, the efficiency of heat removal rates will rely on the analysis of airflow through the DSF. In chapter 6, a comparative assessment of the airflow fields inside the facade with variations in the cavity depth is explained.

5.7 CONCLUSIONS

An experimental chamber of a Box-Double Skin Facade with adjacent room has been built at the University of Nottingham. This was to test the thermal behaviour of the DSF and evaluate the processes involved in overheating, which develops inside a DSF cavity and a living space.

The main aspects observed on this experimental assessment were as follows:

- Temperatures inside the DSF chamber increase rapidly when the cavity is sealed (ST). There is an average increase of 56% above external temperature.
- There was a dramatic reduction in heat accumulated in the DSF when the cavity was ventilated (STV). The average cavity temperature was reduced by nearly 32%.
- The difference in temperatures between the cavity and the exterior (ΔT_{ce}) were reduced by 63% when the cavity was ventilated.
- The inlet to outlet size ratio of the cavity has critical implications for the efficiency of the DSF in removing heat.
- The incident radiation had a direct influence on the buoyancy created inside the DSF.

- Increasing the reflectivity of the cavity surfaces, shading devices or glazed skins increased convective heat transfer inside the cavity.
- The improvement of convective heat transfer rates inside the cavity combined with constant air movement led to improved reduction in temperature levels.
- The location of the shading devices close to the external skin led to better control of direct radiation and heat removal in the cavity.
- Cross ventilation combined with the natural convection of the cavity induced a better performance of the temperature field in the occupied space.
- The relationship between the depth and height of the cavity had profound implications on the stack effect and resultant temperatures inside the cavity.
- The optical properties of the glass type had a particular influence on the direct gains and greenhouse effects inside the DSF cavity.
- Illuminance levels were greatly affected by the optical properties of the glass type and shading ratios.
- Convective heat transfer mainly affects the thermal performance of the cavity.
- The thermal performance of the room was mainly influenced by the resultant incident of direct radiation passing through the inner skin.

The factors that cause the development of overheating under critical conditions of incident radiation include the total heat gain received by the room, which is influenced by the thermal loads from the facade; the thermal loads from the cavity; and the heat losses inside the room, which, in turn, is dependent on the air movement. It was found that DSF with inlets/outlets open reduces temperatures in the cavity. However this resulted in a reduced quantity of heat from being received

by the room. The convective forces inside the facade could be advantageous in improving the air extraction from the room.

The thermal behaviour of the experimental chamber has provided some evidence to indicate that controlling direct heat gains from the DSF cavity is a key factor in reducing both room temperature and overheating. These reductions can be encouraged with adequate sizing of shading devices combined with a constant airflow within the cavity; in order to reduce direct heat gains from the external facade and promote heat removal. The effective reduction of heat is obtained when shading devices are located close to the external skin. The nature of the DSF in which long-wave IR is reflected, creates a greenhouse effect and the convective and radiative gains developed inside the cavity are the main reasons why the cavity acts as a thermal buffer to improve insulation. Conversely however these same issues become the main disadvantages when the facade is exposed to high radiation levels.

It was determined that direct heat gains from the cavity (Q_c) have a material impact on the rise of temperatures inside the room. It was also observed that the reduction in the external facade gains (Q_f) had a direct influence on the reduction of the total gains (Q_f) of the room.

This assessment has illustrated that some of the main issues that cause overheating are as follows:

- Inefficient removal of the heat stored in the facade and the room due to reduced airflow.
- Inadequate location and size of shading devices inside the cavity.

- Rapid overheating development due to excessive heat stored in the cavity as a result of increased U-values.
- The greenhouse effect developed by convective heat transfer in the cavity, is a key factor in removing heat but is also the main cause of overheating.
- The stack effect due to the natural convection developed inside the cavity is a useful means of removing heat and also the cause of overheating on upper parts of the facade.

REFERENCES

1. Brandle, K. and R.F. Boehm. Airflow windows: performance and applications. in Proceedings of the ASHRAE/DOE conference: Thermal Performance of the Exterior, Envelopes of the Building II. 1982. Clearwater Beach.
2. Müller, H. and M. Balowski, Waste Air Ventilated Windows for Offices. Heizung Luftung und Haustechnik, 1983. 34(10): p. 412-417.
3. Inoue, T., Y. Matsuo, and T. Ibamoto. Study on the thermal performance of ventilation window. in Proceedings of the International Symposium on Thermal Application of Solar Energy. 1985. Hakone.
4. Bonveni, F., et al. Air flow windows. in Proceedings of 2nd European conference on architecture. 1989. Paris.
5. Poirazis, H., Double Skin Facades - A Literature Review. 2004, Division of Energy and Building Design, Department of Construction and Architecture, Lund Institute of Technology: Lund. p.196.
6. Park, C.-S., et al., Calibration of a lumped simulation model for double-skin facade systems. Energy and Buildings, 2004. 36(11): p. 1117-1130.
7. Saelens, D., Energy Performance Assessment of Single Storey Multiple-Skin Facades, in Faculteit Toegepaste Wetenschappen, Arenbergkasteel. 2002, Katholieke Universiteit Leuven,: Kasteelpark Arenberg 51, B-3001 Leuven, Belgium. p. 272.
8. Gore, W.L. and Associates-GmbH, GORE™ TENARA® Architectural Fabric specifications. 2007: Wernher-von-Braun-Straße 18, D-85640 Putzbrunn, Germany. http://www.gore.com/en_xx/products/fabrics/architectural/tenara_light.html
9. Skyspan, Skyspan (Europe) GmbH. 2003: Nordstrasse 10, D-83253 Rimsting, Germany. Website: http://www.skyspan.com/07_Material.html
10. Pilkington Group Limited, The Glass Range for Architects and Specifiers. 2006, Pilkington Group Limited: UK. p.18. <http://www.pilkington.com/resources/glassrangebroanddatasheetjune2006.pdf>
<http://www.pilkington.com/pilkington2004/both/images/productdirectory/flash/optiflo.html>

CHAPTER VI

CFD ANALYSIS OF THE DSF EXPERIMENTAL CHAMBER

6.1 INTRODUCTION

Double Skin Facades not only have gained much interest and popularity among architects in Central Europe but also recently have had an influence in the UK, where various commercial DSF buildings have been developed [1]. DSFs play a significant role in the cooling load of the building and on the thermal comfort of its occupants during summertime. Their application increased dramatically due to the reaction about concerns on the environmental impact of buildings, specifically on active facades [2,3]. Double Skin Facades are currently designed and built on new and existing buildings as a resource to improve air quality and thermal insulation [4,5]. The airflow created within the cavity is the key factor on which the use of DSF is based.

According to Djunaedy, E. et al (2002) [6], there are various categories depending on the resolution and complexity in which airflow is resolved. The authors describe them as:

- *Building Energy Balance (BEB) models that basically rely on airflow guess estimates.*
 - *Zone airflow network (AFN) models that are based on (macroscopic) zone balance and inter-zone flow-pressure relationship; typically for a whole building.*
- CFD that is based on energy, mass and momentum conservation in all (minuscule) cells that make up the flow domain; typically a single building zone.”*

The use of computational fluid dynamics (CFD) to predict internal and external flows has been increasingly used in the building industry in the past few years. CFD may be used successfully to predict flow fields inside and outside buildings [7]. For flow fields inside the building, it is used to predict thermal performance, contamination and air quality, energy transport and smoke propagation. For flow fields outside the building, it is applied for the distribution of pressure or pollutants on building surfaces, to predict airflow on urban spaces, and the loading of building facades. According to Versteeg and Malalsekera [8], “*modelling fluid flow and heat transfer is a complex task that cannot be satisfactorily performed without continued reference to experimental validation*”. Champagne (2002) highlighted the importance of validating a proposed design to ensure proper performance by means of experimental or numerical methods. The author stressed that experimental methods are very reliable when performed in controlled environments, however they are expensive and time consuming, as the author pointed out “*CFD is a numerical approach that is informative while also saving time and money*”.

There are previous studies in which data from experimental measurements has been used to develop numerical models to calculate temperature fields inside DSFs. Saelens [9] stressed that most models are developed for mechanically ventilated DSFs and that there are very few models for naturally ventilated facades available. Gan G [10] developed a numerical method for the prediction of thermal transmittance of multiple glazing based on CFD. There are some studies where buoyancy driven, naturally ventilated cavities, using CFD, have been compared to experimental controlled measurements. Gan G. and Riffat, S.B (1998) [11] investigated the performance of a glazed solar chimney for heat recovery in naturally

ventilated buildings using CFD. They validated the performance against experimental data from previous literature. Chiu, Y. and Shao L. (2001) [12] compared the measured data of an experimental chamber with the commercial CFD code, to determine the reliability of CFD. Most authors are in agreement regarding the measured and modelled data using CFD.

There is hardly any information available regarding the performance of Double Skin Facades driven by the buoyancy effect depending on the variation of the cavity, which is the working principle of the facade. Therefore, measuring the performance, in a controlled environment, of buoyancy driven airflow in the facade, and comparing with CFD modelling, is a useful tool to visualize and optimize its performance.

This chapter illustrates the study carried out using Computational Fluid Dynamics (CFD) software based on the previous results of the full-scale laboratory chamber of a DSF used for parametric analysis. As the experimental study was formulated based on various configurations of a DSF and the identification of the causes of overheating in critical radiation conditions, 2D models of the experimental chamber were built and modelled by CFD in order to visualise and assess the airflow within the system.

Commercial CFD software was used to predict the flow and movement of air and temperature response of the laboratory model. FLUENT [13] is a widely used computer program for modelling engineering fluid flows, due to its robustness, accuracy and user-friendliness. In FLUENT, equations for the conservation of heat,

mass, momentum and other transport equations are solved using a control-volume technique. The software is capable of solving multiphase fluid flow problems in a three-dimensional body-fitted coordinate system. This type of coordinated system is necessary for the accurate representation of a two-dimensional model of the DSF. The air flow and the temperature response are modelled, assuming a steady state of radiation in the facade cavity.

The models will include an assessment of the following issues:

- Thermal performance of the facade and adjacent room, during critical summer conditions with the same geometry, which was based on the experimental cases.
- Natural ventilation performance of the facade and its interaction with the room.

The aim of this study was to apply and assess CFD to illustrate the thermal behaviour under experimental conditions of a Double Skin Facade chamber, in order to give a better understanding of the key elements which affect the thermal response of the facade under critical conditions. It demonstrated the feasibility and versatility of the application of CFD for the thermal modelling of a DSF model based on the data previously obtained by experimentation. It also has demonstrated that accurate values of the air flow and temperature can be achieved when detailed assessment of the model and its boundary conditions are inputted into the CFD model.

6.2 FUNDAMENTALS OF AIRFLOW MODELS

The air flow model of the DSF is calculated using the conservation equations for mass and momentum. Thermal buoyancy is the main mechanism of airflow inside the cavity of a DSF and as this flow also involves heat transfer, an additional

equation for energy conservation is solved. Additional transport equations are also solved when the flow is turbulent. The conservation equations for laminar flow in an inertial (non-accelerating) reference frame are presented. The equation for conservation of mass, or the continuity equation, can be written as follows [14]:

$$\frac{\partial \rho}{\partial t} + \nabla \cdot (\rho \vec{v}) = S_m \quad (6.1)$$

This equation is the general form of the mass conservation equation and is valid for incompressible as well as compressible flows. The source S_m is the mass added to the continuous phase from the dispersed second phase.

The conservation of momentum in an inertial (non-accelerating) reference frame is described by:

$$\frac{\partial}{\partial t}(\rho \vec{v}) + \nabla \cdot (\rho \vec{v} \vec{v}) = -\nabla p + \nabla \cdot (\bar{\tau}) + \rho \vec{g} + \vec{F} \quad (6.2)$$

Where p is the static pressure; $\bar{\tau}$ is the stress tensor (described below); and $\rho \vec{g}$ and \vec{F} , respectively, are the gravitational and external body forces (e.g., that arise from interaction with the dispersed phase). Note that \vec{F} , also contains other model-dependent source terms such as porous-media and user-defined sources.

The stress tensor $\bar{\tau}$ is given by:

$$\bar{\tau} = \mu \left[(\nabla \vec{v} + \nabla \vec{v}^T) - \frac{2}{3} \nabla \cdot \vec{v} I \right] \quad (6.3)$$

Where μ is the molecular viscosity; \mathbf{I} is the unit tensor; and the second term on the right hand side is the effect of volume dilation.

As the flow model in the DSF is influenced by the incidence of heat flow from the light source that passes through different types of media, there is a flow of thermal energy from the air, (which occupies one region in space), to the glass, (which occupies a different region in space); this is known as heat transfer. Heat transfer can occur by three main methods: conduction, convection, and radiation. Physical models involving only conduction and/or convection are the simplest, while buoyancy-driven flow, or natural convection, and radiation models are more complex. The Energy Equation can be expressed in the following form:

$$\frac{\partial}{\partial t}(\rho E) + \nabla \cdot (\vec{v}(\rho E + p)) = \nabla \cdot \left(k_{\text{eff}} \nabla T - \sum_j h_j \vec{J}_j + (\vec{\tau}_{\text{eff}} \cdot \vec{v}) \right) + S_h \quad (6.4)$$

Where k_{eff} is the effective conductivity ($k + k_t$); where k_t is the turbulent thermal conductivity defined according to the turbulence model being used; and \vec{J}_j is the diffusion flux of species j . The first three terms on the right-hand side of the equation represent energy transfer due to conduction, species diffusion, and viscous dissipation, respectively. S_h includes the heat of chemical reaction and any other volumetric heat sources.

6.2.1 Computational Fluid Dynamics Model

CFD software is used to predict the flow and movement of the air and temperature response of the laboratory model. FLUENT [13] is a widely used computer program for modelling engineering fluid flows, due to its robustness, accuracy and user-

friendliness. In FLUENT, equations for the conservation of heat, mass, momentum and other transport equations are solved using a control-volume technique. The software is capable of solving multiphase fluid flow problems in a three-dimensional body-fitted co-ordinate system. This type of co-ordinate system is necessary for the accurate representation of a model of the DSF. The air flow and temperature response are modelled assuming a steady state of radiation in the facade cavity.

When this complex process is modelled using Computational Fluid Dynamics Software (CFD), the continuity equations are solved by discretization. The model can be expressed as [10]:

$$\frac{\partial}{\partial x_i} (\rho U_i \phi) = \frac{\partial}{\partial x_i} \left(\Gamma_\phi \frac{\partial \phi}{\partial x_i} \right) + S_\phi \quad (6.5)$$

The flow model consists of the governing conservation equations of mass, momentum, heat transfer and turbulence. In this equation ρ is the air density (kg/m³); ϕ is the flow variable such as the mean velocity component; U_i (m/s) is the pressure, temperature and turbulent parameters in x_i (m) direction; Γ_ϕ represents the diffusion coefficient (N s/m²); and S_ϕ is the source term.

6.2.2 Turbulence Model

The Standard k - ϵ model is one of the simplest and most complete two-equation calculation methods used in fluid dynamics. It is also the most common turbulence model for fluid flow simulations used by commercial software.

In this method, the solution of two separate equations allows turbulent velocity and length scale to be independently calculated. It is a reasonably accurate method for the calculation of overall turbulent flow. The transport equations of the k - ϵ model are expressed by B.E Launder [15,16] as follows:

For the kinetic energy k :

$$\frac{\partial}{\partial t}(\rho k) + \frac{\partial}{\partial x_i}(\rho k u_i) = \frac{\partial}{\partial x_j} \left[\left(\mu + \frac{\mu_t}{\sigma_k} \right) \frac{\partial k}{\partial x_j} \right] + P_k + P_b - \rho \epsilon - Y_M + S_k \quad (6.6)$$

For the dissipation epsilon:

$$\frac{\partial}{\partial t}(\rho \epsilon) + \frac{\partial}{\partial x_i}(\rho \epsilon u_i) = \frac{\partial}{\partial x_j} \left[\left(\mu + \frac{\mu_t}{\sigma_\epsilon} \right) \frac{\partial \epsilon}{\partial x_j} \right] + C_{1\epsilon} \frac{\epsilon}{k} (P_k + C_{3\epsilon} P_b) - C_{2\epsilon} \rho \frac{\epsilon^2}{k} + S_\epsilon \quad (6.7)$$

Where the turbulence viscosity is expressed by:

$$\mu_t = \rho C_\mu \frac{k^2}{\epsilon} \quad (6.8)$$

The production of k is expressed by:

$$P_k = -\overline{\rho u'_i u'_j} \frac{\partial u_j}{\partial x_i} \quad (6.9)$$

$$P_k = \mu_t S^2 \quad (6.10)$$

The source term S (the mean rate-of-strain tensor) is expressed by;

$$S \equiv \sqrt{2S_{ij}S_{ij}} \quad (6.11)$$

The buoyancy effect on the flow is expressed by:

$$P_b = \beta g_i \frac{\mu_t}{Pr_t} \frac{\partial T}{\partial x_i} \quad (6.12)$$

Where Pr_t is the turbulent Prandtl number for energy; and g_i is the component of the gravitational vector in i directions. For the standard and realizable - models, the default value of Pr_t is 0.85.

The coefficient of thermal expansion β , is defined as;

$$\beta = -\frac{1}{\rho} \left(\frac{\partial \rho}{\partial T} \right)_p \quad (6.13)$$

The model has defined as constant the following;

$$C_{1\epsilon} = 1.44, \quad C_{2\epsilon} = 1.92, \quad C_\mu = 0.09, \quad \sigma_k = 1.0, \quad \sigma_\epsilon = 1.3 \quad (6.14)$$

Although the standard $k-\epsilon$ models are widely used today in the prediction of mean properties of turbulent flow fields, the accuracy of the two model near-wall boundaries is debated. Bernard (1986) [17] compared two different Reynolds numbers between the measured turbulent kinetic energy in channel flow and the prediction of various near-wall variants of the $k-\epsilon$ closure. The author observed a

discrepancy between the high Reynolds number models and the measured experimental values of peak kinetic energy near the wall regions. Avva, R. et al [18] compared two approaches using a high Reynolds number $k-\epsilon$ model with near wall functions and a Low Reynolds number $k-\epsilon$ model with near wall resolution. The author highlighted that contrary to the commonly held view, that overall a high-Re model gives better results compared to a Low-Re model, on the problems compared. Low-Re is sensitive to grid clustering near the walls.

In the case of heat transfer prediction through developing flows, Raisse M., et al [19] compared predicted and measured data of a turbulent flow in rectangular channels using Low-Re $k-\epsilon$ models. The authors determined that among the models studied, a non linear Low-Re $k-\epsilon$ model produces better heat transfer predictions.

The Standard $k-\epsilon$ model produces a reasonably precise picture of the overall behaviour of the airflow within the system. However, the standard model works with a high Reynolds number, which is basically present in turbulent flows. In the case of the buoyancy-induced models, the accuracy of the boundaries is significantly reduced when working with a high Reynolds number. Although DSF presents airflows ranging from laminar to turbulent with low air velocities, the Low Reynolds number $k-\epsilon$ is chosen for more accuracy in glazed boundary layers.

6.2.3 Radiation Model

As previously discussed in 3.4.1, heat can also be transferred by radiation without the presence of a medium. Thermal radiation is the form of electromagnetic waves in the IR waveband. As with light, it travels in straight lines and can be reflected, with

its intensity obeying the inverse square law. The amount of radiation emitted by a body depends on its temperature and the quality of its surface; for example its colour or texture [20]. FLUENT software [13] is able to calculate radiation using one of the following five radiation models [21]:

- Discrete transfer radiation model (DTRM) [22].
- P-1 radiation model [23]
- Rosseland radiation model [24]
- Surface-to-surface (S2S) radiation model [24]
- Discrete ordinates (DO) radiation model [25]

According to the FLUENT users' manual [21]:

- *The main assumption of the DTRM is that the radiation leaving the surface element in a certain range of solid angles can be approximated by a single ray.*
- *The P-1 radiation model is the simplest form of the more general P-N model, which is based on the expansion of the radiation intensity into an orthogonal series of spherical harmonics.*
- *The Rosseland or diffusion approximation for radiation is valid when the medium is optically thick. It is recommended for use in problems where the optical thickness is greater than 3. It can be derived from the P-1 model equations, with some approximations. This section provides details about the equations used in the Rosseland model.*
- *The discrete ordinates (DO) radiation model solves the radiative transfer equation (RTE) for a finite number of discrete solid angles, each associated with a vector direction fixed in the global Cartesian system. The fineness of the angular discretization is controlled by the user, analogous to choosing the*

number of rays for the DTRM. Unlike the DTRM, however, the DO model does not perform ray tracing.

- *The surface-to-surface radiation model (S2S) can be used to account for the radiation exchange in an enclosure of grey-diffuse surfaces. The energy exchange between two surfaces depends in part on their size, separation distance, and orientation. These parameters are accounted for by a geometric function called a "view factor." The main assumption of the S2S model is that any absorption, emission, or scattering of radiation, can be ignored; therefore, only "surface-to-surface" radiation need be considered for analysis."*

For simulating heat transfer in the Double Skin Facade model, the most suitable radiation methods are DTRM and S2S. The primary advantage of the DTRM is the simplicity of the model, with its possibility to adjust accuracy to increase the number of rays. The surface-to-surface radiation model is good for modelling the enclosure radiative transfer without participating media. According to the software manufacturer, *"when comparing the DTRM and the DO radiation models, the S2S model has a much faster time per iteration, although the view factor calculation itself is CPU-intensive"*.

For this reason, the accuracy of the DTRM model is limited essentially by the number of rays traced and the computational grid. The 'ray tracing' technique used in the DTRM provides a prediction of radiative heat transfer between surfaces without explicit view-factor calculations. As a result the DTRM was selected for calculating radiation on the DSF model.

6.3 MODEL SETUP FOR CFD SIMULATIONS

The airflow model of the DSF, buoyancy-induced natural convection, involves both laminar and turbulent flows. Buoyant flow in multiple glazing can range from laminar to turbulent, creating a stratification of temperature levels, which increase with height. It is stated that the flow created by the buoyancy within glazed cavities is mainly generated by convective flows [26]. These flows are considered to have low air velocities.

The accurate analysis of convective airflows requires precise calculations around boundaries. The mesh generation for CFD calculation has to be finely defined near wall surfaces while accuracy is required on calculations near the boundaries. In the case of the DSF model, it is required to model a very fine mesh near the glazed surfaces, where the main convective forces are created.

6.3.1 Model Grid

In order to visualize the different responses to the cavity and the chamber using the most computational resources available for this research; the following types of grids were built: A 2D mesh of the experimental chamber on ST and STV, and a series of 2D grid models of the cavity for the different configurations of the DSF. The model grids were set according to the dimensions of the full-scale experimental chamber.

The basic domain of the first model was set in two zones:

The first zone represents the cavity and the second zone represents the room. The basic dimensions for the model are as follows (w x h):

Chamber zone: 3200 x 2400 (mm)
Cavity zone: 800 x 2400 (mm)
Room zone: 2400 x 2400 (mm).

The grid of the model illustrated in figure 6.1 was meshed with a basic quadrangular cell unit of 50mm x 50mm. The boundary layers near the glazed area were meshed by 10 layers next to the external and internal glass in the cavity and room, a fine mesh of 1mm. The figure illustrates a 2D case of the experimental chamber. It was built for the complete model of the cavity and room.

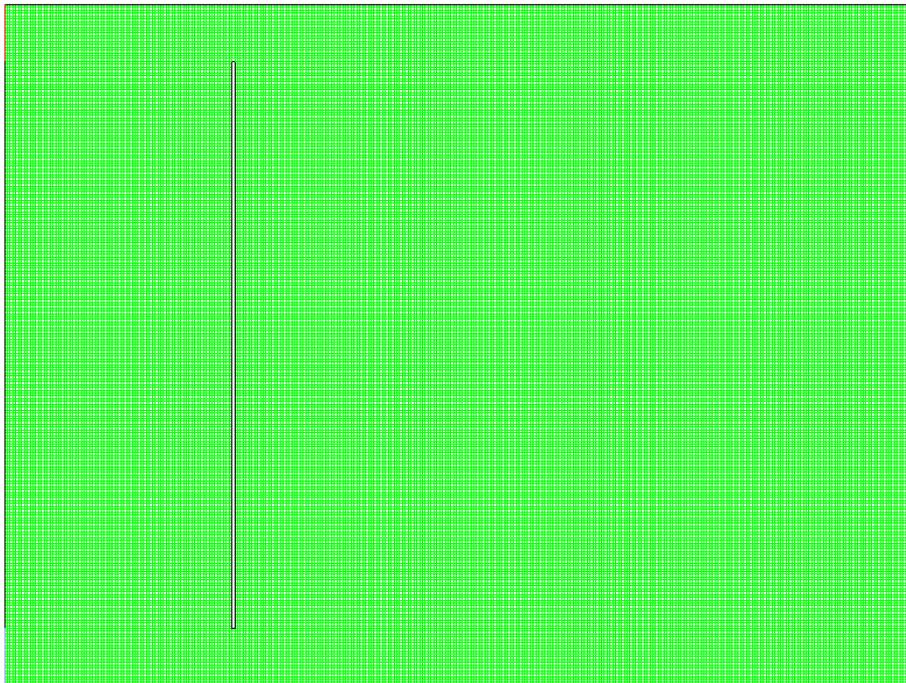


Figure 6.1 2D grid of the two zones of the DSF experimental chamber model.

For a comparative analysis of the experimental model of the DSF; a specific mesh of the cavity was built with a domain of 800mm x 2400mm and adjusted with the configurations made on the experimental cavity. Figure 6.2 shows the basic configuration of the 2D mesh of the cavity.

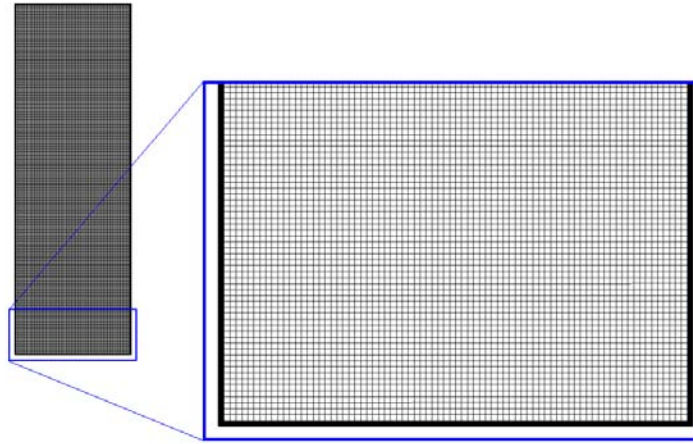


Figure 6.2 2 dimensional grid model of the cavity with fine mesh near the boundaries.

6.3.2 Model Settings

The experimental chamber model was set to simulate the main cavity configurations in ST and STV, in order to compare the overall behaviour of the experimental chamber. The model was then configured in a series of 2D models to compare the specific airflow and thermal behaviour of the cavity. The models were arranged based on the parameters previously assessed in the experimental analysis. The CFD models were set according to the Cavity and room opening positions, DSF structure, Glass type and Cavity depth.

- **DSF Openings Position**

The cavity model was set on these models with the variation of the inlet and outlet type on the boundary conditions. In the ST case, the inlet and outlet were considered as wall boundaries and the cavity domain was sealed with no air exchange outside the domain. In the STV case, the inlet boundary was considered as the inlet-vent for buoyancy to re-create the convective air flow. The upper opening was considered as the outlet boundary. The external and internal walls were set as wall boundaries with a fixed heat flow. The floor and ceiling were set as wall boundaries with a fixed

temperature. The heat flow was calculated for convective and radiative heat transfer by the discretization of the equations of continuity, energy and turbulence. Figure 6.3 shows the main settings of the cavity for non ventilated and ventilated cavity cases.

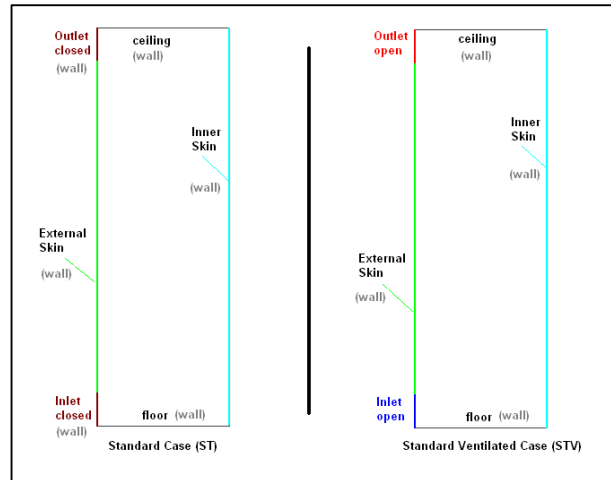


Figure 6.3 Main configurations of the 2D model boundaries for ST and STV.

The ventilated cases were also simulated by adjusting the size of the inlet and outlet on the cavity. Figure 6.4 shows the adjustments made on the inlet and outlet using sizes of 200, 150, 100, 50 and 25mm. These sizes were also simulated based on those used in the experimental analysis.

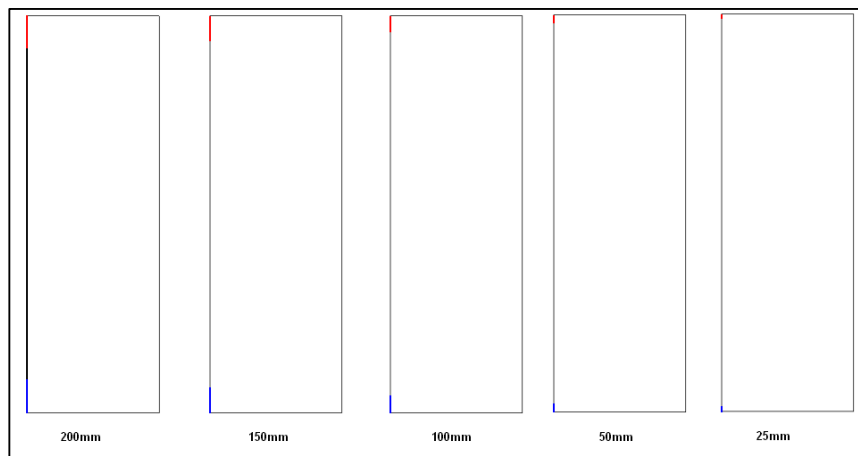


Figure 6.4 Cavity configurations for various inlet and outlet sizes on external skins.

- **Room Openings Position**

To analyse the airflow behaviour of the cavity in relation to the room, a 2D model of the experimental chamber (shown in figure 6.5) was constructed with inlets on the bottom and outlets on the top of the cavity and the back of the room. The inner skin was set as a boundary wall of 4mm. The openings on the bottom and the top were tested on various configurations to analyse their flow behaviour with cross ventilation.

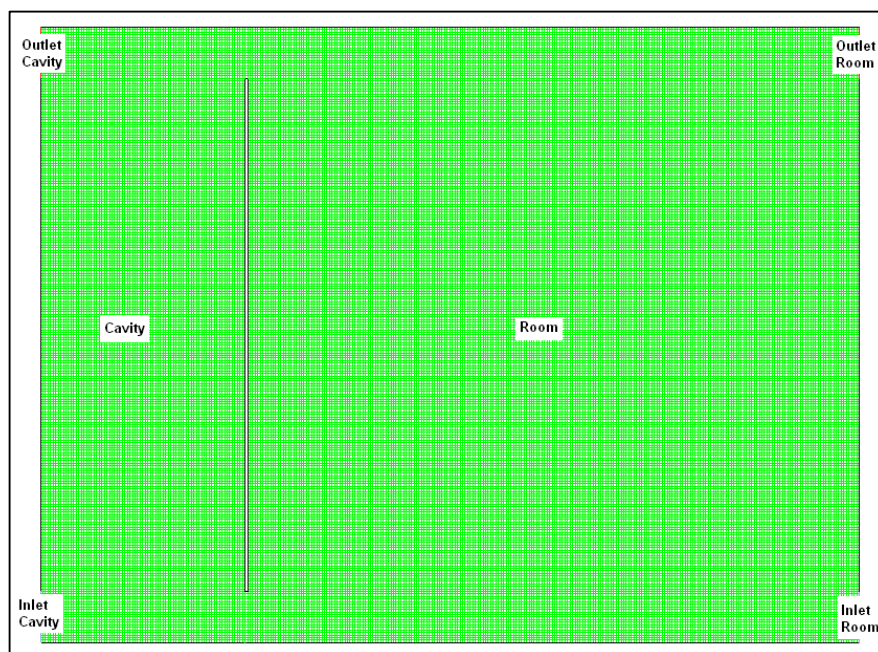


Figure 6.5 Openings locations in the 2D model of the experimental chamber.

- **DSF Structure**

The 2D cavity model was also adjusted to simulate the different configurations of the DSF using shading devices for radiation control. Figure 6.6 illustrates the configurations of the cavity for shading control on the glazed walls, louvers next to the external skin, centre and close to the inner skin. These cases were simulated in the ST and the STV.

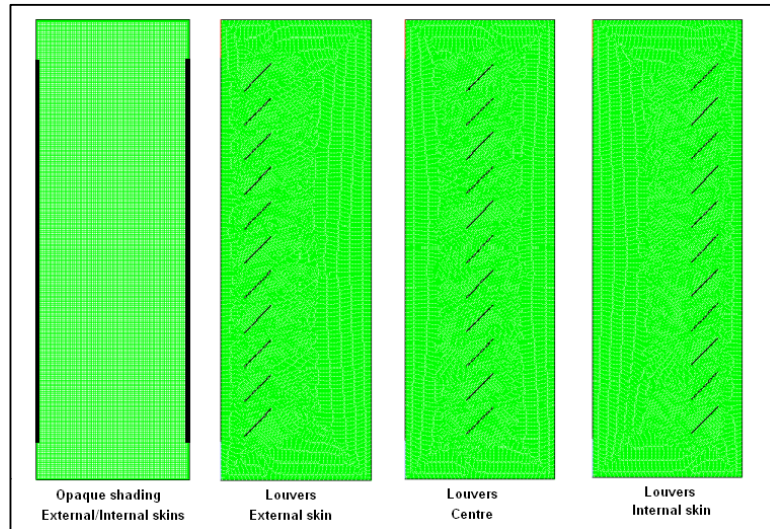


Figure 6.6 Model settings for shading control of glazing and inside the cavity with shading devices.

- **Glass Type**

In order to simulate the 2D model adjustment of glass type; the basic grid model of the cavity (as shown in figure 6.2) was used. In these cases, the boundary settings were assumed according to the total energy transmitted and reflected by each type of glass and the optical properties of the types of glass used in the experimental assessment. The models were simulated with the combination of glass type on external, internal and on both skins. All models were also simulated on the ST and STV.

- **Cavity Depth**

For the variation on the cavity depth of the 2D model, the domain of the model was gradually reduced on x direction from 800, to 600, 400, 200 and then to 100mm. The size of the cells was also proportionally reduced in order to keep the same total of cells in the domain. Also constructed were 2D models of the cavity, including louvers at 45° on the cavity models comprising sizes on the x direction of 600 and

400mm. Figure 6.7 shows the domain settings for the cavity with the varying depths on the x direction.

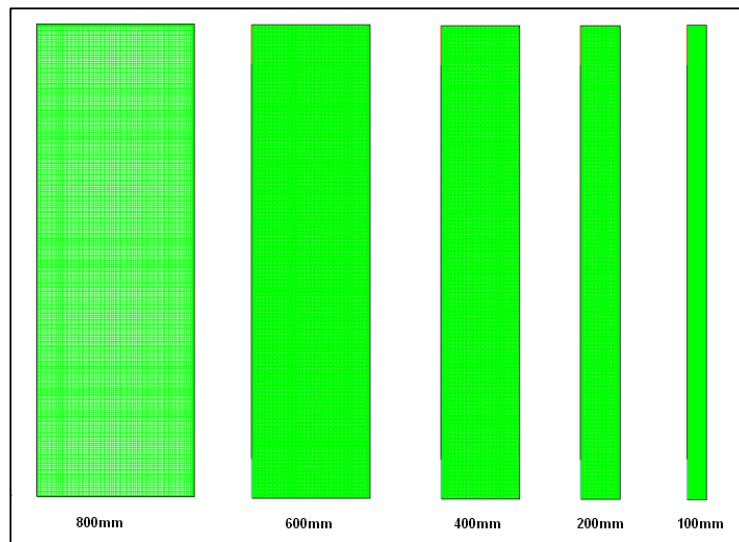


Figure 6.7 Grid models for various cavity depths.

6.3.3 Boundary Conditions

Two main configurations of the DSF model were used, shown in figure 6.8; the Standard (ST) and Standard Ventilated type (STV). The difference between the ST and STV model boundaries was that the inlets and outlets were replaced by a wall boundary on the ST.

- Standard case (ST): Inlets and outlets closed.
- Standard Ventilated case (STV): Inlets and outlets open.

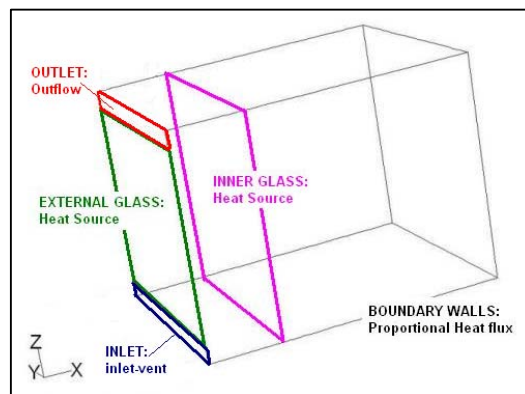


Figure 6.8 Boundary definition of the DSF Experimental Chamber.

The main parameters based on the experimental conditions are described in the following tables:

Table 6.1 Main parameters of the chamber's experimental conditions

Walls transmittance (U-Value):	0,22W/mt ² K [27]
Chamber floor (U-Value):	0,25W/mt ² K [28]
Emissivity silver louvers:	0,89 [29]
Emissivity white louvers:	0,90 [29]
Emissivity black louvers:	0,96 [29]
Glass transmittance -clear 4mm:	0,82 [30]
Glass transmittance -textured 4mm:	0,79 [30]
Glass transmittance -green 4mm:	0,75 [30]

Table 6.2 Main boundary conditions of the experimental model

Net heat source (External glass):	205.2 W/m ²
Net heat source (Internal glass):	63.4 W/m ²
External temperature:	25°C (298°K)
Inlet:	Inlet Vent.
Outlet (Outflow, ext-temp method):	25°C (298°K)
Materials:	
Walls:	Insulation panel
Floor:	Concrete slab
Glass:	Standard 4mm clear/textured/green tinted glass.

The air flow and the temperature response were modelled using a steady state model of radiation that directly affects the Double Skin Facade. The total internal heat gains (TIHG) shown in Table 6.3 were based on the steady state total heat flux calculated for each selected case, which is based on the data measured in the experimental chamber. These gains were set in each zone for the CFD model. For wall and floor surface temperatures, a fixed value was set in each of the cases assessed. Table 6.1 shows the main values used as boundary conditions for temperature and heat gains inside the DSF.

CASE	Main boundary conditions DSF				
	Temperature shading devices	Surface temperature Walls	Surface temperature Ceiling	Surface temperature Floor	Total Internal Heat Gains (TIHG)
	°C	°C	°C	°C	W/m ²
Sealed Cavity ST	-	34,80	35,20	30,10	253,86
Ventilated Cavity STV	-	30,50	31,00	24,50	205,79
DSF structure (STV) shading ext-skin	34,00	29,32	30,80	24,30	178,21
DSF structure (STV) shading int-skin	40,00	32,10	32,10	26,20	219,91
Louvers (STV) aluminium	52,00	31,00	33,00	24,70	215,62
Louvers (STV) white	48,00	31,00	31,00	24,70	194,98
Louvers (STV) black	57,00	31,00	35,00	24,70	228,43
Clear Glass STV	-	30,50	31,00	22,00	205,79
Textured Glass STV	-	29,00	29,10	22,00	195,50
Green Glass STV	-	28,60	28,85	22,00	181,10

Table 6.3 Main boundary conditions and Total Internal Heat Gains (TIHG) of the facade cavity.

6.4 AIRFLOW DESCRIPTION

The CFD models of the experimental chamber are used to visualize the air movement and the resultant temperatures within the cavity. Each model fundamentally simulates buoyancy-induced airflow. The CFD models of the experimental chamber are used to visualize the air movement and resultant temperatures within the cavity. Each model fundamentally simulates buoyancy-induced airflow. The airflow performances are simulated in 2D models of the cavity and the experimental chamber. Although this flow is likely to have significant features in 3D models, the purpose of this study is mainly to assess and compare the vertical airflow within the DSF. For this reason, the 2D models were a feasible alternative that required less demanding computational resources.

6.4.1 DSF Openings Position

The airflow performance is simulated in 2D models of the cavity and the experimental chamber. The positions of the openings are based on the main configuration of the DSF: a sealed cavity with the inlet and outlets closed (ST), and a ventilated cavity with the inlet and outlets open (STV).

6.4.1.1 Sealed Cavity (ST)

The airflow modelled in a sealed DSF resulted in a series of small eddies developing along the height of the cavity. Although the velocity and direction of the flow were variable, the values of velocity magnitude were very small fluctuating between 0.01 to 0.05 m/s. Figure 6.9 shows the development of very clear turbulent flows with very low air velocities inside the sealed cavity. The figure also demonstrates how the incident and reflected heat from external and internal skins created a buoyant

induced movement of air along the glass surfaces. The difference in pressure within the cavity is determined by this effect. The convective heat transfer from the surfaces to the air determines the development of eddies along the cavity. As the airflow is pushed upwards, heat is gradually accumulated on the upper level of the cavity, indicating that in sealed cavities overheating dramatically increases with height. Figure 6.9 also shows the contours of temperatures inside the cavity, which increase steadily from the floor to the ceiling. The maximum temperatures are developed on top of the cavity, reaching values of about 47°C, with a difference of temperature between top and bottom of 21°C.

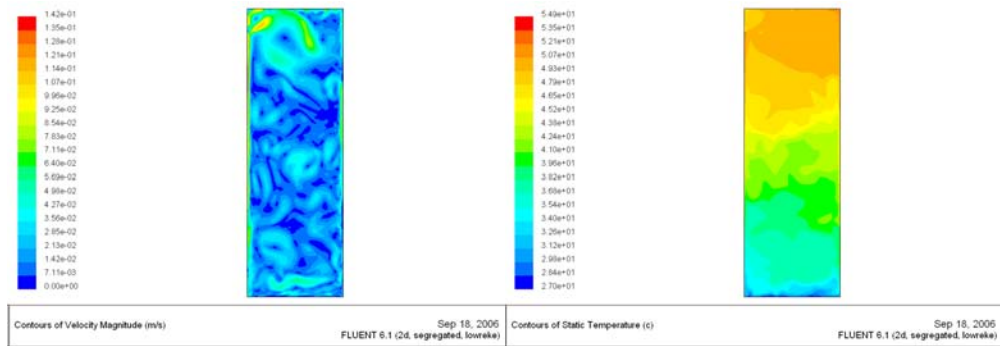


Figure 6.9 Air velocity and temperature contours of the cavity in ST.

The airflow behaviour of the room is directly influenced by the net incident heat load; produced by the inner glass (Q_r). The air next to the inner glass tends to flow upward developing a cyclical flow from the front to the rear wall. The differences in the overall airflow behaviour inside the cavity and the room as illustrated in figures 6.10 and 6.11 are contrary. On one hand, the increased greenhouse effect in the sealed cavity causes the development of noticeable turbulent flows while at the same time the airflow in the room is reduced due to the lack of air exchanged between the cavity and the exterior. The convective heat transfer of the room is mainly

determined by the resultant heat flux from the inner glass and then by the heat reflected by the inner surfaces.

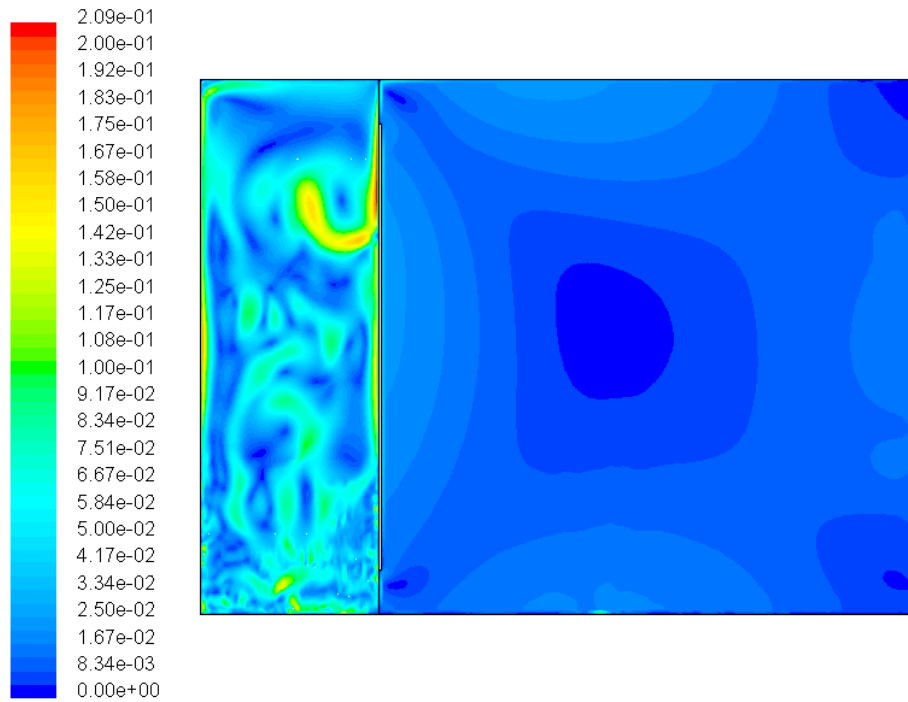


Figure 6.10 Velocity magnitude contours section of the experimental chamber in ST.

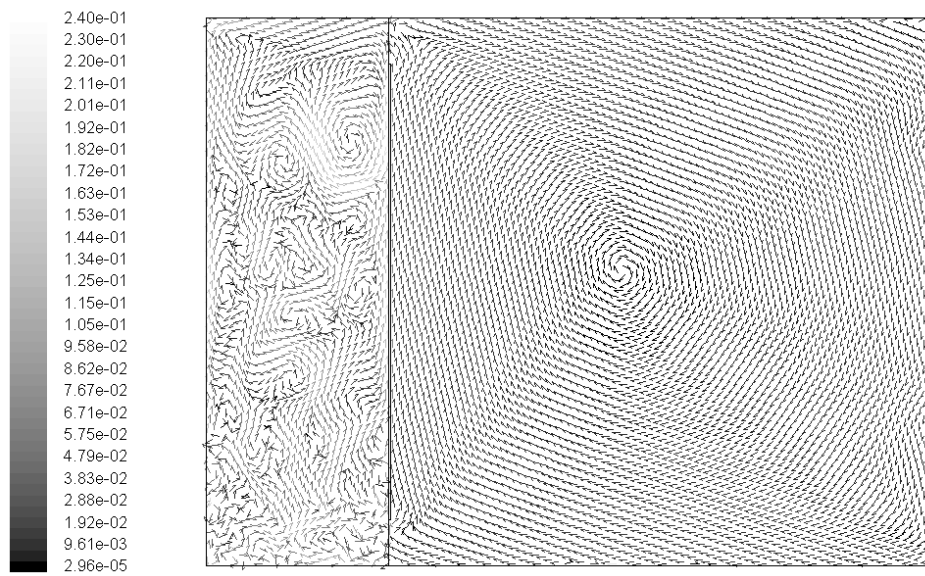


Figure 6.11 Velocity vectors grey scaled by velocity magnitude (m/s) in ST.

6.4.1.2 Ventilated Cavity (STV)

In the case of the behaviour of the airflow inside a ventilated cavity, there is a clear laminar flow from the inlet to the outlet (figure 6.12). Air tends to flow towards the inner glass and upwards to the outlet with a very distinctive eddy forming just behind the external glass, forcing the air stream to flow close to the inner skin. It was observed that air velocities within this vortex were dramatically lower in comparison to those along the laminar flow. This indicates that the size of the cavity has a significant effect on the overall air velocity. The values of the velocity magnitude ranged from 0.01 to 0.09 m/s, with the lowest values within the large eddy and the highest along the laminar flow. Figure 6.12 also illustrates the contours of temperature within the cavity. A dramatic reduction in the temperature levels was observed. The figure shows that temperatures were lowest along the continuous flow while they were highest along the vortex behind the external skin. These values oscillated between 28.7°C to 37.8°C respectively. The incident and reflected heat on the external and internal skin encouraged the airflow from the lower inlet to the outlet. Although airflow was allowed through the cavity, a formation of sub-zones with turbulent eddies where temperature levels were highest, and air velocity was considerably reduced, were observed. Buoyancy induced airflow is still determined by the incident heat flow but the continuous air movement determines the reduction of the convective heat transfer inside the cavity. In the ventilated cavity, the maximum temperature developed on the top of the cavity reached around 37.8°C, with a difference in temperature on the exterior of about 12.3°C. Nevertheless these values are considerably lower within the areas of laminar airflow.

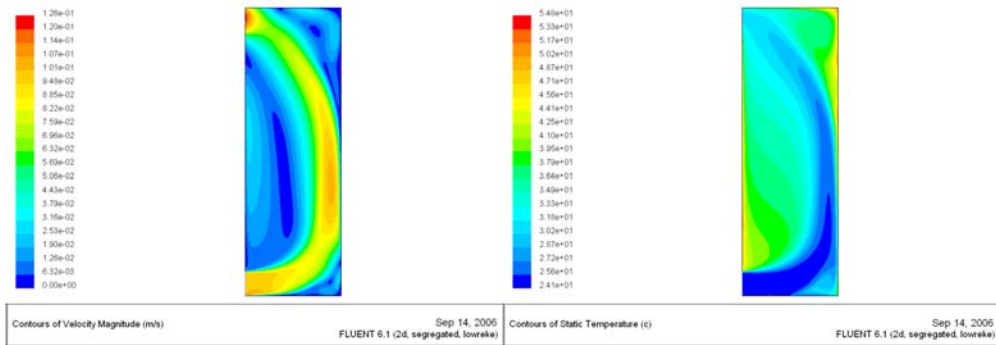


Figure 6.12 Air velocity and temperature contours in STV.

The airflow inside the room behaved similarly to the ST. Although the net incident load from the inner glass (Q_r) is slightly reduced, the resultant airflow still develops an upward flow from the inner skin, which tends to circulate to the back wall creating a cyclical flow within the room (figure 6.13). This indicates that the overall behaviour of the cavity has little impact on the room performance when no air exchange is present between the cavity and the room.

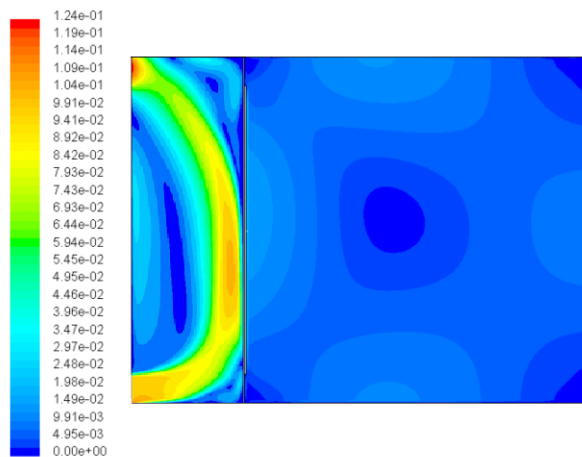


Figure 6.13 Velocity magnitude contours section of the experimental chamber in STV (m/s).

There is a clear reduction in overall temperature values inside the cavity when it is ventilated. The total temperature values inside the cavity are shown in figure 6.14. The figure shows how the temperatures steadily increased in the ST, and how there

were fluctuations in the temperature values on the STV. Although there were some increments in the values of the STV within the areas where eddies were created, there was an overall reduction of 10°C in the average temperature when the cavity was ventilated, which demonstrates the importance of continuous airflow in reducing overheating.

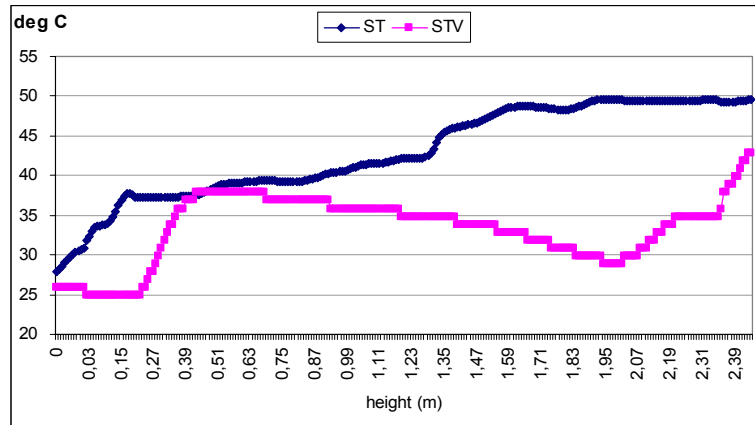


Figure 6.14 Calculated temperature values in the vertical centre of the cavity in ST and STV.

There is a very distinctive difference in the temperature performance of each case. In the case of the ST the increase is reasonably steady and reaches high values, whereas with the STV the increase is variable, due to the displacement of the main flow towards the inner skin reaching lower values than the ST. Thus it is evident that there is a difference in temperature inside the cavity when it is sealed from when it is ventilated. For the airflow inside the cavity, Figure 6.15 also provides evidence of how there is continuous air movement due to the constant airflow from inlet to outlet. The higher velocity values were obtained at the height of the inlet and outlets, decreasing in the centre due to the reduction of magnitude and direction within the vortex behind the external skin. The air velocity magnitude is lower but more variable on the ST, which is due to the appearance of turbulent eddies trapped in a

confined space. It is clear that overheating develops when there is no constant airflow inside the DSF.

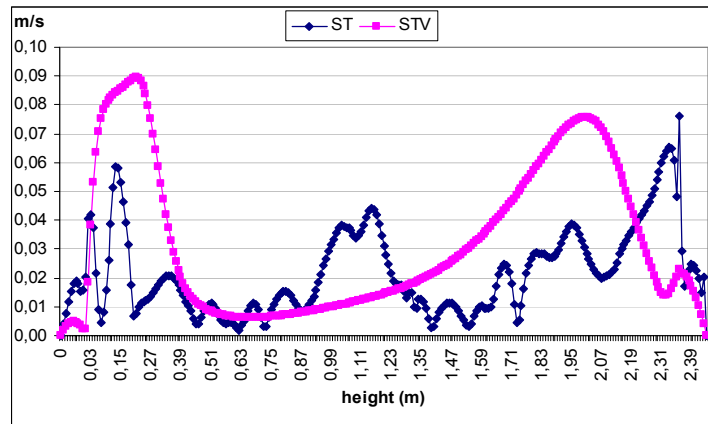


Figure 6.15 Calculated values of air velocity in the centre of the cavity in ST and STV.

6.4.1.3 Inlet / Outlet size

As previously described, the inlet and outlet sizes were adjusted from 200mm to 12.5mm. The airflow performance of the cavity was simulated in the 2D models. The size of the inlets and outlets were compared according to the following correlations:

- Equal variation on inlet and outlet sizes.
- Variable inlet and fixed outlet sizes.
- Fixed inlet and variable outlet sizes.

On the first correlation, it was generally observed that a regular reduction in inlet and outlet sizes resulted in a gradual increase in the overall temperature values inside the cavity. Figure 6.16 shows the plots of the calculated values of temperatures inside the cavity with inlet and outlet sizes of 150, 100, 50, 25 and 12.5mm. The figure illustrates how the temperature performance increased slightly when the size was reduced from 150 to 100mm; this resulted in a steady increase in the temperatures as the sizes were reduced.

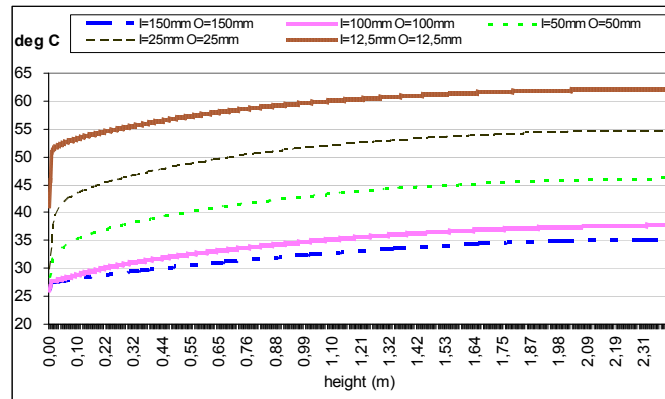


Figure 6.16 Temperature performances for various opening sizes of the cavity.

The influence of the airflow behaviour inside the cavity is a key factor in the overall thermal performance of the ventilated cavity. The values of temperatures obtained inside the cavity varied considerably according to the inlet and outlet sizes. Figure 6.17 shows the different airflow behaviours calculated inside the cavity depending on the variation of inlet and outlet sizes. The figure shows how the velocity magnitude values in the cavity decreased as the size of the openings was reduced. It was noticeable that the laminar airflow became turbulent as soon as the opening sizes were reduced. However, this transition determined the manifestation of relatively steady velocity values within most of the cavity when the inlet and outlet sizes were 150mm, indicating a more constant removal of air from the cavity.

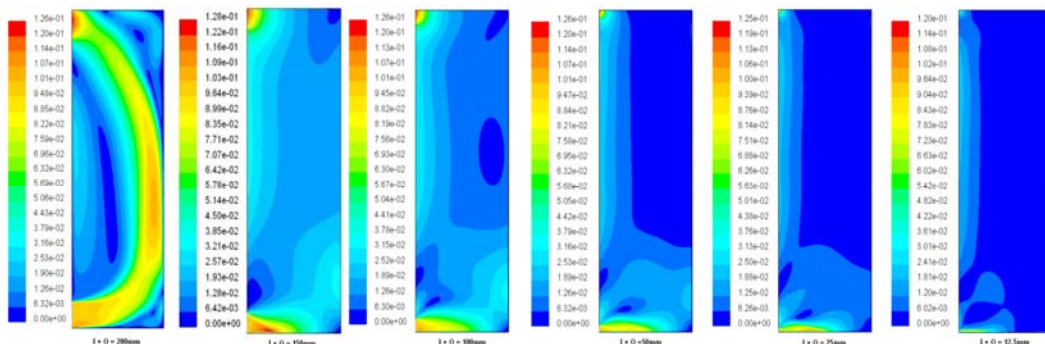


Figure 6.17 Velocity magnitude (m/s) contours inside the cavity for various inlet/outlet openings sizes.

On the second correlation, the outlet size was kept fixed and the inlet sizes were decreased gradually. Figure 6.18 shows the contours of velocity magnitude inside the cavity depending on the variation of the inlet size. It was also observed that the overall velocities decreased gradually when inlet sizes were reduced. In addition the airflow started to behave in a laminar stream between three eddies from when the openings were 200mm, to a reduced but steady flow when the openings were 150 and 100mm. As soon as the opening sizes were reduced further; overall velocities started to decrease dramatically and a small laminar flow began to appear alongside the external skin.

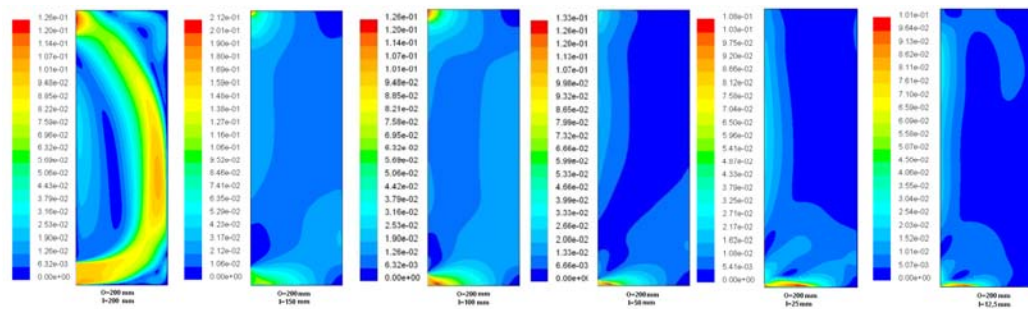


Figure 6.18 Velocity magnitude contours (m/s) inside the cavity for various inlet sizes and 200mm fixed outlet.

The third correlation shown in figure 6.19 was carried out with fixed inlet sizes but with variable outlet sizes. As the outlet sizes were decreased, an overall and gradual reduction of air velocities was observed. However, it became evident that the overall velocity magnitude values (when the outlet sizes were 150 and 100mm) were slightly higher than the ones obtained on the previous settings, indicating more constant air velocities and exchanges from the cavity.

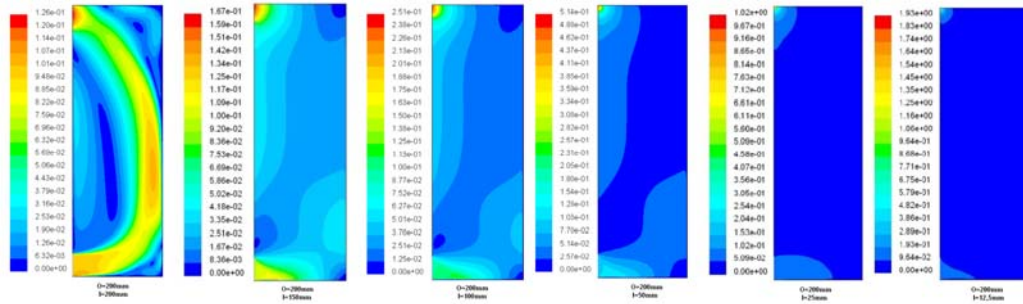


Figure 6.19 Velocity magnitude contours (m/s) inside the cavity with fixed 200mm inlet size and various outlet sizes.

The highest temperature values were obtained when either the inlet or the outlet opening size was set at 12.5mm. With this setting the cavity behaved almost identically to the ST configuration. The lowest temperature values were obtained when the inlet/outlet size ratio was higher than 0.50mm. This proves that a reduction in the opening size ratio has a direct influence on overheating. It was also found that the appearance of slightly lower velocity magnitude values with reduced turbulence was a key factor in controlling overheating within the cavity.

6.4.2 Room Opening Positions

For this parameter, the experimental chamber was modelled using 2D models of the cavity and the room zones linked together. The models were simulated with ventilated cavity variants on the position of the openings in the internal skin and the back wall of the room.

For the cases when varying the internal skin, three models were simulated alternating the position of the upper and lower openings between the cavity and the room. Figure 6.20 shows the velocity magnitude vectors of the airflow inside the cavity and the room in each case. It was shown that air exchange between the cavity and the

room appeared when the inner skin was open at the top. There was a noticeable airflow exchange when both openings were open and only reduced when it was open at the top. This indicated that the stack effect in the cavity encourages air removal from the room through the top of the inner skin. Nevertheless, this air removal is dramatically reduced when the inner skin is open only at the top. The difference in pressure between the lower and upper openings was a key factor in encouraging natural ventilation through the cavity. Although this phenomenon is suitable when using incoming preheated air in wintry conditions, it could contribute to a dramatically increased heat load, which may cause the room to overheat during summery conditions.

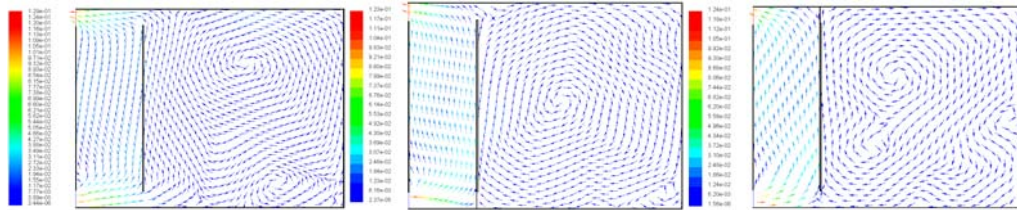


Figure 6.20 Velocity magnitude vectors inside the experimental chamber for various opening positions on the internal skin.

When the openings at the back of the room were adjusted, it was observed that the effect of cross ventilation between the cavity and the room was greatly enhanced. The airflow direction varied accordingly with the position of the back wall openings. Figure 6.21 shows three different airflow behaviours inside the room depending on the position of the openings on the back wall.

The first case (far left) has an opening at the top of the back wall, acting as an outlet shaft, which created a continuous flow from both openings of the inner skin. In the second case, (middle) the opening on the bottom of the back wall acted as an inlet

shaft that created an incoming flow from the back of the room towards the inner skin. This configuration showed that the stack effect of the cavity and the flow created by this configuration could be used for natural ventilation and for passive air removal.

In the third case (far right), both openings on the back wall were open. There was a continuous airflow from the bottom to the top of the room and a secondary flow towards the cavity. However, there was also a tertiary incoming flow on top of the cavity entering the room, indicating that heated air from the cavity was flowing into the room. Although this configuration showed constant cross ventilation from the back wall of the room, the introduction of hot air at the top of the inner skin could cause a problem, as hot air entering the room could increase the total heat load from the inner skin.

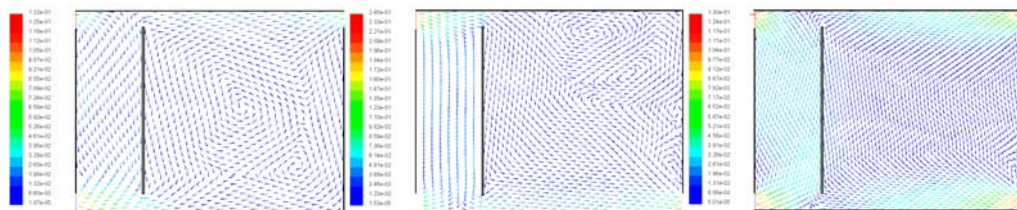


Figure 6.21 Velocity magnitude vectors inside the experimental chamber for various opening positions on the back wall of the room.

6.4.3 DSF Structure

6.4.3.1 Shading panels on Glazed Skins

In this parameter, 2D models of the cavity were simulated reducing the TIHG inside the cavity and adjusting the heat flux on the external and internal skins. Both cases were simulated in the ST and the STV. The thermal and airflow performances were also compared.

The first cases were simulated by reducing 30% of the direct heat flux from the external skin due to an increase in the shading ratio. The airflow behaviour and thermal performances on the ST and the STV of the cavity are shown in figure 6.22. The figure shows that the overall airflow behaviour is relatively similar to the initial ST and STV cases without shading surfaces. Although the reduction of heat flux from the external skin has little impact on the airflow behaviour, the temperatures inside the cavity are slightly reduced by 4.78°C as a result of the reduction in the total heat load entering the cavity.

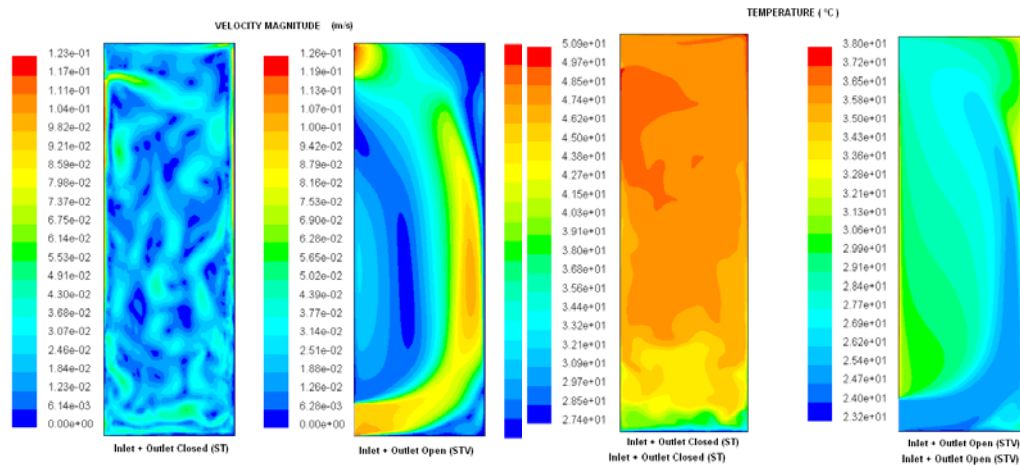


Figure 6.22 Velocity magnitude and temperature contours of the cavity assuming shading panels on the external skin.

The second experiment simulated increasing the heat reflected in the inner skin by 30%. Figure 6.23 shows how the reflected heat from the inner glass had a direct impact on the airflow in the STV, increasing the overall velocity magnitude levels in the cavity. The reflected heat had a dramatic impact on the temperature levels. Average temperature levels were increased by 7.23°C in the ST. These performances demonstrate clearly the increase in overheating in the ST and the increased stack effect in the STV when the inner skin reflects more radiation.

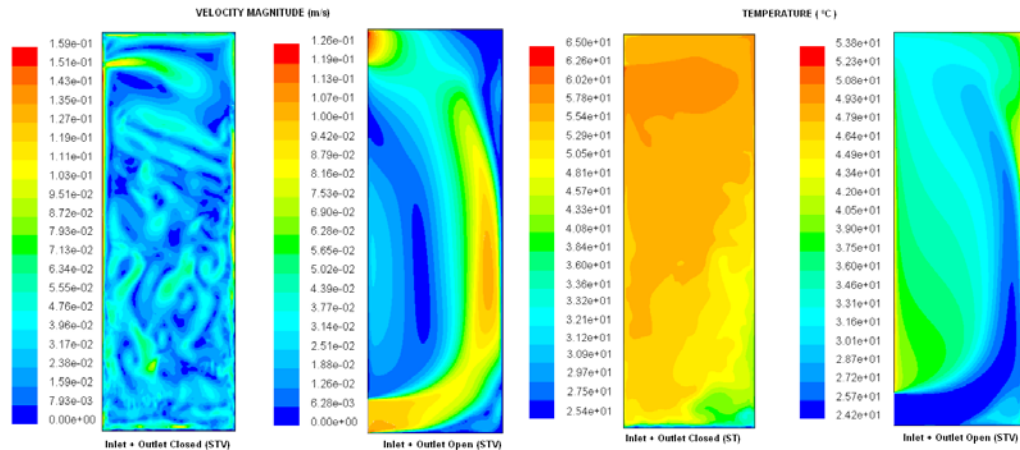


Figure 6.23 Velocity magnitude and temperature contours of the cavity assuming shading panels on the internal skin.

The temperature levels reached in the models are shown in Figure 6.24. The highest temperature levels were reached when the cavity was sealed and the internal skin was partially shaded. The lowest temperatures were obtained when the cavity was ventilated and the external skin was shaded. Although temperature levels in the STV (with reflective surfaces on the internal skin) are higher than the ones obtained with external shading, the levels are still lower than any of the ones obtained in the ST. This confirms that constant airflow within the cavity is a key factor in preventing overheating.

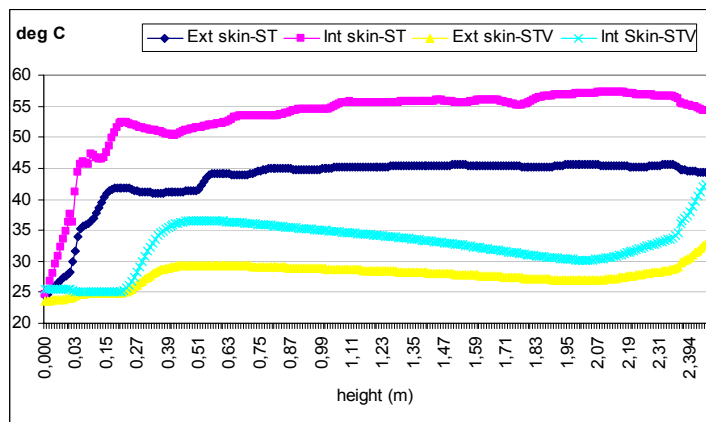


Figure 6.24 Temperature performances of the cavity for various positions of shading surfaces on external and internal skins.

Figure 6.25 shows the velocity magnitude values calculated along the vertical centre of the cavity. The graph shows that preventing air exchange within the exterior of the ST causes fluctuating and turbulent flows with smaller velocity magnitude values. However, the continuous air exchange within the exterior of the STV also causes the appearance of laminar and constant flows close the inlet and outlet, which increase magnitude levels,.

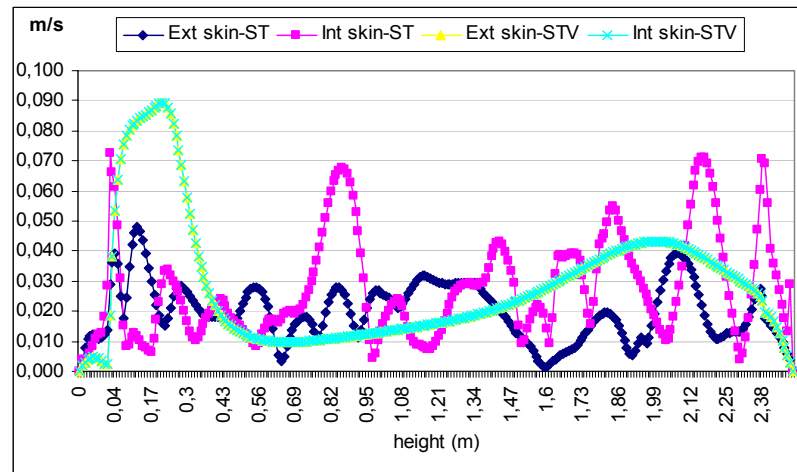


Figure 6.25 Air velocities in the cavity with various positions of shaded surfaces on the external and internal skins.

6.4.3.2 Louvers

In this parameter, the 2D models of the cavity were simulated according to the position and colour of the shading devices placed inside. All cases were simulated in the STV and the thermal and airflow performances compared.

- **Position of Louvers**

The models were built with tilted and horizontal devices positioned at three different points inside the cavity: next to the external skin, on the vertical and next to the internal skin.

In relation to the models with tilted louvers, the airflow behaviour for each position are described in figure 6.26. The models show the displacement of the vertical flow depending on the location of the louvers. It was observed that the heat reflected by the surface of the louvers determined the development of the continuous flow with regard to the proximity of the louvers. However, it was also noted that the displacement of these surfaces either toward the external, or internal skin, encouraged the airflow to develop between the shading devices and the glazed surfaces. The volume of air within this small area was heated rapidly, thus increasing the stack effect, and encouraging higher velocities within this area.

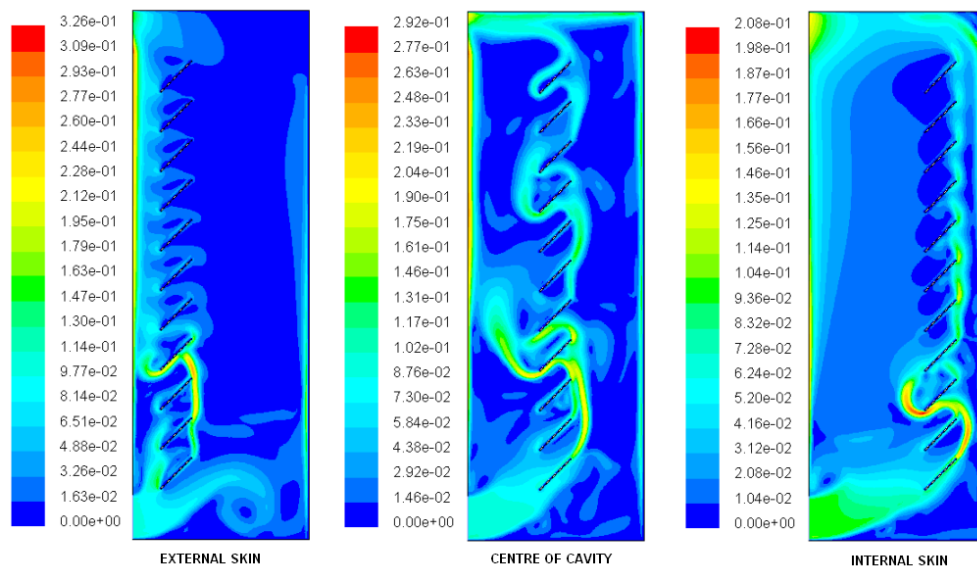


Figure 6.26 Velocity magnitudes contours (m/s) for various positions of louvers at 45° inside the cavity.

The airflow behaviour of each model with horizontal louvers is shown in figure 6.27. These models also show the displacement of the vertical flow depending on the location of the louvers. Although the airflow was still displaced towards the glazed skins, depending of the proximity of the louvers, the horizontal position of the

louvers was not as conducive to the circulation of the air as it was in the previous case. This horizontal position created more resistance to the overall flow reduction of the velocity inside the cavity.

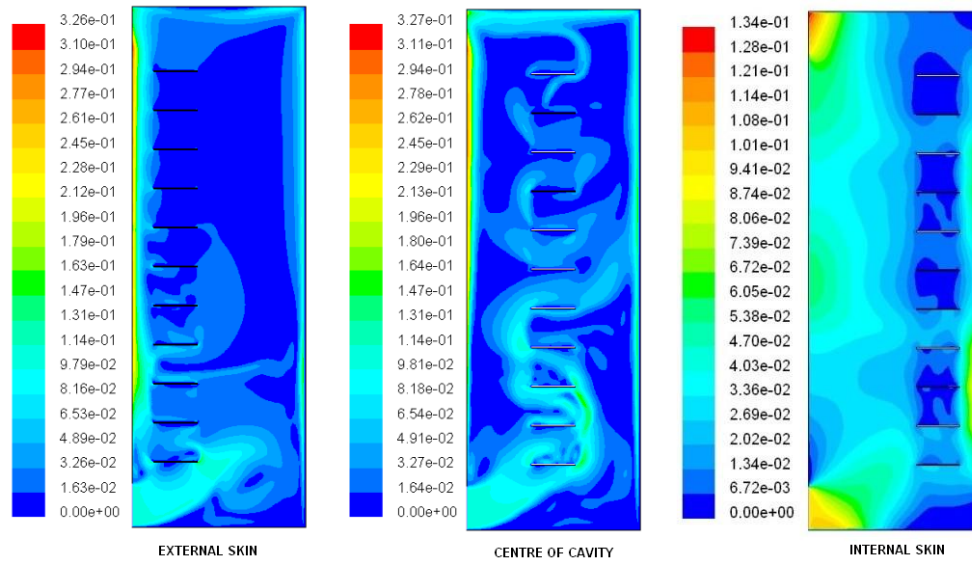


Figure 6.27 Velocity magnitude contours (m/s) for various positions of horizontal louvers inside the cavity.

The thermal response of the cavity depending of the position of the louvers is illustrated in figure 6.28. The graph shows the calculated values on the vertical centre of the cavity. The figure shows how slightly higher temperatures were obtained with louvers placed next to the inner skin. The lowest levels of temperature were obtained when the louvers were placed next to the external skin. The graph also shows the fluctuating levels of the temperature calculated in the centre of the cavity. Here the peak values reflect the significant influence of the heat transfer from the shading devices.

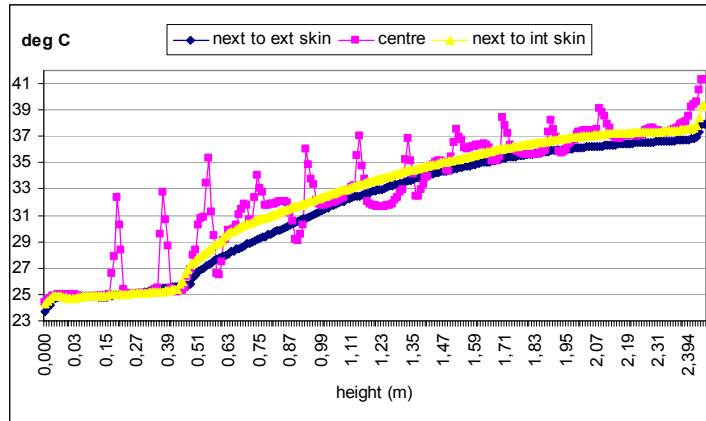


Figure 6.28 Temperature performances of the cavity calculated for variously positioned louvers.

- **Colour of Louvers**

For this parameter, the models were built to modify the emissivity in the boundary conditions of the surface of the louvers, according to the values shown in 6.33 for silver, white and black colours. The airflow behaviour of each model, depending on the colour of the surface of the tilted louvers, is located in the centre of the cavity, as shown in figure 6.29.

The airflow models behaved relatively similar in all three cases. The highest velocity magnitude values were obtained in the areas close to the louvers. The average air velocities in the cavity with silver and white louvers were 0.0363 and 0.366m/s, respectively. A slightly higher average velocity of 0.041m/s was obtained by using a black louver. This clearly indicates an improvement in the stack effect as a result of the increased heat emitted by the darker surfaces.

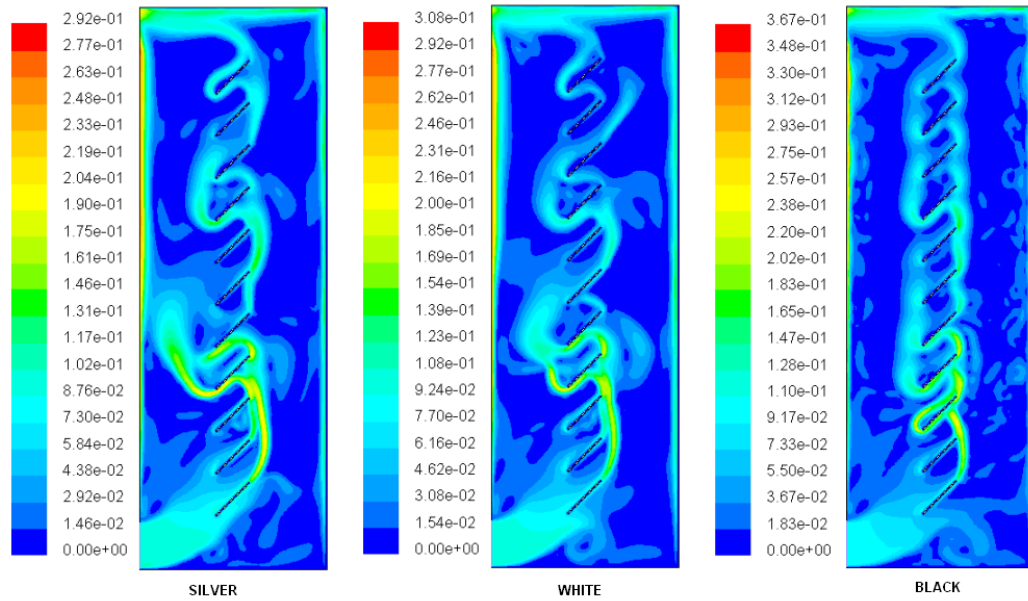


Figure 6.29 Velocity magnitude contours (m/s) inside the cavity for various colours of louver surfaces.

Figure 6.30 shows the calculated values of velocity magnitude along the vertical centre of the cavity, and the fluctuations and peak values in the cells close to the shading devices. As can be see from Figure 6.29, these peak values are evidently due to the laminar flows close to the tilted surface of the louvers; which favour these upward flows.

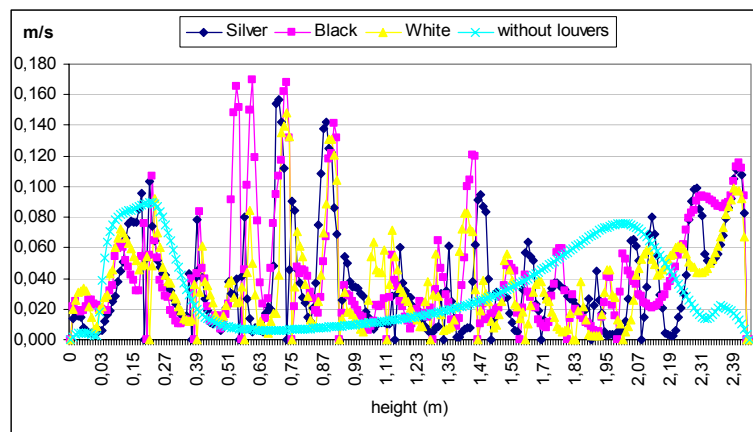


Figure 6.30 Air velocity performances inside the cavity for various surface colours of louvers.

The temperatures obtained in each model are clearly affected by the emissivity of the louvers. Figure 6.31 shows how the increase in emissivity causes resultant increases in temperature. The highest average values were obtained using black, and the lowest using white. Although the emissivity of shading devices is directly related to the increased temperatures inside the cavity, the stack effect is also increased and can be used to remove air from the facade or the inner spaces.

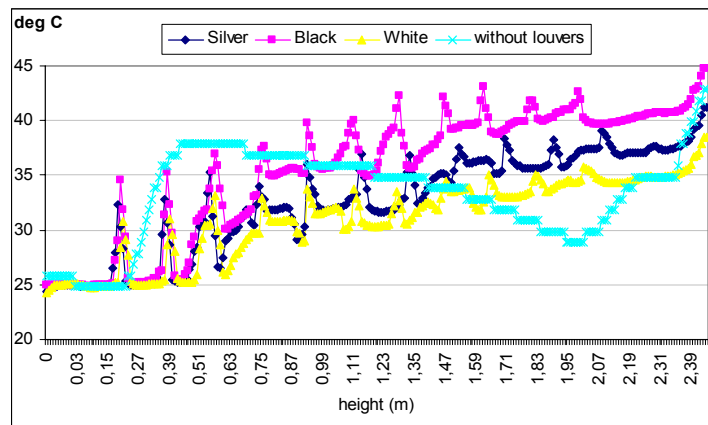


Figure 6.31 Temperature values of the cavity for various surface colours of louvers.

6.4.4 Glass Type

In this parameter, 2D models of the cavity were simulated using different levels of TIHG inside the cavity. The heat flux in the external and internal skins was adjusted according to the transmittance values of clear, textured and green glass [29]. All cases were simulated in the STV. The airflow and thermal performances were compared.

The airflow performances inside the cavity depended on the variation of glass type from the external skin, as illustrated in figure 6.32. In all three cases, the displacement of the laminar flow behaved relatively similarly. However, there were minor reductions in air velocities when correlated with the variation of glass

transmittance. The average air velocities obtained with clear glass settings were 0.032m/s; with textured glass 0.027m/s; and with green glass 0.029m/s. Thus the reduction of glass transmittance had a reduced but gradual influence on the average air velocities inside the DSF.

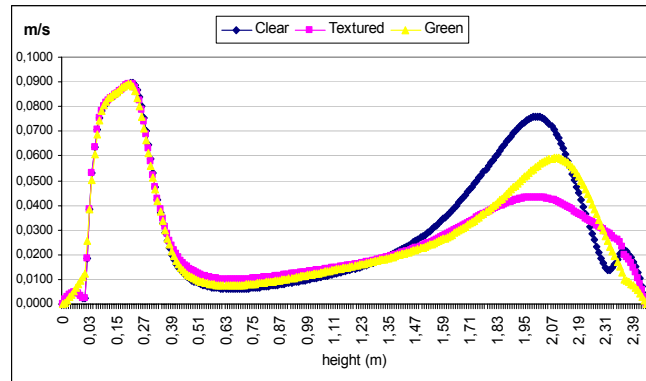


Figure 6.32 Velocity magnitudes along the centre of the cavity for various glass types.

As the model assumed a slight increase in reflected radiation in the inner skin, in the case of green glass, the increase in average velocities was consistent with this factor. Figure 6.33 shows (from right to left), the velocity magnitude contours in each case. It can be seen that slightly higher coloured contours appeared in the case of clear glass, while the performances of textured and green glass were quite similar. The main differences can be observed in the velocities near the outlet.

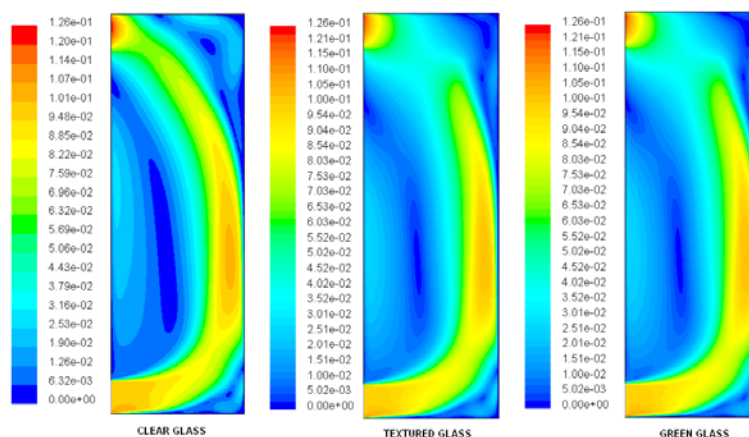


Figure 6.33 Velocity magnitude contours (m/s) inside the cavity for various glass types.

The thermal performance inside the cavity is directly affected by the amount of light transmitted through the glass. Figure 6.34 shows the gradual attenuation of the values obtained as transmittance levels were reduced slightly for textured and green glass.

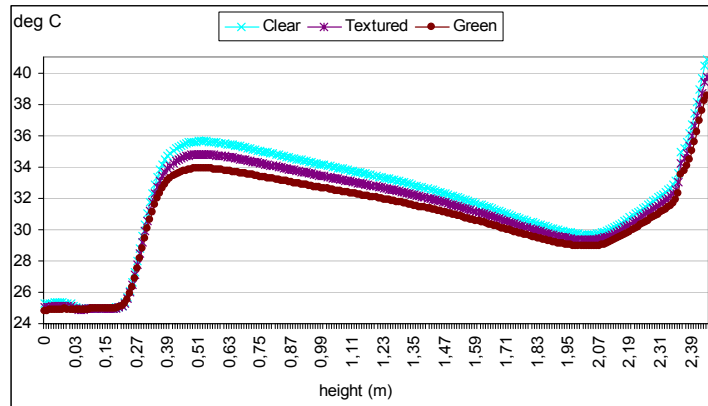


Figure 6.34 Temperature in the centre of the cavity for various glass types.

6.4.5 Cavity Depth

The 2D models of the cavity were simulated in two configurations for comparison purposes. Firstly, by adjusting the cavity's depth using five different positions and secondly, by adjusting its depth using three positions including horizontal louvers in its centre. All cases were simulated in the STV and the airflow performances and thermal behaviour were analysed.

6.4.5.1 Depth Variation

In this parameter, the models of the cavity were simulated according to depths of 800, 600, 400, 200 and 100mm on the x axis. Figure 6.35 shows the variation of airflow patterns and velocity magnitudes inside the cavity for each case. The contours show a pattern of reduction in the values of velocity magnitude; it can be seen that the wider cavity tended to create zones with eddies at low velocities while

at higher velocities a clearly defined laminar flow was created. In the other cases it is clear how overall velocities tend to decrease. It can be seen that the airflow tended to change from more turbulent to laminar as soon as the depth was reduced. The airflow is gradually displaced to each of the radiant surfaces where the convective heat transfer encourages upward flow. Previous research has suggested that there is an optimum width in which DSFs can reach their maximum airflow rate [31]. These tests also showed how the correlation between width and height of the cavity influences the airflow rate inside it. The height of the cavity allowed a more volumetric and constant airflow of 600mm and a higher laminar close to the radiant surfaces. As this model of the DSF is only one story high, the case with 600mm allows for better airflow and constant heat removal.

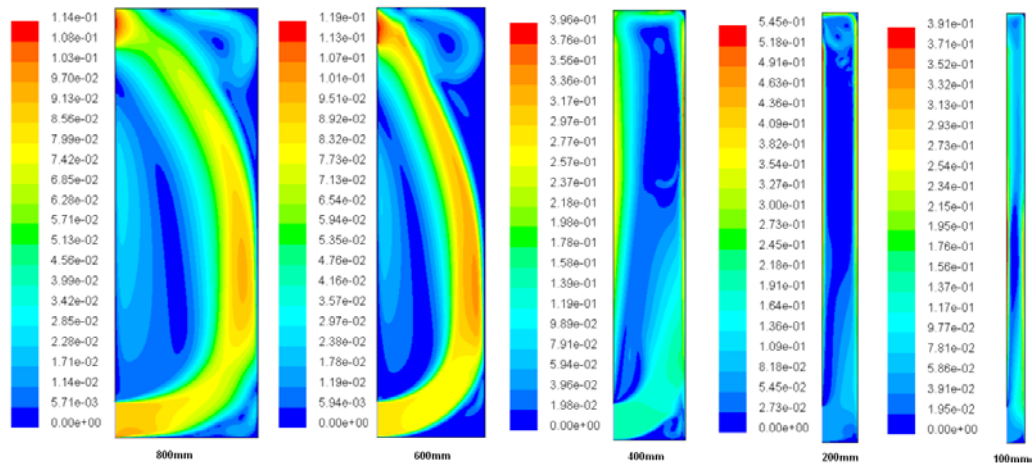


Figure 6.35 Velocity magnitude contours (m/s) for various cavity depths.

The relationship of depth to air velocity has a dramatic impact on the thermal performance of the cavity. Increasing the airflow inside the cavity also causes better heat removal from the cavity. Figure 6.36 shows the calculated values of temperature in the vertical centre of the cavity. The cavity tends to develop high temperatures at specific points when the depth is increased. This behaviour is indicated by the appearance of turbulent eddies. The correlation between depth and

height determines the reduction of the temperature values within an optimum depth of between 600mm and 400mm. This means that an optimum depth must be assessed for each case of DSF.

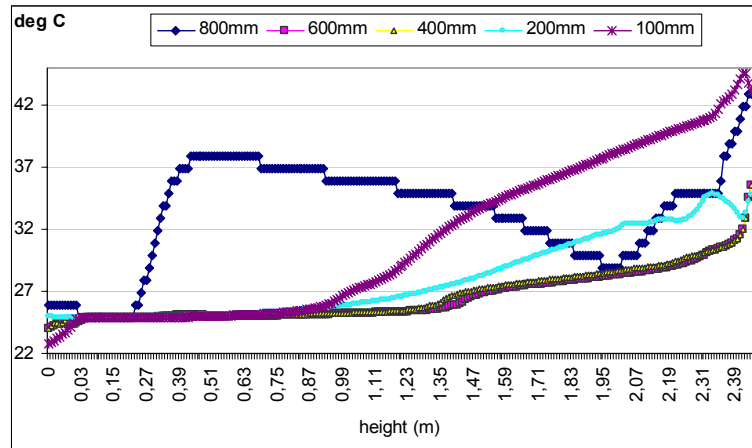


Figure 6.36 Temperature performances in the cavity for various cavity depths in STV.

6.4.5.2 Depth Variation with Louvers

In this parameter, the models were simulated according to depth sizes of 800mm, 600mm and 400mm on the x axis with louvers located along the vertical centre of the cavity. Figure 6.37 shows the variation in airflow patterns and the velocity magnitude inside the cavity in each case. It was observed how the diminution of the size of the cavity permitted a more efficient increase in laminar flows, both in front of and behind the louvers. The proximity to the glass and the increase of the reflective surfaces permitted the rapid development of upward flows between them. Although velocity magnitudes were increased along these areas, the flow rates within the louvers zones remained relatively similar. Similar patterns and behaviours of the airflow next to the louvers surfaces were observed yet a slight reduction in the average air velocity alongside the vertical centre of the cavity could also be seen.

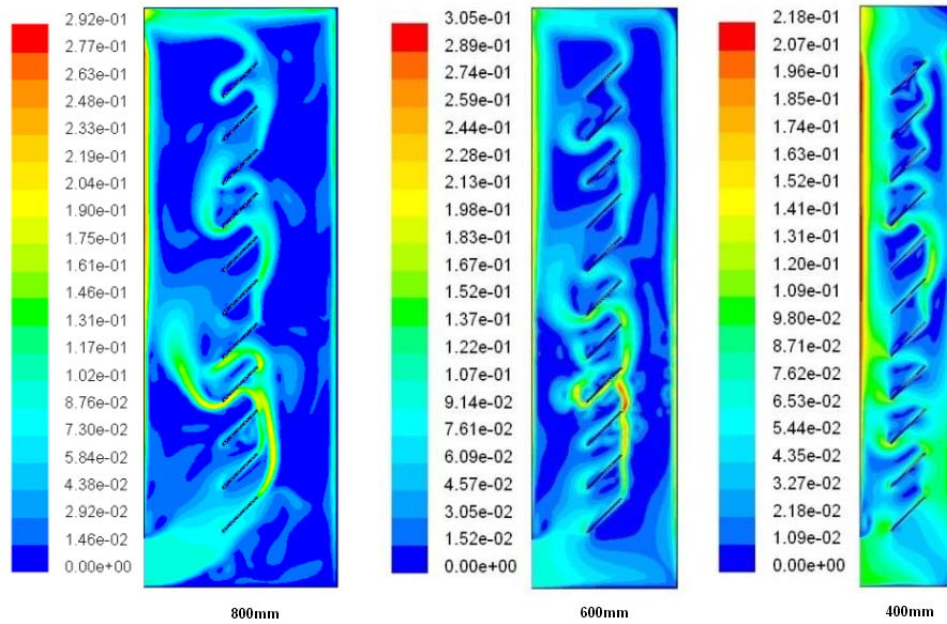


Figure 6.37 Velocity magnitude contours (m/s) for various cavity depths with louvers.

The variation in the airflow behaviour between the glazed surfaces and the louvers allows an increasing buoyancy-induced flow that help to remove the heat that has accumulated within the cavity. Figure 6.38 illustrates how temperature values fall as the depth is reduced. In these cases, it is possible to visualize how, as the depth is reduced, a greater volume of heated air is accumulated at the top of the cavity and how the improvement of the flow contributes to this area. In the cases of the central louvers, the importance of improving the stack effect associated with laminar flows between the louvers and the glazed surfaces becomes noticeable. The improvement in the airflow inside the cavity helps to reduce the temperatures in the DSF.

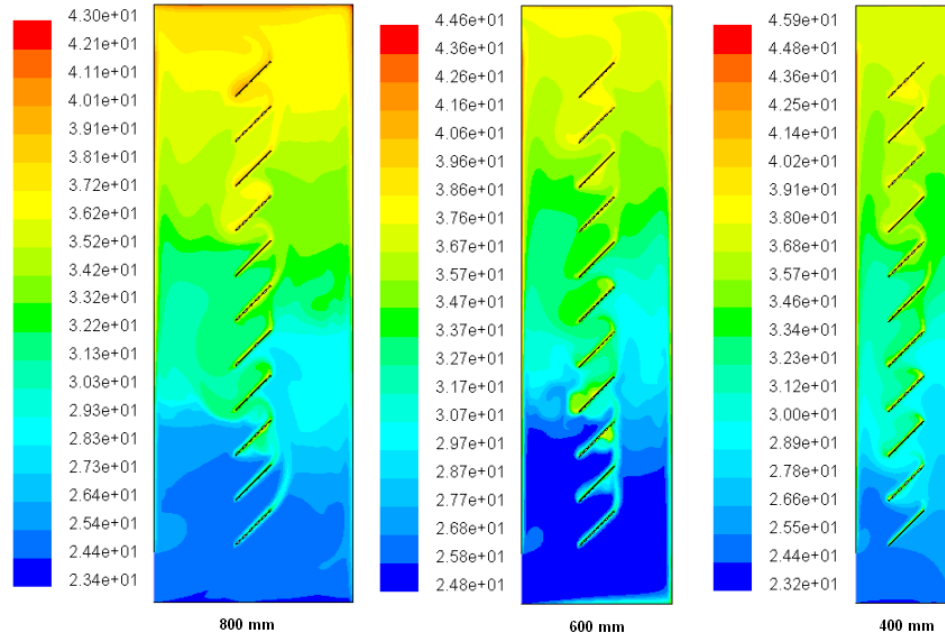


Figure 6.38 Temperature contours (°C) for various cavity depths with louvers.

6.5 DISCUSSION OF RESULTS

6.5.1 Air Velocity

As previously discussed in Chapter 5, the position of inlets and outlets has a dramatic impact on the average air velocities inside the cavity. The CFD simulations also allowed the demonstration of increased mean velocities on ventilated DSF. Figure 6.39 illustrates how mean velocities inside the cavity are higher in the STV. Although mean velocities inside the cavity are low, mean velocities in the STV are 0.01m/s higher than the ST. Thus, a ventilated cavity is an essential configuration to control overheating..

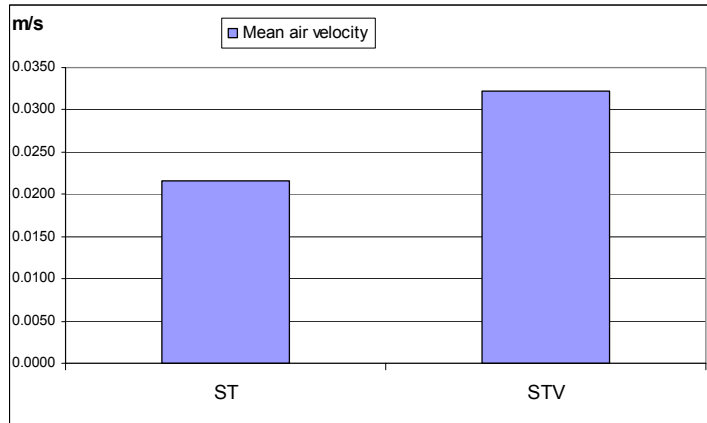


Figure 6.39 Mean air velocity magnitude in sealed (ST) and ventilated (STV) cavity.

The size of the openings is another factor that directly influences the overall performance of the airflow inside the cavity. Figure 6.40 shows how the reduction of inlet and outlet sizes has a direct impact on the reduction of the average air velocities. The equal reduction of inlet and outlet sizes has a direct influence on reducing air velocities and improving air extraction efficiency.

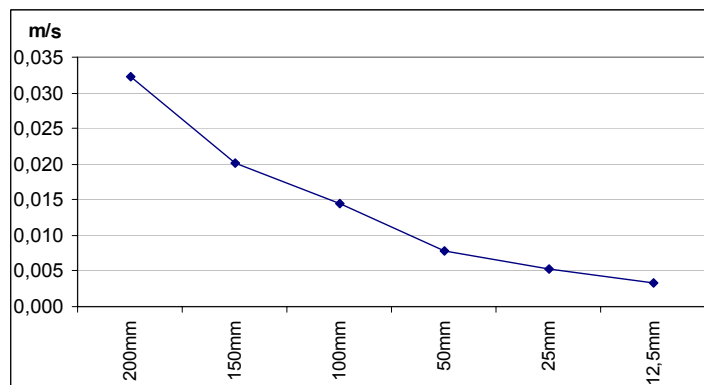


Figure 6.40 Average velocity magnitude values inside the cavity for various opening sizes.

The colour of the surfaces inside the cavity also has interesting implications for the airflow behaviour in the cavity. It was observed that darker colours encouraged higher air velocities inside a ventilated cavity. Figure 6.41 illustrates how higher

mean velocities were reached with black louvers. Thus, darker colours encourage slightly higher velocities and stack effects; however this also increases the heat reflected, so special care must be taken to balance the airflow and temperature performance of the cavity in order to prevent overheating from occurring.

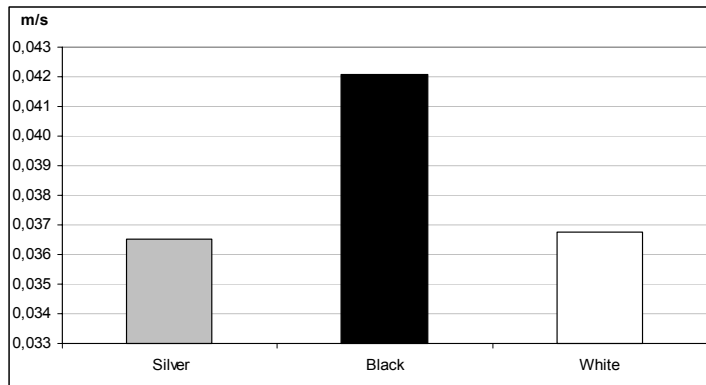


Figure 6.41 Mean velocity magnitude inside the cavity for various surface colours of louvers.

The variation of the depth of the cavity also has an influence on the behaviour of the airflow. As can be seen in Figure 6.4.5.1 airflow patterns tend to veer from turbulent to laminar when both the depth and the volume of heated air is reduced. Thus, there is a balance where depth and airflow favour air velocities inside the cavity. Figure 6.42 shows how velocity magnitude values slightly increase as the depth is reduced to 600mm and then steadily decrease according to the reduction in size. Therefore, the optimum balance between height and depth of a DSF must be gauged in order to prevent overheating from occurring.

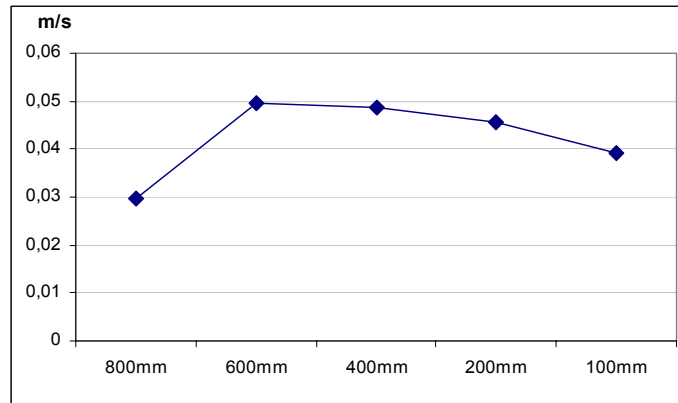


Figure 6.42 Average velocity magnitude values inside the cavity for various depths of the DSF.

6.5.2 Temperature

The positioning of the inlets and outlets also has a dramatic impact on thermal performance inside the cavity. It was observed through the CFD models that higher temperatures were obtained with a sealed cavity. Figure 6.43 shows the average temperature calculated in the ST and the STV. There is a reduction of 9.65°C on the mean temperature when the cavity is ventilated. This also shows the importance of having a ventilated cavity in order to reduce overheating development in the DSF.

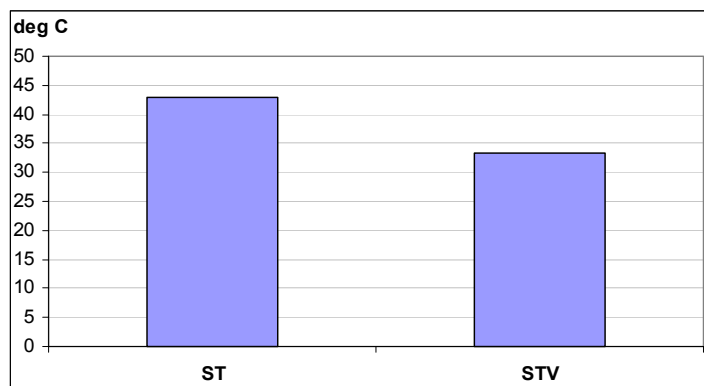


Figure 6.43 Mean temperature values calculated inside the cavity in sealed (ST) and ventilated cavity (STV).

The reduction of opening sizes has the opposite effect on thermal performance in the cavity. The resultant temperatures inside the cavity dramatically increase when the size of the inlets and outlets is reduced. There is a direct correlation between the air

velocities inside the cavity and the resultant temperatures, indicating that heat removal from the cavity is more effective with larger opening sizes. Figure 6.44 illustrates how mean temperatures decrease dramatically, when opening sizes are increased. Nevertheless, slightly lower temperatures with opening sizes of 150mm were noted. As can be seen in Figure 6.4.1.3, more constant air flows inside the cavity were obtained with this configuration. As a result of this, there is also an optimum correlation between the inlet and outlet sizes, which has a direct implication for overheating control.

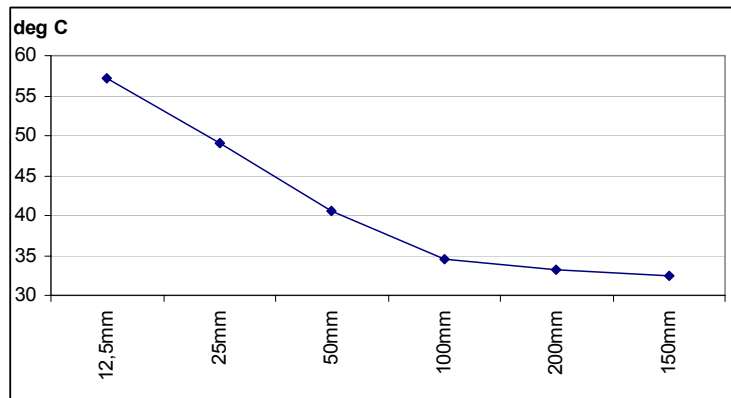


Figure 6.44 Average temperature values inside the cavity for various opening sizes.

The emissivity of the surfaces inside the cavity also has a direct influence on the overall thermal performance of the cavity. The highest temperatures were obtained when using black surfaces inside the cavity. Figure 6.45 illustrates the average calculated temperatures, when using coloured louvers inside the cavity. These values decreased gradually with a reduction in emissivity on silver and white colours on the louvers surface. However, it was observed that compared with the temperatures of the cavity without louvers, lower temperatures were obtained when using silver and white louvers, which indicate that moderately reflected radiation from the louvers, encourages stack effect and heat removal in the cavity.

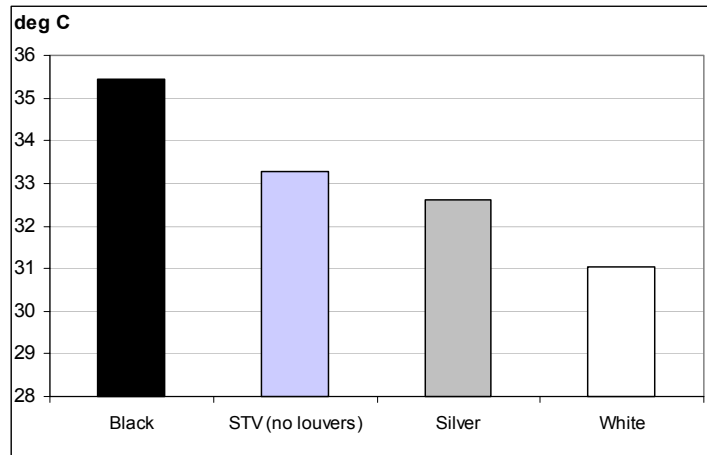


Figure 6.45 Average temperatures inside the cavity for various surface colours of louvers.

The thermal performance of the cavity is also affected by the variation of its depth. The average temperature values initially tend to decrease when the size is reduced. However, at an optimum depth of between 400mm and 600mm, the temperature gradually increased with the reduction in the depth of the cavity. Figure 6.46 illustrates this behaviour in which a minimum of around 26.87°C is reached, with a depth of between 400 and 600mm.

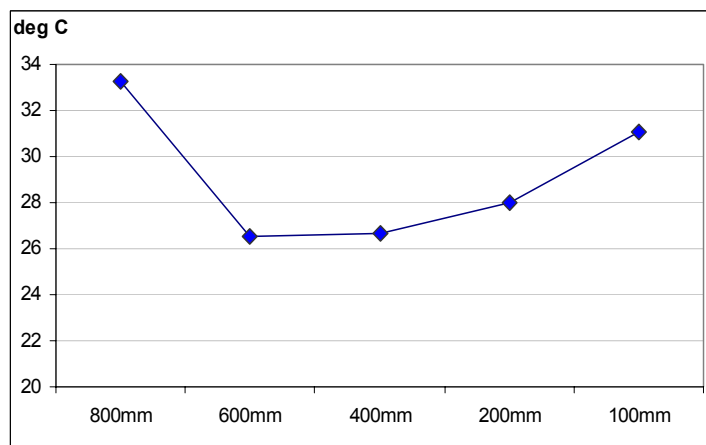


Figure 6.46 Average temperatures along the vertical centre of the DSF, calculated using CFD for various cavity depths.

6.5.3 Validation of Results

The validation of the CFD modelling was performed by comparing steady state value temperatures in three points of the facade test chamber, where the ones obtained were, when using the CFD model. Figure 6.47, shows that both simulated and measured values were very similar, in cases that incorporated a variety of opening positions. The average difference between the predicted and measured temperatures was 6.11% for the ST and 5.03% for the STV.

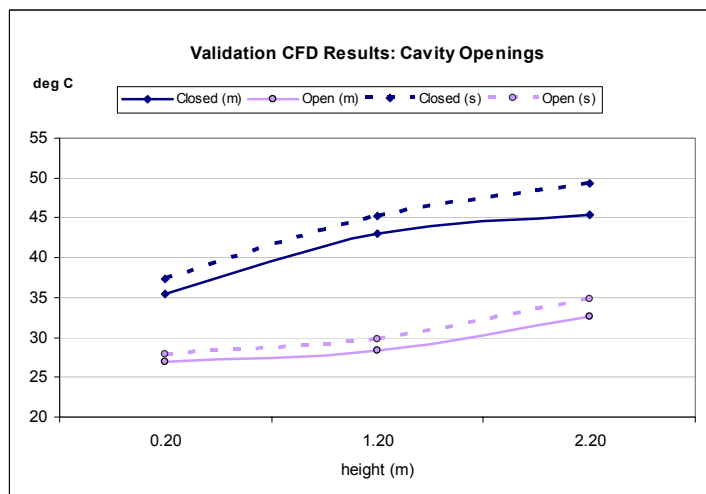


Figure 6.47 Temperature Values at three points for the experimental (m) and simulated cases (s) for various cavity openings positions.

When making comparisons between the ventilated cavity, both with and without shading devices (figure 6.48), the average difference between the predicted and measured temperatures was about 6.14%.

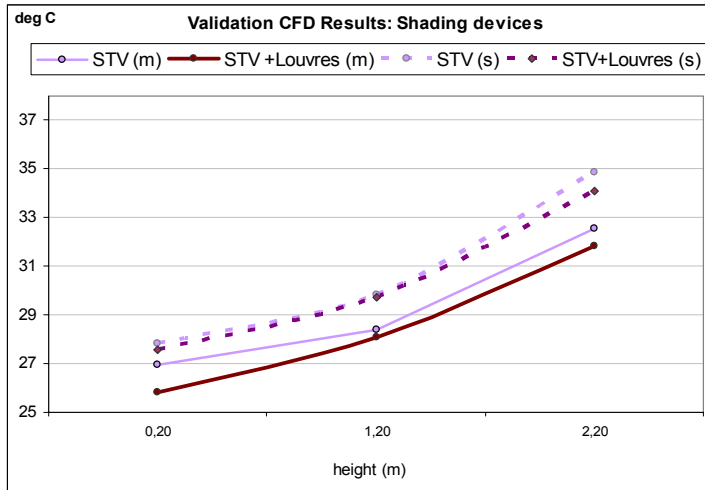


Figure 6.48 Temperature values at three points inside the cavity for the experimental (m) and simulated (s) cases using shading devices.

Figure 6.49 shows the average difference between the predicted and the measured temperatures in the STV cases, with varying cavity depths. It was observed that there was an average difference of 5.03% for 800mm, a 5.36% for 600mm and a 3.39% for 400mm. The relative difference was slightly higher on the simulation of 600mm.

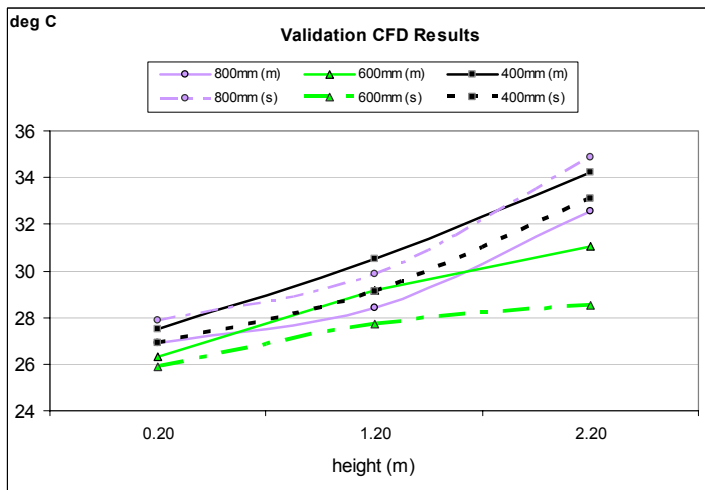


Figure 6.49 Temperature values at three points for the experimental (m) and simulated cases (s) using depths of 800, 600 and 400mm.

Figure 6.50 shows a relatively close correlation between the simulated and the measured values in the STV cases with glass variation. The average differences between the predicted and measured temperatures were 5.04% for clear glass; 2.7% for textured glass; and 1.35% for green glass. These results show the feasibility of using CFD for the analysis of airflow inside ventilated cavities.

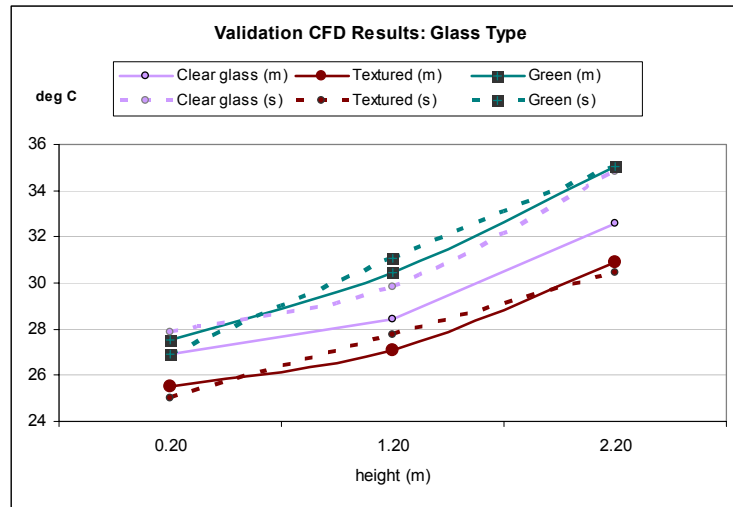


Figure 6.50 Temperature values at three points for the experimental (m) and simulated cases (s) for various glass types on the cavity's external and internal skins.

6.6 CONCLUSIONS

Computational Fluid Dynamics models were built to simulate the airflow and thermal performance of the experimental chamber of a Box-Double Skin Facade, in order to analyse the processes involved in overheating development. Commercial software, FLUENT [13], was used to simulate turbulent airflow and heat transfer.

It was seen that the cavity of a DSF encourages buoyancy and induces air movement. However, this reduces the heat received by the internal room, when the balance of heat gain/losses of this space is not controlled and air movement inside the room is not promoted. The convective forces inside the cavity could be used positively to

improve air extraction from the room, although there is also a requirement to promote air movement within the room to release the excess of the heat received.

The nature of the DSF is to improve insulation based on the long-wave IR trapped inside the glazed skins, and to use the cavity to avoid external protections. It is necessary to take into account the convective and radiative gains generated inside the cavity, due to the fact that this space acts as a thermal buffer, improving insulation but also threatening overheating development.

The main aspects observed in this CFD analysis are the following:

- A sealed DSF determines the development of turbulent flows and the dramatic increase in temperature levels stratified along the height of the DSF.
- Convective heat transfer of the room is mainly determined by the resultant heat flux from the inner skin.
- Continuous airflow inside the cavity reduces average temperatures by almost 10°C, indicating the importance of ventilated DSF as a key to control or reduce overheating.
- The size reduction of the opening shafts of the facade contributes to overheating development.
- The stack effect developed inside the cavity encourages air exchange with the exterior and heat removal from the cavity and the room.
- Constant airflow inside the cavity and the position of louvers close to the external skin favours heat removal from the cavity.

- The variation on the position of louvers determines the displacement of the vertical airflow inside the cavity.
- Emissivity increments on the surfaces inside the cavity have direct impacts on the increase in resultant air temperatures and efficiency of air velocities inside the cavity.
- The reduction of glass transmittance has minor effects on air velocities but an important influence on the greenhouse effect inside the cavity.
- The correlation between size and height of the cavity on the airflow is a key factor required to determine the flow rate and efficiency of the stack effect of a DSF. Further research is required on this field.

This study confirmed that the precise approach of CFD models to the experiment depends on the accuracy of setting the boundary conditions. The mesh and geometry of the model determines the complexity and precision of the CFD model.

Simulation of fluid dynamics based on natural convection flows with low air velocities requires extensive calculation time in order to get the desired converged residuals. The data results of the CFD model can be compared with experimental data.

Although CFD is a powerful tool to visualize the flow movement of a DSF model, the conditions have to be selected and inputted precisely in order to obtain accurate results. The conscious and responsible use of this tool makes it possible to obtain valued data for validation with experimental results.

REFERENCES

1. Manz, H., A. Schaelin, and H. Simmler, Airflow patterns and thermal behavior of mechanically ventilated glass double facades. *Building and Environment*, 2004. 39(9): p. 1023-1033.
2. Holmes, M.J., Optimisation of the thermal performance of mechanically and naturally ventilated glazed facades. *Renewable Energy*, 1994. 5(5-8): p. 1091-1098.
3. Wang, F., et al. The design of double skin facade: Modelling study on some design parameters affecting indoor thermal conditions. *Proceedings of CIBSE National Conference*. 1999. UK.
4. Dorer, V. and A. Weber. Simulation of passive cooling and natural facade driven ventilation. in *Proceedings of AIVE Conference*. 1994.
5. Lee, E.J., et al. Double facades: The reduction of cooling energy in summer and the use of solar energy during the winter. in *Proceedings of WREC*. 1998.
6. Djunaedy, E., J.L.M. Hensen, and M.G.L.C. Loomans, Towards a Strategy for Airflow Simulation, in *Building Design Center for Building & Systems TNO - TU/e*. 2002, Technische Universiteit Eindhoven: The Netherlands.
7. Manz, H., Numerical simulation of heat transfer by natural convection in cavities of facade elements. *Energy and Buildings*, 2003. 35(3): p. 305-311.
8. Versteeg, H.K. and W. Malalasekera, *An introduction to computational fluid dynamics : the finite volume method*. 2nd ed. 2007: Harlow : Pearson Prentice Hall. 503.
9. Saelens, D., Energy Performance Assessment of Single Storey Multiple-Skin Facades, in *Faculteit Toegepaste Wetenschappen, Arenbergkasteel*. 2002, Katholieke Universiteit Leuven,: Kasteelpark Arenberg 51, B-3001 Leuven, Belgium. p. 272.
10. Gan, G., Thermal transmittance of multiple glazing: computational fluid dynamics prediction. *Applied Thermal Engineering*, 2001. 21(15): p. 1583-1592.
11. Gan, G. and S.B. Riffat, A numerical study of solar chimney for natural ventilation of buildings with heat recovery. *Applied Thermal Engineering*, 1998. 18(12): p. 1171-1187.
12. Chiu, Y.-H. and L. Shao. An Investigation into the effect of solar double skin facade with buoyancy-driven natural ventilation. in *2001 CIBSE National Conference*. 2001: Chartered Institution of Building Services Engineers.
13. FLUENT 6.1 User's Guide. 2001, Fluent Inc: 10 Cavendish Court, Lebanon, U.S.A. Website: <http://www.fluent.com/software/fluent>.
14. Warsi, Z.U.A., *Fluid Dynamics: Theoretical and Computational Approaches*. 3rd ed. 2006, Boca Raton, Fla; London: CRC Press-Taylor and Francis Group. 845.
15. Launder, B.E. and D.B. Spalding, *Lectures in Mathematical Models of Turbulence*. 1st ed. 1972, London: Academic Press Inc. 169.

16. Launder, B.E. and D.B. Spalding, The Numerical Computation of Turbulent Flows. Computer Methods in Applied Mechanics and Engineering, 1974. 3: p. 269-289.
17. Bernard, P.S., Limitations of the Near-Wall k-e Turbulence Model. AIAA:, 1986. 24(4): p. 619-622.
18. Avva, R.K., C.E. Smith, and A.K. Singhal. Comparative Study of High and Low Reynolds Number Version of k-e Models. in Aerospace Sciences Meeting, 28th. 1990. Reno, NV: AIAA.
19. Raisee, M. and S.H. Hejazi, Application of linear and non-linear low-Re k- ϵ models in two-dimensional predictions of convective heat transfer in passages with sudden contractions. International Journal of Heat and Fluid Flow, 2007. 28(3): p. 429-440.
20. Booth, C.N., Thermal Physics: Unit 7 - Transfer of Heat (2) - Radiation. 1998, Department of Physics and Astronomy, The University of Sheffield: Sheffield, UK. Website: <http://www.shef.ac.uk/physics/teaching/phy001/unit7.html>.
21. FLUENT, Fluent Software v6.1 Documentation: Introduction to Radiative Heat Transfer. 2001, Fluent Inc: 10 Cavendish Court, Lebanon, U.S.A. p. (12)1-128. Website: <http://www.fluent.com>
22. Carvalho, M.G., T. Farias, and P. Fontes, Predicting Radiative Heat Transfer in Absorbing, Emitting, and Scattering Media Using the Discrete Transfer Method. Fundamentals of Radiation Heat Transfer. Vol. volume 160. 1991: ASME HTD. pages 17-26.
23. Cheng, P., Two-Dimensional Radiating Gas Flow by a Moment Method. AIAA Journal, 1964. 2: p. 1662-1664.
24. Siegel, R. and J.R. Howell, Thermal Radiation Heat Transfer. 1992, Washington D.C, USA: Hemisphere Publishing Corporation.
25. Chui, E.H. and G.D. Raithby, Computation of Radiant Heat Transfer on a Non-Orthogonal Mesh Using the Finite-Volume Method. Numerical Heat Transfer, Part B. Vol. 23. 1993. 269-288.
26. Gan, G., Simulation of buoyancy-induced flow in open cavities for natural ventilation. Energy and Buildings, 2006. 38(5): p. 410-420.
27. Kingspan, Rigid Insulation System Thermal Performance. 2004, Kingspan Insulation Limited: Pembroke, Leominster, Herefordshire HR6 9LA, UK. Website: http://www.tek.kingspan.com/uk/thermal_performance.htm
28. DTLR, Building Regulations: Approved Document Part L2: Conservation of fuel and power in buildings other than dwellings. 2003, Office of the Deputy Prime Minister: UK. p. 75.
29. Omega.com®, Transactions: In measurement and Control. 1998, Putman Publishing Company and OMEGA Press LLC. p. 86
http://www.omega.com/literature/transactions/Transactions_Vol_I.pdf.

30. Pilkington, The Glass Range for Architects and Specifiers. 2006, Pilkington Group Limited: UK. p.18.
<http://www.pilkington.com/resources/glassrangebroanddatasheetjune2006.pdf>
<http://www.pilkington.com/pilkington2004/both/images/productdirectory/flash/optifloat.html>
31. Gan, G., CFD Simulation of buoyancy-induced flow in open cavities for natural ventilation. Energy and Buildings, 2006. 38(5): p. 410-420.

CHAPTER VII

FIELD CASE STUDY OF MONITORING A DOUBLE SKIN FACADE:

7.1 INTRODUCTION

The basic principle of a Double Skin Facade is to enhance the thermal and acoustic insulation in urban areas. It was previously mentioned that overheating is produced when the amount of heat stored within the cavity of the façade is combined with the solar radiation directly gained through glazing to increase the heat transfer by radiation, convection and conduction to the adjacent spaces [1]. Convective gains inside the channel are considerably higher when solar shading devices are placed inside the DSF.

Preliminary research on the performance of Double Facades has confirmed the possibility that the energy consumption of the building; may be reduced by using natural ventilated facades [2]. However, there is currently no extensive data available regarding thermal behaviour of Double Skin Façades in the UK. The cost implications and the risk of overheating create a necessity to thoroughly assess the performance of local buildings as a foundation for guidelines on the design of DSF systems. Such results would make it possible to relay solutions that are more cost-effective and more suitable for UK requirements.

This chapter illustrates the results of a field case monitoring of a Double Skin Façade system of a building in London. The study was carried out for the duration of one year in order to identify the thermal behaviour of the facade and provide a pilot methodology and procedures to monitor Double Skin Facades in Commercial

Buildings in the UK. The current chapter outlines a pilot study exercise carried out in ARUP Headquarters building at 13 Fitzroy Street, London. The objective of the pilot study was to test the methodology and to acquire a preliminary set of measured data.

The objective of monitoring the performance of the existing double façade cavity of 13 Fitzroy Street was to investigate possible overheating problems and daylighting performance under summer and winter conditions. This included the assessment of the following issues:

- Thermal performance in the vertical section of the facade and its shading devices.
- Thermal performance of the selected space during summer and winter conditions, which include measurements of their environmental conditions.
- Daylighting variations during the day in comparison with the total solar radiation received by the building.
- Solar flux assessment of the facade and selected room next to the facade.

- **Façade Performance**

The data collected offered information regarding the possible factors that contribute to overheating of the occupied spaces. It provided key information understanding the direct implication of any overall interaction of the DSF within an occupied building.

- **Airflow Analysis**

The data collected through real-time monitoring provided the basis for the CFD model, which made data available on the thermal and airflow behaviours of the DSF cavity under summer and winter conditions. Data collected from both seasons was useful for a comparative assessment of the facade in critical conditions. For this analysis, CFD modelling of the facade was performed using FLUENT software [3] to analyse a steady state thermal performance of the facade on a seasonal model to visualize its airflow behaviour.

- **Occupant's response**

For the Occupant's perception, the occupants of the monitored room answered a series of surveys. The influence of the facade on natural lighting, ventilation and operation of the facade were investigated.

7.2 CLIMATE AND WEATHER DATA

Central London is located at 51° 30' 25" North and 0° 7' 39" West. It has a temperate climate, with regular but generally light precipitation throughout the year. Summer temperatures do not often exceed 33°C, however, higher temperatures have become more frequent recently. The highest temperature ever recorded in London was 38.1 °C, measured in Kew Gardens during the European Heat Wave of 2003. London's large built-up area creates a microclimate (known as "urban heat island"), where heat is stored in the city's buildings. Sometimes temperatures are 5 °C warmer in the city than in the surrounding areas. Figure 7.1 shows the average climate data for 1971 to 2000 at the Met Office station in the London borough of Greenwich, which is the closest station to the centre of London [4].

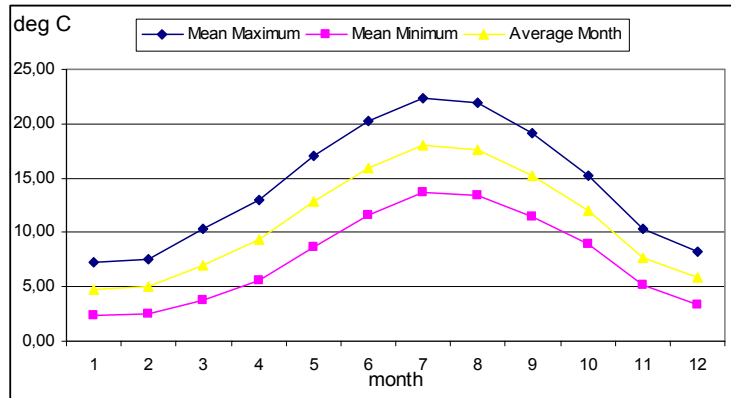


Figure 7.1 Monthly average temperatures values for London (Greenwich station).

The values of temperature in the monitored site were recorded from February 2006 to January 2007. The readings were taken at 4.05 metres from street level at the inlet of the southeast DSF. Figure 7.2 shows the daily temperature values recorded every 30 minutes from the 6th of February. The minimum temperature reached in the year was -0.55°C on the 10th February and the maximum was 34.42°C on 19th of July. There were some points when there were peak values of temperature above 30°C from June to August. Nevertheless, these peak temperatures were isolated on specific dates and did not show a trend on the mean temperature.

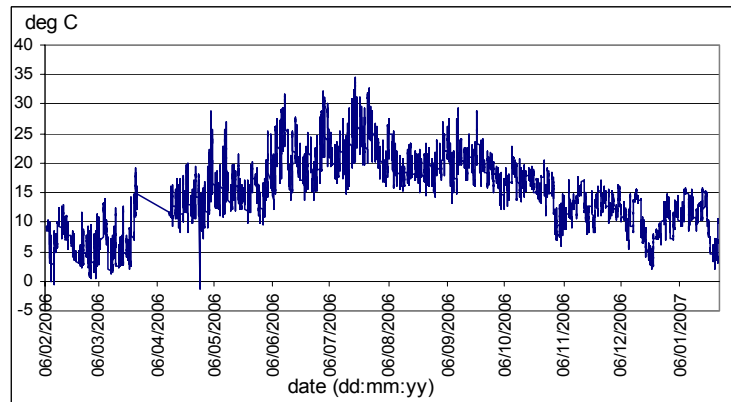


Figure 7.2 Recorded hourly inlet temperature values for ARUP HQ on south-east facing façade.

Figure 7.3 illustrates the mean monthly temperatures in 2006. The temperature values ranged from a minimum average value of 2.5°C in winter to a maximum of 24.8°C in summer. Although, the values obtained during the year were relatively similar to past historical values; there is evidence that in recent years there has been a small and gradual increment in the average values of daily maximum temperatures.

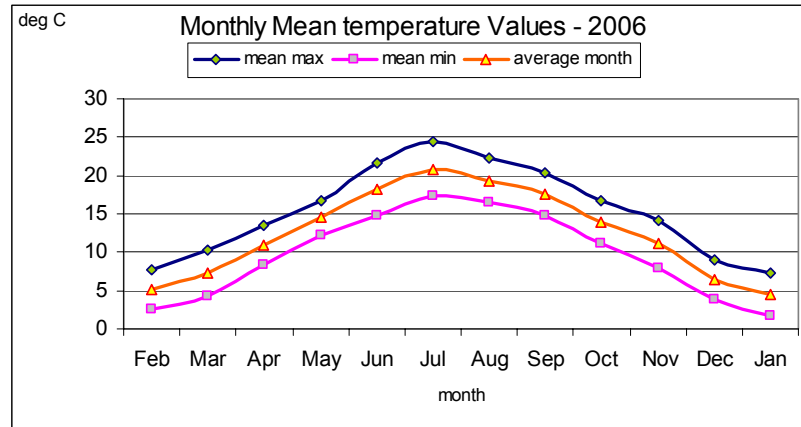


Figure 7.3 Mean temperature values measured at inlet level for 2006-07.

7.3 PILOT MONITORING

The objective of monitoring the performance of the existing double façade cavity was to investigate possible overheating problems and daylight performance under summer and winter conditions. This included the assessment of the following issues:

- Thermal performance in the vertical section of the facade and its shading devices.
- Thermal performance of the selected space during summer and winter conditions, which include the measurements of their relative humidity variations.
- Daylight variations during the day in comparison with the total solar radiation received by the building.
- Solar flux assessment of the facade and selected room next to the facade.

- Occupant perception survey of the immediate influence of the facade and shading devices.

7.3.1 Monitored Building

The site selected for monitoring was an office building refurbished by ARUP as part of the redevelopment plan within the London Borough of Camden [5]. The selected case for this pilot study was the building for their main headquarters in the UK. This building was refurbished as part of their image strategy. Arup’s officials stated, *“The project will establish a coherent campus that will reflect both externally and internally what Arup stands for. It will provide an exciting and inspirational workplace to support and encourage the firm’s philosophy of creativity and innovation”*. The refurbishment of the Fitzrovia building was the first step in their urban plan. The main characteristics of this building are described in the following table [6]:

Table 7.1 General information ARUP Headquarters Building

Official name:	ARUP HQ, Fitzrovia Building.
Location:	Central London.
Address:	13 Fitzroy Street, W1T 4BQ
Bordering street:	Fitzroy, Howland Street
Complex:	Fitzrovia Estate
Number of floors:	7
Original construction:	1960s
Refurbishment end:	2002
Façade:	Clear Glazed Double Skin with horizontal sun-shading devices on each floor.
Type of DSF:	Multi story facade
Type of construction:	High-rise building

Climatic Controls:	Mechanical HVAC system.
Area	125,000-square-foot
Main usages:	Offices
Status:	completed
Consultant:	Arup Associates
Architect:	Sheppard Robson
Real estate management:	London Merchant Securities plc (LMS)

7.3.2 Monitored Areas

The areas selected for monitoring are located on the southeast facade; this facade has a ventilated cavity with double fully glazed skins. It is a multi storey facade with open cavity through the facade section. The design of the facade also includes sunshading devices, which consist of a set of 5 fixed horizontal louvers placed on each floor. The cavity of this facade also contains horizontal ducts, which are components of the mechanical ventilation system of the building. Figure 7.4 shows the location of the facade chosen for monitoring.

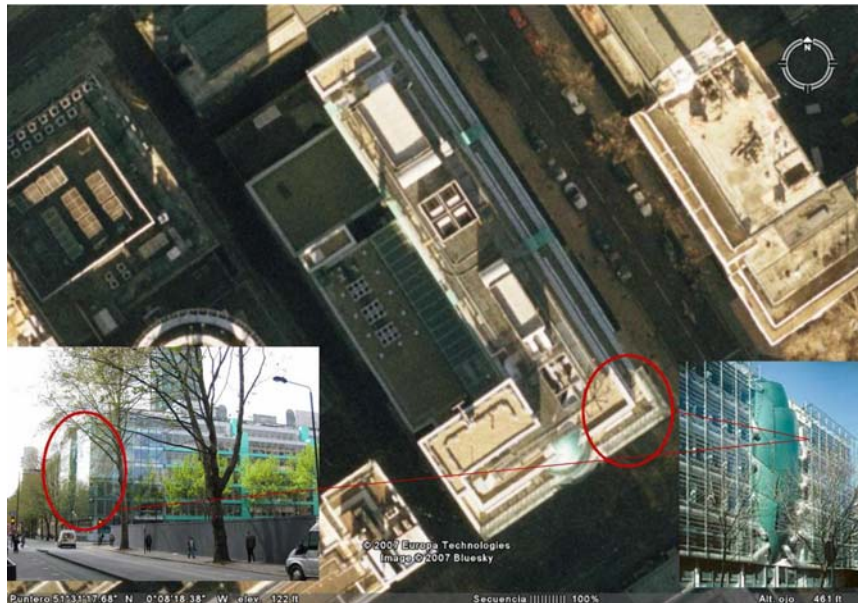


Figure 7.4 Facade selected for monitoring, highlighting the location of monitored area. Source aerial photo: Google earth.

The cavity and the room selected on the 5th floor next to the DSF were monitored and the measurements were focused specifically on the southeast-facing facade. The sensors and logging equipment measured environmental variations from February 2006 to January 2007 with periodical inspections each month. Figure 7.5 illustrates the location of the facade and the room selected for this study.

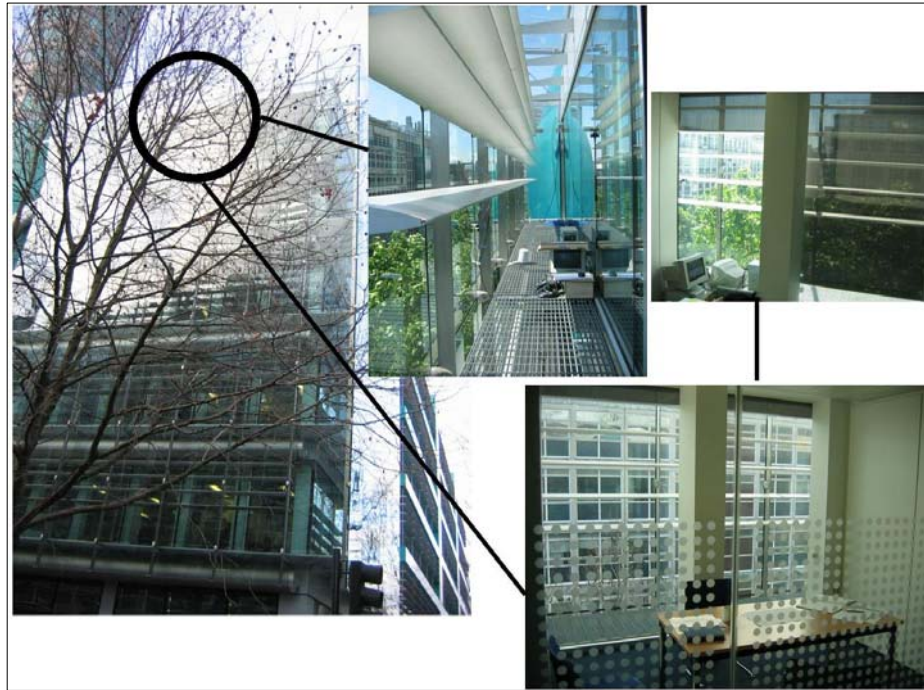


Figure 7.5 Location of equipment and room selected for monitoring.

This pilot monitoring study focused mainly on the thermal behaviour of the facade, based on the collection of temperature values within the cavity. For this purpose, K-type thermocouples were placed, one on each floor throughout the facade section. Figure 7.6 illustrates a section of the specific location of sensors within the DSF channel from the 1st to the 5th floors.

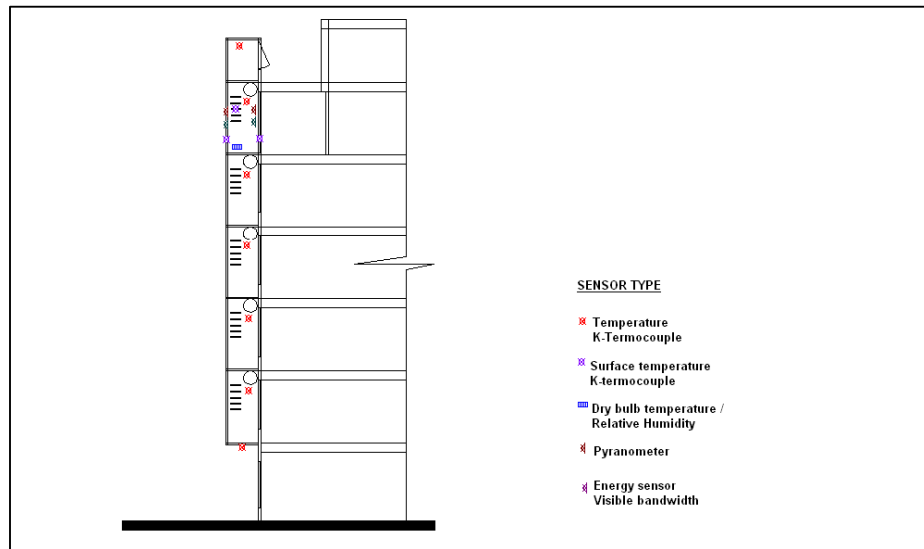


Figure 7.6 Vertical section of sensors location within the facade cavity.

The total solar radiation energy transmitted through the facade was measured using sensors placed on the 5th floor inside the facade cavity and next to the inner glass of the room selected. Illumination levels were measured inside the selected room with sensors located next to the inner-skin glass and next to the back wall of the room. Dry bulb temperature and relative humidity were also measured. Figure 7.7 illustrates a detailed location of the sensors on the 5th floor and selected room.

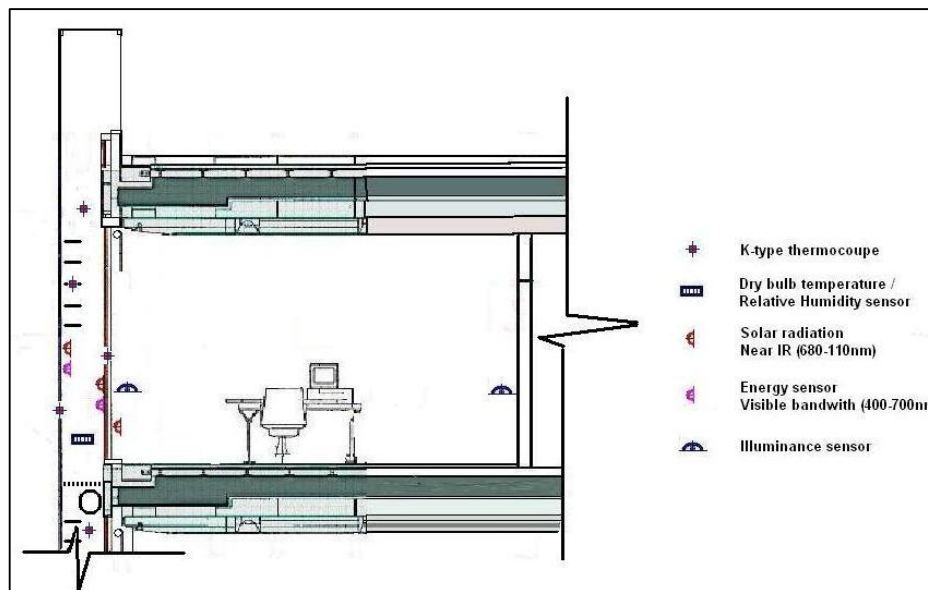


Figure 7.7 Location of sensors inside the selected room

7.3.3 Parameters assessed

Outdoor Climate:

- Total solar irradiance (behind external glass cavity).
- External Ambient temperature (1 height, at 4.05m from ground level, outside lower inlet of the façade channel).

Facade Cavity Measurements:

The building has two sections of a Multi-storey type of DSF on the southeast facade (figure 7.4). The monitoring equipment was located on the easternmost of these two sections. The physical parameters were taken as follows:

- Glass surface temperatures inside the facade cavity (4 points measured with K-type thermocouples. 2 were located on the outer glass and 2 were placed on the inner glass of the cavity at 5th floor level).
- Facade cavity temperatures (5 points measured with K-type thermocouples at 5 heights: One point each on the 1st, 2nd, 3rd, 4th and 5th floor inside the DSF channel). Figure 6 illustrates these positions.
- Solar radiation transmitted through the outer façade and inner glazing measured on 5th floor inside the cavity (2 positions): Solar radiation energy on visible bandwidth (380-680nm) and solar radiation energy on near shortwave bandwidth (680-1050nm) on vertical surface.
- Surface temperature of shading devices on the 5th floor (2 positions measured with K-type thermocouples).
- Dry bulb temperature and Relative humidity measured at 5th floor level inside the DSF channel.

Room Measurements:

The room positioned on the 5th floor, is currently used for meetings. It is not used on a permanent basis and its occupancy patterns are variable so were not analysed. The physical parameters measured are described as it follows:

- Ambient Dry bulb temperature and Relative Humidity (1 point, measured at 1,60m from floor level, at a distance of 1,75m from the inner glass of the façade).
- Glass surface temperatures (2 points measured with K-type thermocouples), located on the inner facade inside the room.
- Indoor illuminance (2 positions): One on the horizontal plane next to the inner glass inside the room, the other on horizontal the plane inside the room at 3.55m from internal glass facade.
- Solar radiation transmitted trough the outer façade and inner glass (2 positions): Visible (380-680nm) and near IR (680-1050nm) and solar flux on inner glass.

7.3.4 Instrumentation

The equipment used for the monitoring is described as it follows:

- 1 Data Logger: Datataker 500 [8].
- 3 Skye Pyranometers (Bandwidth 680-1050nm).
- 2 Skye Visible light energy sensors (Bandwidth 380-680nm).
- 2 Skye Illuminance sensors (480-630nm)
- 2 Skye Humidity/Temperature probes rht+ type.
- 14 K-type thermocouples for temperature measurement.
- 1 DeLogger Plus Software for recording and Monitoring.
- 1 PC for data storage.

The technical specifications and detailed description of the instruments used is provided on the following table:

Instrument	Manufacturer	Parameter measured description	Parameter Units	Sensitivity	Working range	calibration date	Accuracy
Energy Sensor	Skye Instruments Ltd [9]	Solar flux within the visible light band range	irradiance W/m ²	380-680nm 1mV/100W/m ²	0-5000 w/m ²	10/05/2005	Absolute typ. <3% to 5% max
Pyranometer	Skye Instruments Ltd [9]	Solar flux within the near infrared range	irradiance W/m ²	680-1050nm 1mV/100W/m ²	0-5000 w/m ²	17/05/2005	Absolute typ. <3% to 5% max
Lux sensor	Skye Instruments Ltd [9]	Levels of light perceived by human eye	illuminance Lux	450-650nm 1mV/10Lux	0-500.000 lux	15/07/2005	Typical ±3 to 5%
pt100 Temperature RH+ sensor	Skye Instruments Ltd [9]	Dry bulb temperature Air Relative Humidity	°C %	0-1V	-40°C+60°C 0-100%	27/07/2005	±0.2°C (-10+60°C) ±2% RH
K-type Thermocouples	Fico Technology	Air temperature	°C	100.2kΩ	-75+250°C		±0.2°C to ±2°C

Table 7.2 Technical description of sensors

7.3.4 Methodology for Monitoring

The post-occupancy data collected inside the Double Skin Facade was based on recording the thermal behaviour and solar radiation incidence of the facade as a physical reference of the influence of the façade on overheating and increased heat loads on fully glazed buildings.

7.3.4.1 Procedures

For the environmental monitoring of the Double Skin Facade of this pilot study; the procedures followed for the location of equipment, rooms to monitor and data collection were based on the spaces that ARUP kindly made available for this study. As a result of this, it was possible to obtain access to the DSF cavity and one room next to the facade. The room offered by ARUP was one meeting room located on the fifth floor.

According to the spaces available for the post-occupancy monitoring, the main procedures arranged for this study are described as follows:

Identification of parameters to measure:

As mentioned before; thermal performance of the facade and room, daylighting levels, total solar radiation and occupant's perception were the main parameters defined for in study.

a) Equipment required: For data collection, a minimum requirement for this study was a data logger and a computer for data storage.

b) Sensor type required: The minimum required sensors must measure at least one parameter on each of the layers of the DSF and the spaces next to the facade. The main sensor types suggested for this study were the following:

- Lux sensors.
- Temperature and Relative humidity sensors.
- Solar radiation energy sensor.
- Thermocouples for surface and air temperature measurement
- Relative Humidity and Dry Bulb temperature sensors.

c) Location of sensors and equipment: The location of sensors was based on the purpose to investigate possible overheating problems and daylighting performance under summer and winter conditions. The most relevant location of sensors was based on obtaining data from each of the facade layers, the DSF cavity, shading devices, inlet temperature, outlet temperature and room environmental

conditions. The position of the sensors depended on the space available and relevance of the situation, in order to provide information for the facade model.

d) Data collection settings: For the initial timescale, it was proposed that this study be carried out for 90 days during the of summer 2006 to cover the peak hot weather conditions, planning also to undertake measurements for 30 to 60 days during winter to early spring 2006. Fortunately, ARUP granted to keep monitoring for one year; starting in February 2006 and finishing on January 2007.

7.3.4.2 Problems encountered

The main difficulties faced during this study are described as follows:

- Limited availability of space to locate monitoring equipment and sensors.
- Installation of two separate monitoring equipments, due to the isolation of the facade cavity and the monitored room. This made it impossible to collect all the information through a single data-logging unit.
- Restricted access to monitored zones during office hours, due to the possible disturbance that this can cause to the building's occupants. However, on Saturdays it was possible to periodically check and adjust the equipment.
- Involuntary alteration of sensor position and/or connections due to facade/building cleaning maintenance.
- Reduction of reliability on continuous power supply for data storage equipment also due to involuntary disconnection by maintenance/cleaning personnel.

As mentioned above, the main problems were due to external factors that depend on more of the physical conditions of the monitored site rather than on the equipment or measuring procedures.

These sorts of limitations make post-occupancy monitoring a difficult task, as buildings do not usually have easy access to specific locations in which sensors can be placed or power supply accessed to produce the required data transmission.

7.3.4.3 Lessons learned

Based on this experience, there were some important issues that have to be considered for future post-occupancy monitoring of DSFs.

- The best suggested option to collect data safely without interruption is to locate the equipment away from the building's occupants and maintenance personnel.
- To avoid wrong data collection and incorrect operation of sensors, periodic inspection of the intervals of sensor positioning and functionality must be set to a maximum of 20 days.
- To avoid power supply loss, it is strongly advisable to have backup batteries for data logging units or at least better memory storage capacity.
- Finally, one of the primary lessons learned was the importance of informing and arranging, in advance, with the building managing officers to coordinate access and periodical inspections of the equipment.

7.4 FACADE PERFORMANCE MONITORING

7.4.1 Facade Cavity

This pilot monitoring study was mainly focused on the thermal behaviour of the facade and the analysis of solar radiation received. The data may be used to visualize the behaviour of the facade in comparison with the amount of solar radiation received and the operation of the facade openings.

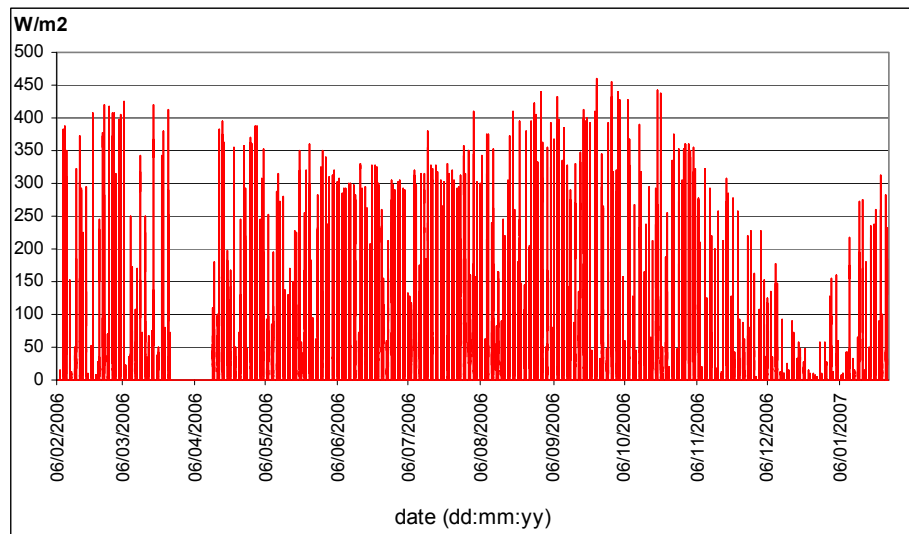


Figure 7.8 Total Solar Radiation on vertical surface measured inside the external skin of the south-east facing DSF (wavelength: 380 -1050 nanometres).

Figure 7.8 shows the total amount of solar radiation received inside the Double Skin Facade. As the selected place for monitoring was on the 5th floor, there was no shading influence from trees or buildings. The solar radiation on vertical surfaces was measured inside the facade behind the outer glass with two sensors, measuring energy on visible and near infrared wavelengths. The amount of energy measured inside the cavity was the total on the visible and near infrared, passing the external glass. According to the manufacturer, the glass has a light transmittance coefficient of 0.85[9]. The graph shows that during times of clear sky, there are reasonably high

levels of solar radiation received on the south-east facing facade; even in winter, as the sun is low in the horizon and the amount of light received is more direct to this facade.

There were some peak values of around 450W/m^2 , however, on average, the values of radiation in winter were about 120W/m^2 . During early spring, it was interesting to find some peak values relatively similar to those reached during the summer months. This was also due to the more direct incidence of the radiation on the vertical south-facing facade - in contrast to summer - due to the high solar altitude, which shows rather similar levels of radiation. Figure 7.9 displays the total solar energy hitting the external and internal glass. The plot indicates the difference of radiation levels on each skin, due to the total transmittance of the glass. The months when the two values reach closer to one another are during mid season and winter, due to the increase of direct radiation hitting the vertical plane of the facade. This plot also illustrates how the amount of radiation is decreased through each layer of glass in the façade.

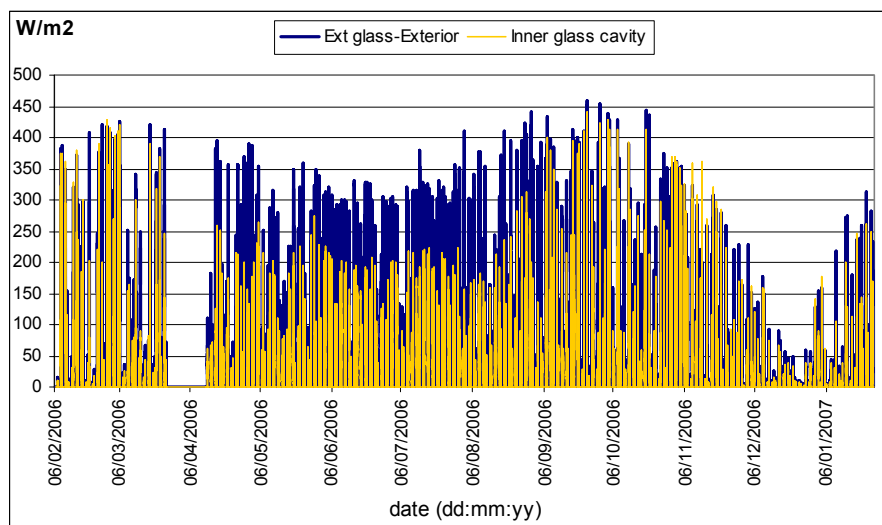


Figure 7.9 Total Solar radiation energy measured on vertical surfaces inside the facade cavity.

Regarding the temperature inside the DSF, figure 7.10 illustrates an overall comparative thermal response to the ambient temperature of the second and fifth floor. This shows a large difference of peak temperatures reached by each floor within the same period of time. It clearly illustrates how the DSF creates stratification of thermal levels due to the stack effect, as a result of IR radiation trapped inside the facade. However, during the night there is a rapid decrease of the ambient temperature due to the facade configuration.

Figure 11 shows a plot of ambient temperature of 3 days measured at 2nd and 5th floor levels during winter. Here, the difference of temperature values is more evident, in relation to the height. This is a consequence of the heat accumulated at upper levels of the facade.

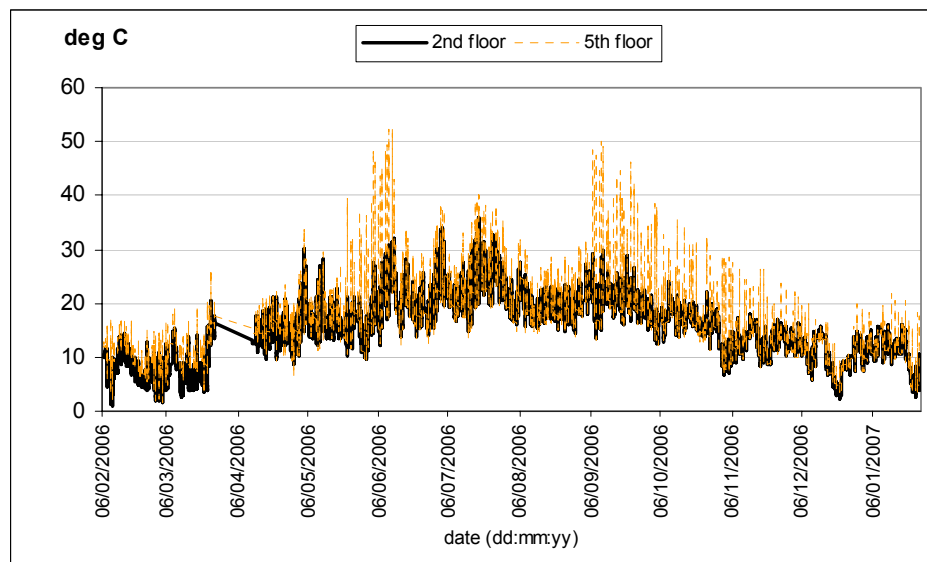


Figure 7.10 Temperature measured inside the DSF cavity.

The graph below shows the rapid drop in temperature values, which is a result of the facade physical configurations, comprised of a fixed open inlet that can cause this rapid decrease of nocturnal temperatures on the facade channel, due to the downdraft

flow created through the lower inlet. In the airflow analysis, this behaviour is illustrated in more detail.

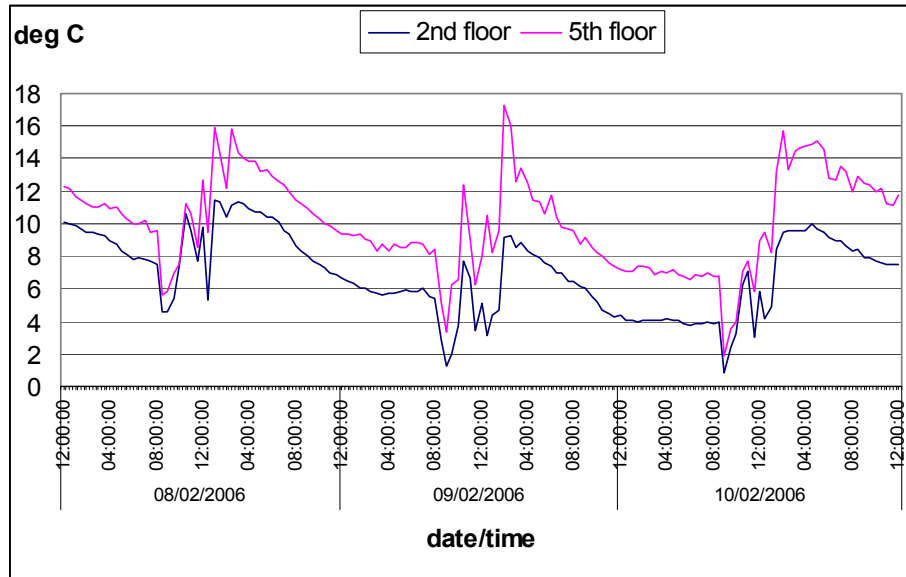


Figure 7.11 Ambient temperatures measured on 2nd and 5th floor levels inside the facade cavity during 3 days of winter.

In the case for spring, the amount of heat accumulated began to decrease when solar radiation was not received directly by the façade, until the next day when it was increased sharply as radiation began to hit the façade. Figure 7.12 shows the difference of temperature between the 2nd and 5th floor, which is caused mainly by heated air inside the façade displaced towards the top by buoyancy. However, the graph shows sharp fluctuations on the values for the 5th floor. This is due to the incidence of direct radiation received, which in turn affects the stack effect in the cavity.

Figure 7.13 illustrates the fluctuations on solar radiation compared with the fluctuations on temperature values on the 5th floor. This indicates that the

fluctuations have a direct influence on the heat accumulated on the upper levels of the façade.

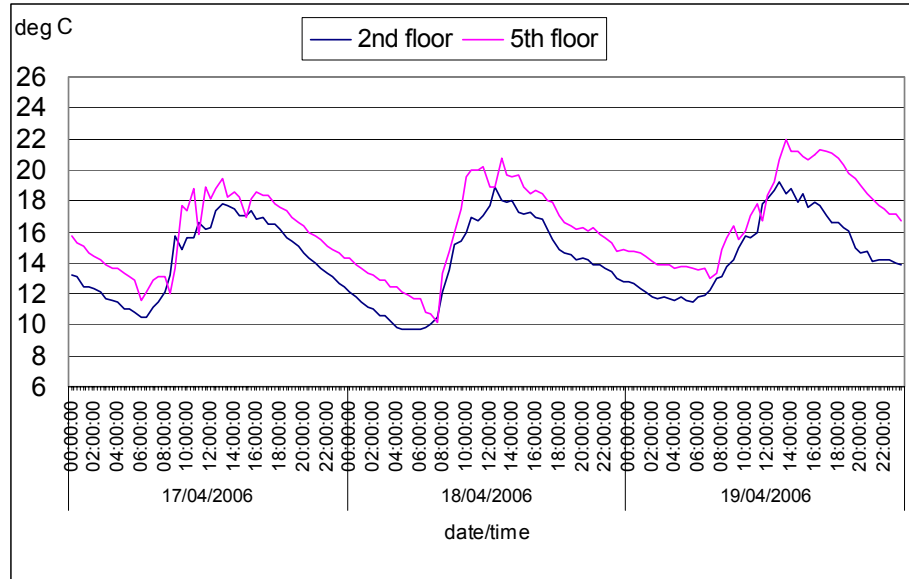


Figure 7.12 Ambient Temperature measured on 2nd and 5th floor levels inside the facade cavity during 3 days of spring.

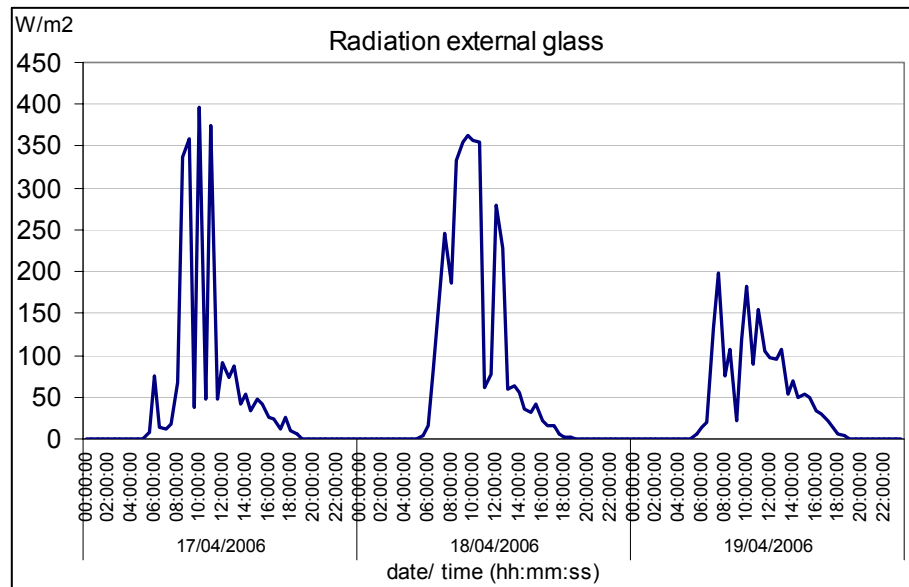


Figure 7.13 Total solar radiation on vertical surface passing through the external glass of the façade.

During a summer period, illustrated in figure 7.14, the same stratification is registered inside the cavity. However, the difference of temperature values between the 5th and 2nd floors is not as high as when compared with the performance in previous seasons. Although the graph shows a very sharp increase in temperature levels, which clearly indicates the buoyancy and stack effect, there is also a quick but gradual decrease of the levels as a result of the ventilated configuration of the façade.

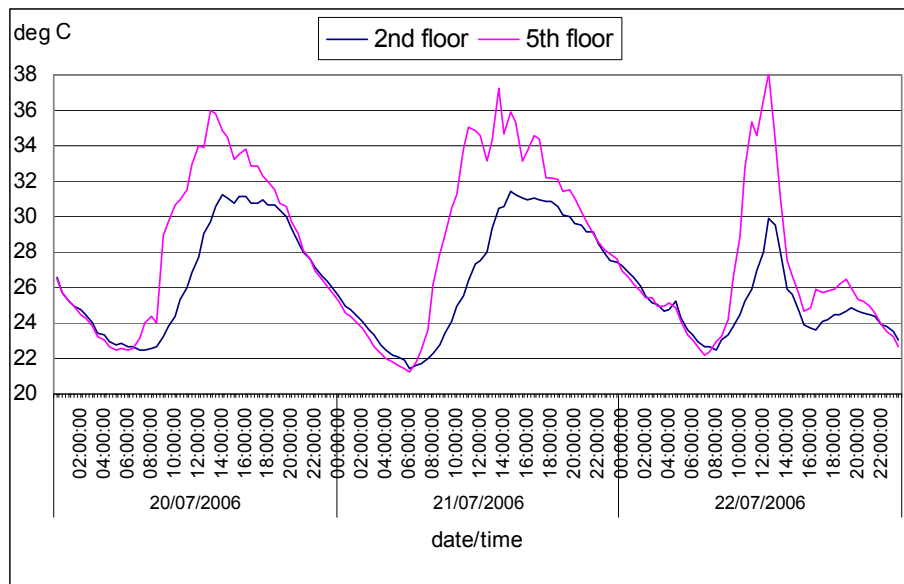


Figure 7.14 Ambient Temperature measured on 2nd and 5th floor levels inside the facade cavity during 3 days of summer.

In September, the outlet shafts were closed. The increment of temperature difference and measured values are displayed in figure 7.15, which shows how severe the effect was on the variation from a ventilated to a non-ventilated façade. Here, overheating began to develop in the façade cavity, reaching temperature differences of up to 25°C.

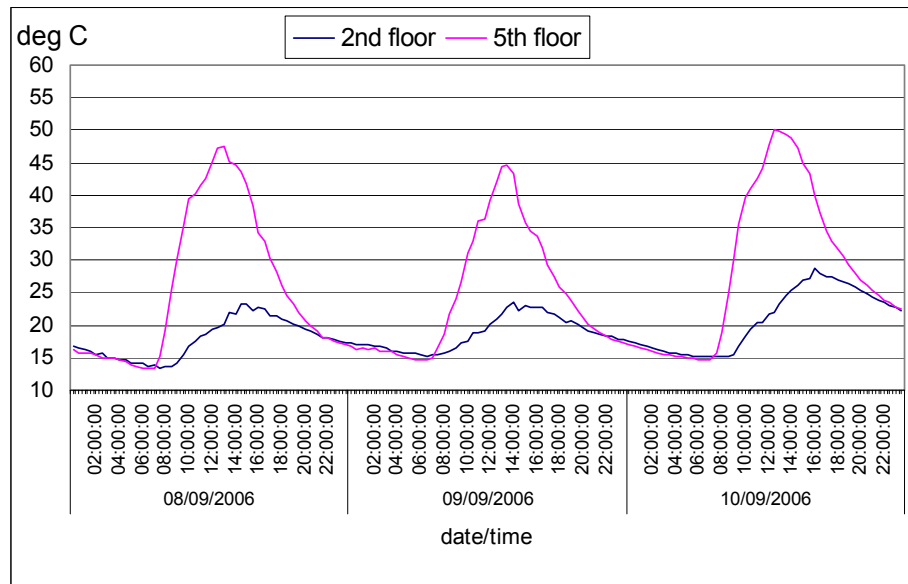


Figure 7.15 Ambient Temperature measured on 2nd and 5th floor levels inside the facade cavity during 3 days of autumn.

In order to measure the ambient values of the dry bulb temperature inside the cavity, one sensor was installed at 5th floor level. The data obtained by this sensor is illustrated in figure 7.16. The plot shows the measured and polynomial averaged values of temperature during the tested timeframe. On one hand, the plot illustrates various peaks of temperature during some days of the year. This is due to the direct link between incident radiation and heat accumulated inside the facade. This behaviour demonstrates the basic principle of DSF in which the greenhouse effect is increased when the glazed facade receives more direct radiation. On the other hand, there is also a repeated trend of successive peaks on the minimum temperature, which has a close relationship with the ones shown in the figures for winter and spring, due to the downdraft through the facade inlet during the night.

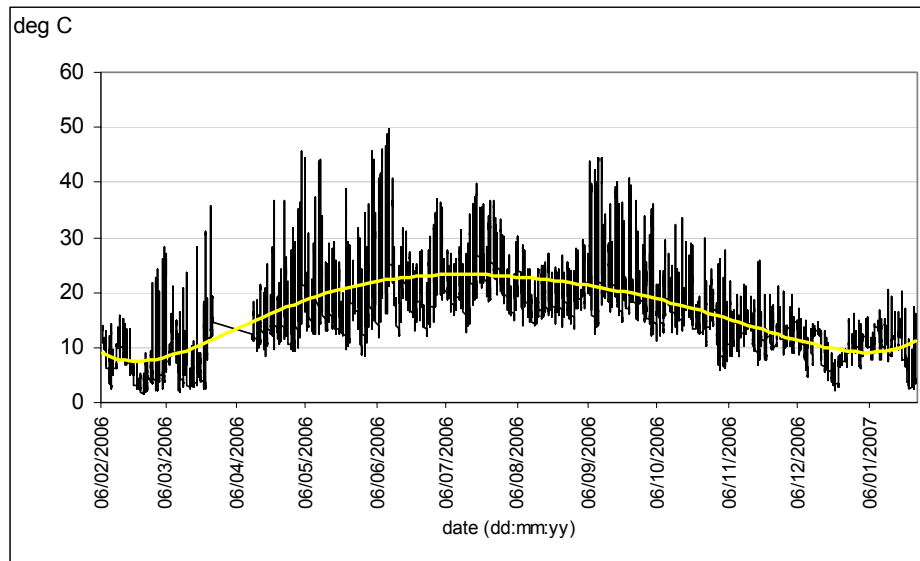


Figure 7.16 Measured and mean dry bulb temperature of the facade cavity at 5th floor level.

The plot in the figure above also shows that these peaks do not have a very strong influence on the total average temperature, which generally ranges from 5°C to 25°C, demonstrating a close relationship with the average measured external temperature. As a result, it may be concluded that a fixed open inlet determines a dramatic increase of heat loss on the facade during the night.

Glass surface temperatures inside the facade are shown in figure 7.17. The range of temperature values of external and internal glass is noticeably different. This is due to the direct influence of heat transfer coefficient on external and internal glass. The measured values prove that the external glass has increased heat losses due to convection outside the facade and also increased heat gains due to the heat accumulated in the facade.

For the inner glass, the temperature variation is reduced - mostly due to the convective heat transfer inside the facade channel. The figure also shows how a slight increment on the mean temperature of the inner glass is obtained, which also corresponds with the periods when the facade had the outlet shafts closed. This is due to the increase of convective heat gains inside the facade as a result of the greenhouse effect.

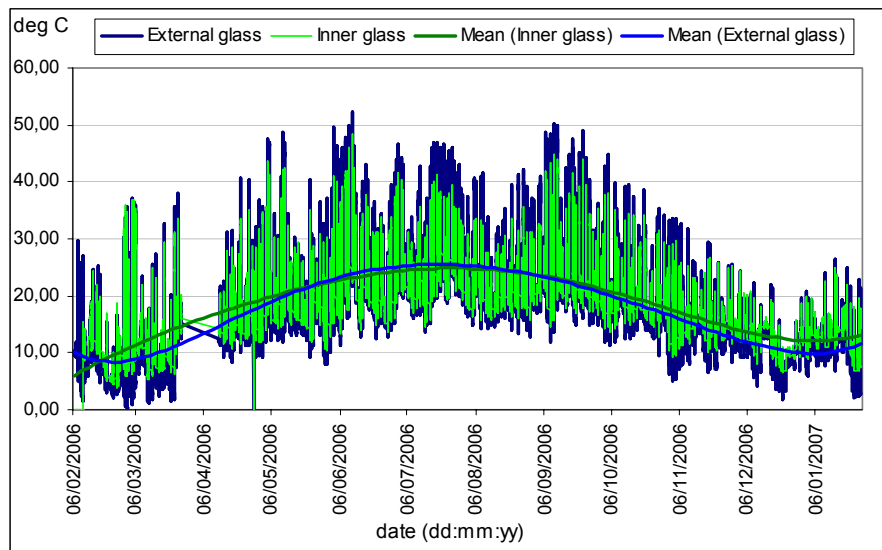


Figure 7.17 Surface temperatures of the two skins of glass inside the facade cavity.

The louvers monitored for this pilot study were located on the 5th floor, as here it was not shadowed by external elements. For future monitoring work, it is suggested that at least one point on *each* floor, be monitored. Figure 7.18 shows their surface temperature measured with thermocouples placed underneath the louvers in the shade, to avoid measuring heat from direct radiation. In general, their thermal performance follows a similar response during the year as the one displayed by the internal glass. However, their thermal range is increased to the maximum temperature, due to the higher absorption coefficient of aluminium. As a consequence of this, the shading devices absorb and store more heat, thus the resultant temperature is higher than the ambient temperature.

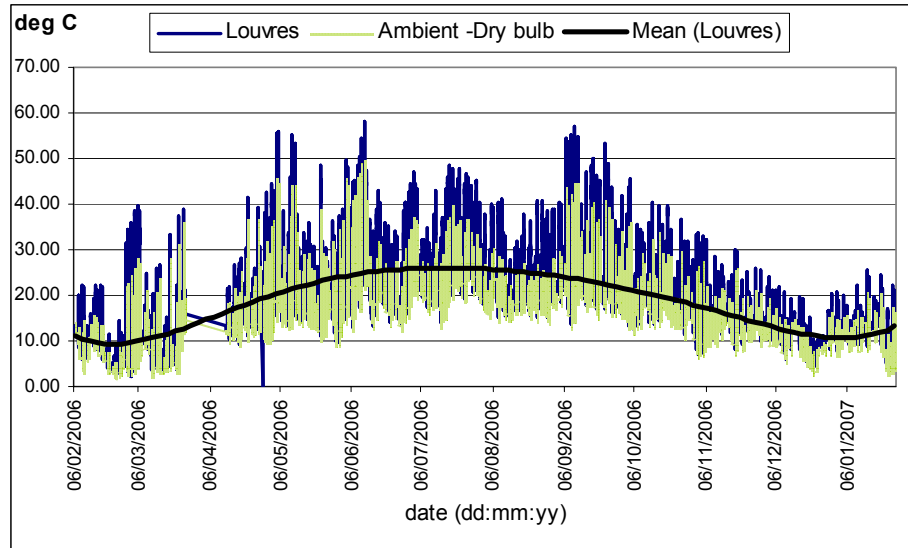


Figure 7.18 Monthly dry bulb and surface temperatures of sun shading devices temperatures measured inside the DSF.

The surface temperature of the louvers presents stratification depending on their location height. Figure 7.19 shows clearly how the temperature reached by the louvers is higher when its location height is increased. Even louvers located within the same floor with just a height increment of 600mm. develop a moderate difference in their temperature as solar radiation hits them. When there is no solar radiation, the figure below also shows that the louvers reach similar temperatures. This proves that, during times without direct radiation, the thermal behaviour depends less on the incident solar radiation and more on the convective heat losses, which makes clear that efficient insulation of the DSF depends on the effective reduction of the heat losses at night or during periods of reduced solar radiation.

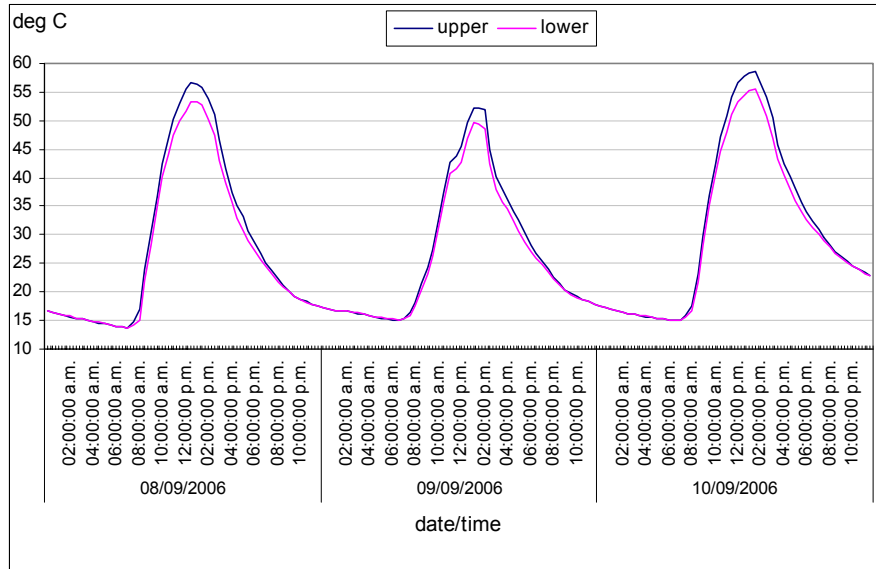


Figure 7.19 Surface temperature measured on upper and lower louvers inside the facade cavity at 5th level during 3 days of late summer.

The values of temperature generated inside the DSF cavity are clearly stratified within it, starting from values close to the external temperature on the lower part of the facade and increasing gradually throughout the channel. However, the increment rate is strongly affected by the configuration of the facade and the incident of solar radiation. Figure 7.20 shows a clear difference on performance and the stratification of temperatures depending on the season. The most dramatic increments of temperature inside the facade were obtained during the summer months. Nevertheless, the sharpest increments were developed when high influence of solar radiation hit the façade, in addition to a non-ventilated configuration. This is shown on the plot for the months of September and June, when the outlet shafts were closed and there were differences of temperatures of about 21°C. Although the lowest temperature differences between top and bottom levels were measured during winter, there was also a clear trend of more heat accumulation on top of the facade. It is now apparent that DSF favours insulation and heat storage but it tends to develop

overheating when the facade is not ventilated and hit by moderate to high levels of direct solar radiation.

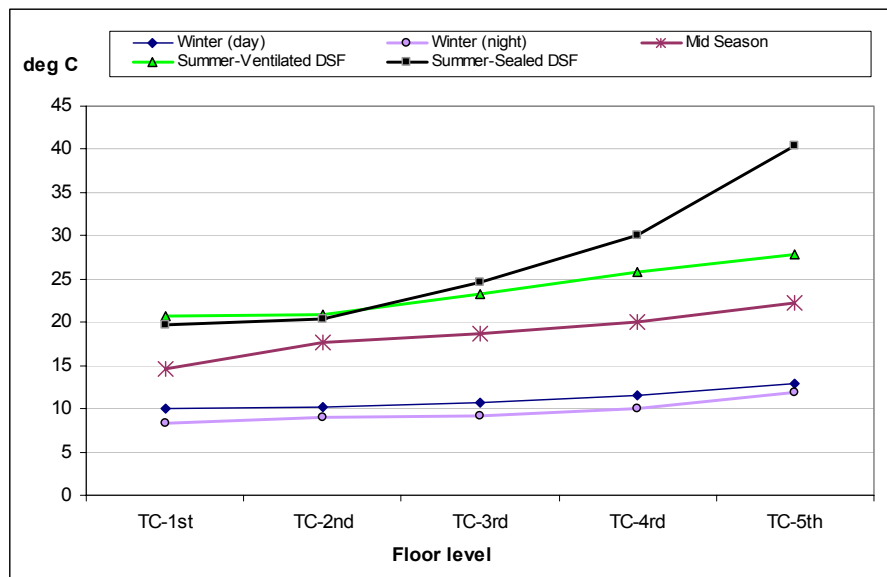


Figure 7.20 Air temperatures inside the cavity measured in one point on each floor at 12:00h for selected dates of each season.

7.4.2 Monitored Room

Although the pilot monitoring mainly focused on the thermal behaviour of the facade, the environmental response of the selected room located on the 5th floor was also measured. For ideal monitoring of the inside of the façade, it is suggested that at least one room from each floor be assessed. However, due to technical and physical restrictions, it was only possible to monitor one room on the 5th floor. The purpose of such an assessment was to observe any implications or direct influence of the DSF on thermal performance and natural lighting levels of the occupied spaces. Although some problems with power supply did not allow detailed data collection from February to April 2006 and to a lesser extent, during short periods in June and July, the rest of the year the equipment collected valuable data to give a general picture of the environmental performance of the room.

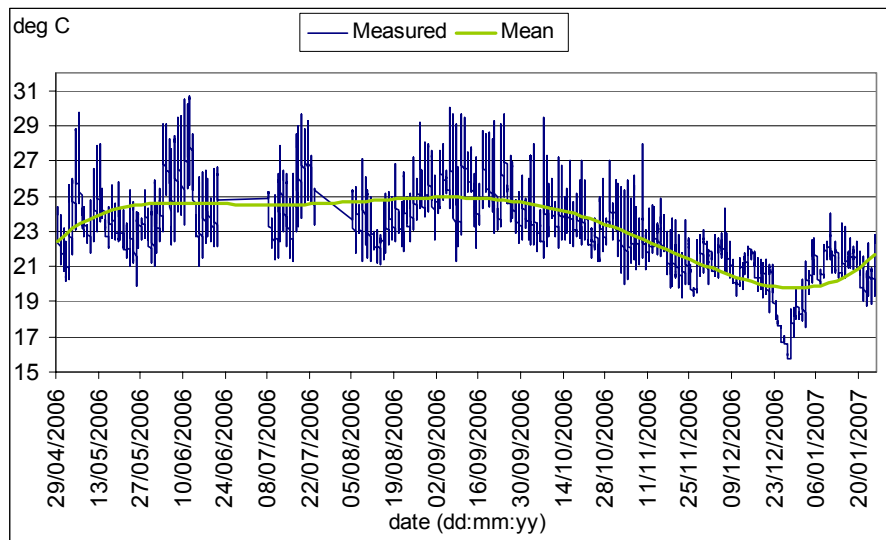


Figure 7.21 Monthly mean and measured Dry Bulb Temperature inside the room.

The ambient dry bulb temperature performance inside the room is illustrated in figure 7.21. This graph shows that the mechanical HVAC system of the building is mainly responsible for the mean resultant temperatures of the room during mid seasons and summer. The chart also shows that mean temperatures are slightly but quite uniformly decreased during winter, meaning that the HVAC system is adjusted to a lower effective temperature during this period. However, the graph shows clear fluctuations on peak maximum and minimum temperatures, mainly caused by the direct incidence of the solar radiation which is not completely blocked by the shading devices inside the facade. Figure 7.23 shows an example during mid season where part of the direct radiation is not blocked by the shading devices. This obviously increases heat gains and peak temperatures, which are noticeably plotted in figure 7.22, illustrating the values of direct solar radiation entering the room through inner glass. The deep fluctuations on these levels are primarily caused by the partial protection provided by the shading devices. For efficient reduction of direct gains and overheating prevention, the amount of direct radiation during mid season and

summer has to be reduced to less than 50W/m^2 , which is a reasonable amount gained by reflected, rather than direct radiation entering the room.

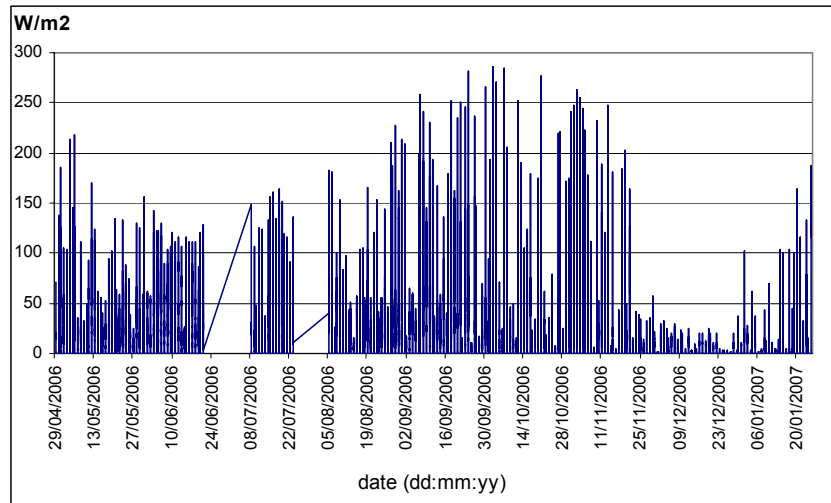


Figure 7.22 Radiation measured inside the room on the vertical plane of the inner glass of the facade.



Figure 7.23 Direct radiation hitting inside the room on walls and floor as the shading devices were not totally able to shield efficiently part of the inner facade.

Ineffective performance of the shading devices during specific hours causes surface temperature of the inner glass to be directly affected. The figure above illustrates how there are peak fluctuations in temperature values instead of gradual variations, which is the optimal expected behaviour of the inner glass facade during summer conditions.

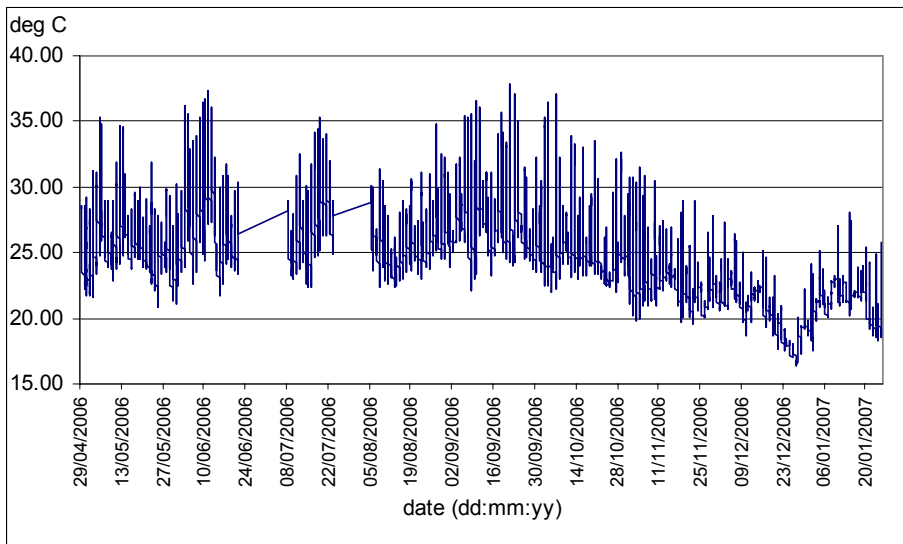


Figure 7.24 Surface temperature of the inner facade glass measured inside the room.

For ambient relative humidity, the measured and average data displayed in figure 7.25 shows a relatively steady behaviour during most of the year. This clearly demonstrates the main influence on the parameters of the HVAC system.

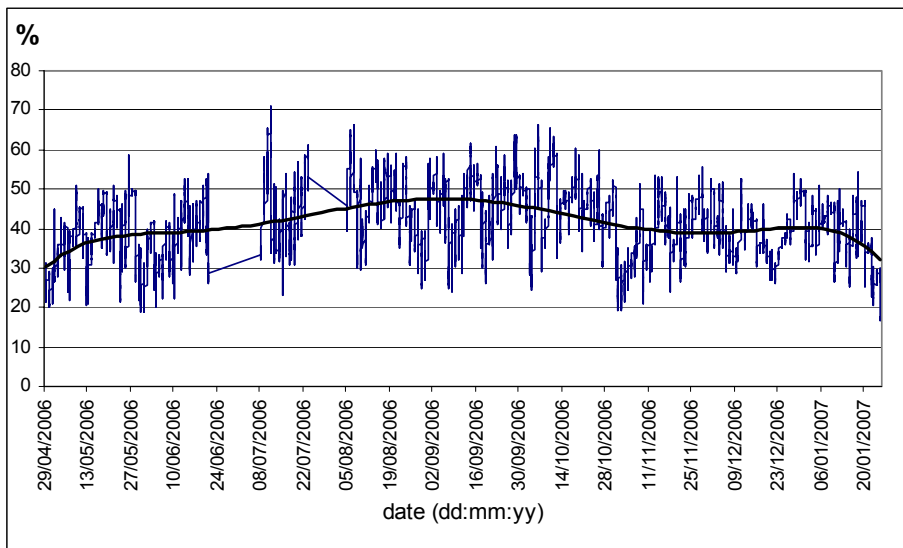


Figure 7.25 Monthly ambient Relative Humidity room.

The amount of visible light that enters the room is greatly affected by the DSF. Figure 7.26 shows a very fluctuating behaviour on the illumination levels close to the facade glass, which are also due to the event mentioned previously. Although the illumination measured at 3.55 metres from the facade glass is significantly reduced, the average levels are within 400-550 lux, which are reasonable for natural lighting (see figure 7.27). Nevertheless, some peaks were measured during winter which indicates glare as an issue that has to be controlled on fully glazed facades when solar altitude is low and direct radiation hits almost perpendicular on the facade. For this reason, inner shading devices are also a requirement on fully glazed facades.

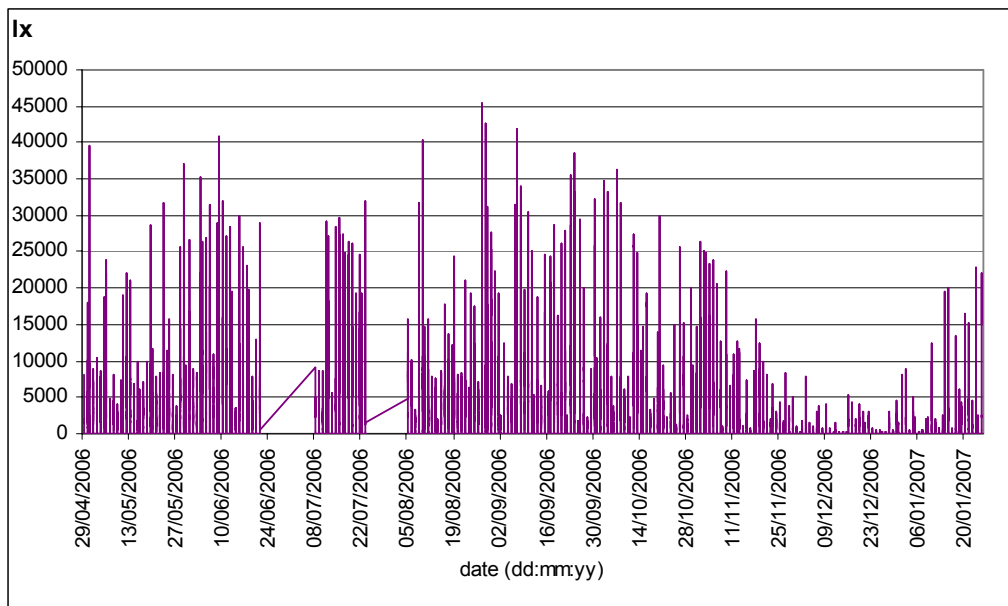


Figure 7.26 Illumination on horizontal surfaces measured next to the inner glass of the facade inside the room.

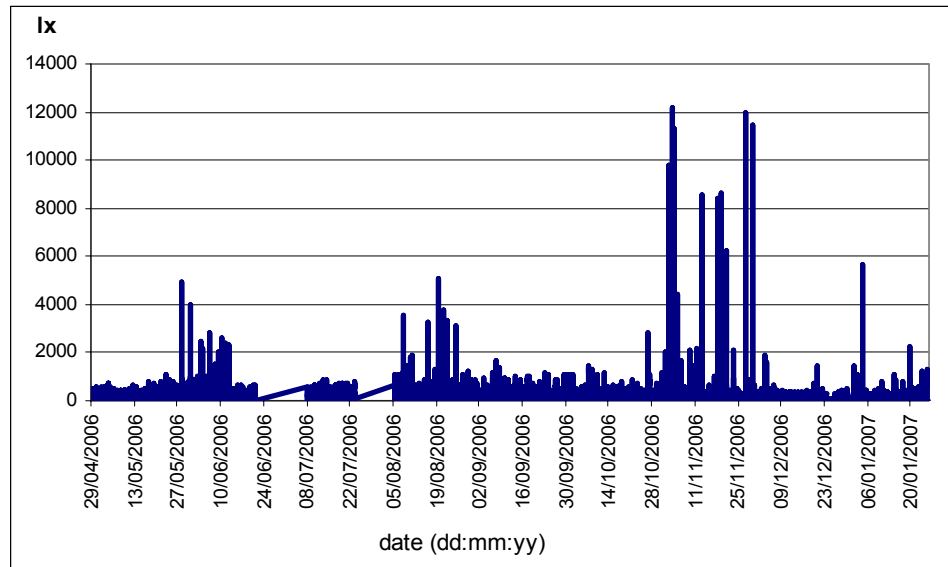


Figure 7.27 Illumination on horizontal surfaces measured on the back wall of the room at 3.55m from the facade.

7.5 DOUBLE SKIN FAÇADE AIRFLOW ANALYSIS

The data collected during the year was used as a reference for the boundary conditions of the CFD model, which in turn was used to compare the measured thermal behaviour. This was done to obtain information in relation to the airflow inside the DSF channel under summer, mid season and winter conditions.

The physical behaviour of the air inside the facade channel provided valuable information regarding the possible factors that contribute to overheating of the Double Skin Facade and the increment of heat loads inside the rooms next to the facade. It also provided key information for the understanding of the direct implication of the overall interaction of the DSF with the building.

7.5.1 Model Description

CFD software was used to predict the flow and movement of air and temperature response in the facade cavity. FLUENT [8] is a widely used computer program for modelling engineering fluid flows, due to its robustness, accuracy and user-friendliness. In FLUENT, equations for the conservation of heat, mass, momentum and other transport factors are solved using a control-volume technique. The software is capable of solving multiphase fluid flow problems in two or three-dimensional body-fitted coordinate systems.

For the turbulence model, the Standard k - ϵ model was applied. This is one of the simplest complete two-equations calculation method used in fluid dynamics. It is also the most common turbulence model for fluid flow simulations used by commercial software. In this method, the solution of two separate equations allows turbulent velocity and length scale to be independently calculated. It is a reasonably accurate method for overall turbulent flow calculation.

For radiation calculation, Discrete Transfer Radiation method (DTRM) was adopted to calculate the energy equation. The model was simplified into a two dimensional section of the Double Skin Façade channel, in order to save computational resources and calculation time.

7.5.2 Model settings and Boundary Conditions

The air flow and the temperature response were modelled using a steady state model of radiation, directly affecting the Double Skin Façade. The total internal heat gain (TIHG) shown in table 7.3 were based on the steady state total heat flux

calculated for the selected dates, based on the data provided by the monitoring instruments. In the CFD model, these gains were set on each floor level. For wall surface temperatures, a fixed value was set to each of the cases assessed. Table 7.3 shows the values used as boundary conditions for temperature and heat gains inside the facade channel.

Boundary conditions variables	Case Model					
	units	Winter (day)	Winter (night)	Mid season	Summer (Open outlet)	Summer (Closed Outlet)
External Temperature	°C	10,00	7,00	13,90	20,00	19,00
Surface Temperature Louvres	°C	12,05	8,00	22,85	32,00	35,00
Surface Temperature A/C ducts	°C	13,00	7,80	21,00	25,00	28,00
TIHG	W/m ²	32,86	-10,50	273,65	306,24	298,26

Table 7.3 Main boundary conditions and Total Internal Heat Gains (TIHG) of the facade cavity set for each model case.

Five different cases were modelled in FLUENT. In every case, the cavity was considered as one continuous space. The different elements inside the facade were assumed as subtracted objects from the calculated domain. For each model, the grid was exactly the same and the boundaries were adjusted according to a basic seasonal value - recorded on one day during 12 hours.

For the winter (day) case, the flow model was calculated based exclusively on buoyancy generated by solar and internal heat gains. The energy equation was calculated through the DTRM model. The reference values for the model were taken from the data collected on 07/02/2006 at 12h. The winter (night) case model was set without solar heat gains while considering a very low additional heat gain from the

internal glass facade with the additional heat losses from the external glass of the cavity.

The mid - season case was set assuming a ventilated cavity with temperature values for the internal facade according to the values recorded on 07/05/2006 at 12:00pm. The first summer case was set also with a ventilated open cavity. The reference temperature values selected for this case were based on the data recorded on 09/08/2006 at 12:00pm. The second summer case was set based on the data recorded on 07/09/2006 at 12:00 in which the monitored facade cavity was already closed.

7.5.3 Airflow Models Results

7.5.3.1 Winter Day Model

In this model, the temperature values obtained inside the façade cavity increased steadily from 9.87°C to 17.02°C (see Figure 7.28). This difference of temperature illustrates how the solar radiation is received through external glass, where the greenhouse effect created within the façade contributes to the improvement of thermal insulation and heat stored by the façade when required in winter.

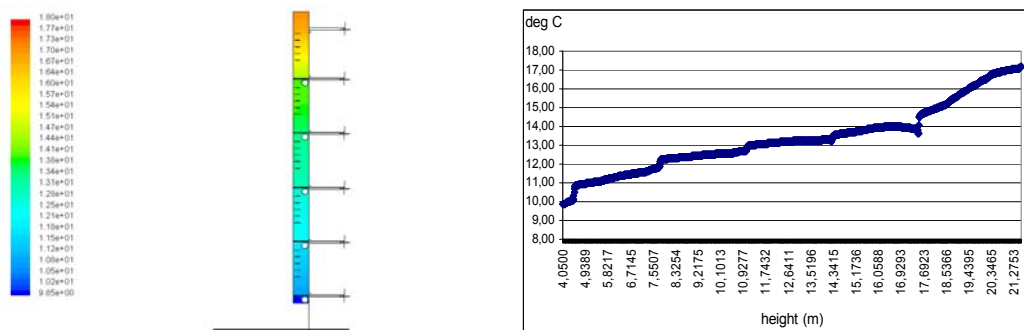


Figure 7.28 Total temperature inside the cavity (°C).

Although the DSF configuration in this building is reasonably helpful to improve insulation, the open inlet contributes to a constant airflow from the bottom of the façade, increasing heat losses by convection and restricting a more efficient storage of heat, which is required during the night. Figure 7.29 shows this behaviour. The velocity magnitude values decrease gradually from the inlet position to the top of the façade. The peak values shown on the plot below are mostly due to the influence of the cylindrical air duct increasing airflow pressures close to their boundary.

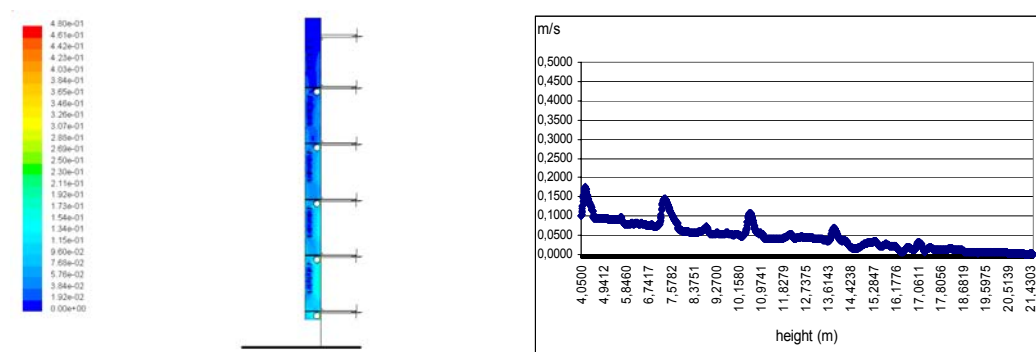


Figure 7.29 Velocity magnitude contours of the winter (day) model (m/s).

7.5.3.2 Winter Night Model

In this simulation, the temperature behaviour differs from the previous case. The values decrease with height as a result of the downdraft flow created by the open inlet, which indicates that heat loss by conduction and convection are higher and the façade acts as a heat sink. Figure 7.30 illustrates the temperature values inside the channel with steady values of 7.7°C decreasing to around 7.0°C, showing how, without radiation hitting the external glass, this trend starts to develop.

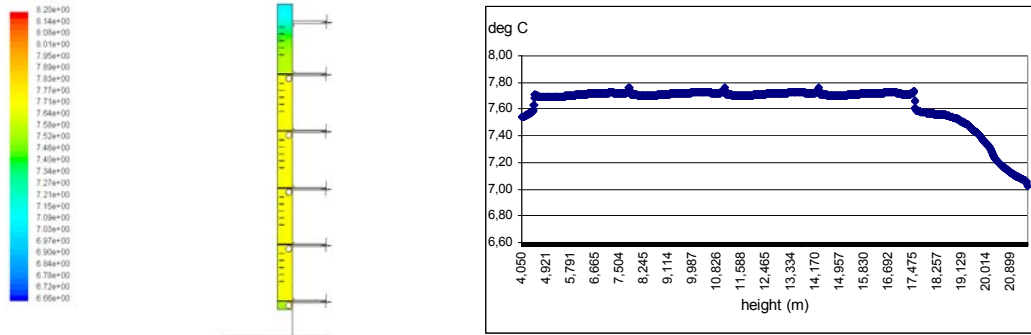


Figure 7.30 Total temperature contours for the winter model at night ($^{\circ}\text{C}$).

The air movement inside the façade cavity is much reduced. However, there is a repeated appearance of air pockets within each floor as a consequence of the small heat gains from the inner glass. This is illustrated by the repeated peaks on the plot and clear vortex on the contours of the diagram in Figure 7.31.

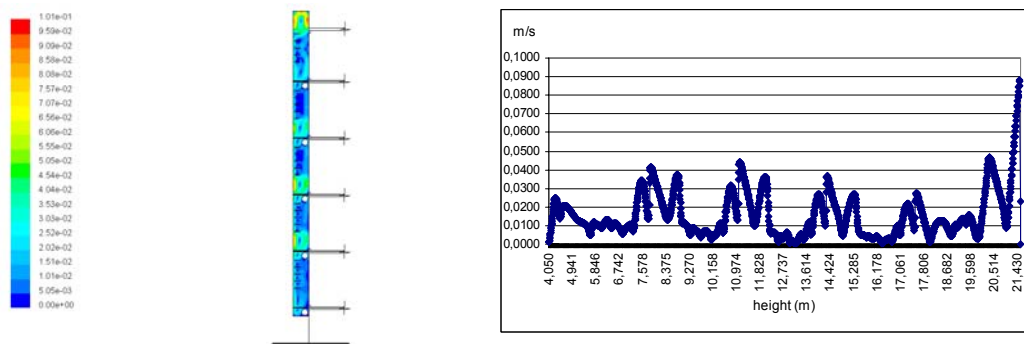


Figure 7.31 Contours of Velocity magnitude for the winter case at night (m/s).

7.5.3.3 Mid Season Model

In this simulation, the increase of temperature is still gradual. This indicates that heat losses by conduction continue playing an important role in the total heat load of the façade. Figure 7.32 illustrates how temperature values inside the channel range from 15°C to nearly 30°C and also how the impact of more radiation hitting the

external glass contributes to a further increase in the difference of temperatures inside and outside.

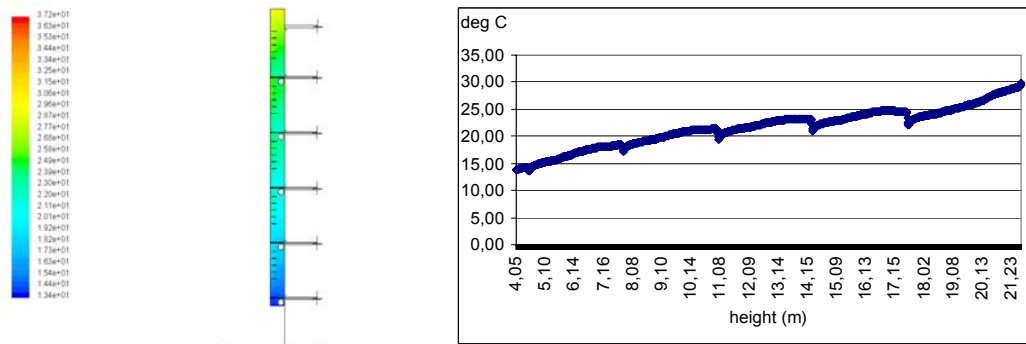


Figure 7.32 Contours of total temperature for the mid season case (°C).

The air movement inside the façade cavity is also improved due to two factors. First, the ventilated configuration of the façade is with an open outlet and secondly, the increase of heat gains inside the façade is a result of the additional convective heat transfer on the glass surfaces and internal elements of the façade. Figure 7.33 illustrates how there is a rather steady air velocity of 0.09m/s inside the façade cavity. The same pattern of 5 peaks on the velocity magnitude is also shown on the velocity plot as a result of the divergence of flow by the ducts.

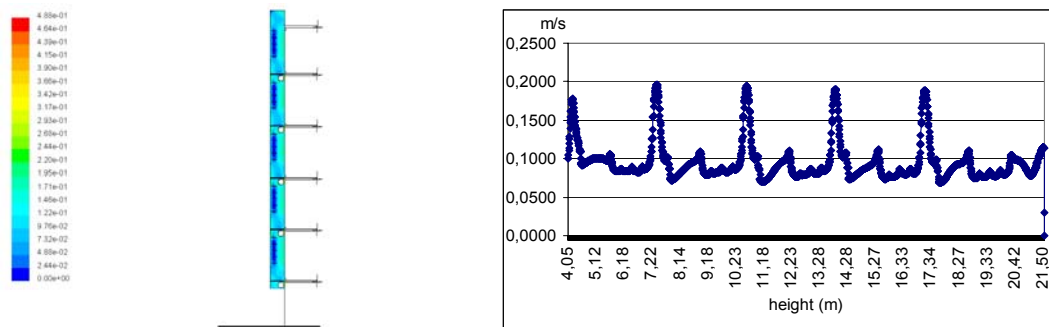


Figure 7.33 Velocity magnitude contours for the airflow inside the facade channel (m/s).

7.5.3.4 Summer model with ventilated cavity

Although the stack effect is improved as a result of the additional solar radiation, the ventilated configuration of the façade favours constant air flow with gradual increments on temperature levels across the cavity section. This indicates that more heat is stored on the upper part of the façade, which behaves like a chimney and favours air extraction. However, this building does not have openings from inside the building to the façade and the possibility of air removal by natural means is not exploited. Therefore, the HVAC solely removes external and internal gains of the building without the help of passive means from the façade, wherein DSF can play a key role of heat removal under summer conditions. Figure 7.34 illustrates how temperature values inside the channel range from 20°C to nearly 35°C, it also shows the impact of extra radiation on the external glass that contribute to a further increase on the stack effect.

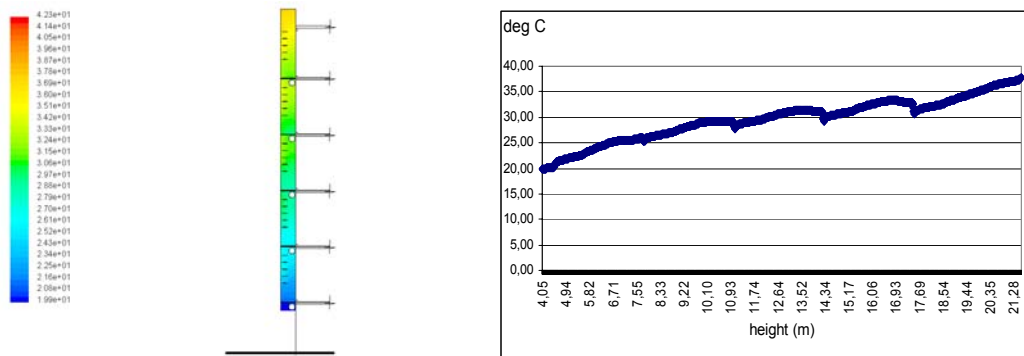


Figure 7.34 Contours of temperature of the Ventilated summer model (°C).

The air movement inside the façade cavity is also improved by the previous two factors - the ventilated configuration of the façade and the increased improvement of the stack effect. Figure 7.35 illustrates the steady air velocity of 0.095m/s on each level of the façade channel and 5 peaks on velocity magnitude close to the cylindrical ducts.

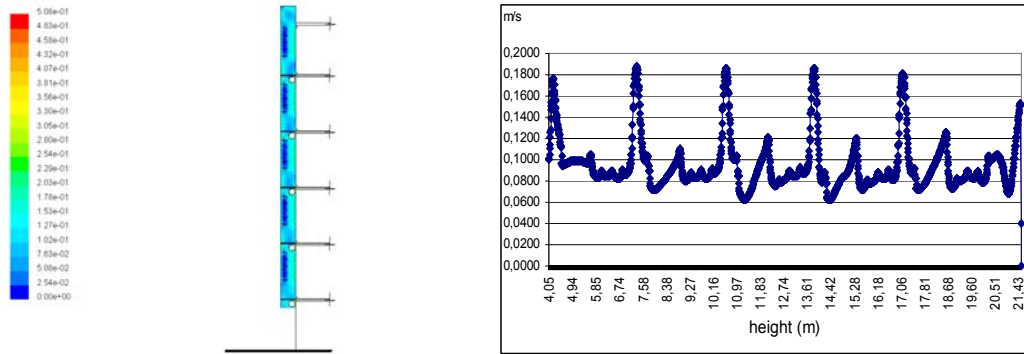


Figure 7.35 Velocity magnitude contours of the summer model with outlet shafts open (m/s).

7.5.3.5 Summer model with cavity closed

In this case, the outlet shafts of the building were closed. The temperature values obtained inside the façade channel increased sharply from 19°C to 45°C (Figure 7.36). This large variation of temperature illustrates how the solar radiation received through external glass, when no openings are available, creates a sharp rise in the greenhouse effect within the facade. This typical example is a clear sign of overheating created by the wrong operation of the façade, which at the end contributes to extra heat loads on the building and increasing the cooling load on the HVAC system.

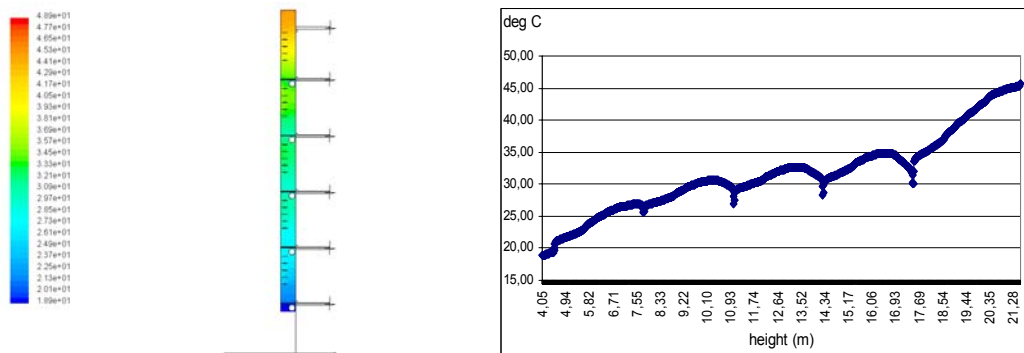


Figure 7.36 Total temperature contours of the closed facade channel on the summer model (°C).

In this case, the DSF configuration of the building does not help to improve energy efficiency of HVAC system. The closed outlet shafts contribute to the amplification of the greenhouse effect and a reduction in airflow inside the façade cavity, where extra heat load is transferred through the inner skin of the façade by delayed conduction. This also can be seen in figure 24 where the surface temperature of glass is greatly affected during early spring and late summer, when the outlets were closed.

Figure 7.37 shows the behaviour of the airflow. The velocity magnitude values decrease gradually from the inlet position to the top of the façade. Here, vortex pockets are also created on each level. The peak values on the plot show the clear trend of decreasing values due to the reduction of the static pressure of the façade.

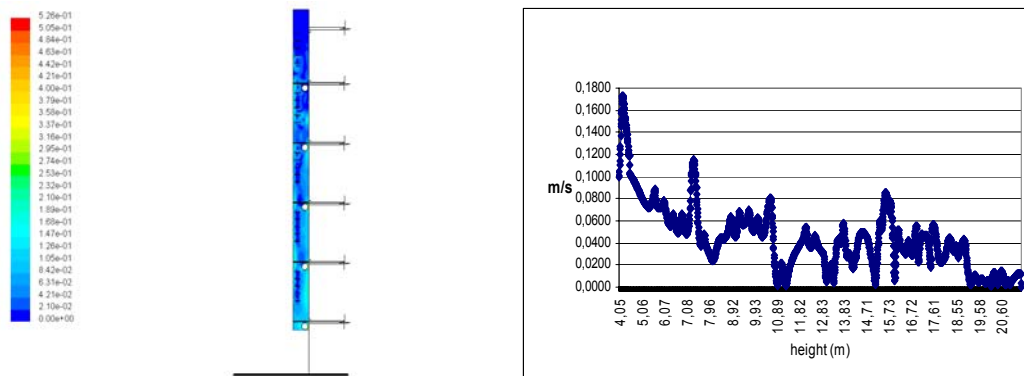


Figure 7.37 Contours of Velocity magnitude inside the facade cavity with closed outlets on the summer model (m/s).

7.5.4 Validation of CFD Results

The validation of the model was performed by comparing the results from the CFD models, with the monitored data from the selected dates of each seasonal case study. The time for all the base models was 12:00 except for the winter night model, which was 05:00. The dates for the models were 7th of January for the winter model, 7th of

May for the mid-season model, 9th of August for the Ventilated Summer model and 7th of September for the summer case with closed outlets.

Figure 7.38 shows a rather good agreement between the simulated and measured values, which was achieved particularly for the summer cases. The average difference between the predicted and measured temperatures was about 6.5%. The relative difference was larger in the nocturnal winter case. (In the domain close to the inlet.) This validation shows that CFD can be used to study the buoyancy-induced flow in open and closed cavities.

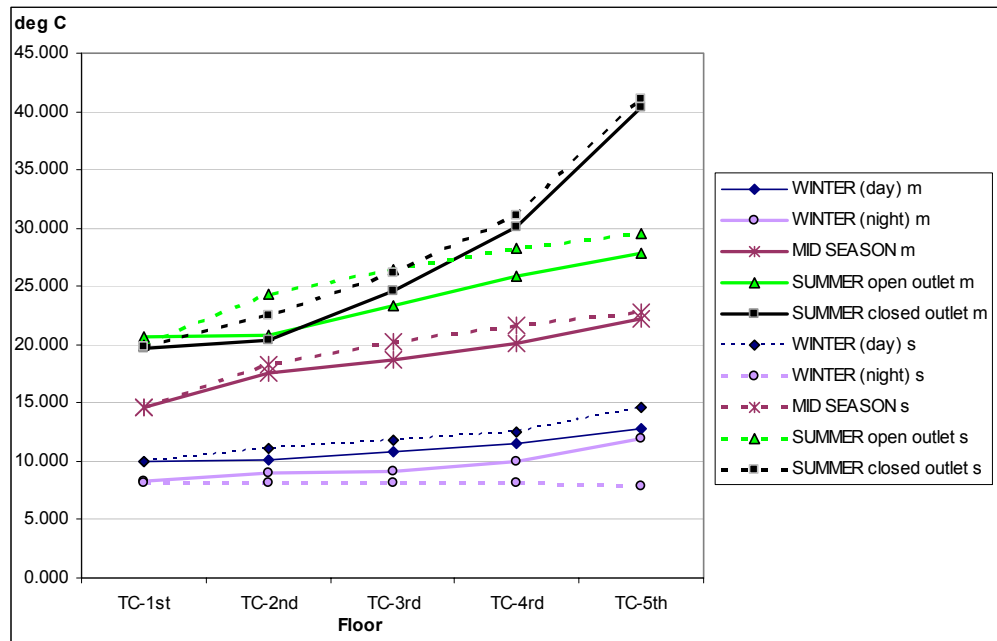


Figure 7.38 Validation of CFD results with the measured steady state temperature values according to each season case.

7.6 OCCUPANTS PERCEPTION ASSESSMENT

For a general understanding of how the occupants perceive the influence of the façade on relation to their well-being, a questionnaire was left in the monitored room. The occupants were free to collect a questionnaire form, which is shown in table 7.4. The survey was carried out for 6 months from September/06 to March/07. A total of 135 people voluntarily answered the questionnaire. The aim of the survey was to provide a general idea of how people see the implications of the Double Skin Facade on natural lighting, comfort and energy efficiency.

Natural Lighting levels satisfaction						
	LIGHTING					
	satisfaction with quality of natural lighting					
	Very Satisfied	Fairly Satisfied	Neither s / d	Fairly dissatisfied	Very dissatisfied	N/A
Glass façade influence	27	81	0	0	27	0
Daylight levels	32	81	0	0	22	0
Artificial lighting requirement	0	27	54	0	54	0
Solar radiation reduction	0	31	26	0	78	0
Facade performance perception						
	PERFORMANCE IMPLICATIONS					
	Agreement with façade influence on performance					
	Strongly Agree	Agree	Neither A/D	Disagree	Disagree strongly	
Improvement of insulation	0	81	54	0	0	
Improvement of thermal comfort	0	0	0	108	27	
External noise reduction	0	81	0	27	27	
Effective Glare control by louvers	0	54	22	31	28	
Requirement of indoor shading devices	54	49	0	5	27	
Energy savings due to façade design	0	0	108	0	27	
Natural ventilation and air quality awareness						
	VENTILATION					
	Influence of DSF on Ventilation					
	Strongly Agree	Agree	Neither A/D	Disagree	Disagree strongly	
Air quality improvement	0	0	27	60	48	
Natural Ventilation improvement	0	0	27	33	75	

Requirement of openings for manual operation		27	54	32	22	0
Adequate room ventilation		0	0	0	54	81
User's interaction with Double Skin Façade and operation						
OTHER FEATURES						
Flexibility for user's controlling the façade						
	Strongly Agree	Agree	Neither A/D	Disagree	Disagree strongly	
Manual operation of openings	50	85	0	0	0	0
Control external louvers	54	81	0	0	0	0
Manual control of lighting levels	57	51	27	0	0	0
Considerable differences with single facades	0	0	135	0	0	0
Improvement of building aesthetics	0	54	81	0	0	0
TOTAL PEOPLE SURVEYED						135

Table 7.4 Occupants Perception survey results.

7.6.1 Natural Lighting levels satisfaction

In terms of natural lighting, the occupants have a reasonably good perception of the quality of light as a result of a fully glazed façade (figure 7.39). Around 60% of the people have considered that natural lighting levels inside the room are satisfactory. There was an important disagreement on a real requirement of artificial lighting, probably due to the reduction of daylight levels on cloudy days. These levels can be observed in figure 7.27, showing the average illumination measured was around 500 lux - with some peak fluctuations due to direct sunlight entering the room.

For the case of satisfaction with the reduction of solar radiation by the façade, there were a majority of people who were very uncomfortable with glare and direct light. 58% of the occupants were very dissatisfied with the capacity of the façade to provide adequate shading. This can be seen in figure 7.23 which clearly illustrates direct light entering the room as the louvers were not able to efficiently shade the inner glass at some periods during mid-season.

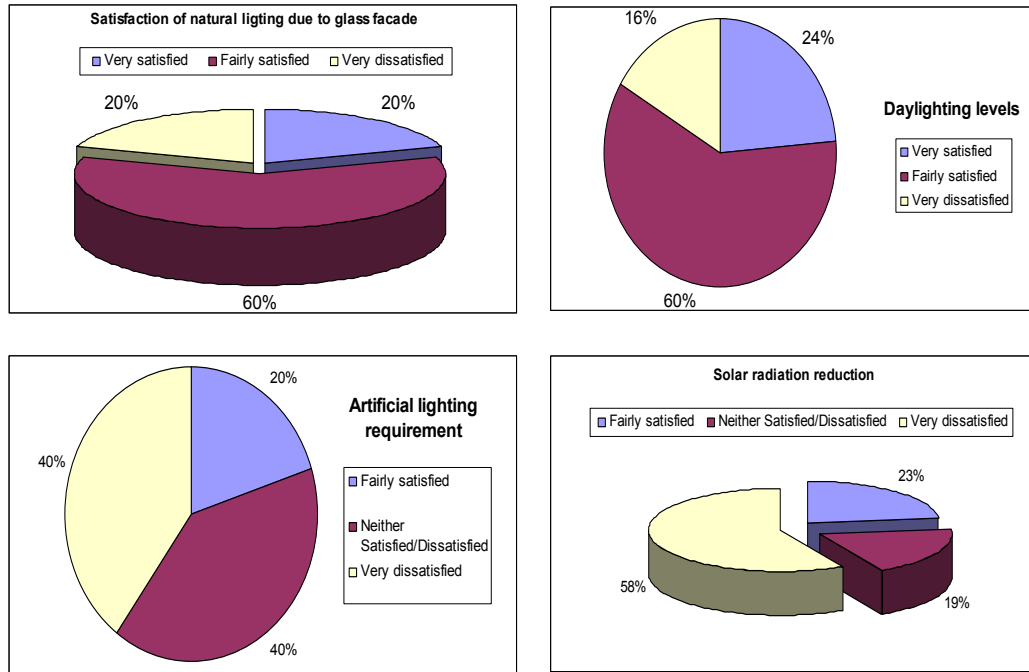


Figure 7.39 Occupants satisfaction with natural light quality and solar radiation control by the DSF.

7.6.2 Façade performance perception

Regarding the effective performance of the façade, 60% of the occupants thought the façade generally improved air-tightness. However the influence of the façade enhancing thermal comfort was mostly seen as a down point. This can be explained, as the high fluctuations of temperature within a short time are a result of not having efficient shading devices. The majority of discontent amongst the people in relation of the louvers performance was 44%.

As stated previously, the façade is quite efficient at blocking external noise. 60% of those surveyed thought the façade accomplished that effectively. Nevertheless there was some disagreement on this (26%) - probably based on the fact that double façades block external noise through the double skin of glass and buffer zone, but also reflect and reverberate sound on the inner one [4].

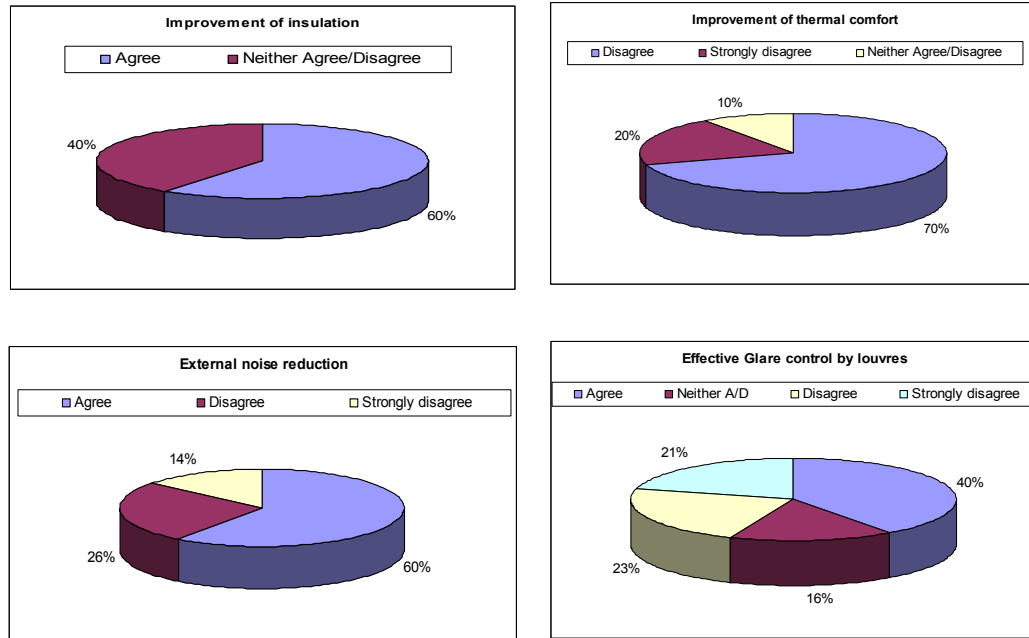


Figure 7.40 Occupants perception of the façade efficiency.

7.6.3 Natural ventilation and air quality awareness

As a result of using a Double Skin Façade in the surveyed room, the occupants mostly perceived the façade as it is... a system that contributes poorly to good levels of natural ventilation. More than half of the people thought there is no improvement on natural ventilation levels using this DSF. This can be explained by the type of façade used on this building, which is completely sealed inside. This type does not allow any control by the users. Research has proved that the occupant's ability to control façade windows or openings improves largely the perception of quality of the indoor air. In this pilot case, those surveyed also thought that air quality was not related to the type of façade used in the room (80% in total). As a matter of fact, the monitored room is fully mechanically ventilated and the façade does not play any roll in this matter.

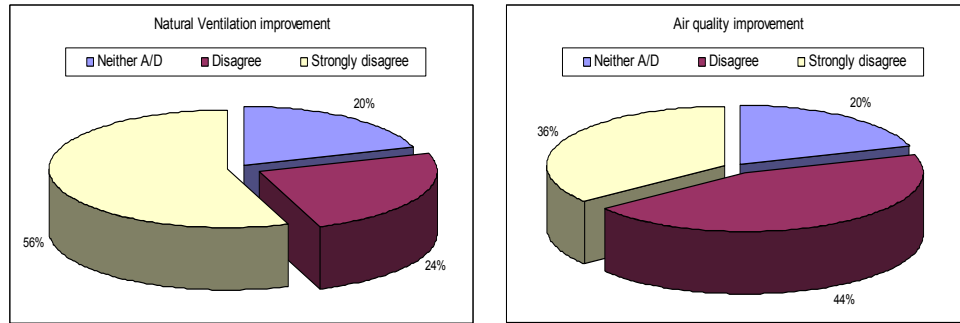


Figure 7.41 Occupants perception of the quality of air and ventilation in relation with the façade.

7.6.4 User's interaction and operation of Double Skin Facade

Regarding the operation of the façade openings and natural lighting, there is a necessity by the occupants to be able to operate the façade openings. In this study, 63% of the people agreed and 37% strongly disagreed with this statement. There was also an important concern about the flexibility of the façade to provide manual control for the external shading devices. This also proves that a problem arises when fixed passive systems do not work efficiently. In general, there is an overall agreement on the flexibility of the façade to facilitate manual operation by the users.

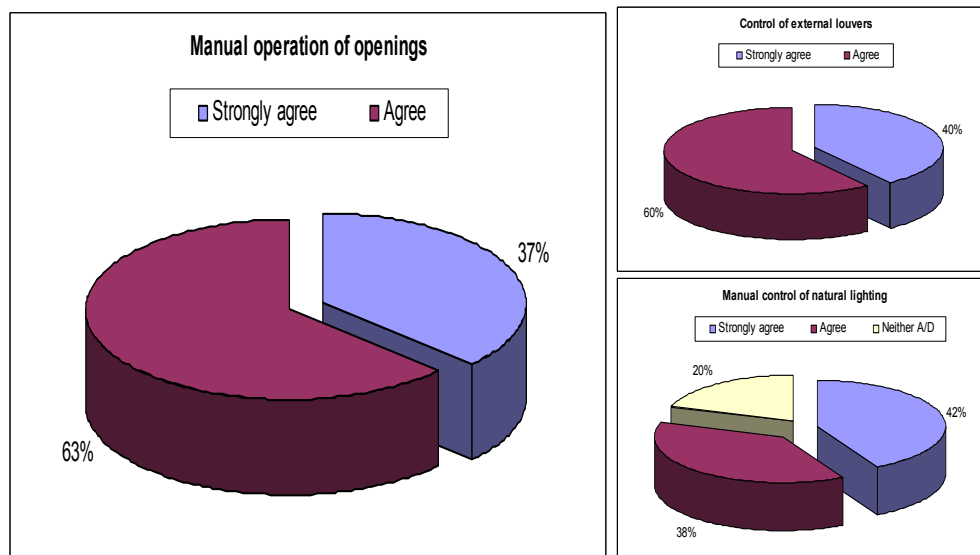


Figure 7.42 Occupants opinion about the possibility of manual operation of lighting levels and solar protections of the façade.

7.7 CONCLUSIONS

A pilot monitoring study was carried out inside the Double Skin Façade cavity in a selected room at ARUP Headquarters building located at 13 Fitzroy Street in London. Information and results provided key elements to develop a method to monitor other buildings with Double Skin Façade based on the following issues:

- Data collection and monitoring of main environmental variables focusing on the thermal behaviour of the façade.
- Data collection and monitoring of main environmental issues of a room connected to the facade also focusing on its thermal performance.
- Evaluation and assessment of the overall performance of the system.
- Comparative analysis using CFD software tools to compare monitored results.
- Occupant's perception assessment in relation to the influence of the façade.

Regarding the thermal behaviour of the DSF and its influence on the environmental performance of the room assessed, the following issues were concluded after this study:

- The thermal performance in the vertical section of the façade is clearly stratified during the day. Highest temperatures were always measured at the top of the façade. The stack effect created by the façade favours air movement when the façade is ventilated. In this building, the façade is sealed on the inner skin; this is a disadvantage of the façade design as the system could contribute to save energy during summer, extracting air by natural means from the building.

- The measured thermal performance of the shading devices showed that the heat stored by them is also a factor that contributes to the stack effect.
- The accurate configuration of the façade is a critical issue. The lack of knowledge of when and how the façade has to be adjusted according to the climate is a factor that largely contributes to the problem of overheating and heat losses.
- The thermal performance of the monitored space was directly influenced by the partial inefficiency of the shading devices and was the major cause of increased temperatures, direct gains and illumination fluctuations.
- The amount of direct incident solar radiation influenced the stack effect. However, overheating was mostly produced by the incorrect configuration of the façade during early and later mid-season, when most of the overheating was produced.
- The purpose of DSF is improvement of insulation during winter, however the incorrect design of a fixed open inlet, encourages downdraft flow during this season, which increases heat losses when no solar radiation is received by the façade.

This study demonstrated that the Double Skin Façade of this building performs reasonably well during mid-season and summer when in ventilated configuration, however the incorrect operation and some problems with shading devices makes the façade contribute negatively with the heat load of the building on this side of the building.

REFERENCES

1. Faggembauu, D., et al. Strategies to reduce thermal overheating in Mediterranean climates using large glazed areas. In Fier 2002: International Forum on Renewable Energies. 2002. Tetuan: FIER 2002.
2. Kragh, M., M. Colombari, and M. Zobeck. Advanced Façades and HVAC Systems: Preliminary results of full-scale monitoring. in: Energy Efficient and Healthy Buildings in Sustainable Cities. 2002. Lyon-France: EPIC AIVC.
3. FLUENT 6.1 User's Guide. 2001, Fluent Inc: 10 Cavendish Court, Lebanon, U.S.A. p. <http://www.fluent.com/software/fluent>.
4. MET Office, UK climate and weather statistics: Monthly Climate Statistics, Greenwich, London. 2000, Met Office: Exeter, EX1 3PB, United Kingdom. <http://www.metoffice.gov.uk/climate/uk/stationdata/index.html>.
5. ARUP, Camden Neighbourhood Regeneration Strategy, in Development Planning. 2001, Ove Arup & Partners Ltd: London, UK. <http://www.arup.com/developmentplanning/feature.cfm?pageid=4699>.
6. Gissen, D., Breathing room: Arup's new London headquarters celebrates its mechanical systems, in Architectural Record. 2005, McGraw-Hill Construction. <http://archrecord.construction.com/features/digital/archives/0507dignews-1.asp>.
7. ARUP, Headquarters Offices in London. 2007, Ove Arup & Partners Ltd: London, UK. <http://www.arup.com/offices.cfm>.
8. Datataker, DT500/600 Specifications. 2007, Datataker Pty Ltd: 7 Seismic Court, Rowville, Australia, VIC 3178. <http://www.datataker.com/products/dt500.html>.
9. Skye-instruments, Technical information. 2007, Skye Instruments Ltd.: 21 Dole Enterprise Park, Llandrindod Wells, United Kingdom, LD1 6DF. <http://www.skyeinstruments.com>

CHAPTER VIII

DISCUSSION AND CONCLUSIONS

The building envelope is a crucial element for the thermal balance of a building, as its influence on the building's energy efficiency creates significant issues for the design of any building. The use of fully glazed facades has generated wide concern about the effect on natural lighting, thermal performance and energy consumption of contemporary buildings. Double Skin Facades were developed to overcome the problem of thermal instability of single glass facades. However, environmental conditions and the configuration and operation of this type of facade exposed to moderate or high radiation levels, are argued to be relevant factors that lead to overheating. This study presents the experimental assessment of overheating and CFD airflow behaviour of an experimental chamber built at the University of Nottingham. It also shows the results of a field case study of a Double Skin Facade building in the UK.

8.1 DISCUSSION OF FINDINGS

8.1.1 Thermal Performance:

The arguable improvement of the thermal insulation of DSFs is highlighted throughout previous literature. However, the utilization of this system in places with high solar gains has shown a link with the development of overheating. A steady stratified increase in temperature levels along the height of the DSF was clearly identified, which determined that the upper parts of the facade are 'critical' in terms of total heat gains on the facade.

The main factors affecting rapid overheating on the facade and in the room, identified in this research, is the rate of convective heat transfer inside the cavity, and the resultant incident direct radiation which determined the total heat gains and resultant temperatures of the occupied spaces. The balance between these two factors is crucial when controlling overheating and thermal discomfort of the building's occupants. The optical properties of glass influences primarily direct gains and greenhouse effects inside the DSF.

A rapid rise in insulation quality and temperature levels on sealed cavities (ST), and a reduction of heat accumulated on ventilated cavities (STV), resulted, when the position of the openings of the facade were adjusted. The size-ratio correlation between inlets and outlets affects the heat reduction in the cavity. A size-ratio correlation of 0.5 between inlet and outlet may achieve the lowest temperature levels inside the cavity and the airflow rates within the DSF.

The adjustment of the surface's emissivity inside the DSF increases convective heat transfer and buoyancy-induced flow inside the cavity. The location of shading devices near the external skin provided better control of radiation and heat removal from the cavity.

Cross ventilation combined with buoyancy-induced natural convection in the cavity, favoured a better performance of the temperature field in the occupied spaces next to the facade. The correlation between height and depth of the DSF has far-reaching consequences regarding the stack effect and resultant temperatures inside the cavity.

8.1.2 Airflow Performance:

It was observed that the incident radiation has direct influence on the buoyancy and airflow rates inside the DSF cavity, favouring air extraction from the facade. It was also visualized that DSF with inlets and outlets open, encourages buoyancy and induces air movement, thus a ventilated cavity is imperative for the control of overheating. The air movement inside the DSF has influence on the spaces next to the facade as long as openings are available between the cavity and the inner spaces. The convective forces in the cavity may also be used to promote air extraction from these spaces. A ventilated cavity promotes constant laminar vertical airflow and a limits the increase in temperature. The position of louvers and elements inside the cavity are critical factors determining the nature and magnitude of the airflow within the DSF.

8.1.3 Natural Lighting:

Previous literature has suggested that DSFs account for a slight reduction in illuminance levels when compared with single glazed facades. It was found that illuminance is primarily affected by the optical properties of glass. Shading coefficients on the external or inner skin are critical factors on the prevention of glare and the control of natural lighting.

8.1.4 User's Perception:

Taking into account the limitations on the number of respondents of those surveyed, it was fundamentally identified that there was a good perception of the quality of light as a result of a fully glazed facade on the building envelope. In the case studied, the moderate efficiency of the shading devices inside the double skin facade

produced dissatisfaction amongst the room users. Nevertheless, the occupants also identified improved efficiency of shading devices during some periods of the year. This indicates that detailed assessment on the performance of shading devices in every season is required. There is still important disagreement on the perception of natural lighting reduction when using DSF on the envelope.

In general, users perceive the facade as an efficient architectural feature that improves thermal and sound insulation. However, there was a negative perception regarding the improvement in thermal comfort during summer conditions as a result of a lack of openings and natural ventilation through the facade. The respondents generally agreed that it is important to allow, by some means, manual control of the facade openings in order for them to perceive that the space is really ventilated.

8.1.5 Design Implications

It was observed that DSF improves insulation for winter conditions when the cavity is sealed, however the design and operation of the opening shafts has to respond to the seasonal requirements of passive heating and/or natural ventilation. The implications of a fully glazed facade have to be assessed in each specific case in order to reduce undesired heat gains even in mid-season and critical summer conditions.

The key elements to be considered when designing a DSF are solar radiation, climatic conditions, building location, orientation, facade design, material properties, user requirements and building regulations. The functionality and efficiency of the facade depends on the analysis of the thermal and airflow performances during the

design stages.

8.2 CONCLUSIONS

The cause of overheating under conditions of incident radiation includes the convective heat transfer of the cavity and the total heat gain received by the room. The thermal loads from the external skin and the thermal loads from the cavity, which in turn depend on the rate of air movement, influence these factors. It was found that a ventilated DSF reduces the temperatures in the cavity if properly operated.

The thermal behaviour of the experimental chamber has provided some evidence indicating that controlling direct heat gains from the DSF cavity, is a key factor in the reduction of cavity overheating and high room temperatures. This may result when part of the heat gained is reduced from within the external facade, with proper sizing and location of shading devices combined with constant airflow for heat removal. The effective reduction of heat results when shading devices are located close to the external skin.

This study has illustrated that the primary issues that cause overheating are as follows:

- 1 Inefficient removal of the heat stored in the facade and the room due to reduced airflow.
- 2 Inadequate location and size of shading devices inside the cavity.
- 3 The greenhouse effect is the main cause of overheating while convective heat

transfer in the cavity is the key to removing heat.

- 4 The stack effect due to the natural convection developed inside the cavity is a useful resource in removing heat from the cavity.
- 5 Inadequate operation of the DSF according to the seasonal requirements of thermal comfort.

8.2 FUTURE WORK

Previous research in this field has provided a wide assessment of thermal and airflow models of DSFs. However, the advancement of more simple design tools for architects is still under-developed. Further analysis is required on the implications of DSF types, forms and orientations as a reference guide for architectural design.

The post-occupancy assessment of existent DSF buildings in the UK requires further in- depth research, into the field of user comfort and energy efficiency. There is a lack of systematic and quantified data regarding the performance of buildings with DSF in the UK.